Design Methods of Sparse and Robust Differential Microphone Arrays

Yaakov Buchris

Design Methods of Sparse and Robust Differential Microphone Arrays

Research Thesis

Submitted in partial fulfillment of the requirements for

degree Doctor of Philosophy

Yaakov Buchris

Submitted to the Senate of the Technion—Israel Institute of Technology

Marheshvan 5780 Haifa November 2019

Acknowledgment

This thesis was done under the supervision of Professor Israel Cohen in the Department of Electrical Engineering. Proffesor Jacob Benesty and Dr. Alon Amar were also involved in this research and contributed greatly to its advancement.

I would like to express my gratitude to my advisors, Professor Israel Cohen, Professor Jacob Benesty, and Dr. Alon Amar, who guided me from the early stages of my studies. Thanks for paving the way for me and taking a significant part in my journey of the PhD studies. I truly appreciate you for that. You gave me many important tools, which will serve me throughout my carrier.

I would like to thank the staff of the Signal and Image Processing Lab (SIPL), Prof. David Malach, Mr. Nimrod Peleg, Mr. Yair Moshe, and Dr. Avi Rozen, for their continuous support, their encouragement and friendship throughout the way.

Lastly, thank you Orit, my amazing wife for being my second half and for your nonstop support on this long term journey. You and our amazing kids, Tair, Eliya-Avidan, Ariel, Amichai, and Eitan, have a non-negligible part on the success of this work. You all make me who I am.

The generous financial support of the Technion, The Israeli Science Foundation (Grants no. 576/16) and the ISF-NSFC joint research program (grant No. 2514/17) is gratefully acknowledged.

List of papers

- Y. Buchris, I. Cohen, and J. Benesty, "First-order differential microphone arrays from a time-domain broadband perspective," in Proc. IEEE International Workshop on Acoustic Signal Enhancement (IWAENC 2016).

- Y. Buchris, I. Cohen, and J. Benesty, "Analysis and design of time-domain first-order circular differential microphone arrays," in Proc. the 22nd International Congress on Acoustics (ICA 2016).

- Y. Buchris, I. Cohen, and J. Benesty, "Asymmetric beampatterns with circular differential microphone arrays," in Proc. IEEE Workshop on Applications of Signal Processing to Audio and Acoustics (WASPAA 2017) (pp. 190-194).

- Y. Buchris, I. Cohen, and J. Benesty, "Asymmetric Supercardioid Beamforming Using Circular Microphone Arrays," in Proc. 26th European Signal Processing Conference (EUSIPCO 2018) (pp. 627-631).

- Y. Buchris, I. Cohen, and J. Benesty, "Frequency-domain design of asymmetric circular differential microphone arrays", IEEE/ACM Transactions on Audio, Speech, and Language Processing, vol. 26, no. 4, pp. 760–773, (2018).

- Y. Buchris, I. Cohen, and J. Benesty, "On the design of time-domain differential microphone arrays", Applied Acoustics, 148 (2019), pp. 212-222.

- Y. Buchris, A. Amar, I. Cohen, and J. Benesty, "Incoherent Synthesis of Sparse Arrays for Frequency-Invariant Beamforming," IEEE/ACM Transactions on Audio, Speech, and Language Processing, vol. 27, no. 3, pp. 482–495, (2019).

- Y. Buchris, I. Cohen, J. Benesty, and A. Amar, "Joint Sparse Concentric Array Design for Frequency and Rotationally Invariant Beampattern," submitted to IEEE/ACM Transactions on Audio, Speech, and Language Processing.

Contents

List of Figures

Abstract

This dissertation addresses advanced design approaches of sparse and robust differential microphone arrays (DMAs) which can be integrated into several acoustic systems like: data service audio devices, video conference rooms, autonomous underwater vehicles (AUVs), drones, and more. Acquiring acoustic data of high quality is a challenging task as the acoustic medium introduces some artifacts like noise and reverberations. In order to mitigate these artifacts, broadband adaptive beamforming techniques are widely used to enhance the signal-to-interference plus noise ratio. One of the promising concepts for broadband adaptive beamforming is the DMAs, which refer to arrays that combine closely spaced sensors to respond to the spatial derivatives of the acoustic field. These small-size arrays yield nearly frequency-invariant (FI) beampatterns and high directivity. In spite of their desired properties, DMAs suffer from noise amplification, especially at low frequencies. Thus, they are highly sensitive to model mismatch errors.

In this thesis, we propose advanced techniques for the design of DMAs, providing better performances in terms of array gain, directivity, computational efforts, and more. We present a time-domain design method of DMAs which is important in some applications where minimal delay is required, such as real-time audio communications. We analytically represent the array input signal vector in a separable form, which enables to apply several array processing algorithms, originally developed in the frequency domain, directly into broadband time-domain DMAs. We also show the convergence of the proposed time-domain model to the traditional model of DMAs.

We also extend the traditional symmetric model of DMAs and establish an analytical asymmetric model for circular DMAs, which allows flexible design of the directivity pattern since additional degrees of freedom are available in placing some directional constraints like directional nulls. Consequently, the proposed model yields better array gain and robustness. We demonstrate these benefits by deriving asymmetric versions for two well-known directivity patterns, namely the hypercardioid and supercardioid, designed to maximize the directivity factor and the front-to-back-ratio, respectively.

In the second part of our work, we focus on sparse designs of DMAs that optimize both the sensors' gains and their locations, resulting in better performance with a smaller number of sensors. Moreover, sparse designs may help to obtain FI beampatterns with higher accuracies and lower sidelobes levels. We develop an incoherent sparse design which first optimizes the array layout for each frequency bin in the bandwidth of interest. Then, all the decisions are fused together using some data mining tools yielding a joint sparse array layout used in the synthesis step. Simulations comparing our design to other previous sparse and uniform designs, show that the proposed design offers a good compromise between array gain and computational complexity. Finally, we generalize this concept and propose a greedy sparse design for more complicated array geometries like concentric arrays, which supports a flexible steering direction of the desired signal. The essential progress obtained along this research will make the integration of such arrays in acoustic systems more feasible, which is important for the future generations of such devices.

Notations

$\mathcal{B}\left[\mathbf{h}(\omega), \theta\right]$	The designed beampattern
$\mathcal{B}\left(\omega, \theta\right)$	The theoretical beampattern
$\mathcal{B}_N\left(\theta\right)$	Beampattern of an Nth order DMA
c	Speed of sound
$\mathbf{d}(\omega, \theta)$	A steering vector
$\mathbf{D}(\omega, \Theta)$	A steering matrix
$\mathcal{D}\left[\mathbf{h}(\omega)\right]$	The directivity index
$E\left[\cdot\right]$	Mathematical expectation
f	Frequency
f_{s}	Sampling frequency
$\mathcal{G}\left[\mathbf{h}(\omega)\right]$	Array gain in SNR
$\mathcal{G}_{\mathrm{wn}}\left[\mathbf{h}(\omega)\right]$	The white noise gain
$\mathcal{G}_{\mathrm{dn}}\left[\mathbf{h}(\omega)\right]$	The directivity factor
$H_m(\omega)$	The complex gain of the mth microphone
$\mathbf{h}(\omega)$	The beamformer coefficients vector
$\mathbf{I}_M$	The $M \times M$ identity matrix
$\mathrm{iSNR}(\omega)$	The input SNR
M	Number of sensors
N	Order of DMA
$\mathrm{oSNR}\left[\mathbf{h}(\omega)\right]$	The output SNR
t	The propagation time from the source to microphone 1
$V_m(\omega)$	The additive noise in the mth microphone

$\mathbf{v}(\omega)$	The additive noise vector
$X(\omega)$	An acoustic source signal
$X_m(\omega)$	The signal arrived to the mth microphone
$Y_m(\omega)$	The noisy signal in the output of the mth microphone
$\mathbf{y}(\omega)$	The beamformer input vector
$Z_{DAS}(\omega)$	The DAS beamformer output vector
$\Gamma_{\mathbf{v}}(\omega)$	The pseudo-coherence matrix of the noise vector
δ	Element spacing
θ	Azimuthal angle
θ_{s}	Steering direction
λ	Wavelength
τ_m	The delay of the signal in the mth microphone
$\phi_{X_1}(\omega)$	The variance of the zero mean signal $X_1(\omega)$
$\phi_X(\omega)$	The variance of the source signal
$\phi_{V_1}(\omega)$	The variance of the noise
$\Phi_{\mathbf{v}}(\omega)$	The correlation matrix of the noise vector
ω	Angular frequency
$(\cdot)^T$	Transpose operator
$(\cdot)^*$	Complex conjugation
$(\cdot)^H$	Conjugate transpose operator

Abbreviations

CDMA	Circular Differential Microphone Array
CSS	Coherent Signal Subspace
DAS	Delay and Sum
DF	Firectivity Facotr
DI	Firectivity Index
DMA	Differential Microphone Array
FBR	Front to Back Ratio
FI	Frequency Invariant
MMSE	Minimum Mean Square Error
OMP	Orthogonal Matching Pursuits
PCA	Principal Component Analysis
SLL	Sidelobes Level
SNR	Signal to Noise Ratio
STFT	Short-Time Fourier Transform
WNG	White Noise Gain

Chapter 1

Introduction

1.1 Background and motivation

One of the essential parts of many real-world systems is the acquisition and processing of acoustic sound signals, widely used in traditional telephones, smart phones, video conference rooms, modern speech service devices and more. As these signals are propagating in harsh acoustic environments that include additive uncorrelated noise, interferences, reverberations, and more, they are received with some distortions and artifacts, which should be removed in order to preserve the original signals and get intelligible versions of them. In order to obtain this goal, microphone arrays are employed [1, 3, 4].

Microphone arrays consist of a number of acoustic sensors, which are organized together in a certain geometry and sample the sound field with spatial diversity. Through processing the array outputs, various functionalities can be implemented including but not limited to: localizing and tracking the sound sources, extracting the signal of interest, suppressing ambient noise, interfering signals, and reverbrations, and separating different sound sources, as presented in Fig. 1.1.

Among several classes of algorithms operating on arrays, beamforming is a general name for a class of several algorithms used to spatially filter the desired signal from undesired noise, echoes and interfering signals [5]. These algorithms

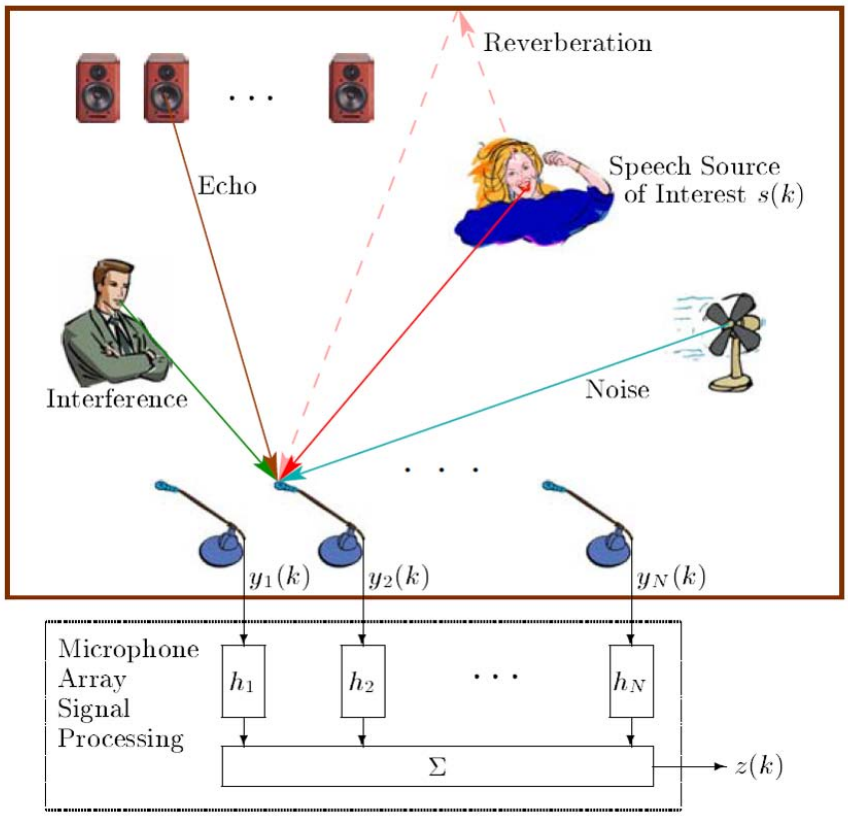

Figure 1.1: An illustration of several typical problems in a room which can be mitigated by microphone arrays [1].

can be designed according to different quality criteria like signal-to-noise ratio (SNR) improvement subject to a specific noise field, adaptivity, and more. These algorithms operate on an array of sensors, each receive a delayed version of a desired signal plus noise and interfering signals,

The basic structure of a beamformer consists of a vector of complex gains, each multiplied by one of the inputs of the array. Then, all the outputs are summed together yielding the beamformer output signal which is typically an enhanced version of the original signal of interest, i.e., a cleaner signal with a reduced level of noise, echoes, and interfering signals arriving from different directions. The

performance measures used to evaluate beamformers are the directivity pattern and the array gain [2]. The directivity pattern is the normalized output power vs. direction, where the output power in the steering direction is normalized to one. The array gain defined as the ratio between the signal to noise ratio (SNR) at the output of the beamformer and the input of the beamformer in the presence of assumed noise field. Usually, two main noise fields are considered: the uncorrelated noise field and the diffuse noise field. The first one is a good indication to the robustness of the beamformer to mismatch and array model errors while the second is called also the directivity factor of the array, indicating to what extent the array is directional.

The above basic structure is a narrowband one, meaning that the beamformer complex gain vector is matched to a specific frequency. As an example, the conventional delay and sum (DS) beamformer [5] whose gains are simple complex exponents which are intended to compensate for the phases of the desired signal arrived at different times for each sensor. These delays depend on frequency and also the directivity pattern. Specifically, its spatial resolution which is dictated by the width of the mainbeam is inversely proportional to the frequency.

In some systems the signals are considered to be broadband. For example, speech and audio signals are broadband since the ratio between their bandwidth and the central frequency is much high (more than a few percents). Sonar and underwater acoustic communication signals are also broadband in nature as their available bandwidth is highly depends on the range between the emitter and the receive array. This fact means that some dispersion effects may occur to such signals in systems consisting the chain of transmission-channel-reception, and processing steps. In particular, using a beamformer in the receiver side, the transmitter side, or in both sides, may introduce several artifacts to the signals due to the beamforming operation. Note that even though beamforming can be implemented it both the receiver side or the transmitter side for application of communication, in our work we may focus on the receiver side.

In the literature, there are several approaches to design of broadband beam-

formers. The simplest approach implements a narroawband beamformer for each frequency bin in the bandwidth of interest. This can be implemented either in the frequency or the time domain. Such approach suffers from the problem that the directivity pattern is frequency varying. Specifically, the mainbeam becomes narrower as the frequency increases. Consequently, each frequency bin of the output signal is processed by a different beamformer leading to a distorted version of the desired signal.

In order to mitigate the distortions caused by the beamformer, several approaches implementing frequency-invariant (FI) beamformers are presented in the literature. These beamformers are designed to yield a FI directivity pattern across all the bandwidth of interest, thus, the output signal is not distorted since each of its frequency components sees the same beamformer.

Some work has been done to obtain FI beampatterns [3, 6–16] by introducing either more hardware and computational complexity, or by allowing model mismatch errors augmentation. One simple sparse structure of FI beamforming is based on the concept of harmonic nested arrays [17, 18] where the total array is composed from several uniform subarrays, each matched to a different frequency subband. Yet, the locations of the sensors are set only according to the spatial sampling constraint in the relevant subband, and are not optimized according to some design constraints like robustness to mismatch errors. Another concept is based on the coherent signal subspace (CSS) [19] where in each frequency bin in the bandwidth of interest, a linear transformation is designed to transform the frequency varying steering matrix into a steering matrix matched to a fix frequency. The output signal has nearly FI steering matrix, thus, a single set of beamformer coefficients is required in order to get a FI directivity pattern.

A different concept is based on differential microphone arrays (DMAs) which refer to arrays that combine closely spaced sensors to respond to the spatial derivatives of the acoustic pressure field. These small-size arrays yield nearly FI beampatterns, and include the well-known superdirective beamformer [6, 20] as a particular case. DMAs are characterized by their order such that the output of an

Nth-order DMA is proportional to up to the Nth derivative of the acoustic pressure field. Practically, Nth-order DMAs may afford up to $N-1$ nulls in their directivity patterns.

DMAs first appeared in the literature in the 1930's, designed to respond to the spatial derivatives of an acoustic pressure field [21], and later were implemented using omnidirectional pressure microphones [22]. These early fixed implementations had a prominent limitation that once they were designed and produced, their properties cannot be changed. The modern concept of DMAs employs pressure microphones, and digital signal processing techniques are used to obtain desired directional responses [23–27]. Based on the modern concept, several works on DMAs appeared during the last two decades. Buck [28], and Derkx and Janse [29] analyzed the performance of the first-order design under array imperfections, and presented solutions for sensors calibration. First- and second-order adaptive DMAs based on fullband as well as on subband algorithms were introduced and examined by Teutsch and Elko [30]. De Sena et al. [31] proposed a general approach to the design of directivity patterns for DMAs of higher-orders. In [2] a more general approach is proposed for the design of DMAs, which ignores the traditional differential structure of DMAs and develops broadband frequency-domain DMAs up to any order from a signal processing perspective. Robust frequency-domain DMAs have been presented by Zhao et al. [32], and Pan et al. [33]. More recent work on DMAs can be found in [34–37].

In spite of their benefits, traditional DMAs suffer from noise amplification, especially at low frequencies, meaning that the array gain of DMAs in the presence of uncorrelated white noise is poor. It is acceptable to relate between the white noise gain (WNG) of an array and the robustness to model mismatch errors and array imperfections. Therefore, the practical consequence of the above drawback is that the traditional DMAs are non robust and their performance may deteriorate in the presence of uncorrelated noise or model errors. This problem is even worsen for lower frequencies and for higher orders of DMAs since the solutions for the DMAs gain vectors depend on the steering matrix of the array which becomes

more and more ill-conditioned as the frequency decreases or the order increases.

In all former works considering DMAs design, it was assumed that the sensors are located either uniformly or nonuniformly in a given aperture which can be linear, planar, or arbitrary. Yet, optimizing the number of sensors and/or their locations was not considered, and only the beamformer coefficients were optimized according to certain design constraints. In sparse arrays, also termed as aperiodic, random, thinned or space tapered arrays, the nonuniform design of the sensors' locations enables to obtain arrays where part of their adjacent sensors have spacing larger than half the wavelength. Yet, the harmful effects of the grating lobes can be completely mitigated. Thus, arrays with a greater aperture and better robustness to array imperfections, but with a smaller number of sensors than in the uniform design, can be designed using the sparse approach. In the context of FI beamformers, sparsity may lead to more flexibility and better design in terms of satisfying constraints on a wider range of frequencies.

While for the narrowband design many advanced techniques have been presented for the synthesis of sparse arrays [40–51], much less work has been done for the sparse design of FI broadband beamformers. One simple sparse structure of FI beamforming is based on the concept of harmonic nested arrays [17, 18]. Analytical approaches for optimization of the sensors positions in order to obtain FI beampattern can be found in [9, 10]. However, in these approaches no consideration regarding issues like robustness to noise has been done. Crocco and Trucco [7] proposed a FI sparse design by joint-optimization of the sensors positions and the beamformer coefficients, using simulated annealing optimization, while assuming a given a-priori number of sensors on the sparse array. In [52], a genetic algorithm combined with a gradient-based method was applied to find a global minimum for the optimization of the cost function. A design of FI beampattern for linear arrays based on the generalized matrix pencil method can be found in [53].

Recently, both Hawes and Liu [54], and Liu et al. [55] proposed sparse designs for broadband beamformers based on an iterative weighted ℓ_1-norm mini-

mization under multiple convex constraints. One of the imposed constraints is a joint-sparsity constraint [56] which ensures that the chosen sensors are joint for all frequency bins in the relevant bandwidth. In other words, the same sensors are used to build the beamformers coefficient vectors for all the frequency bins in the bandwidth of interest. As the optimization of sensors positions and beamformer coefficients is performed simultaneously for all the frequency bins in the relevant bandwidth, we may refer to this design approach as a coherent sparse design. While good results were reported, this method is limited when the number of candidate sensors is an order of magnitude of hundreds or more.

1.2 Main Contributions

In light of the above stated drawbacks this research is focused in several practical design aspects of DMAs and superdirective beamformers. There are four main contributions to this research:

- A new formulation in the time domain for DMAs design, which may be useful in cases where minimal delay is required, and consumes less computational resources when short filters are sufficient.

- Derivation of a general asymmetric model for circular DMAs which provides more flexible designs with higher array gains, compared to symmetric circular DMAs.

- An incoherent sparse design for DMAs which obtains superior performance in terms of array gains, robustness, and frequency-invariant beampattern, with a reduced number of sensors. Moreover, as it optimizes each frequency bin in the bandwidth of interest separately, this approach is feasible for practical applications where the array layout may contain higher number of sensors.

- A greedy based sparse design of DMAs for other geometries like concentric

arrays, where the beampattern can be steered azimuthally to any direction, since the signal of interest is not confined to arrive from a certain direction.

In the remainder of this chapter, we describe these issues and indicate the scientific gaps that motivated our work.

1.3 Overview of the Thesis

In Chapter 3, we introduce a time-domain implementation of DMAs, which is of a great importance for applications requiring small delays such as real-time audio communications [38]. We present a framework for a broadband time-domain equivalent design of Nth-order DMAs. We develop broadband frequency-domain DMAs up to any order from a signal processing perspective. It includes the formulation of equivalent time-domain expressions for the array incoming signal, the covariance matrices of the noise and signal, and some other useful performance measures like time-domain beampattern, WNG, and directivity factor (DF). We also derive the WNG for the case that there are some model mismatch errors. The array input signal is manipulated to represent it in a separable form, meaning that the input signal is a product of a desired-signal-dependent term and a second term which depends only on the array geometry. This representation enables to apply several array processing algorithms, which were originally developed in the frequency domain, directly into broadband time-domain DMAs. We derive a closed-form solution for time-domain Nth-order DMAs for any given number of sensors. We show that under the DMA's assumption, the derived time-domain beampattern complies with the theoretical beampattern of traditional DMA designs [24]. Finally in the experimental results, we evaluate the performance of the time-domain DMAs in comparison with that of the frequency-domain implementation and demonstrate some of its fundamental properties.

Chapter 4 introduces an innovative theoretical model for asymmetric DMAs. Most of the previous works on DMAs, both for linear or circular geometry, consider only the case of symmetric beampatterns, which is an inherent property of

the linear geometry and confines the design process by some aspects. For linear arrays, a symmetric beampattern means that the beampattern is symmetric with respect to the axis of the array. Such a symmetry is not required in different array geometries like the circular geometry, thus, removing this requirement may lead to a substantial performance improvement. We term such beampatterns as asymmetric beampatterns.

We address the above limitation by deriving an analytical model for asymmetric Circular Differential Microphone Arrays (CDMAs) which includes also the traditional symmetric model as a particular case. We begin with an extension of the well-known analytical expression for the directivity pattern of the traditional DMAs, to a generalized expression which supports also the asymmetric case. Next, we derive asymmetric versions for two popular directivity patterns usually applied in the context of microphone arrays, namely the hypercardioid and the supercardioid which are designed to maximize the DF and the Front to Back Ratio (FBR), respectively [24]. Originally, both directivity patterns were developed for the symmetric framework as unconstrained versions, i.e., no directional constraints were imposed except the distortionless constraint in the desired source direction. We derive constrained versions where additional directional attenuation constraints are imposed. For that case, the asymmetric design achieves better performance with respect to the traditional one, since it enables more flexible design. As expected, the solutions for the asymmetric design are reduced to the solutions presented in [24] where no additional directional attenuation constraints are imposed.

Simulations show that the asymmetric model achieves better performance in terms of WNG, DF, and FBR due to a more flexible design, which takes into account the requirements regarding the null directions. Furthermore, additional degrees of freedom are available for a given number of null directions which can be utilized to choose CDMAs of reduced orders with respect to the minimal order in the symmetric model, and improve robustness to array imperfections.

In Chapter 5, we propose a new incoherent sparse array design FI beamformer,

based on a convex optimization. Assuming an initial grid of candidate sensors, it first solves an ℓ_1-constrained optimization problem separately for each frequency bin in the bandwidth of interest, and get a sparse vector of sensor positions complying some desired constraints. One of them is the joint sparse constraint which ensures that the chosen sensors are joint for all frequency bins in the bandwidth of interest, thus, some hardware and computational resources are saved. All these sparse vectors are fused together using data mining tools, yielding a single set of sensors which are jointly sparse, used to synthesize the desired FI beampattern in the final step.

Simulations illustrate the benefits of the proposed incoherent sparse design with respect to the coherent one and also to the uniform array design. The incoherent design is a compromise between robustness and frequency-invariant beampattern and can be implemented in a reasonable computational complexity with respect to the coherent one.

The incoherent sparse design obtains superior performance in terms of directivity and WNG but suffers from the strong limitation that it has a fixed steering direction. Therefore, in Chapter 6 we extend our recent work on a joint-sparse design of frequency-invariant (FI) beamforming [57], and propose a new greedy orthogonal matching pursuits (OMP) [58,59] based joint-sparse design for FI concentric arrays, which optimizes both the number of sensors and the number of rings while taking into consideration the requirement regarding the rotationally-invariant property. Therefore, the obtained sparse array layout may allow to get a similar array response for different azimuthal directions of steering. Moreover, it also supports the case that one is interested on a similar array response only for an azimuthal range or for a discrete number of azimuthal directions. The proposed approach is more general with respect to [57] as it allows more than a one fixed steering direction.

Simulation results compare between the proposed greedy sparse design, a uniform array design and a random array design. It is shown that the greedy sparse design yields an FI rotationally-invariant beamformer with high robustness to ar-

ray imperfections and high directivity. In contrast, the uniform designs suffer from high sidelobe level (SLL) and sensitivity to noise, while the random design provides unstable and fluctuated results. In addition, the sparse design requires reasonable resource consumption leading to a practical design for applications involving large arrays with hundreds of candidate sensors.

1.4 Organization

This thesis is organized as follows. Chapter 2 briefly outlines the basic theories and methods which were used during this research. The original contribution of this research starts in Chapter 3, where a time-domain implementation of DMAs is introduced. Chapter 4 introduces an innovative theoretical model for asymmetric DMAs. In Chapter 5, we propose a new incoherent joint-sparse array design for FI beamformer, and in Chapter 6 we extend it and propose a new greedy based joint-sparse design for FI concentric arrays. Chapter 7 concludes and summarizes the main contributions of this dissertation and presents some future research directions.

Chapter 2

Scientific Background

In this chapter, we briefly review research methods which were useful during this research. We start by introducing several definitions regarding broadband beamformers. Then we focus on DMAs and superdirective beamformers and present some motivation to sparse designs of arrays. For the sake of simplicity, we focus on a linear array geometry, yet, all the presented definitions can be extended to more geometries as presented in next chapters of this thesis.

2.1 General principles of microphone arrays

We consider an acoustic source signal (plane wave), $X(\omega)$, with ω being the angular frequency, that propagates in an anechoic acoustic environment at the speed of sound, i.e., $c \approx 340\ \mathrm{m/s}$, and impinges on a linear array consisting of M omnidirectional microphones, where the distance between two successive sensors is equal to δ. The direction of the source signal to the array is denoted by the azimuth angle θ, as illustrated in Fig 2.1. In the frequency domain, the signal model is given by

$$\begin{aligned} Y_m(\omega) &= X_m(\omega) + V_m(\omega) \\ &= X(\omega)e^{-\jmath\omega(t+\tau_m)} + V_m(\omega), \quad m = 1, 2, ..., M, \end{aligned} \tag{2.1}$$

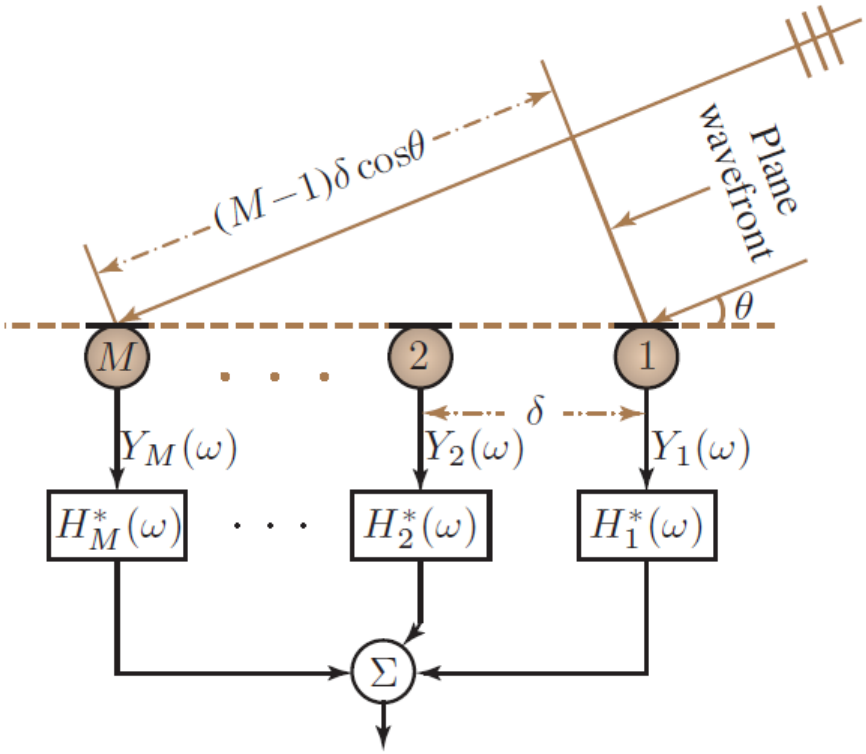

Figure 2.1: A uniform linear microphone array with processing units [2].

where t is the propagation time from the source $X(\omega)$ to microphone 1 (reference point), and $\jmath = \sqrt{-1}$. With a uniform linear array and a farfield source, the delays τ_m can be expressed as

$$\tau_m = \frac{(m-1)\delta\cos\theta}{c} \quad m = 1, 2, ..., M. \tag{2.2}$$

Collecting all the outputs into vector $\mathbf{y}(\omega)$, we get the following structure

$$\mathbf{y}(\omega) = [Y_1(\omega), Y_2(\omega), ..., Y_M(\omega)]^T = X(\omega)\mathbf{d}(\omega, \theta), \tag{2.3}$$

where

$$\mathbf{d}\left(\omega,\theta\right)=\left[e^{-\jmath\omega(t+\tau_1(\theta))},e^{-\jmath\omega(t+\tau_2(\theta))}\cdots e^{-\jmath\omega(t+\tau_M(\theta))}\right]^T \tag{2.4}$$

is the steering vector which contains the spatial information of the array, and the superscript ^{T} is the transpose operator.

The beamformer output is calculated by multiplying the complex weights, $H_m^*(\omega), m=1,2,...,M$, at the output of each microphone, $Y_m(\omega), m=1,2,...,M$, respectively, where the superscript * denotes complex conjugation. The weighted outputs are then summed together to form the beamformer output

$$\begin{aligned} Z(\omega) &= \sum_{m=1}^{M} H_m^*(\omega)Y_m(\omega) \\ &= \mathbf{h}^H(\omega)\mathbf{y}(\omega) \\ &= \mathbf{h}^H(\omega)\mathbf{d}(\omega,\theta)X(\omega)+\mathbf{h}^H(\omega)\mathbf{v}(\omega), \end{aligned} \tag{2.5}$$

where

$$\mathbf{h}(\omega)=\left[H_1(\omega),H_2(\omega),...,H_M(\omega)\right]^T \tag{2.6}$$

is the beamformer coefficients vector of length M, and the superscript ^{H} is the conjugate transpose operator. The vector $\mathbf{v}(\omega)$ is defined similarly to the vector $\mathbf{h}(\omega)$. In the next two subsections we discuss about some performance measures taken into consideration when designing beamformers.

2.2 Beampattern

Each beamformer has a pattern of directional sensitivity, i.e., it has different sensitivities for signals arriving from different directions. The beampattern or directivity pattern describes the sensitivity of the beamformer to a plane wave (source signal) impinging on the array from the direction θ. Mathematically, it is defined

as

$$\mathcal{B}\left[\mathbf{h}(\omega),\theta\right] = \mathbf{h}^{H}(\omega)\mathbf{d}(\omega,\theta). \tag{2.7}$$

Figure 2.2 presents a basic structure of a directivity pattern. It composed from a steerable main-lobe region which transfers the desired signal, and a side-lobes region. Denoting by $BW_{3\mathrm{dB}}$ the angular width where the mainbeam decreases below $3\mathrm{dB}$ with respect to its maximal value. This quantity is important as it related to the spatial resolution of the beamformer. It is also desired to reduce the side-lobes power so that undesired interfering signals and noise will be attenuated at the output of the beamformer. Specifically, in some beamforming algorithms it is possible to reject directional interferences by imposing nulls in certain directions.

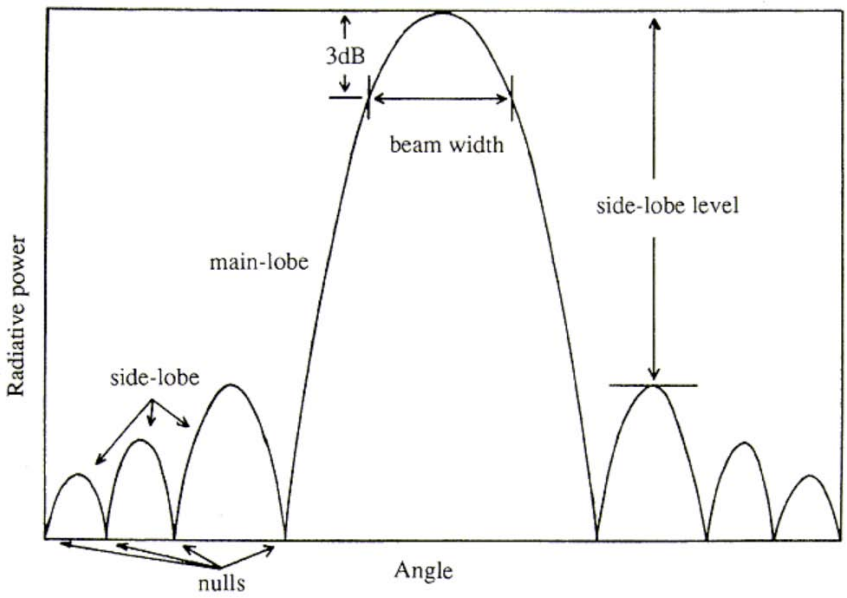

Figure 2.2: A basic structure of a directivity pattern.

2.3 Array gain

In order to evaluate the performance of a beamformer it is common to consider its array gain which is defined as the ratio between the SNR at the beamformer output and the SNR at the input to the beamformer, subject to a certain noise field. The input SNR is defined as the SNR at the first (reference) microphone, i.e.,

$$\mathrm{iSNR}(\omega) = \frac{\phi_{X_1}(\omega)}{\phi_{V_1}(\omega)} = \frac{\phi_X(\omega)}{\phi_{V_1}(\omega)}, \tag{2.8}$$

where $\phi_{X_1}(\omega) = E\left[|X_1(\omega)|^2\right]$, $\phi_{V_1}(\omega) = E\left[|V_1(\omega)|^2\right]$, and $\phi_X(\omega) = E\left[|X(\omega)|^2\right]$, with $E\left[\cdot\right]$ denoting mathematical expectation.

The output SNR is defined as

$$\begin{aligned}\mathrm{oSNR}\left[\mathbf{h}(\omega)\right] &= \phi_X(\omega)\frac{|\mathbf{h}^H(\omega)\mathbf{d}(\omega,\theta)|^2}{\mathbf{h}^H(\omega)\Phi_{\mathbf{v}}(\omega)\mathbf{h}(\omega)} \\ &= \frac{\phi_X(\omega)}{\phi_{V_1}(\omega)}\frac{|\mathbf{h}^H(\omega)\mathbf{d}(\omega,\theta)|^2}{\mathbf{h}^H(\omega)\Gamma_{\mathbf{v}}(\omega)\mathbf{h}(\omega)},\end{aligned} \tag{2.9}$$

where

$$\Phi_{\mathbf{v}}(\omega) = E\left[\mathbf{v}(\omega)\mathbf{v}^H(\omega)\right], \tag{2.10}$$

and

$$\Gamma_{\mathbf{v}}(\omega) = \frac{\Phi_{\mathbf{v}}(\omega)}{\phi_{V_1}(\omega)} \tag{2.11}$$

are the correlation and pseudo-coherence matrices of $\mathbf{v}(\omega)$, respectively. The definition of the array gain in SNR is easily derived from the two previous definitions, i.e.,

$$\mathcal{G}\left[\mathbf{h}(\omega)\right] = \frac{\mathrm{oSNR}\left[\mathbf{h}(\omega)\right]}{\mathrm{iSNR}(\omega)} = \frac{|\mathbf{h}^H(\omega)\mathbf{d}(\omega,\theta)|^2}{\mathbf{h}^H(\omega)\Gamma_{\mathbf{v}}(\omega)\mathbf{h}(\omega)}. \tag{2.12}$$

Usually, two types of noise field are of high interest :

- The temporally and spatially white noise with the same variance at all microphones. In this case, $\Gamma_{\mathbf{v}}(\omega) = \mathbf{I}_M$, where $\mathbf{I}_M$ is the $M \times M$ identity matrix. Therefore, the WNG is

$$\mathcal{G}_{\text{wn}}\left[\mathbf{h}(\omega)\right] = \frac{|\mathbf{h}^H(\omega)\mathbf{d}(\omega,\theta)|^2}{\mathbf{h}^H(\omega)\mathbf{h}(\omega)} = \frac{1}{\mathbf{h}^H(\omega)\mathbf{h}(\omega)}, \tag{2.13}$$

  where the last transition is due to the distortionless assumption, i.e., the beamformer coefficient vector is designed to yield an undistorted unity gain in the desired signal direction.

- The diffuse noise where

$$\left[\Gamma_{\mathbf{v}}(\omega)\right]_{i,j} = \left[\Gamma_{\text{dn}}(\omega)\right]_{i,j} = \frac{\sin(\omega(j-i)\tau_0)}{\omega(j-i)\tau_0} = \text{sinc}(\omega(j-i)\tau_0), \tag{2.14}$$

  where $\tau_0 = \delta/c$. In this scenario, the gain in SNR, $\mathcal{G}_{\text{dn}}\left[\mathbf{h}(\omega)\right]$, is called the directivity factor and the directivity index is simply defined as

$$\mathcal{D}\left[\mathbf{h}(\omega)\right] = 10\log_{10}\mathcal{G}_{\text{dn}}\left[\mathbf{h}(\omega)\right]. \tag{2.15}$$

  With diffuse noise, the filter $\mathbf{h}(\omega)$ is often found by maximizing the directivity factor.

2.4 A Narrowband beamformer

Note that the above formulation (2.5) is termed as a filter and sum implementation, which is the general form to the simple narrowband model of a beamformer. In its basic structure, beamformer is a narrowband in a sense that its response depends on frequency. Therefore, when the system is broadband, i.e., the signals to be processed by the beamformer contain multiple frequency components, one should consider a broadband structure of beamforming. Simple implementations

of broadband beaformers can be found either in the frequency domain or equivalently, in the time domain [3], as presented in Fig. 2.3 and Fig. 2.4, respectively.

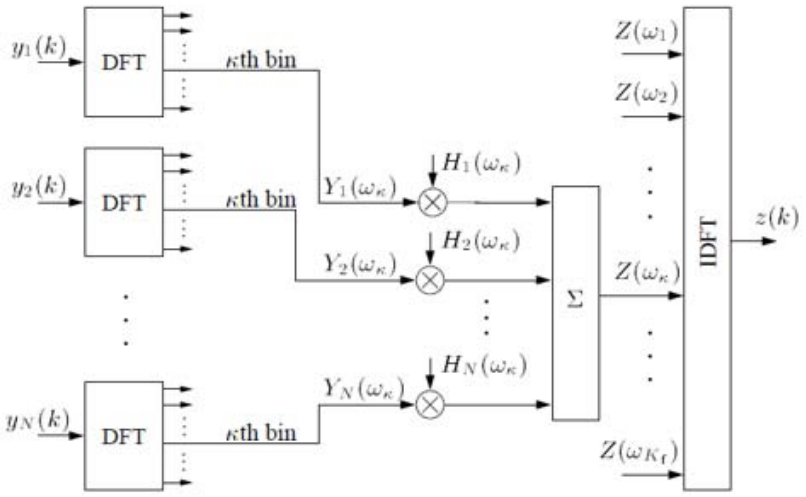

Figure 2.3: A basic structure of broadband beamformer in the frequency domain [3].

Although their simplicity, the above braodband structures suffer from an inherent drawback as they introduce some artifacts to the beamformer output signal. In order to exemplify it, we may focus on one of the commonly used private cases for the above structure - the so-called DAS beamformer. The basic principle of this approach is that it compensates $Y_m(\omega)$ with a delay τ_m to align all the M microphone signals, by multipling $Y_m(\omega)$ with $H_m(\omega) = e^{\jmath\omega\tau_m}$, and then averages all the results together. The DAS beamformer output is then

$$Z_{DAS}(\omega) = \frac{1}{M}\sum_{m=1}^{M} Y_m(\omega)e^{\jmath\omega\tau_m} = X(\omega)e^{-\jmath\omega t} + \frac{1}{M}\sum_{m=1}^{M} V_m(\omega)e^{\jmath\omega\tau_m}. \quad (2.16)$$

For that case it can be shown that the beampattern of this beamformer is given

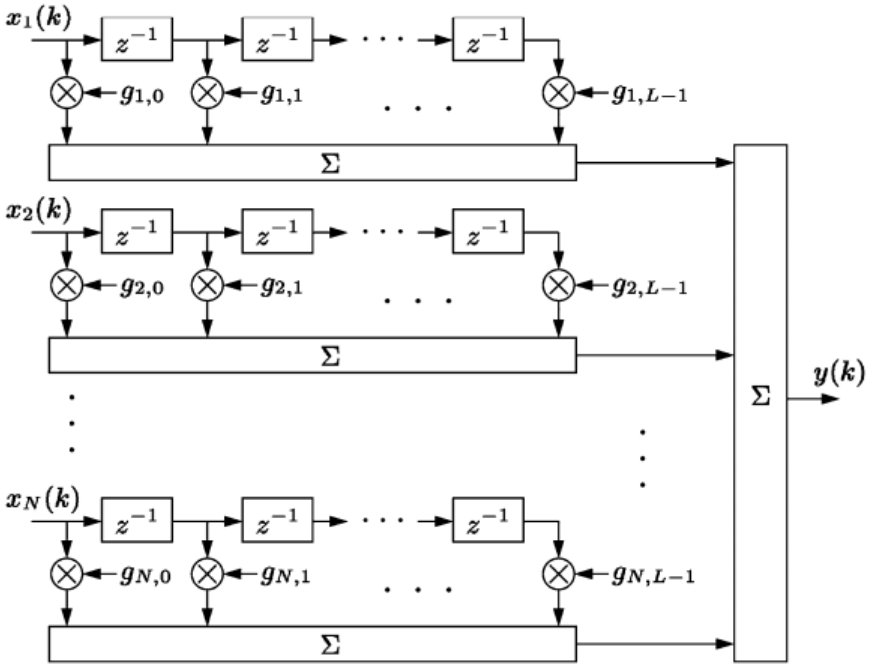

Figure 2.4: A basic structure of broadband beamformer in the time domain [3].

by [2]

$$\mathcal{B}(\omega,\theta)=\left|\frac{\sin\left[M\omega\delta(\cos\theta-\cos\theta_{\mathrm{s}})/(2c)\right]}{M\sin\left[\omega\delta(\cos\theta-\cos\theta_{\mathrm{s}})/(2c)\right]}\right|, \tag{2.17}$$

where θ_{s} is the steering direction. It can be shown that $BW_{3dB}\propto\cos^{-1}(c/M\delta f)$, meaning that the beamwidth becomes narrower as the frequency increases as can be seen from Fig. 2.5 which demonstrates the beampattern (2.17) for different frequencies, for a simple example of DAS beamformer with a linear array of $M=10$ microphones and $\delta=0.08$ [m]. One can see that for signals arriving from directions which are different from the steering direction θ_{s}, one may get some artifacts due to different gains in different frequencies.

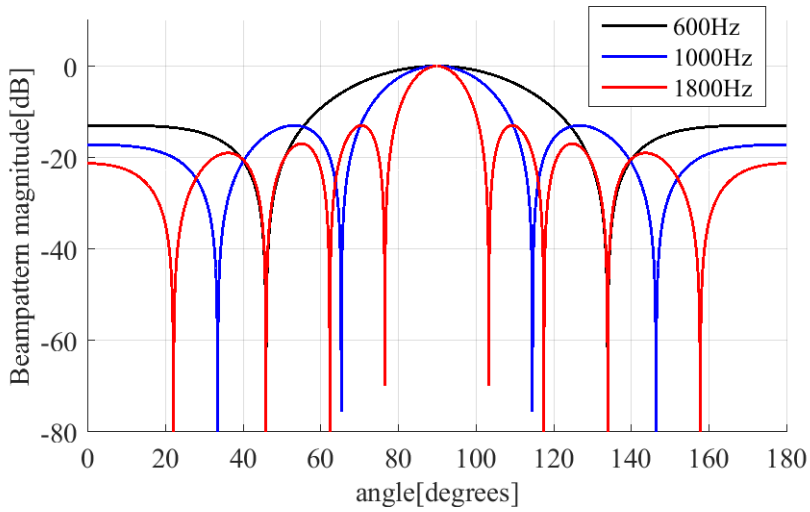

Figure 2.5: The beampattern (2.17) for different frequencies, for a simple example of DAS beamformer with a linear array of $M = 10$ microphones and $\delta = 0.08$ [m].

2.5 Differential Microphone Arrays

In order to cope with this problem, several design approaches implementing FI beamformers were presented in the literature (a detailed overview can be found in the previous chapter). Among them the concept of DMAs can provide FI superdirective small size arrays which can be applied to broadband beamforming. They are responsive to the spatial derivatives of the acoustic pressure field. When implementing linear DMAs, two model assumptions are exist. The first one is that the desired signal arrives from the endfire, i.e., from $\theta_{\mathrm{s}} = 0°$. The second is that the element spacing is much smaller than the wavelength, i.e.,

$$\delta \ll \lambda. \tag{2.18}$$

Under the above assumptions, it can be shown that the FI beampattern of an Nth-order DMA is given by

$$\mathcal{B}_N(\theta) = \sum_{n=0}^{N} a_{N,n} \cos^n \theta. \tag{2.19}$$

While the original implementations were fixed hardware implementations, modern implementations of DMAs consist of a number of pressure microphones arranged into a particular geometry and digital signal processing techniques are then used to process the microphones' outputs to obtain the desired directional response. Figure 2.6 illustrates how first-, second-, and third-order DMAs are constructed with a linear geometry. A new and a more general implementation of

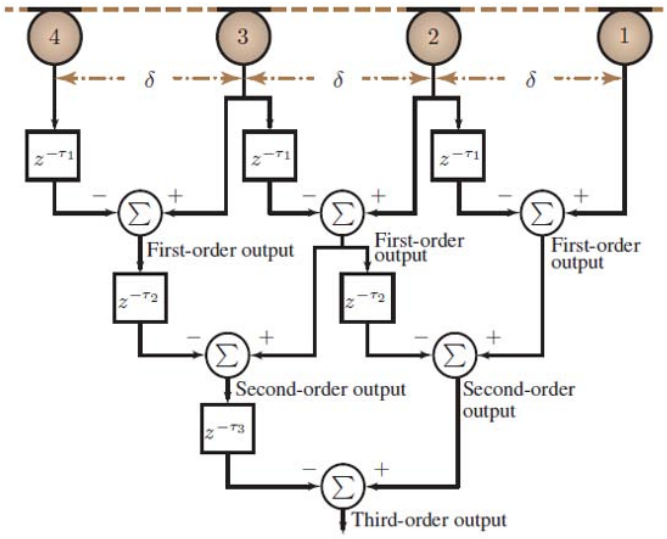

Figure 2.6: A schematic diagram of construction of first-, second-, and third-order DMAs [2].

DMAs is presented in Fig 2.7 [2]. This frequency-domain implementation can be applied to design several FI directivity patterns with similar properties like in the traditional implementations of DMAs. Although it has no differential structure, one can get similar FI beampatterns like in the classic DMAs implementations.

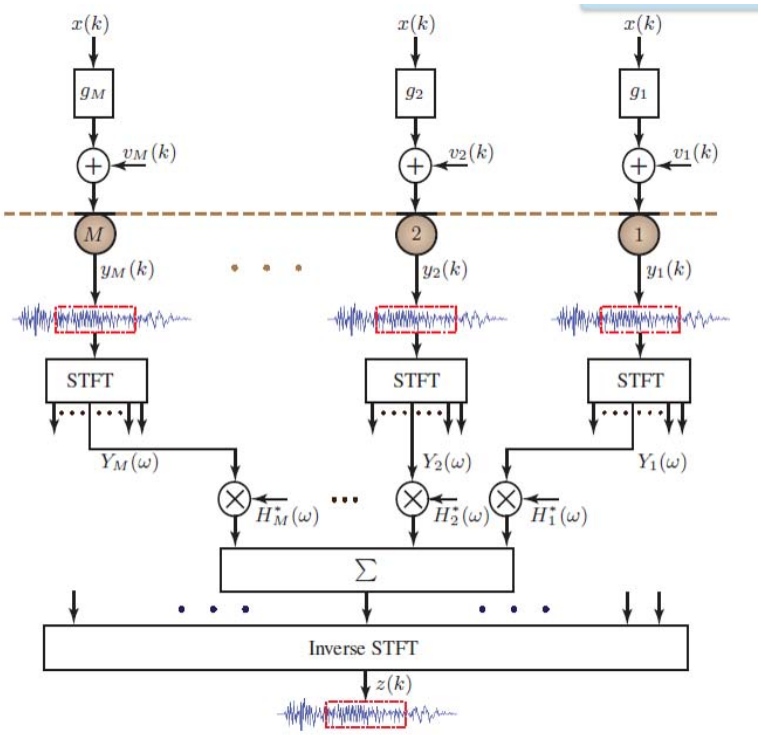

Figure 2.7: General block diagram of a DMA system implemented in the frequency domain [2].

Besides their small size, DMAs have the following number of advantages in comparison with a standard arrays. They can form FI beampatten and, therefore, there are more suitable to process broadband speech signals. For a given number of sensors, DMAs have the potential to attain maximum directional gain. In order to get some insight regarding the last attribute, Fig. 2.8 shows typical beampatterns of DAS beamformers while Fig. 2.9 presents a beampattern of a superdirective beamformer like DMAs. It can be shown that for the standard DAS beamformers there is an ambiguity in the direction of the incoming desired signal meaning that some extra noise and undesired interfering signals may enter into the beamformer. In contrast, the superdirective beamformer does not suffer from such ambiguity leading to a better directivity.

In spite of all the aforementioned benefits of DMAs, they have the following

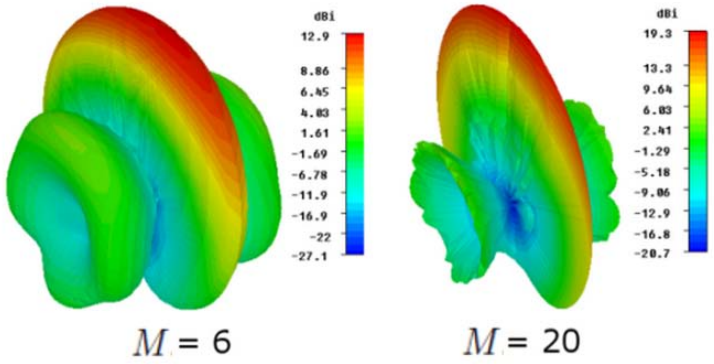

Figure 2.8: Beamptterns of DAS beamformers.

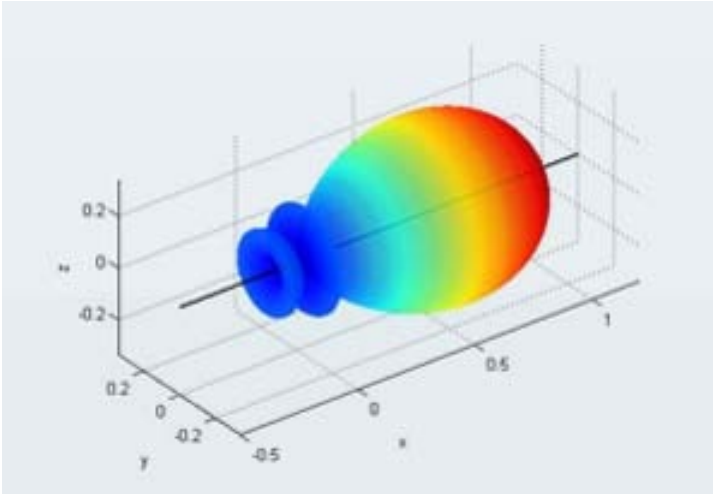

Figure 2.9: Beampattern of DMAs and superdirective beamformers.

drawbacks. First, for a linear geometry, the desired signal direction is confined to arrive from the endfire direction, while for arriving from different directions, it decreased dramatically. Second, DMAs suffer greatly from white noise amplification, particularly at low frequencies. The practical meaning of the last drawback is that DMAs are highly sensitive to model mismatch errors and array imperfections. Figure 2.10 shows the WNG of a second-order hypercardioid versus frequency for different values of the element spacing δ. One can see the WNG problem becomes

even worsen at lower frequencies. The WNG is improved as the element spacing δ is increased. Figure 2.11 shows the directivity index (DI) of a second-order hypercardioid versus frequency for different values of the element spacing δ. In that case, the DI becomes less FI as the element spacing increased. We can conclude that the element spacing δ has an essential role in the design of DMAs and it is responsible for the trade-off between FI directivity and robustness to array imperfections.

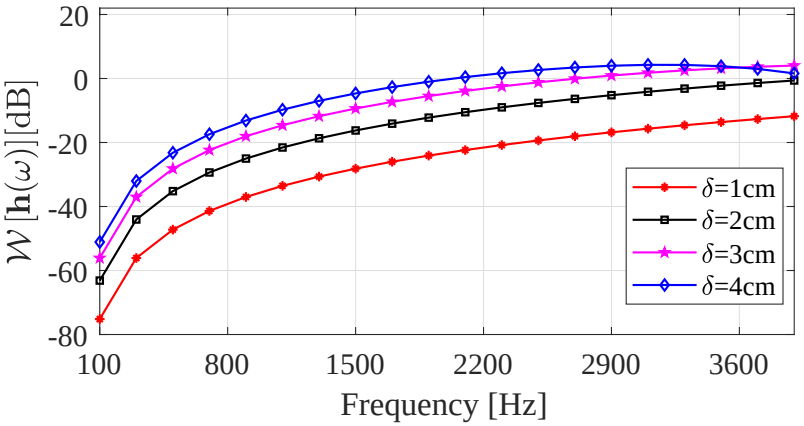

Figure 2.10: WNG vs. frequency for different values of the element spacing δ.

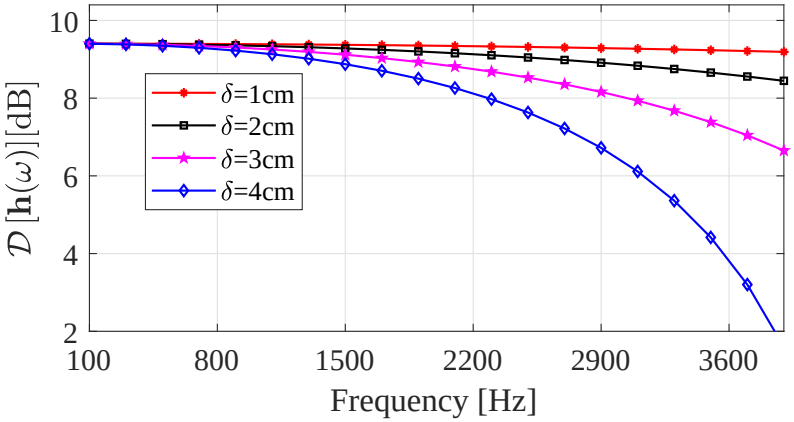

Figure 2.11: DI vs. frequency for different values of the element spacing δ.

2.6 Sparse Designs of Microphone Arrays

As discussed in the previous chapter, there are some benefits to sparse design of arrays, where both the number of sensors, their locations and their gains are optimized, over the standard uniform array design. In particular, broadband sparse design is even more worthwhile since it enables to get several desired properties for a wide range of frequencies, such as FI directivity pattern. In the following, we provide some insight about the last point.

Lets consider the following trade-off regarding the ratio between the wavelength of the signal and the element spacing, δ, of the array. It is well-known that temporal aliasing occurs when the sampling frequency, f_{s}, is smaller than twice the maximal frequency of the signal, as demonstrated in Fig. 2.12. Anal-

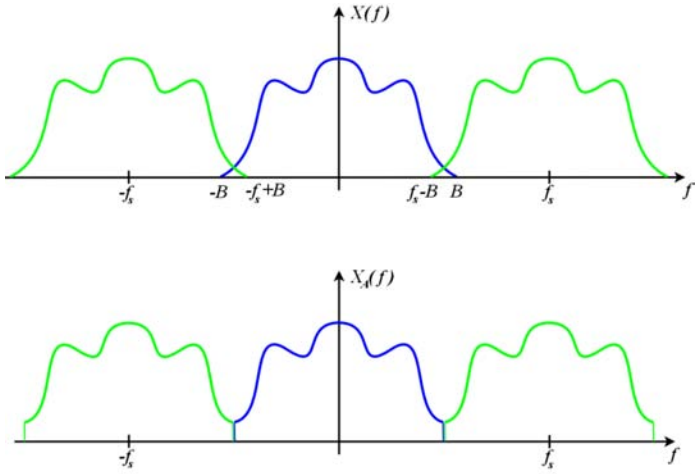

Figure 2.12: Temporal aliasing effect.

ogously, similar effect occurs in the spatial domain. For the case that $\delta > \lambda/2$, spatial aliasing produces some grating lobes as presented in Fig. 2.13. We can conclude that the element spacing of an array cannot be increased beyond a certain value which relates to the minimal wavelength of the signal. On the other hand, for the case that $\delta \ll \frac{\lambda}{2}$, white noise amplification is occurred since usually

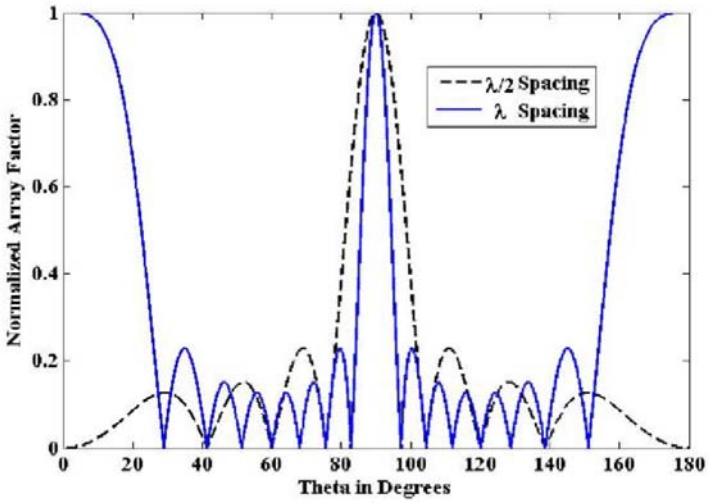

Figure 2.13: Grating lobes effect due to spatial aliasing.

$\mathbf{h}(\omega) = f(\mathbf{R}^{-1}(\mathbf{D}(\omega, \Theta)), \mathbf{D}^{-1}(\omega, \Theta))$ where

$$\mathbf{D}(\omega, \Theta) = [\mathbf{d}(\omega, \theta_1), \mathbf{d}(\omega, \theta_2), \mathbf{d}(\omega, \theta_3), ..., \mathbf{d}(\omega, \theta_L)] \tag{2.20}$$

is the steering matrix, typically an ill-conditioned, especially at low frequencies, as can be shown from Fig. 2.10, and $\mathbf{R}(\cdot)$ denotes a covariance matrix.

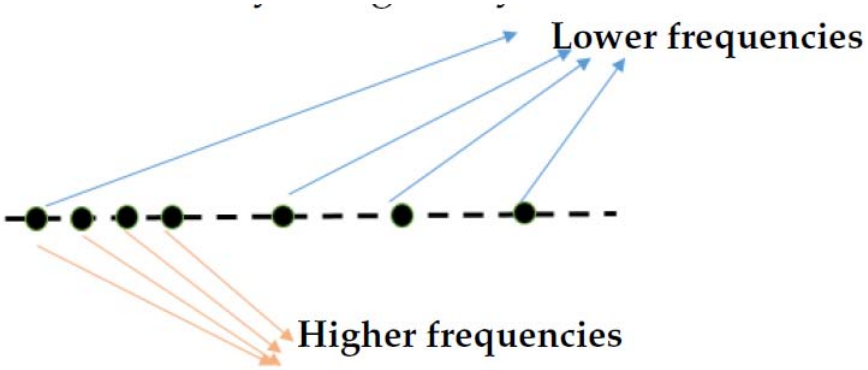

Figure 2.14: The concept of sparse array for broadband signals.

The aforementioned trade-off dictates small element spacing for broadband

signals and uniform arrays. Instead, nonuniform array design may relax this trade-off as exemplified in Fig. 2.14. It shows that for the broadband case, the nonuniform structure can be exploited by using different sets of sensors to different band of frequencies. Therefore, sparse approaches which optimize both the number of sensors and their locations, are expected to yield robust arrays with reduced amount of sensors and without grating lobes, with enhanced flexibility in the design of FI beamformers.

Chapter 3

On the design of time-domain differential microphone arrays

This chapter contains the following manuscript:

Y. Buchris, I. Cohen, and J. Benesty, “On the design of time-domain differential microphone arrays”, Applied Acoustics, 148 (2019), pp. 212-222.

On the Design of Time-Domain Differential Microphone Arrays

Yaakov Buchris, *Member, IEEE*, Israel Cohen, *Fellow, IEEE*, and Jacob Benesty

***Abstract*—Differential microphone arrays (DMAs) are characterized as compact superdirective beamformers whose beampatterns are almost frequency invariant. In this work, we present a time-domain design of Nth-order DMAs, which is important in some applications where minimal delay is required, such as real-time audio communications. Moreover, design in the time domain can reduce the computational efforts, compared to the frequency-domain design, especially when short filters are sufficient. We present design examples for DMAs illustrating some of the fundamental properties of the time-domain implementation as well as the equivalence to the frequency-domain design approach.**

***Index terms*—** Differential microphone arrays, time-domain processing, broadband beamforming.

I. Introduction

Differential microphone arrays (DMAs) constitute a promising solution to some real-world beamforming applications involving speech signals, e.g., hands-free telecommunication, mobile phones, hearing aids, and others. Relative to their physical length, DMAs are characterized by high directivity leading to greatly intelligible speech signals even in heavy reverberant and noisy areas. DMAs first appeared in the literature in the 1930's, designed to respond to the spatial derivatives of an acoustic pressure field [1], [2].

In comparison with additive arrays [3], DMAs have several advantages in processing speech signals. First, DMAs may inherently form frequency-invariant beampatterns which are effective for processing both high- and low- frequency signals. In contrast to DMAs, some work has been done on additive arrays to achieve frequency-invariant beampatterns [4], [5], [6], [7], [8], [9], [10], [11], [12], [13], [14], [15], [16] by introducing either more hardware and computational complexity, or by allowing model mismatch errors augmentation. Second, DMAs have the potential to attain maximum directional gain with a given number of sensors [17]. Furthermore, DMAs are generally small in size relative to the acoustic wavelength, due to the inherent assumption that the true pressure differentials can be approximated by finite differences of the microphone outputs. Therefore, DMAs can be easily integrated into communication devices. Due to these benefits, DMAs have attracted a significant amount of interest in the field of microphone array processing during the past years (see [18], [19], [20], [21], [22], [23], [24], [25], [26], [27], [28], [29], [30], [31], [32], [33], [34] and the references therein).

This research was supported by the Israel Science Foundation (grant no. 576/16), the ISF-NSFC joint research program (grant No. 2514/17) and MAFAAT-Israel Ministry of Defense.

Broadband array processing algorithms can be implemented both in the time and frequency domains. Design in the time domain is of a great importance for applications requiring small delays such as real-time audio communications [35]. Second, processing in the time domain circumvents the edge effects between successive snapshots of the incoming signals, that are typical to the frequency-domain implementation. Furthermore, in some cases the implementation of time-domain filters is computationally more efficient than the equivalent frequency-domain filters, especially when short filters are sufficient. The benefits of the frequency-domain implementation is mainly due to the ability to implement some widely-used frequency dependent processing algorithms like frequency-selective null-steering and efficient calculation of the sample matrix inversion (SMI) [36]. Although algorithms to reduce the associated delay in the frequency domain exist, they usually introduce non-negligible penalty of high computational complexity [36]; thus, they are rarely used.

Previous works in the design of time-domain beamformers mainly focused on the narrowband case. Recent works have investigated time-domain frequency-invariant broadband beamformers [37], [38], [39], [40], [41], [42], [43], [44], [19], [26], [25]. The general approach to design time-domain FIR filters is to solve an optimization problem which incorporates several constraints in the frequency domain. The constraint of a frequency-invariant beampattern is imposed either in all angular directions or only on specific directions such as the mainbeam's direction. Other constraints may be imposed to ensure an adequate performance level such as the white noise gain (WNG) limitation.

In this work, we extend our recent preliminary work [45], [46] and present a framework for a broadband time-domain equivalent design of Nth-order DMAs. We use a similar approach like the one in [23] which ignores the traditional differential structure of DMAs and develops broadband frequency-domain DMAs up to any order from a signal processing perspective. In contrast to previous approaches to frequency-invariant beampattern design, this framework performs both the design process and the beamforming process in the time domain. It includes formulation of equivalent time-domain expressions for the array incoming signal, the covariance matrices of the noise and signal, and some other useful performance measures like time-domain beampattern, WNG, and directivity factor (DF). We also derive the WNG for the case that there are some model mismatch errors. The array input signal is manipulated to represent it in a separable form, meaning that the input signal is a product of a desired-signal-dependent term and a second term which depends only on the

array geometry. This representation enables to apply several array processing algorithms, which were originally developed in the frequency domain, directly into broadband time-domain DMAs. We derive a closed-form solution for time-domain Nth-order DMAs for any given number of sensors. Due to the DMA assumption, the derived solution is much simpler compared to [37], [38], [39], [40], [41], [42], [43], [44], since in the latter works several constraints should be imposed in order to ensure the frequency-invariance property. Furthermore, we show that under the DMA's assumption, the derived time-domain beampattern complies with the theoretical beampattern of traditional DMA designs [24]. Finally in the experimental results, we evaluate the performance of the time-domain DMAs in comparison with that of the frequency-domain implementation and demonstrate some of its fundamental properties.

The paper is organized as follows. In Section II, we formulate the signal model. In Section III, we define some useful performance measures to evaluate time-domain DMAs. In Section IV, we extend the array gain derived in the previous section, to fit also to the case of model mismatch errors. In Section V, we develop a general closed-form solution for the Nth-order DMAs. In Section VI, we present design examples for up to third-order DMAs, along with some simulation results confirming the validity of the developed time-domain solution. Section VII deals with computational complexity and compares time- and frequency- domain designs.

II. Signal Model

We consider a broadband source signal, $s(n)$, in the far-field scenario, where n is the discrete-time index, that propagates in an anechoic acoustic environment at the speed of sound, i.e., $c = 340$ m/s, and impinges on a uniform linear sensor array consisting of M omni-directional microphones, where the distance between two successive sensors is equal to δ. The direction of the source signal to the array is parameterized by the angle θ, where $\theta = 0^\circ$ corresponds to the endfire direction. In the rest, microphone 1 is chosen as the reference sensor. We should say, in passing, that the anechoic far-field model is also used to design conventional DMAs [23]. The proposed approach is more general, though, since the source is considered as broadband instead of narrowband and the design is performed directly in the time domain which has several advantages as discussed before. In this scenario, the signal measured at the mth microphone is given by

$$\begin{aligned} y_m(n) &= s\left[n - \Delta - f_{\mathrm{s}}\tau_m(\theta)\right] + v_m(n) \\ &= x_m(n) + v_m(n), \end{aligned} \tag{1}$$

where f_{s} is the sampling frequency, Δ is the propagation time from the position of the source, $s(n)$, to the reference sensor;

$$\tau_m(\theta) = (m-1)\frac{\delta\cos\theta}{c} \tag{2}$$

is the time delay between the first and the mth sensor which can be positive or negative, and $v_m(n)$ is the noise picked up by the mth sensor. For the general case where $f_{\mathrm{s}}\tau_m(\theta)$ is not an integer, we may apply the Shannon's sampling theorem [47], which implies that

$$\begin{aligned} y_m(n) &= \sum_{l=-\infty}^{\infty} s\left[n-\Delta-l\right]\mathrm{sinc}\left[l - f_{\mathrm{s}}\tau_m(\theta)\right] + v_m(n) \\ &\approx \sum_{l=-P}^{P+\mu L_h} s\left[n-\Delta-l\right]\mathrm{sinc}\left[l - f_{\mathrm{s}}\tau_m(\theta)\right] + v_m(n), \end{aligned} \tag{3}$$

where $\mathrm{sinc}(x) = \sin x/x$, $P \gg f_{\mathrm{s}}\tau_m(\theta)$, μ is a fractional number, and L_h is the length of the FIR filter to be defined later. Hence, we can also express (1) as

$$y_m(n) = \mathbf{g}_m^T(\theta)\mathbf{s}\left(n-\Delta\right) + v_m(n), \tag{4}$$

where the superscript ^{T} is the transpose operator, the vector $\mathbf{g}_m(\theta)$ is a vector containing the coefficients of the interpolation kernel function, and the vector $\mathbf{s}\left(n-\Delta\right)$ contains $L = 2P + \mu L_h$ successive samples of the signal $s\left(n-\Delta\right)$:

$$\begin{aligned} \mathbf{s}\left(n-\Delta\right) = \big[\ & s\left(n-\Delta+P\right) \quad \cdots \\ & s\left(n-\Delta\right) \quad \cdots \quad s\left(n-\Delta-P-\mu L_h+1\right)\ \big]^T. \end{aligned} \tag{5}$$

By considering L_h successive time samples of the mth microphone signal, (4) becomes a vector of length L_h:

$$\mathbf{y}_m(n) = \mathbf{G}_m(\theta)\mathbf{s}\left(n-\Delta\right) + \mathbf{v}_m(n), \tag{6}$$

where $\mathbf{G}_m(\theta)$ is a $L_h \times L$ Toeplitz matrix with the elements:

$$\left[\mathbf{G}_m(\theta)\right]_{i,j} = \mathrm{sinc}\left[-P-i+j-f_{\mathrm{s}}\tau_m(\theta)\right], \tag{7}$$

where $i = 1, ..., L_h$ and $j = 1, ..., L$. The vector $\mathbf{v}_m(n)$ is a vector of length L_h containing the noise samples, i.e.,

$$\mathbf{v}_m(n) = \big[\ v_m(n) \quad \cdots \quad v_m(n-L_h+1)\ \big]^T. \tag{8}$$

Now, by concatenating the observations from the M microphones, we get a vector of length ML_h:

$$\begin{aligned} \underline{\mathbf{y}}(n) &= \big[\ \mathbf{y}_1^T(n) \quad \mathbf{y}_2^T(n) \quad \cdots \quad \mathbf{y}_M^T(n)\ \big]^T \\ &= \underline{\mathbf{G}}(\theta)\mathbf{s}\left(n-\Delta\right) + \underline{\mathbf{v}}(n), \end{aligned} \tag{9}$$

where

$$\underline{\mathbf{G}}(\theta) = \begin{bmatrix} \mathbf{G}_1(\theta) \\ \mathbf{G}_2(\theta) \\ \vdots \\ \mathbf{G}_M(\theta) \end{bmatrix} \tag{10}$$

is a matrix of size $ML_h \times L$ and

$$\underline{\mathbf{v}}(n) = \big[\ \mathbf{v}_1^T(n) \quad \mathbf{v}_2^T(n) \quad \cdots \quad \mathbf{v}_M^T(n)\ \big]^T \tag{11}$$

is a vector of length ML_h.

In the model of the DMAs, it is assumed that δ is much smaller than the wavelength of the incoming signal, i.e.,

$$\delta \ll \lambda, \tag{12}$$

and the desired signal propagates at the endfire, i.e., at the angle $\theta = 0$, therefore, the desired signal vector is

$$\underline{\mathbf{y}}(n) = \underline{\mathbf{G}}(0)\mathbf{s}\left(n-\Delta\right) + \underline{\mathbf{v}}(n). \tag{13}$$

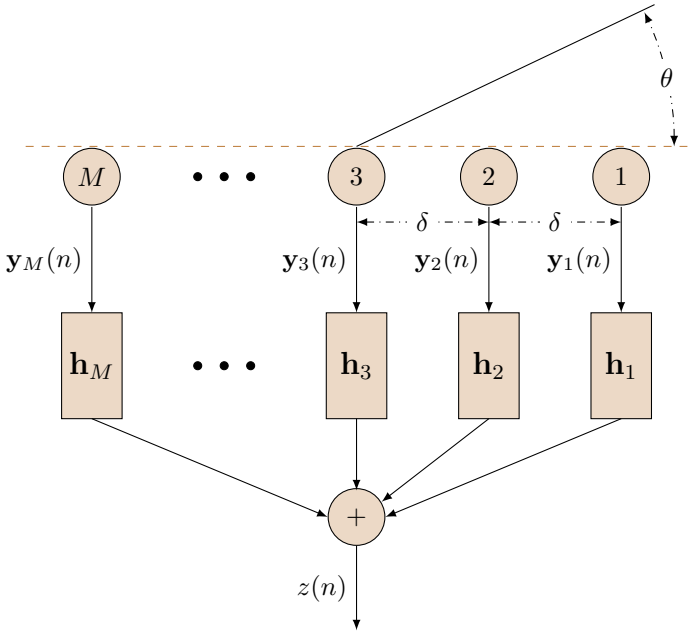

Fig. 1: A block diagram of the time-domain differential array beamformer.

It is worth to emphasize that the vector $\underline{\mathbf{y}}(n)$ has a separable representation meaning that ignoring the noise term, it is a product between a signal dependent term and a second term which depends only on the array geometry. This structure also exists in the frequency domain. Therefore, we can treat $\underline{\mathbf{G}}(0)$ as a broadband time-domain steering matrix. Moreover, it implies on the next required steps of imposing distortionless and null constraints in order to cancel the influence of the steering matrix $\underline{\mathbf{G}}(0)$ as usually done in the frequency-domain design. Then, we can design all kinds of broadband DMAs, where the main lobe is at the angle $\theta = 0$, with a real-valued spatiotemporal filter of length ML_h:

$$\underline{\mathbf{h}} = \left[\begin{array}{cccc} \mathbf{h}_1^T & \mathbf{h}_2^T & \cdots & \mathbf{h}_M^T \end{array} \right]^T, \tag{14}$$

where $\mathbf{h}_m,\ m = 1, 2, \ldots, M$ are temporal filters of length L_h.

By applying the filter $\underline{\mathbf{h}}$ to the observation vector $\underline{\mathbf{y}}(n)$, we obtain the output of the broadband beamformer:

$$z(n) = \sum_{m=1}^{M} \mathbf{h}_m^T \mathbf{y}_m(n) = \underline{\mathbf{h}}^T \underline{\mathbf{y}}(n) = x_{\mathrm{fd}}(n) + v_{\mathrm{rn}}(n), \tag{15}$$

where

$$\begin{aligned} x_{\mathrm{fd}}(n) &= \sum_{m=1}^{M} \mathbf{h}_m^T \mathbf{G}_m(0) \mathbf{s}\left(n - \Delta\right) \\ &= \underline{\mathbf{h}}^T \underline{\mathbf{G}}(0) \mathbf{s}\left(n - \Delta\right) \end{aligned} \tag{16}$$

is the filtered desired signal and

$$v_{\mathrm{rn}}(n) = \sum_{m=1}^{M} \mathbf{h}_m^T \mathbf{v}_m(n) = \underline{\mathbf{h}}^T \underline{\mathbf{v}}(n) \tag{17}$$

is the residual noise. Figure 1 presents a block diagram of the time-domain differential array beamformer.

III. Performance Measures

In this section, we introduce several quality measures commonly used in the context of array processing. These measures are usually defined in the frequency domain for the case of broadband beamforming (see e.g. [23]). Herein, we establish their analogous time-domain versions.

Since our concern is broadband beamforming, we assume for convenience that the source signal, $s(n)$, is white; this way, the whole spectrum is taken into account. Assuming microphone 1 to be the reference sensor, the broadband input signal-to-noise ratio (SNR) is computed from the first L_h components of $\underline{\mathbf{y}}(n)$ as defined in (13), i.e., $\mathbf{y}_1(n) = \mathbf{s}(n - \Delta) + \mathbf{v}_1(n)$. We easily find that

$$\mathrm{iSNR} = \frac{\mathrm{tr}\left(\mathbf{R}_{\mathbf{s}}\right)}{\mathrm{tr}\left(\mathbf{R}_{\mathbf{v}_1}\right)} = \frac{\sigma_s^2}{\sigma_{v_1}^2}, \tag{18}$$

where $\mathrm{tr}(\cdot)$ denotes the trace of a square matrix, $\mathbf{R}_{\mathbf{s}}$ and $\mathbf{R}_{\mathbf{v}_1}$ are the correlation matrices of $\mathbf{s}(n - \Delta)$ and $\mathbf{v}_1(n)$, respectively, and $\sigma_{v_1}^2$ and σ_s^2 are the variances of $v_1(n)$ and $s(n)$, respectively. The broadband output SNR is given by

$$\begin{aligned} \mathrm{oSNR}\left(\underline{\mathbf{h}}\right) &= \frac{\sigma_{x_{\mathrm{fd}}}^2}{\sigma_{v_{\mathrm{rn}}}^2} \\ &= \frac{\sigma_s^2 \underline{\mathbf{h}}^T \underline{\mathbf{G}}(0) \underline{\mathbf{G}}^T(0) \underline{\mathbf{h}}}{\underline{\mathbf{h}}^T \mathbf{R}_{\underline{\mathbf{v}}} \underline{\mathbf{h}}} \\ &= \frac{\sigma_s^2}{\sigma_{v_1}^2} \times \frac{\underline{\mathbf{h}}^T \underline{\mathbf{G}}(0) \underline{\mathbf{G}}^T(0) \underline{\mathbf{h}}}{\underline{\mathbf{h}}^T \mathbf{\Gamma}_{\underline{\mathbf{v}}} \underline{\mathbf{h}}}, \end{aligned} \tag{19}$$

where

$$\mathbf{\Gamma}_{\underline{\mathbf{v}}} = \frac{\mathbf{R}_{\underline{\mathbf{v}}}}{\sigma_{v_1}^2} \tag{20}$$

is the pseudo-correlation matrix of $\underline{\mathbf{v}}(t)$. We see from (19) that the gain in SNR is

$$\mathcal{G}\left(\underline{\mathbf{h}}\right) = \frac{\mathrm{oSNR}\left(\underline{\mathbf{h}}\right)}{\mathrm{iSNR}} = \frac{\underline{\mathbf{h}}^T \underline{\mathbf{G}}(0) \underline{\mathbf{G}}^T(0) \underline{\mathbf{h}}}{\underline{\mathbf{h}}^T \mathbf{\Gamma}_{\underline{\mathbf{v}}} \underline{\mathbf{h}}}. \tag{21}$$

The WNG is obtained by taking $\mathbf{\Gamma}_{\underline{\mathbf{v}}} = \mathbf{I}_{ML_h}$, where $\mathbf{I}_{ML_h}$ is the $ML_h \times ML_h$ identity matrix, i.e.,

$$\mathcal{W}\left(\underline{\mathbf{h}}\right) = \frac{\underline{\mathbf{h}}^T \underline{\mathbf{G}}(0) \underline{\mathbf{G}}^T(0) \underline{\mathbf{h}}}{\underline{\mathbf{h}}^H \underline{\mathbf{h}}}. \tag{22}$$

We can also define the broadband beampattern or broadband directivity pattern as

$$\left|\mathcal{B}\left(\underline{\mathbf{h}}, \theta\right)\right|^2 = \underline{\mathbf{h}}^T \underline{\mathbf{G}}(\theta) \underline{\mathbf{G}}^T(\theta) \underline{\mathbf{h}}. \tag{23}$$

The theoretical frequency-invariant beampattern of an Nth-order DMA is defined as [24]

$$\mathcal{B}_N\left(\theta\right) = \sum_{n=0}^{N} a_{N,n} \cos^n \theta, \tag{24}$$

where $a_{N,n}, n = 0, 1, ..., N$ are real coefficients that are set according to some desired properties, like null directions, maximal directivity, and more. In the appendix, we show that for small values of δ we get

$$\left|\mathcal{B}\left(\underline{\mathbf{h}}, \theta\right)\right|^2 \underset{\delta \ll \lambda}{\longrightarrow} \mathcal{B}_N^2\left(\theta\right). \tag{25}$$

This result is meaningful since it shows how our general model converges to the theoretical beampattern of DMAs, when the DMA assumptions are satisfied.

We may also define the normalized beampattern error, E_{BP}, to be the integral over θ of the absolute error between the time-domain beampattern (23) and $\mathcal{B}_N^2(\theta)$ (24), divided by the integral over θ of the square of the theoretical beampattern:

$$E_{\mathrm{BP}} = \frac{\int_0^\pi \left| |\mathcal{B}(\underline{\mathbf{h}},\theta)|^2 - \mathcal{B}_N^2(\theta) \right| d\theta}{\int_0^\pi \mathcal{B}_N^2(\theta)\, d\theta}. \tag{26}$$

Finally, we define the DF of the array which is the gain in SNR for the case of spherical isotropic noise. One way to calculate the DF is to use (21) and substitute the time-domain version of $\mathbf{\Gamma}_{\underline{\mathbf{v}}}$ for diffuse noise. Yet, an explicit expression for $\mathbf{\Gamma}_{\underline{\mathbf{v}}}$ in the time domain is unavailable. Instead, we can use directly the definition of the DF (see for example at [48, ch.2]):

$$\mathcal{D}(\underline{\mathbf{h}}) = \frac{2}{\int_0^\pi |\mathcal{B}(\underline{\mathbf{h}},\theta)|^2 \sin\theta d\theta}, \tag{27}$$

where $\mathcal{B}(\underline{\mathbf{h}},\theta)$ is defined in (23) and the filter is assumed to be distortionless. These definitions of the SNR, gains, and beampattern, which are extremely useful for the evaluation of any type of beamformer, conclude this section.

IV. Performance In the Presence of Array Perturbations

In this section, we extend the analytical expression of the array gain (21) also to the practical case where the actual array has some perturbations from the nominal model.

Array perturbations usually arise from some errors in the gain, phase, as well as the locations of the sensors. Returning to our proposed model of the received signal (9), we may model the array perturbations by adding an error matrix to the steering matrix $\underline{\mathbf{G}}(\theta)$:

$$\underline{\mathbf{G}}_{\mathrm{pert}}(\theta) = \underline{\mathbf{G}}(\theta) + \mathbf{\Delta}\underline{\mathbf{G}}, \tag{28}$$

where $\mathbf{\Delta}\underline{\mathbf{G}}$ is the error matrix whose entries are given by

$$[\mathbf{\Delta}\underline{\mathbf{G}}]_{i,j} = \epsilon_{i,j}, \qquad \epsilon_{i,j} \approx N(0,\sigma^2). \tag{29}$$

This model is reasonable because the matrix $\underline{\mathbf{G}}(\theta)$ is considered as the time-domain steering matrix which depends only on the array geometry.

Substituting the matrix $\underline{\mathbf{G}}_{\mathrm{pert}}(\theta)$ into (9), we get that

$$\underline{\mathbf{y}}(n) = \underline{\mathbf{G}}(\theta)\mathbf{s}(n-\Delta) + \tilde{\underline{\mathbf{v}}}(n), \tag{30}$$

where

$$\tilde{\underline{\mathbf{v}}}(n) = \mathbf{\Delta}\underline{\mathbf{G}}\mathbf{s}(n-\Delta) + \underline{\mathbf{v}}(n) \tag{31}$$

is a vector containing the additive backgorund noise and the perturbation noise.

The correlation matrix of the noise vector $\tilde{\underline{\mathbf{v}}}(n)$ is given by

$$\mathbf{R}_{\tilde{\underline{\mathbf{v}}}} = \sigma_s^2\mathbf{D} + \sigma_{v_1}^2\mathbf{\Gamma}_{\underline{\mathbf{v}}}, \tag{32}$$

where $\mathbf{D} = \mathrm{diag}\left(\left[\sigma^2,\sigma^2,...,\sigma^2\right]^T\right)$ is an $ML_h \times ML_h$ diagonal matrix. The WNG for that case is given by

$$\mathcal{W}_{\mathrm{pert}}(\underline{\mathbf{h}}) = \frac{\underline{\mathbf{h}}^T\underline{\mathbf{G}}(0)\underline{\mathbf{G}}^T(0)\underline{\mathbf{h}}}{\underline{\mathbf{h}}^T(\mathrm{iSNR}\mathbf{D}+\mathbf{I})\underline{\mathbf{h}}}. \tag{33}$$

Note that for the ideal case when there are no model mismatch errors (i.e., $\sigma = 0$), (33) reduced to (22). We now move to present the design of time-domain DMAs up to any desired order.

V. Design of Nth-Order DMAs

It is well known that the design of Nth-order DMAs requires at least $N+1$ microphones [23], [24]. We present here the general derivation for time-domain design of DMAs for any order $N \geq 1$ and any number of sensors $M \geq N+1$. The number of constraints is exactly equal to $N+1$. The first one is a distortionless constraint which can be formulated as follows. We see from (16) that the distortionless constraint is

$$\underline{\mathbf{h}}^T\underline{\mathbf{G}}(0) = \mathbf{i}^T(D), \tag{34}$$

where $\mathbf{i}(D)$ is a vector of length L with all its elements equal to zero except for its Dth element. The remaining N constraints are of the form:

$$\underline{\mathbf{h}}^T\underline{\mathbf{G}}(\theta_n) = \alpha_n\mathbf{i}^T(D), \quad n = 1,2,...,N, \tag{35}$$

where $\alpha_n,\ n = 1,2,\ldots,N$, are the attenuation parameters, with $0 \leq \alpha_n \leq 1$. Combining these $N+1$ constraints together, we get the following linear system to solve

$$\mathbf{C}_{N,M}(\boldsymbol{\theta})\underline{\mathbf{h}} = \underline{\mathbf{i}}_N(\boldsymbol{\alpha},D), \tag{36}$$

where

$$\mathbf{C}_{N,M}(\boldsymbol{\theta}) = \begin{bmatrix} \mathbf{G}_1^T(0) & \mathbf{G}_2^T(0) & \cdots & \mathbf{G}_M^T(0) \\ \mathbf{G}_1^T(\theta_1) & \mathbf{G}_2^T(\theta_1) & \cdots & \mathbf{G}_M^T(\theta_1) \\ \vdots & \vdots & \ddots & \vdots \\ \mathbf{G}_1^T(\theta_N) & \mathbf{G}_2^T(\theta_N) & \cdots & \mathbf{G}_M^T(\theta_N) \end{bmatrix} \tag{37}$$

is the $(N+1)L \times ML_h$ constraints matrix, $\theta_n \in (0,\pi],\ n = 1,2,\ldots,N$, with $\theta_1 \neq \theta_2 \neq \cdots \neq \theta_N$, are the corresponding directions where the attenuations are desired. The vector:

$$\underline{\mathbf{i}}_N(\boldsymbol{\alpha},D) = \begin{bmatrix} \mathbf{i}^T(D) & \alpha_1\mathbf{i}^T(D) & \cdots & \alpha_N\mathbf{i}^T(D) \end{bmatrix}^T \tag{38}$$

is of length NL. We can derive the beamformer using the pseudo-inverse solution:

$$\underline{\mathbf{h}}_{N,M;\mathrm{Pinv}} = \mathbf{P}^\dagger_{\mathbf{C}_{N,M}}(\boldsymbol{\theta})\underline{\mathbf{i}}_N(\boldsymbol{\alpha},D), \tag{39}$$

where

$$\mathbf{P}^\dagger_{\mathbf{C}_{N,M}}(\boldsymbol{\theta}) = \left[\mathbf{C}_{N,M}^T(\boldsymbol{\theta})\mathbf{C}_{N,M}(\boldsymbol{\theta}) + \eta\mathbf{I}\right]^{-1}\mathbf{C}_{N,M}^T(\boldsymbol{\theta}) \tag{40}$$

is the pseudo-inverse of the matrix $\mathbf{C}_{N,M}(\boldsymbol{\theta})$, and the scalar η is a regularization parameter.

In order to set the appropriate delay, D, we suggest to choose the value that minimizes the error introduced by the solution of (39), i.e.

$$D^{\mathrm{opt}} = \min_D \quad ||\mathbf{C}_{N,M}(\boldsymbol{\theta})\underline{\mathbf{h}}_{N,M;\mathrm{Pinv}} - \underline{\mathbf{i}}_N(\boldsymbol{\alpha},D)||^2. \tag{41}$$

Figure 2 shows the error defined by (41) as a function of the delay, D. One can see that the optimal delay is not necessary the theoretical value expected from the model of (5). This means that we have a degree of freedom by allowing an additional delay to the DMA's output signals and improving

their performance. Using this value of delay provides the best results with respect to other values. Finding improved solutions that both achieve a reduced delay and sufficient level of performance is a future research topic.

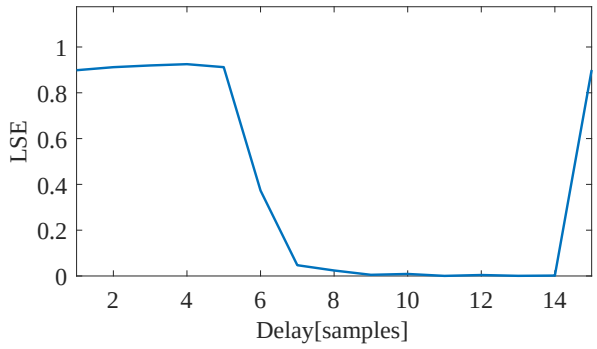

Fig. 2: The least-squares error (LSE) (41) Vs. D.

Note also that in order to solve (36) in the direct way, one have to invert the matrix $\mathbf{C}_{N,M}(\boldsymbol{\theta})$. This operation is computationally expensive as it will be discussed later. Instead, we may exploit the structure of this matrix. This matrix is composed of several sub-matrices, each contains the sinc function in a circulant structure. This implies that $\mathbf{C}_{N,M}(\boldsymbol{\theta})$ is a rank deficient matrix. Therefore, we can calculate the singular value decomposition (SVD) of $\mathbf{C}_{N,M}(\boldsymbol{\theta})$ and invert it using only the most dominant singular values. Figure 3 shows an image of a typical matrix, $\mathbf{C}_{N,M}(\boldsymbol{\theta})$ for the case of second order DMAs with $M = 3$ sensors (a), and its singular values (b). One can see that this matrix is indeed a rank-deficient matrix and its effective rank is approximately equal to L, therefore, we can exploit it for more efficient calculation of its pseudo-inverse. Using the SVD decomposition, we can derive the r - rank approximation of the matrix $\mathbf{C}_{N,M}(\boldsymbol{\theta})$:

$$\mathbf{C}^{(r)}_{N,M}(\boldsymbol{\theta}) \approx \sum_{l=1}^{r} \sigma_l \mathbf{u}_l \mathbf{v}_l^T, \tag{42}$$

where σ_l, $\mathbf{v}_l$, and $\mathbf{u}_l$ are the lth singular value, lth right-singular vector, and lth left-singular vector of the matrix $\mathbf{C}_{N,M}(\boldsymbol{\theta})$, respectively. The parameter r may be chosen according to

$$||\mathbf{C}_{N,M}(\boldsymbol{\theta}) - \mathbf{C}^{(r)}_{N,M}(\boldsymbol{\theta})||^2 \leq \epsilon, \tag{43}$$

where ϵ is a small positive integer that control the accuracy of the r-rank approximation of the matrix $\mathbf{C}_{N,M}(\boldsymbol{\theta})$. We can invert the matrix using the following formula:

$$\mathbf{P}^{\dagger,(r)}_{\mathbf{C}_{N,M}}(\boldsymbol{\theta}) \approx \sum_{l=1}^{r} \frac{1}{\sigma_l} \mathbf{v}_l \mathbf{u}_l^T. \tag{44}$$

Note that by using (44) and setting an appropriate value for ϵ, we can also achieve a stable solution.

In the simulation section, we study the design of time-domain DMAs up to the third order. We also evaluate the performance of the various orders and patterns by means of the beampattern, WNG, DF, and E_{BP} as defined in Section III. We start with the design of first-order time-domain DMAs, then we move to higher orders.

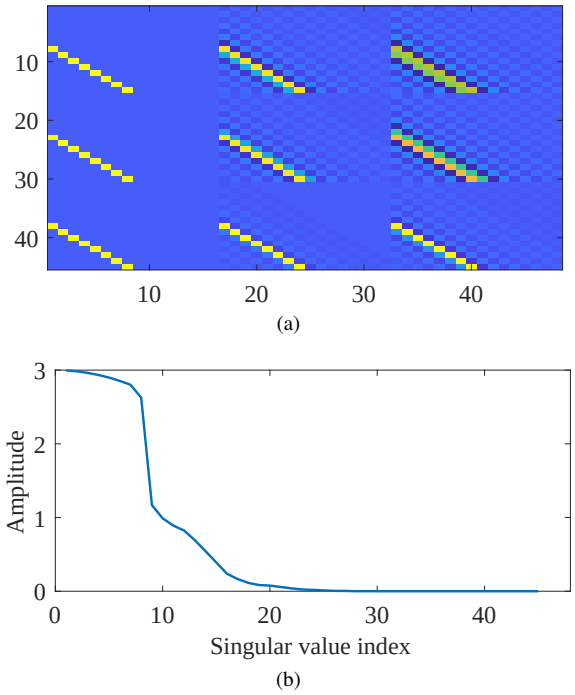

Fig. 3: An example of a typical image of the matrix $\mathbf{C}_{N,M}(\boldsymbol{\theta})$ (a), and its singular values (b).

VI. Simulations

A. First-order DMAs

The first-order standard DMAs directivity patterns are dipole, cardioid, hypercardioid, and supercardioid, each with one distinct null in the following directions: $\theta_{\mathrm{Dp}} = \pi/2, \theta_{\mathrm{Cd}} = \pi, \theta_{\mathrm{Hc}} = 2\pi/3$, and $\theta_{\mathrm{Sc}} = 3\pi/4$. We choose the sensor spacing $\delta = 1$ cm as this value is much smaller with respect to the maximal wavelength of the signal, and first examine the case of $M = N + 1 = 2$ sensors, where $N = 1$ stands for the order. We choose the fractional delay length $P = 6$ taps which is a sufficient value for practical implementations and $\mu = 0.5$ and get $L = 24$ taps. We choose the filter length $L_h = 16$ taps and the sampling frequency to be $f_{\mathrm{s}} = 8000$ Hz. The parameter ϵ is set to be 10^{-3}.

Figure 4 shows a comparison between the broadband beampattern of the time-domain implementation (39) (black dashed line), and the theoretical beampattern [23, ch.2] (blue circles line). Using (24), it is easy to show that the theoretical beampatterns of first-order DMAs have the following forms:

$$\mathcal{B}_1(\theta) = (1 - a_{1,1}) + a_{1,1} \cos\theta, \tag{45}$$

where the parameter $a_{1,1}$ is obtained by imposing the null constraint on (45). These patterns were also achieved by the frequency-domain implementation in [23, ch.3]. The comparison illustrates the equivalence between the time- and frequency- domain implementations.

Table I summarizes the results for the four basic shapes by means of $\mathcal{W}(\underline{\mathbf{h}})$, $\mathcal{D}(\underline{\mathbf{h}})$, and E_{BP}. The main difference between the WNG and the DF of the frequency-domain implementation presented at [23, ch.3] to the values in Table I

TABLE I: Results of $\mathcal{W}(\underline{\mathbf{h}})$, $\mathcal{D}(\underline{\mathbf{h}})$, and E_{BP} for the four basic shapes of first-order DMAs.

Pattern	$\mathcal{W}(\underline{\mathbf{h}})$ [dB]	$\mathcal{D}(\underline{\mathbf{h}})$ [dB]	E_{BP}
Dipole	-14.4	4.90	0.040
Cardioid	-8.68	4.75	0.007
Hypercardioid	-11.00	5.84	0.010
Supercardioid	-10.00	5.42	0.007

is that for the frequency-domain case, these quantities are frequency-dependent while for the time-domain case each of these quantities is a scalar. Yet, the mean values of the theoretical WNG and the DF over the frequency obtained in [23, ch.3] are very close to the corresponding values in Table I. This fact shows also the equivalence between the time-domain approach and the frequency-domain approach.

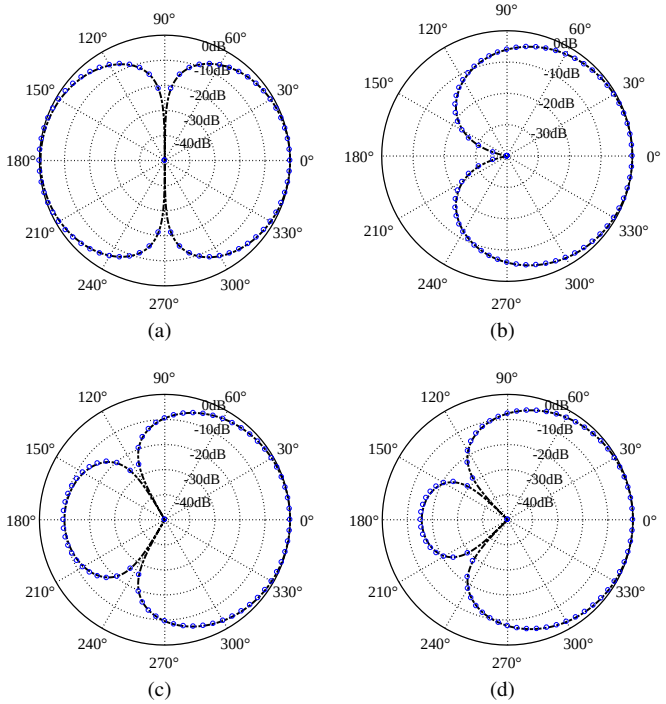

Fig. 4: Beampatterns for the four basic shapes of first-order DMAs produced by the time-domain implementation (dark dashed line): (a) dipole, (b) cardioid, (c) hypercardioid, and (d) supercardioid. The theoretical patterns are also presented (blue circles line).

The obtained filters were tested by simulating a speech signal, whose spectrogram is presented in Fig. 5, impinging on the DMA using the model of (6). The received vector was fed into the temporal filters (39). Figure 6 shows the time-domain waveform (dark blue line) of the signals arrived from the endfire direction, the null direction, and an arbitrary direction of $\theta = 88^\circ$ for the supercardioid beamformer. It also shows the waveforms of the recovered signals in the output of the DMA (light red line). One can see that the produced filters provide perfect recovery of the desired endfire signal while completely suppressing the signal arriving from

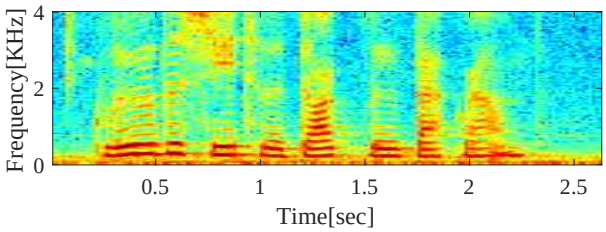

Fig. 5: Spectrogram of the speech signal.

TABLE II: Normalized energy of the output signals for the case of a first-order supercardioid DMA.

	Endfire signal	Null signal	Arbitrary signal
$\mathbf{E}_{\mathrm{norm}}[\mathrm{dB}]$	-0.009	-46.810	-6.569

the null direction. For signals impinging from an arbitrary direction which the DMA was not designed to suppress at all, the output signal is reasonably suppressed as compared to the input signal. Table II shows the normalized energy of the output signal for all the three signals:

$$\mathbf{E}_{\mathrm{norm}}(\theta) = \frac{\mathbf{E}_{\mathrm{out}}(\theta)}{\mathbf{E}_{\mathrm{i}}(\theta)}, \tag{46}$$

where $\mathbf{E}_{\mathrm{i}}(\theta)$ is the energy of a signal arrived from direction θ measured at the reference sensor (dark blue line), and $\mathbf{E}_{\mathrm{out}}(\theta)$ is the energy of the output array signal due to the input signal from direction θ (light red line). There is a reduction of about 6 dB for the signal arriving from $\theta = 88^\circ$ which corresponds to the gain of the beampattern of a supercardioid plotted in Fig. 4(d) in the direction of $\theta = 88^\circ$. These results demonstrate the practical ability of first-order DMAs to spatially filter undesired signals while perfectly recovering the endfire desired signal.

Note that unlike the traditional [24] and the frequency-domain [23] implementations of DMAs where the beamformers coefficient vectors can be explicitly expressed and the differential structure is presented, in the time-domain design each sensor is filtered by an FIR filter vector and the differential structure cannot be presented explicitly. Yet, both implementations obtain almost identical frequency-invariant beampattern as reflected from Figs. 4 and 6, meaning that the proposed design indeed implements a differential beamformer.

Figure 7 shows the time-domain WNG and the time-domain DF as a function of the number of sensors, M, for the case of a first-order hypercardioid. One can see that the WNG increases with the number of sensors while the DF is slightly above the value of 5 dB and does not change at all. From this result, we can infer that one of the effective ways to increase the robustness of DMAs in to add more sensors. Increasing the number of sensors is an effective way to improve the WNG also for the case of additive arrays. For example, the delay and sum (DAS) beamformer obtains the largest WNG for a given number of sensors which is [48]

$$\mathcal{W}_{\mathrm{DAS}} = M. \tag{47}$$

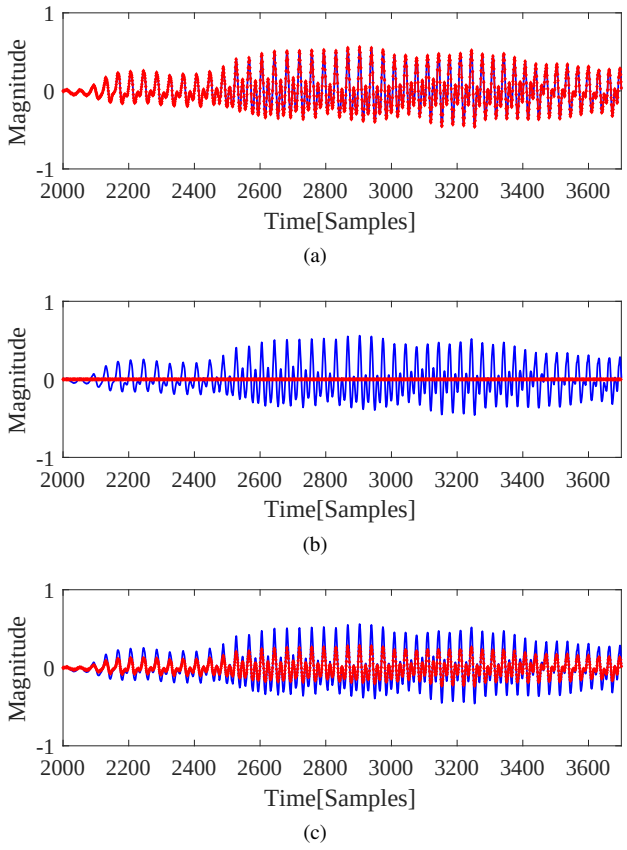

Fig. 6: Time-domain waveforms of the original signals (dark blue line) and the output recovered signals (light red line) for the supercardioid: (a) source in the endfire direction, (b) source in the null direction, and (c) source in an arbitrary direction of 88°.

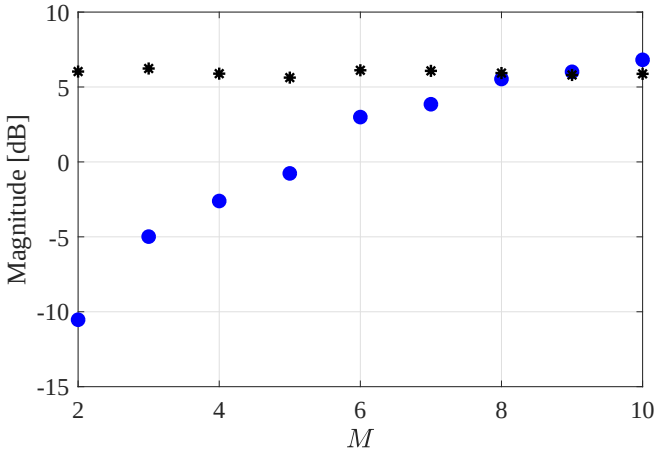

Fig. 7: WNG (circles) and DF (stars) vs. M, for the case of a first-order hypercardioid.

While the WNG of the DMA beamformer is about -10dB for two microphones, the WNG of a DAS beamformer for two microphones is 3dB.

Figure 8 shows the time-domain WNG as a function of the number of sensors, M, for the case that some model mismatch

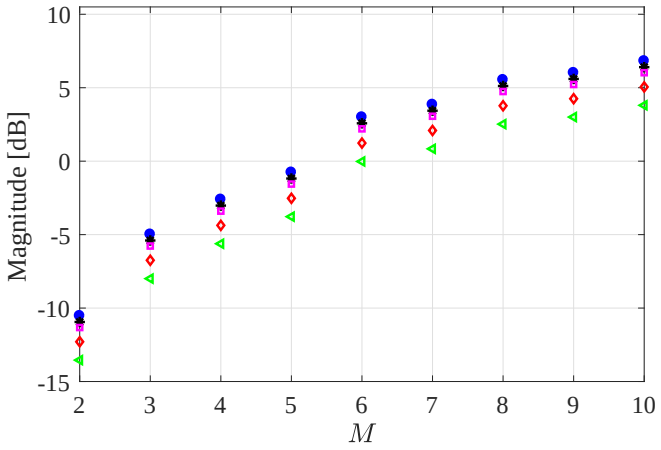

Fig. 8: WNG (blue circles) vs. M, for the case of a first-order hypercardioid. Five cases are compared: $\sigma^2 = 0$ (blue circles), $\sigma^2 = 0.05$ and iSNR $= 2$ (black stars), $\sigma^2 = 0.25$ and iSNR $= 2$ (red diamonds), $\sigma^2 = 0.05$ and iSNR $= 4$ (magenta squares), and $\sigma^2 = 0.25$ and iSNR $= 4$ (green triangles).

errors exist as derived in Section IV. It compares between the following cases: $\sigma^2 = 0$ (blue circles), $\sigma^2 = 0.05$ and iSNR $=$ 2 (black stars), $\sigma^2 = 0.25$ and iSNR $= 2$ (red diamonds), $\sigma^2 = 0.05$ and iSNR $= 4$ (magenta squares), and $\sigma^2 = 0.25$ and iSNR $= 4$ (green triangles). As expected, the WNG is influenced by the variance of the mismatch error. It is also influenced by the input SNR since as the SNR increased, the mismatch noise is more dominant than the background noise. For all these cases, the WNG is still an increasing function of the number of sensors, M.

Before we move to higher orders of DMAs, we present two more design aspects of DMAs. The first aspect is related to the minimal required filter length, L_h, and the second aspect is related to the element spacing parameter, δ.

1) Minimal Required Filter Length : We examine the issue of the minimal required length of the filter vector, $\underline{\mathbf{h}}_{N,M;\text{Pinv}}$, as given in (39). In Fig. 9, the time-domain waveforms of the filters for the case of a first-order hypercardioid with $M = 2$ sensors are plotted as a function of the number of taps. In the bottom plot, the filters cumulative energy as a function of the number of taps is plotted. The dashed line in the bottom plot is the total energy of the filters, justifying the assumption that in practice, a small number of coefficients is sufficient. In this case, most of the filters energy is concentrated in the 15 first coefficients.

Figure 10 shows the performance by means of WNG and DF as a function of the filter length, L_h, for the case of a first-order hypercardioid with $M = 2$ sensors. It shows that up to $L_h = 15$ taps there are fluctuations and the performance is unstable, but starting from the length of $L_h = 15$ taps, the performance is almost constant. Similar results were obtained for the other checked patterns of first order DMAs. From this example we can see that the required length of the filter should be on the order of 10 to 20 taps which makes the time-domain design computationally more efficient in some cases as will be discussed later.

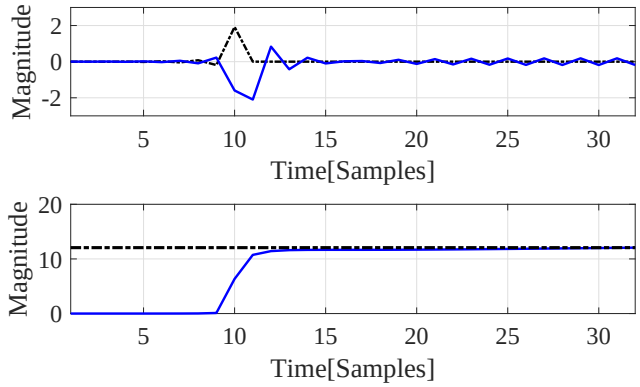

Fig. 9: Waveform of the filters for the case of a first-order hypercardioid with $M = 2$ sensors as a function of time (top). The cumulative energy vs. time (solid line) and the total filters energy (dashed line) (bottom).

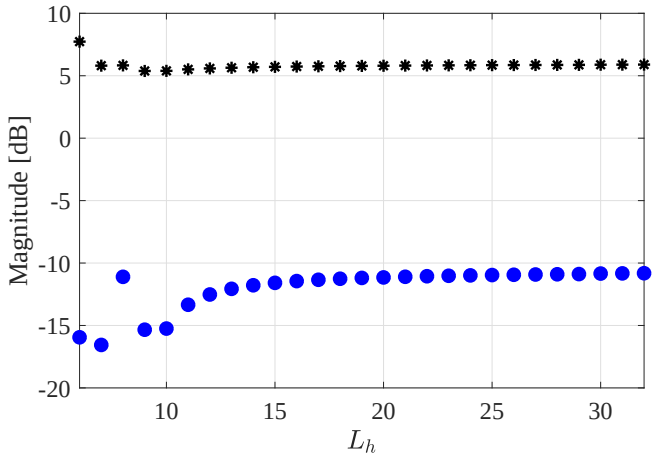

Fig. 10: WNG (circles) and DF (stars) vs. L_h for the case of a first-order hypercardioid with $M = 2$.

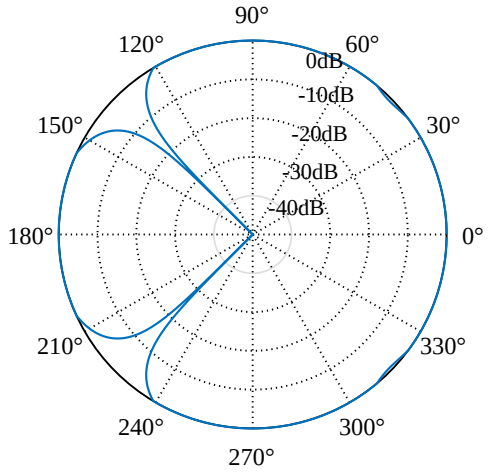

Fig. 11: Beampattern of a first-order hypercardioid ($M = 2$) for the case of $\delta = 15$ cm.

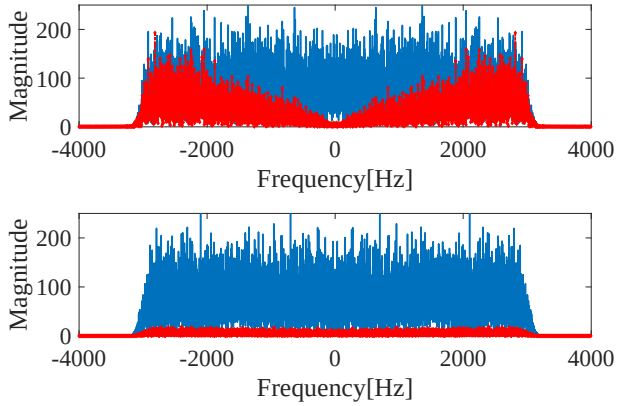

Fig. 12: Waveform for the case of $\delta = 15$ cm (top) and for the case of $\delta = 1$ cm (bottom) for a signal arrived from 145°. The dark blue spectrum is the original spectrum and the light red one is the output signal spectrum.

2) Spacing Between Two Sensors : As discussed before, DMAs are very small and can provide high directivity relative to their small physical length. Moreover, when broadband signals are employed, they can provide nearly constant directivity patterns. In the case of a time-domain implementation, there is no clear definition of a frequency dependent WNG and DF. So, we try to exhibit the influence of the sensor spacing, δ, by simulation results. Figure 11 shows the beampattern of a first-order hypercardioid with element spacing $\delta = 15$ cm. We can see that both the mainbeam and the sidelobes are saturated which are expected to behave like that because for such a choice of δ, the mainbeam cannot be constant over the entire bandwidth. We expect good spatial properties in the low frequencies and poor results in the high frequency range. To prove this fact, Fig. 12 shows the output spectrum (light red line) and the original spectrum (dark blue line) for the case of $\delta = 15$ cm (top) and for the case of $\delta = 1$ cm (bottom) for a white signal impinging on the array from direction of $\theta = 145°$. While for the case of a small value of δ, the entire output spectrum is flat implying a frequency-invariant beampattern, it is not the case when δ is large, resulting in a very good attenuation in low frequencies while insufficient attenuation in high frequencies. This result demonstrates the claim that under the DMAs assumption, the proposed solution is sufficient to provide frequency-invariant beampattern. However, when the assumption is not valid anymore, solutions with additional constraints should be applied in order to achieve frequency-invariant beampattern.

The results presented in this section show equivalence between time- and frequency- domain implementations of first-order DMAs. Moreover, testing the time-domain filters with actual broadband signals confirms that the desired endfire signal is undistorted while suppressing the undesired signals, even those not arriving exactly from a null direction. We now move to design examples of higher orders of DMAs.

B. Second-order DMAs

In this section, we present the design of the second-order DMAs. The second-order standard DMAs directivity patterns are dipole, cardioid, hypercardioid, and supercardioid. The second-order dipole has one null in $\theta_{\mathrm{Dp},1} = \pi/2$ and a

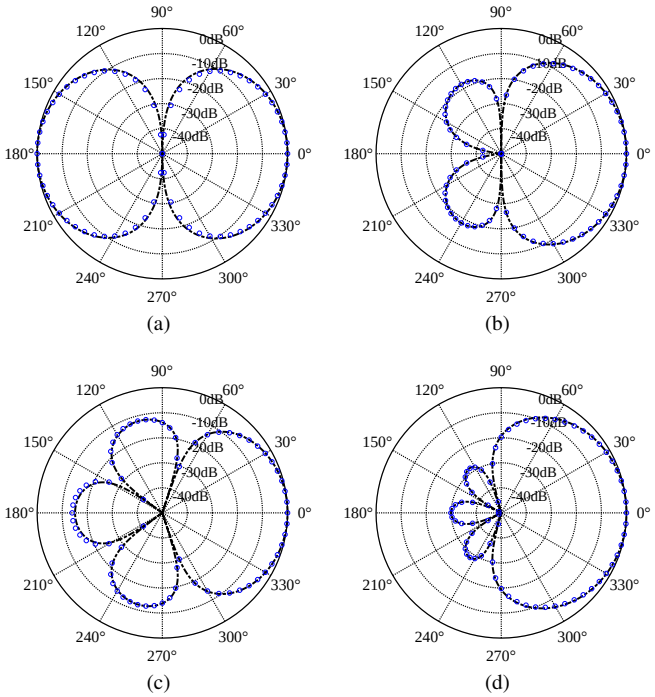

Fig. 13: Beampatterns for the four basic shapes of second-order DMAs produced by the time-domain implementation(dark dashed line): (a) dipole, (b) cardioid, (c) hypercardioid, and (d) supercardioid. The theoretical patterns are also presented (blue circles line).

TABLE III: Results of $\mathcal{W}(\underline{\mathbf{h}})$, $\mathcal{D}(\underline{\mathbf{h}})$, and E_{BP} for the four basic shapes of second-order DMAs.

Pattern	$\mathcal{W}(\underline{\mathbf{h}})$ [dB]	$\mathcal{D}(\underline{\mathbf{h}})$ [dB]	E_{BP}
Dipole	-29.18	6.70	0.03
Cardioid	-25.48	8.60	0.02
Hypercardioid	-29.30	9.36	0.01
Supercardioid	-23.91	8.01	0.03

second distortionless constraint at $\theta_{\mathrm{Dp},2}=\pi$. The three other shapes have two distinct nulls in the following directions: $\theta_{\mathrm{Cd},1}=\pi/2, \theta_{\mathrm{Cd},2}=\pi, \theta_{\mathrm{Hc},1}=0.8005\pi, \theta_{\mathrm{Hc},2}=0.3997\pi$, and $\theta_{\mathrm{Sc},1}=0.8493\pi, \theta_{\mathrm{Sc},2}=0.5903\pi$. We choose $L_h=20$ taps. All the rest design parameters are identical to those of the first-order example.

Figure 13 shows the time-domain implementation (dark dashed line) and the theoretical (blue circles line) beampatterns of the four basic shapes of second-order DMAs. Table III summarizes the performance measures by means of $\mathcal{W}(\underline{\mathbf{h}})$, $\mathcal{D}(\underline{\mathbf{h}})$, and E_{BP}. Using (24), it is easy to show that the theoretical beampatterns of second-order DMAs have the following form:

$$\mathcal{B}_2(\theta)=(1-a_{2,1}-a_{2,2})+a_{2,1}\cos\theta+a_{2,2}\cos^2\theta, \quad (48)$$

where the parameters $a_{2,1}$ and $a_{2,2}$ are obtained by imposing the null constraints on (48).

Figure 14 shows the time-domain WNG and DF as a function of the number of sensors, M, for the case of a second-order cardioid. In Fig. 15 the corresponding beampatterns are plotted for (a) $M=5$ and (b) $M=8$ sensors, respectively. One can see that the directivity patterns is close to the theoretical value also for the robust case of increased number of sensors.

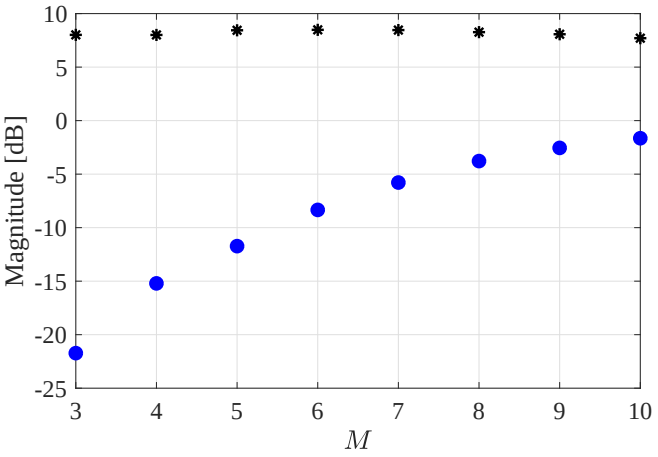

Fig. 14: WNG (circles) and DF (stars) vs. M, for the case of a second-order cardioid.

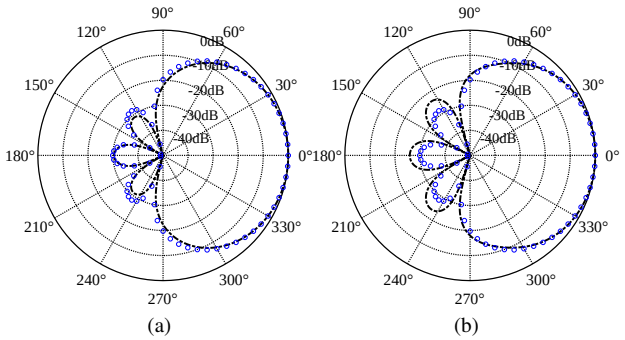

Fig. 15: Beampatterns for the case of a second-order cardioid for the case of (a) $M=5$ sensors, and (b) $M=8$ sensors .

From the above examples of the second-order DMAs, one can inspect similar trends like those presented in the first-order case. These trends are also compatible to the theoretical results and to the frequency-domain results (see [23, ch.4]).

C. Third-order DMAs

In the case of third-order DMAs, we choose to present two out of the three patterns presented at [23, ch.5], because these patterns contain three distinct nulls in the following directions: $\theta_{\mathrm{case1},1}=\frac{\pi}{2}, \theta_{\mathrm{case1},2}=\frac{2\pi}{3}, \theta_{\mathrm{case1},3}=\pi$, and $\theta_{\mathrm{case2},1}=\frac{\pi}{3}, \theta_{\mathrm{case2},2}=\frac{2\pi}{3}, \theta_{\mathrm{case2},3}=\pi$. We choose $L_h=24$ taps and $M=4$ sensors. All the rest design parameters are like those in the previous examples. In Fig. 16 the beampatterns of the two basic shapes are plotted.

Table IV summarizes the results for the two basic shapes by means of $\mathcal{W}(\underline{\mathbf{h}})$, $\mathcal{D}(\underline{\mathbf{h}})$, and E_{BP}, where the last measure is calculated using the following theoretical beampattern for

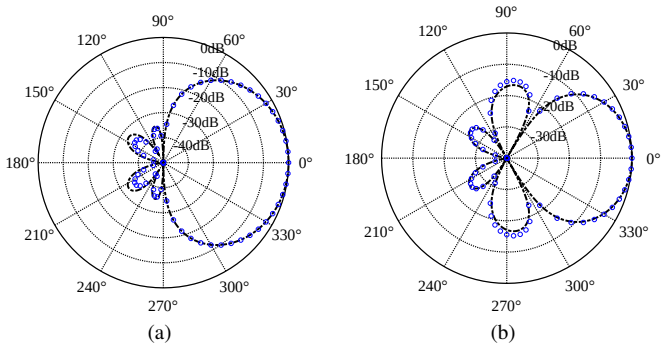

Fig. 16: Beampatterns for two cases of third-order DMAs with 3 distinct nulls, produced by the time-domain implementation (dark dashed line): (a) case 1, and (b) case 2. The theoretical patterns are also presented (blue circles line).

TABLE IV: Results of $\mathcal{W}(\underline{\mathbf{h}})$, $\mathcal{D}(\underline{\mathbf{h}})$, and E_{BP} for the two basic shapes of third-order DMAs.

Pattern	$\mathcal{W}(\underline{\mathbf{h}})$ [dB]	$\mathcal{D}(\underline{\mathbf{h}})$ [dB]	E_{BP}
Case 1	-29.32	10.16	0.007
Case 2	-36.78	11.78	0.030

third-order DMAs:

$$\mathcal{B}_3(\theta) = (1 - a_{3,1} - a_{3,2} - a_{3,3}) + a_{3,1}\cos\theta + a_{3,2}\cos^2\theta + a_{3,3}\cos^3\theta, \qquad (49)$$

where the parameters $a_{3,1}, a_{3,2}$, and $a_{3,3}$ are obtained by imposing the three null constraints on (49).

We finally plot in Fig. 17 the time-domain WNG and DF for various values of the number of sensors, M, for a third-order DMA (case 1). Comparing between the WNG and DF of the first-, second-, and third-order DMAs one can see that as the DMA's order increases proportionally, the WNG decreases but the DF increases proportionally to $(N+1)^2$ with accordance to the case of superdirective beamformers [17].

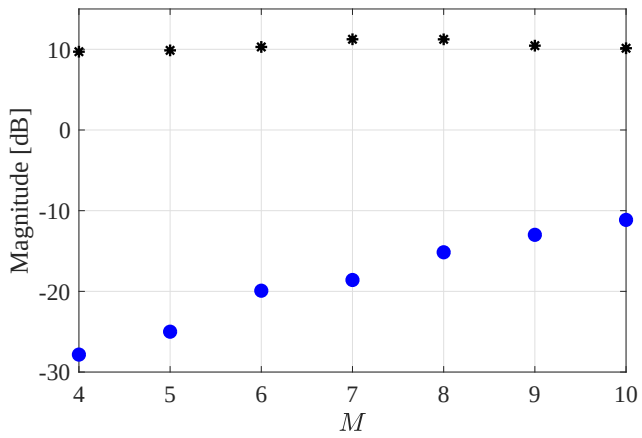

Fig. 17: WNG (circles) and DF (stars) vs. M, for the case of a third-order DMA (case 1).

Other results presented in previous sections are valid also for the third-order case and are not presented here. Comparing between the results of all orders one can see similar trends of the WNG and the DF also in the frequency-domain implementation presented in [23]. This fact is important because a time-domain framework for the design of DMAs up to any order is useful in a large variety of applications with some hard design considerations like small-delay, memory, computational complexity and more. In the next section, we evaluate the computational complexity of the time-domain implementation and compare it to that of the frequency-domain implementation.

VII. Computational Complexity

As discussed in the introduction, there are some benefits to implementing DMAs in the time domain rather than in the frequency domain. One of the most important benefits is reduced computational complexity in some design cases. Let us consider separately the filter design stage and the convolution stage in which the incoming data is filtered.

In the filter design stage, the most expensive operation in the time-domain implementation is the pseudo-inverse operation (39). Direct implementation according to (39) involves multiplication of the transpose of $\mathbf{C}_{N,M}(\boldsymbol{\theta})$ by itself, its inverse and another multiplication by the transpose of $\mathbf{C}_{N,M}(\boldsymbol{\theta})$. These operations require approximately $3M^3L_h^3$ multiplications and a similar number of additions. Lower complexity may be achieved by using the SVD method in (44) since we can use a reduced number of singular values.

If we implement the filters in the frequency domain and return to the time domain, this requires us to design the filter in each frequency bin, and then use inverse fast Fourier transform (FFT). Assuming that the number of frequency bins is also L_h, so it requires approximately $4M^3L_h^2\log_2 L_h$ multiplications and a similar number of additions, where the factor four is due to the complex operations. Moreover, the evaluated number of operations for the frequency-domain implementation assumes that L_h is an integer power of two. If this is not satisfied, a zero padding operation should be performed which increases the computational complexity even further.

Comparing the last two results, one can easily be convinced that there are non-negligible number of cases in which there will be fewer operations in direct design in time, especially for small values of the filter length, L_h. Indeed, the experimental results of the previous sections claim for a typical filter length in the range between 10 to 30 taps.

In the convolution stage, one may refer to [49, ch.5] where a detailed comparison between the computational complexities of the time and frequency convolutions is presented. The bottom line is that the choice between time or frequency implementation is related to the length of the filter and to the length of the incoming signal.

VIII. Conclusions

We have presented a framework for time-domain implementation of DMAs. A closed-form solution for temporal DMAs filters of any order and any number of sensors was provided.

We have also formulated time-domain performance measures for microphone arrays. The proposed solution is very simple with respect to other methods due to the DMA assumption which enables to get frequency-invariant beampatterns without additional constraints in the frequency domain.

We showed that the proposed model converges to the classical DMAs model since the time-domain beampattern converges to the theoretical beampattern. Several design examples were presented in the simulation part demonstrating the equivalence of the time- and frequency- domain implementations. Each of the possible implementations involves some benefits and shortcomings. The time-domain implementation has some benefits like a short delay, which is essential in some applications such as real-time communications. On the other hand, a frequency-domain implementation enables frequency-dependent null steering, which can be useful in frequency-selective fading channels.

From a computational point of view, depending on the length of the filters, the time-domain design can be advantageous in some cases, especially when short filters are sufficient, while the design in the frequency domain may be preferred in other cases. The possibility to choose time- or frequency- domain implementation for a specific system, is of a great importance because it provides flexibility in the design considerations of several real-world applications involving DMAs.

Future research directions may focus on time-domain implementation for different array geometries, robustness issues, extension of the proposed time-domain design to support also reverberant environments, and comparisons to more advanced frequency-implementations like subband filtering implementation.

IX. Appendix: Proof of the equivalence between (23) and (24) for $\delta \ll \lambda$

The analytic term for the time-domain beampattern (23) contains the product of the matrix $\underline{\mathbf{G}}(\theta)$ with its transpose:

$$\underline{\mathbf{G}}(\theta)\underline{\mathbf{G}}^T(\theta) = \begin{bmatrix} \mathbf{G}_1(\theta)\mathbf{G}_1^T(\theta) & \cdots & \mathbf{G}_1(\theta)\mathbf{G}_M^T(\theta) \\ \vdots & \vdots & \vdots \\ \mathbf{G}_M(\theta)\mathbf{G}_1^T(\theta) & \cdots & \mathbf{G}_M(\theta)\mathbf{G}_M^T(\theta) \end{bmatrix}. \tag{50}$$

According to (7), the matrix $\mathbf{G}_i(\theta)$ has the following structure:

$$\mathbf{G}_i(\theta) = \begin{bmatrix} \mathbf{t}^T\left(l - \tau_i(\theta) f_s\right) \\ \mathbf{t}^T\left(l - 1 - \tau_i(\theta) f_s\right) \\ \vdots \\ \mathbf{t}^T\left(l - L_h + 1 - \tau_i(\theta) f_s\right) \end{bmatrix}, \tag{51}$$

where $\mathbf{t}\left(l - \tau_i(\theta) f_s\right) = \mathrm{sinc}\left[-P - 1 + l - f_s \tau_i(\theta)\right], \quad l = 1, ..., L$ is a column vector. From now on, we omit the dependency of $\tau_i(\theta)$ on θ for notation simplicity. In order to simplify (50), we may exploit the following property of the scalar product between two time-shifted sinc functions:

$$\mathbf{t}^T(\tau_1)\,\mathbf{t}(\tau_2) \approx \begin{cases} \xi_{\tau_1,\tau_2} & , \ |\tau_1 - \tau_2| < 1 \\ 0 & , \ |\tau_1 - \tau_2| > 1 \end{cases}, \tag{52}$$

where

$$\xi_{\tau_1,\tau_2} = \mathrm{sinc}^2\left(\frac{\tau_1 + \tau_2}{2} f_\mathrm{s}\right) \tag{53}$$

is a scalar which expresses the value of the shifted version of the sinc function at the best matching point between $\mathbf{t}(\tau_1)$ and $\mathbf{t}(\tau_2)$. Therefore, each block of (50) can be simplified to

$$\mathbf{G}_i(\theta)\mathbf{G}_j^T(\theta) \approx \mathrm{sinc}^2\left(\frac{\tau_i + \tau_j}{2} f_\mathrm{s}\right)\mathbf{I}, \tag{54}$$

where $\mathbf{I}$ is an $L_h \times L_h$ identity matrix. We may conclude that $\underline{\mathbf{G}}(\theta)\underline{\mathbf{G}}^T(\theta)$ is a matrix which is composed of diagonal sub-matrices of the form (54).

Substituting the last result into (23) we get the following:

$$\begin{aligned} \underline{\mathbf{h}}^T\underline{\mathbf{G}}(\theta)\underline{\mathbf{G}}^T(\theta)\underline{\mathbf{h}} &\approx \sum_{i=1}^{M}\sum_{j=1}^{M} \mathbf{h}_i^T\mathbf{G}_i(\theta)\mathbf{G}_j^T(\theta)\mathbf{h}_j \\ &= \sum_{i=1}^{M}\sum_{j=1}^{M} \mathrm{sinc}^2\left(\frac{\tau_i + \tau_j}{2} f_\mathrm{s}\right)\mathbf{h}_i^T\mathbf{h}_j \\ &= \sum_{i=1}^{M}\sum_{j=1}^{M} \mathrm{sinc}^2\left(\frac{\delta f_\mathrm{s}\mu_{i,j}}{c}\cos\theta\right)\mathbf{h}_i^T\mathbf{h}_j, \end{aligned} \tag{55}$$

where $\mu_{i,j} = i + j - 2$. According to the DMA assumption [23], $\frac{2\pi f \delta}{c} \ll 2\pi$, therefore, $\frac{f_\mathrm{s}\delta}{c} \approx \frac{f_\mathrm{max}\delta}{c} \ll 1$, where f_max is the highest frequency bin of the signal. Let us assign $x_{i,j} \equiv \mu_{i,j}\frac{f_\mathrm{s}\delta}{c}\cos\theta$ and approximate $f(x_{i,j}) = \mathrm{sinc}^2(x_{i,j})$ using Taylor series around the point x_0:

$$f(x) = \sum_{n=0}^{\infty} \frac{f^{(n)}(x_0)}{n!}(x - x_0)^n. \tag{56}$$

We can calculate (56) by using the well-known Taylor series $\mathrm{sinc(x)} = \sum_{n=0}^{\infty}\beta_n(-1)^n x^{2n}$ and its derivatives which lead to the following general form:

$$\mathrm{sinc}^2(x_{i,j}) \approx \sum_{n=0}^{2N} f_n(x_{i,j})\frac{\delta f_\mathrm{s}\mu_{i,j}}{c}(\cos\theta - 1)^n, \tag{57}$$

where we choose x_0 as the corresponding to the case of $\theta = 0^\circ$ and cut the infinite series after $2N$ terms. The functions f_n contain the derivatives of the sinc function. Opening the brackets in the last expression and substituting into (55) we get the general structure:

$$\underline{\mathbf{h}}^T\underline{\mathbf{G}}(\theta)\underline{\mathbf{G}}^T(\theta)\underline{\mathbf{h}} \approx \sum_{n=0}^{2N} \varrho_{N,n}(\Theta)\cos^n\theta, \tag{58}$$

where Θ is the parameters vector containing all the above parameters like δ, c, $\underline{\mathbf{h}}$, etc.

On the other hand, the square of (24) is

$$\mathcal{B}_N^2(\theta) = \left(\sum_{n=0}^{N} a_{N,n}\cos^n\theta\right)^2 = \sum_{n=0}^{2N}\tilde{a}_{N,n}\cos^n\theta. \quad (59)$$

Comparing between (58) and (59), it is obvious that both are equivalent.
Q.E.D

REFERENCES

[1] H. F. Olson, "A uni-directional ribbon microphone," *J. Acoust. Soc. Amer.*, vol. 3, pp. 139–147, Oct. 1932.

[2] ——, "Gradient microphones," *J. Acoust. Soc. Amer.*, vol. 17, pp. 192–198, Jan. 1946.

[3] J. Benesty, J. Chen, and Y. Huang, *Microphone Array Signal Processing*. Berlin, Germany: Springer-Verlag, 2008.

[4] M. Crocco and A. Trucco, "Design of robust superdirective arrays with a tunable tradeoff between directivity and frequency-invariance," *IEEE Trans. Signal Process.*, vol. 59, no. 5, pp. 2169–2181, May 2011.

[5] ——, "Stochastic and analytic optimization of sparse aperiodic arrays and broadband beamformers with robust superdirective patterns," *IEEE Trans. Audio, Speech, Language Process.*, vol. 20, no. 9, pp. 2433–2447, Nov. 2012.

[6] Y. Buchris, I. Cohen, and M. Doron, "Bayesian focusing for coherent wideband beamforming," *IEEE Trans. Audio, Speech, Language Process.*, vol. 20, no. 4, pp. 1282–1295, May 2012.

[7] J. Flangan, D. Berkeley, G. Elko, J. West, and M. Sondhi, "Autodirective microphone systems," *Acustica*, vol. 73, pp. 58–71, 1991.

[8] I. J. H. Doles and F. D. Benedict, "Broad-band array design using the asymptotic theory of unequally spaced arrays," *IEEE Trans. Antennas Propagat.*, vol. 36, pp. 27–33, Jan. 1991.

[9] D. B. Ward, R. A. Kennedy, and R. C. Williamson, "Theory and design of broadband sensor arrays with frequency invariant farfield beampatterns," *J. Acoust. Soc. Amer.*, vol. 97, no. 2, pp. 1023–1034, Feb. 1995.

[10] S. C. Chan and H. H. Chen, "Uniform concentric circular arrays with frequency-invariant characteristics - theory, design, adaptive beamforming and doa estimation," *IEEE Trans. Signal Process.*, vol. 55, pp. 165–177, Jan. 2007.

[11] W. Liu and S. Weiss, "Design of frequency invariant beamformers for broadband arrays," *IEEE Trans. Signal Process.*, vol. 56, no. 2, pp. 855–860, Feb. 2008.

[12] S. Doclo and M. Moonen, "Design of broadband beamformers robust against gain and phase errors in the microphone array characteristics," *IEEE Trans. Signal Process.*, vol. 51, no. 10, pp. 2511–2526, Oct. 2003.

[13] B. D. Van Veen and K. V. Buckley, "Beamforming: A versatile approach to spatial filtering," *IEEE Mag. Acoust., Speech, Signal Process.*, vol. 5, pp. 4–24, Apr. 1988.

[14] E. Mabande, A. Schad, and W. Kellermann, "Design of robust superdirective beamformers as a convex optimization problem," *Int. Conf. Acoust., Speech, Signal Process., Taipei, Taiwan*, Apr. 2009.

[15] J. Benesty, J. Chen, Y. Huang, and J. Dmochowski, "On microphone-array beamforming from a MIMO acoustic signal processing perspective," *IEEE Trans. Audio, Speech, Language Process.*, vol. 15, no. 3, pp. 1053–1065, Mar. 2007.

[16] T. Do-Hong and P. Russer, "Spatial signal processing for wideband beamforming," in *Proc.VII International Symposium on Theoretical Electrical Engineering*, 2003, pp. 73–76.

[17] G. W. Elko and J. Meyer, "Microphone arrays," in *Springer Handbook of Speech Processing*, J. Benesty, M. M. Sondhi, and Y. Huang, Eds. Berlin, Germany: Springer-Verlag, 2008, ch. 50, Part I, pp. 1021–1041.

[18] J. Benesty, M. Souden, and Y. Huang, "A perspective on differential microphone arrays in the context of noise reduction," *IEEE Trans. Audio, Speech, Language Process.*, vol. 20, no. 2, pp. 699–704, Feb. 2012.

[19] E. De Sena, H. Hacihabibğlu, and Z. Cavetković, "On the design and implementation of higher order differential microphones," *IEEE Trans. Audio, Speech, Language Process.*, vol. 20, no. 1, pp. 162–174, Jan. 2012.

[20] T. D. Abhayapala and A. Gupta, "Higher order differential-integral microphone arrays," *J. Acoust. Soc. Amer.*, vol. 127, pp. 227–233, May 2010.

[21] M. Buck, "Aspects of first-order differential microphone arrays in the presence of sensor imperfections," *European Trans. Telecommunications*, vol. 13, pp. 115–122, Mar. 2002.

[22] M. Kolundžija, C. Faller, and M. Vetterli, "Spatiotemporal gradient analysis of differential microphone arrays," *J. Audio Eng. Soc.*, vol. 59, pp. 20–28, Feb. 2011.

[23] J. Benesty and J. Chen, *Study and Design of Differential Microphone Arrays*. Berlin, Germany: Springer-Verlag, 2012.

[24] G. W. Elko, "Superdirectional microphone arrays," in *Acoustic Signal Processing for Telecommunication*, S. L. Gay and J. Benesty, Eds. Boston, MA: Kluwer Academic Publishers, 2000, ch. 10, pp. 181–237.

[25] ——, "Differential microphone arrays," in *in Audio Signal Processing for Next-Generation Multimedia Communication Systems*, Y. Huang and J. Benesty, Eds. Norwell, MA: Kluwer, 2004, ch. 2, pp. 11–65.

[26] H. Teutsch and G. W. Elko, "First- and second-order adaptive differential microphone arrays," in *Darmstadt, Germany: 7th International Workshop on Acoustic Echo and Noise Control*, 2001, pp. 57–60.

[27] G. W. Elko and A. T. N. Pong, "A simple first-order differential microphone," in *Proc. IEEE Workshop Applicat. Signal Process. Audio Acoust. (WASPAA)*, 1995, pp. 169–172.

[28] ——, "A steerable and variable firstorder differential microphone array," in *Proc. ICASSP*, 1997, pp. 223–226.

[29] R. M. M. Derkx and K. Janse, "Theoretical analysis of a first-order azimuth-steerable superdirective microphone array," *IEEE Trans. Audio, Speech, Language Process.*, vol. 17, pp. 150–162, Jan. 2009.

[30] J. Chen and J. Benesty, "A general approach to the design and implementation of linear differential microphone arrays," in *Signal and Information Processing Association Annual Summit and Conference (APSIPA)*, Asia-Pacific, Oct. 2013, pp. 1–7.

[31] L. Zhao, J. Benesty, and J. Chen, "Design of robust differential microphone arrays," *IEEE Trans. Audio, Speech, Language Process.*, vol. 22, no. 10, pp. 1455–1464, Oct. 2014.

[32] P. Chao, J. Benesty, and J. Chen, "Design of robust differential microphone arrays with orthogonal polynomials," *The Journal of the Acoustical Society of America*, vol. 138, no. 2, pp. 1079–1089, Aug. 2015.

[33] H. Zhang, J. Chen, and J. Benesty, "Study of nonuniform linear differential microphone arrays with the minimum-norm filter," *Applied Acoustics*, vol. 98, pp. 62–69, May 2015.

[34] P. Chao, J. Chen, and J. Benesty, "Theoretical analysis of differential microphone array beamforming and an improved solution," *IEEE Trans. Audio, Speech, Language Process.*, vol. 23, no. 11, pp. 2093–2105, Nov. 2015.

[35] L. C. Godara, "Application of the fast fourier transform to broadband beamforming," *J. Acoust. Soc. Amer.*, vol. 98, no. 1, pp. 230–240, July 1995.

[36] R. T. Compton, "The relationship between tapped delay-line and FFT processing in adaptive arrays," *IEEE Trans. Antennas and Propagation.*, vol. 36, no. 1, pp. 15–26, Jan. 1988.

[37] R. C. Nongpiur and D. J. Shpak, "*L*-infinity norm design of linear-phase robust broadband beamformers using constrained optimization," *IEEE Trans. Signal Process.*, vol. 61, no. 23, pp. 6034–6046, Dec. 2013.

[38] E. Mabande, A. Schad, and W. Kellermann, "A time-domain implementation of data-independent robust broadband beamformers with low filter order," in *Proc. Joint Workshop on Hands-free Speech Commun. Microphone Arrays, Edinburgh, U.K*, May 2011.

[39] L. C. Godara and M. R. S. Jahromi, "Convolution constraints for broadband antenna arrays," *IEEE Trans. Anthennas and propagation*, vol. 55, no. 11, pp. 3146–3154, Nov. 2007.

[40] S. Yan, Y. L. Ma, and C. H. Hou, "Optimal array pattern synthesis for broadband arrays," *J. Acoust. Soc. Amer.*, vol. 122, no. 5, pp. 2686–2696, Nov. 2007.

[41] S. Yan, "Optimal design of fir beamformer with frequency invariant patterns," *Appl. Acoust.*, vol. 67, pp. 511–528, Nov. 2006.

[42] H. H. Chen, S. C. Chan, and K. L. Ho, "Adaptive beamforming using frequency invariant uniform concentric circular arrays," *IEEE Trans.Circuits Syst. I, Reg. Papers*, vol. 54, no. 9, pp. 1938–1949, Sept. 2007.

[43] D. B. Ward, R. A. Kennedy, and R. C. Williamson, "FIR filter design for frequency invariant beamformers," *IEEE Signal Process. Lett.*, vol. 3, pp. 69–71, Mar. 1996.

[44] S. Yan, H. Sun, X. Ma, P. U. Svensson, and C. Hou, "Time-domain implementation of broadband beamformer in spherical harmonics domain," *IEEE Trans. Audio, Speech, Language Process.*, vol. 19, no. 5, pp. 1221–1230, Jul. 2011.

[45] Y. Buchris, I. Cohen, and J. Benesty, "First-order differential microphone arrays from a time-domain broadband perspective," in *International Workshop on Acoustic Echo and Noise Control (IWAENC) 2016 conf.*

[46] ——, “Analysis and design of time-domain first-order circular differential microphone arrays,” in *the 22nd International Congress on Acoustics (ICA)*, 2016.
[47] C. E. Shannon, “Communications in the presence of noise,” *Proc. IRE*, vol. 37, pp. 10–21, 1949.
[48] H. L. Van-trees, *Detection, Estimation and Modulation Theory, Part IV - Optimum Array Processing*. New York: Wiley Interscience, 2002.
[49] B. Porat, *A Course in Digital Signal Processing*. John Wiley & Sons, INC., 1997.

Chapter 4

Frequency-Domain Design of Asymmetric Circular Differential Microphone Arrays

This chapter contains the following manuscript:

Y. Buchris, I. Cohen, and J. Benesty, "Frequency-domain design of asymmetric circular differential microphone arrays", IEEE/ACM Transactions on Audio, Speech, and Language Processing, vol. 26, no. 4, pp. 760–773, (2018).

Frequency-Domain Design of Asymmetric Circular Differential Microphone Arrays

Yaakov Buchris, *Member, IEEE*, Israel Cohen, *Fellow, IEEE*, and Jacob Benesty

***Abstract*—Circular differential microphone arrays (CDMAs) facilitate compact superdirective beamformers whose beampatterns are nearly frequency invariant. In contrast to linear differential microphone arrays where the optimal steering direction is at the endfire, CDMAs provide perfect steering for all azimuthal directions. Herein, we extend the traditional symmetric model of DMAs and establish an analytical asymmetric model for Nth-order CDMAs. This model exploits the circular geometry to eliminate the inherent limitation of symmetric beampatterns associated with a linear geometry and allows also asymmetric beampatterns. This new model is then used to develop asymmetric versions of two optimal commonly used beampatterns namely the hypercardioid and the supercardioid. Experimental results demonstrate the advantages of the asymmetric model compared to the traditional symmetric one, when additional directional constraints are imposed. The proposed model yields superior performance in terms of white noise gain, directivity factor, and front-to-back ratio, as well as more flexible design of nulls for the interfering signals.**

***Index terms*—** Circular differential microphone arrays, asymmetric beampatterns, broadband beamforming, hypercardioid, supercardioid.

I. Introduction

Differential microphone arrays (DMAs) refer to arrays that combine closely spaced sensors to respond to the spatial derivatives of the acoustic pressure field. These small-size arrays yield nearly frequency-invariant beampatterns. Moreover, DMAs include the well-known superdirective beamformer [1], [2] as a particular case. Therefore, DMAs have attracted much research interest in recent years.

DMAs first appeared in the literature in the 1930's, designed to respond to the spatial derivatives of an acoustic pressure field [3], and later were implemented using omnidirectional pressure microphones [4]. These early fixed implementations had a prominent limitation that once they were designed and produced, their properties cannot be changed. The modern concept of DMAs employs pressure microphones, and digital signal processing techniques are used to obtain desired directional responses [5]–[9]. Based on the modern concept, several works on DMAs appeared during the last two decades. Buck [10], and Derkx and Janse [11] analyzed the performance of the first-order design under array imperfections, and presented solutions for sensors calibration. First- and second- order adaptive DMAs based on fullband as well as on subband algorithms were introduced and examined by Teutsch and Elko [12]. De Sena et al. [13] proposed a general approach to the design of directivity patterns of higher-order DMAs. In [14] a more general approach is proposed for the design of DMAs, which ignores the traditional differential structure of DMAs and develops broadband frequency-domain DMAs up to any order from a signal processing perspective. Robust frequency-domain DMAs have been presented by Zhao et al. [15], and Pan et al. [16]. More recent work on DMAs can be found in [17]–[20].

Most of the work on DMAs deals with a linear array geometry. The geometry of microphone arrays plays an important role in the formulation, solution, and performance of the algorithms. The selection of the geometry, however, depends heavily on the application requirements. For example, in devices like smartphones, tablet PCs, and smart televisions, a linear geometry is preferable as this type of arrays can be easily integrated into the devices. But linear arrays may not have the same response at different directions as shown in [21]. In applications like teleconferencing and 3D sound recording where the signal of interest may come from any direction, it is necessary for the microphone array to have similar, if not the same response from one direction to another. In such cases, circular arrays are advantageous.

Design schemes of circular arrays can be classified into two main categories. The first category relies on narrowband methods for the design of frequency-varying beampatterns [22]–[28]. The second category incorporates methods that produce frequency-invariant beampatterns [29]–[32]. A general approach for the design of frequency-invariant broadband beamformers is to solve an optimization problem which enforces several constraints in the frequency domain, such as frequency-invariant beampattern either in all angular directions or only in specific directions like the mainbeam direction. Other constraints may be imposed to ensure an adequate performance level such as maximum white noise gain (WNG). Recently, Benesty et al. [33] presented a study of the most basic concepts and fundamental techniques used in the design and implementation of different orders of circular differential microphone arrays (CDMAs). In [34], we introduced a time-domain design for first-order CDMAs.

Existing works on DMAs, for linear or circular geometry, consider only the case of symmetric beampatterns, which is an inherent property of the linear geometry and confines the design process by some aspects. For linear arrays, a symmetric beampattern means that the beampattern is symmetric with respect to the axis of the array. Such a symmetry is not required in different array geometries like the circular geometry, thus, removing this requirement may lead to a substantial performance improvement. We term such beampatterns as

This research was supported by the Israel Science Foundation (grant no. 576/16), the ISF-NSFC joint research program (grant No. 2514/17) and MAFAAT-Israel Ministry of Defense.

asymmetric beampatterns.

In this paper, we derive an analytical model for asymmetric CDMAs which includes also the traditional symmetric model as a particular case. We begin with an extension of the well-known analytical expression for the directivity pattern of the traditional DMAs, to a generalized expression which supports also the asymmetric case. Next, we derive asymmetric versions for two popular directivity patterns usually applied in the context of microphone arrays, namely the hypercardioid and the supercardioid which are designed to maximize the directivity factor (DF) and the front-to-back ratio (FBR), respectively [6]. Originally, both directivity patterns were developed for the symmetric framework as unconstrained versions, i.e., no directional constraints were imposed except the distortionless constraint in the desired source direction. Herein, we derive constrained versions where additional directional attenuation constraints are imposed. For that case, the asymmetric design achieves better performance with respect to the traditional one, since it enables more flexible design. As expected, the solutions for the asymmetric design are reduced to the solutions presented in [6] where no additional directional attenuation constraints are imposed.

We should note that an asymmetric design of CDMAs was already presented in [33, ch.6] but only for the case of a superdirective beamformer with a single distortionless constraint in the desired source direction. Herein, we present a more general framework for asymmetric design of CDMAs, which is based on the analytical proposed model of the asymmetric beampattern, and enables to derive analytical expressions for both the asymmetric hypercardioid and the supercardioid directivity patterns as well as other general directivity patterns. Yet, for the particular case of optimizing the DF under the distortionless constraint, both solutions are consolidated.

The frequency-invariant beampattern produced by the proposed analytical asymmetric model is then used as the input desired beampattern for a general practical design of Nth-order CDMAs, which enables perfect steering to any azimuthal direction. We show that the solution design proposed in [33], which is based on symmetry, is a particular case of the proposed practical design. In the simulations section, we demonstrate the main advantages of the asymmetric model and compare it to the symmetric one. It is shown that the asymmetric model achieves better performance in terms of WNG, DF, and FBR due to a more flexible design, which takes into account the requirements regarding the null directions. Furthermore, additional degrees of freedom are available for a given number of null directions which can be utilized to choose CDMAs of reduced orders with respect to the minimal order in the symmetric model, and improve robustness to array imperfections.

The paper is organized as follows. In Section II, we formulate the signal model. In Section III, we concisely present the traditional symmetric model of Nth-order CDMAs. In Section IV, we derive asymmetric beampatterns for CDMAs and also develop the equivalent asymmetric hypercardioid and supercardioid. In Section V, we present an Nth-order CDMA practical design for a given number of sensors. Section VI demonstrates some design examples.

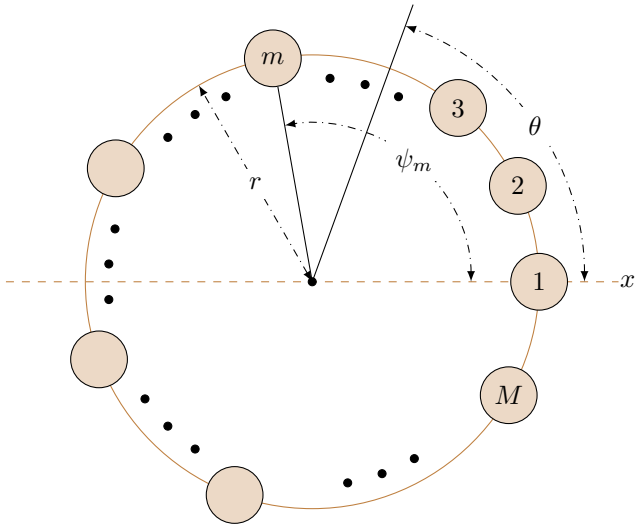

Fig. 1: Illustration of a uniform circular microphone array in the Cartesian coordinate system.

II. Signal Model

We consider an acoustic source signal, $X(\omega)$, with ω being the angular frequency, that propagates in an anechoic acoustic environment at the speed of sound, i.e., $c \approx 340$ m/s, and impinges on a uniform circular array (UCA) of radius r, consisting of M omnidirectional microphones, where the distance between two successive sensors is equal to

$$\delta = 2r \sin\left(\frac{\pi}{M}\right) \approx \frac{2\pi r}{M}. \tag{1}$$

The direction of the source signal to the array is denoted by the azimuth angle $\theta_{\rm s}$. We assume that the center of the UCA coincides with the origin of the Cartesian coordinate system and serves also as the reference. Azimuth angles are measured anti-clockwise from the x axis, i.e., at $\theta = 0°$, and sensor 1 of the array is placed on the x axis, i.e., at $\theta = 0°$, as illustrated in Fig. 1.

Assuming the far-field propagation, the time delay between the mth microphone and the center of the array is

$$t_m(\theta_{\rm s}) = \frac{r}{c}\cos(\theta_{\rm s} - \psi_m), \quad m = 1, 2, ..., M, \tag{2}$$

where

$$\psi_m = \frac{2\pi(m-1)}{M} \tag{3}$$

is the angular position of the mth array element. The mth microphone signal is given by

$$Y_m(\omega) = e^{j\varpi\cos(\theta_{\rm s}-\psi_m)}X(\omega) + V_m(\omega), \ m = 1, ..., M, \tag{4}$$

where $\varpi = \frac{\omega r}{c}$, $j = \sqrt{-1}$ is the imaginary unit, and $V_m(\omega)$ is the additive noise at the mth microphone. In a vector form, (4) becomes

$$\begin{aligned} \mathbf{y}(\omega) &= \begin{bmatrix} Y_1(\omega) & Y_2(\omega) & \cdots & Y_M(\omega) \end{bmatrix}^T \\ &= \mathbf{d}\left(\omega, \theta_{\rm s}\right) X(\omega) + \mathbf{v}(\omega), \end{aligned} \tag{5}$$

where the superscript ^{T} denotes the transpose operator, $\mathbf{d}(\omega, \theta_s)$ is the steering vector at $\theta = \theta_s$, i.e.,

$$\mathbf{d}(\omega, \theta_s) = \left[e^{j\omega t_1(\theta_s)} \cdots e^{j\omega t_M(\theta_s)}\right]^T = \left[e^{j\varpi \cos(\theta_s - \psi_1)} \cdots e^{j\varpi \cos(\theta_s - \psi_M)}\right]^T, \quad (6)$$

the vector $\mathbf{v}(\omega)$ is defined similarly to $\mathbf{y}(\omega)$, and the acoustic wavelength is $\lambda = c/f$. According to the model of the DMAs, it is assumed that the element spacing, δ, is much smaller than the wavelength of the incoming signal, i.e,

$$\delta \ll \lambda, \quad (7)$$

or, equivalently,

$$\varpi \ll M, \quad (8)$$

in order to approximate the differential of the pressure signal.

III. Traditional Symmetric Nth-Order CDMAs

Traditional Nth-order CDMAs were designed to have a symmetric directivity pattern. The directivity pattern describes the sensitivity of the beamformer to a plane wave impinging on the UCA from the direction specified by the pair (θ, ϕ) where θ is the azimuth and ϕ is the elevation. In this paper, we confine ourselves to the 2D case of $\phi = \pi/2$, i.e., the plane where the UCA is laid. The 3D case is a subject to a future research. For the 2D case, the frequency-invariant beampattern of an Nth-order DMA is given, for any steering angle θ_s, as [6]

$$\mathcal{B}_N(\theta - \theta_s) = \sum_{n=0}^{N} a_{N,n} \cos^n(\theta - \theta_s), \quad (9)$$

where $\{a_{N,n}\}_{n=0}^{N}$ are real coefficients. The beampattern $\mathcal{B}_N(\theta - \theta_s)$ is an even function as it is a power series of the cosine function.

Modern Nth-order DMAs have a time-domain hierarchical delay-and-subtract structure and originally proposed for the linear geometry [6]. In general, the response of an Nth-order DMA is proportional to a linear combination of signals derived from spatial derivatives from order 0 to (including) order N and corresponds to the Nth level in the hierarchical structure.

Traditional designs of DMAs focused mainly on the linear geometry which inherently dictates a symmetric beampattern, thus (9) was sufficient for the description of frequency-invariant beampatterns associated with DMAs. Herein, we introduce an asymmetric model for the directivity pattern of Nth-order CDMAs, which exploits the circular structure and incorporates both symmetric and asymmetric beampatterns.

IV. Asymmetric beampattern for CDMAs

In this section, we extend the traditional analytical symmetric beampattern (9) and derive an asymmetric beampattern for CDMAs, where asymmetry means that the beampattern is not confined to be symmetric with respect to the steering angle θ_s, i.e., in the general case $\mathcal{B}_N(\theta - \theta_s) \neq \mathcal{B}_N(-\theta + \theta_s)$. Later, we will see that such a generalized model leads to a more flexible design of CDMAs.

A. Asymmetric Beampattern of Nth-Order CDMAs

We start with the simple first-order asymmetric case and then we generalize it for any desired order, N. First-order CDMAs can be designed with at least three microphones (the case of only two microphones is consolidated with the linear case which was extensively investigated in [14]). The geometry of first-order CDMAs is an equilateral triangle of radius r and the sensor spacing is $\delta = 2r\sin(\pi/3) = \sqrt{3}r$. The positions of the three microphones are

$$\psi_1 = 0, \psi_2 = \frac{2\pi}{3}, \psi_3 = \frac{4\pi}{3}. \quad (10)$$

Assuming a 2D propagation model (i.e., $\phi = \pi/2$), the acoustic propagation field received at each sensor can be expressed as

$$p(k, r, \theta, \psi_m) = P_0 e^{-j\varpi \cos(\theta - \psi_m)}, \quad m = 1, 2, 3, \quad (11)$$

where P_0 is the plane-wave amplitude, and $k = \frac{\omega}{c}$ is the wave number. We may add a complex gain $c_m e^{-j\omega\tau_m}$ at each sensor, sum all the sensors' outputs, and get the output pressure:

$$p_o(k, r, \theta) = P_0 \sum_{m=1}^{3} c_m e^{-j\omega\tau_m} e^{-j\varpi \cos(\theta - \psi_m)}, \quad (12)$$

where c_m is a real number, and τ_m is a temporal delay added to the signal acquired by the mth microphone. Without loss of generality, we assume that $P_0 = 1$, $c_1 = 1$, and $\tau_1 = 0$. Using the approximation that $e^{-x} \approx 1 - x$, (12) becomes

$$p_o(k, r, \theta) \approx 1 + c_2 + c_3 - j\omega \sum_{m=1}^{3} c_m \left[\tau_m + \frac{r}{c}\cos(\theta - \psi_m)\right], \quad (13)$$

where this approximation holds for small values of $\omega\tau_m$ and ϖ in accordance with the DMAs' model assumptions (7) and (8). In order to cancel DC components which have no influence on the shape of the directional response of the array, we impose $c_1 + c_2 + c_3 = 0$, leading to $c_2 + c_3 = -1$, and define

$$\alpha_1 = \frac{\sum_{m=1}^{3} c_m \tau_m}{\sum_{m=1}^{3} c_m \left(\tau_m + \frac{r}{c}\cos\psi_m\right)}, \quad (14)$$

$$1 - \alpha_1 = \frac{\sum_{m=1}^{3} c_m \frac{r}{c}\cos\psi_m}{\sum_{m=1}^{3} c_m \left(\tau_m + \frac{r}{c}\cos\psi_m\right)}, \quad (15)$$

$$\beta_1 = \frac{\sum_{m=1}^{3} c_m \frac{r}{c}\sin\psi_m}{\sum_{m=1}^{3} c_m \left(\tau_m + \frac{r}{c}\cos\psi_m\right)}. \quad (16)$$

Now we can write the normalized response of the first-order asymmetric CDMA as

$$\mathcal{B}_1(\theta) = \frac{p_o(k, r, \theta)}{p_o(k, r, 0)} = \alpha_1 + (1 - \alpha_1)\cos\theta + \beta_1 \sin\theta. \quad (17)$$

It can be easily noticed that the last expression is a generalization of the well-known first-order DMA response [6]. Thus, the proposed design includes also the symmetric design as a particular case. It should be noted that although the normalized response is frequency invariant, the output pressure (13) includes also a first-order high-pass frequency response,

which can be compensated by a first-order low-pass filter [5], [6]. We later see in Section V that by implementing asymmetric CDMAs using a more general design approach in the frequency domain, this high-pass response is inherently compensated.

Note that since we imposed $c_2 + c_3 = -1$, (12) can be rewritten as

$$p_{\mathrm{o}}(k,r,\theta) = x\left[e^{-j\varpi\cos(\theta-\psi_1)} - e^{-j\omega\tau_2 - j\varpi\cos(\theta-\psi_2)}\right] + (1-x)\left[e^{-j\varpi\cos(\theta-\psi_1)} - e^{-j\omega\tau_3 - j\varpi\cos(\theta-\psi_3)}\right], \tag{18}$$

where $x = -c_2$. Therefore, (18) can be interpreted as a weighted sum of the differential of the pressure measured between sensor 1 and sensor 2 and the differential of the pressure measured between sensor 1 and sensor 3. In other words, the first-order output of CDMAs is a linear combination of two first-order linear DMAs outputs.

The fact that DMAs have a hierarchical multistage structure [6] implies that the response of Nth-order DMAs can be described as a cascade of first-order responses, i.e., the total response of Nth-order CDMAs is a product of N responses of first-order DMAs. For example, every two outputs of first-order DMAs on the first stage are the inputs to another first-order DMA in the next stage. When a beamformer is implemented in a multistage way, its beampattern equals the product of the beampatterns of all the different stages [18]. Therefore, the second-order asymmetric CDMA's beampattern can be written as a product of two first-order terms, i.e.,

$$\mathcal{B}_2(\theta) = \prod_{i=1}^{2}\left[\alpha_i + (1-\alpha_i)\cos\theta + \beta_i\sin\theta\right], \tag{19}$$

from which we can easily derive the general form of the second-order asymmetric CDMA:

$$\mathcal{B}_2(\theta) = \upsilon_0 + \upsilon_1\cos\theta + \upsilon_2\cos^2\theta + \upsilon_3\sin\theta\cos\theta + \upsilon_4\sin\theta, \tag{20}$$

where $\{\upsilon_i\}_{i=0}^{4}$ are real coefficients which depend on $\{\alpha_i,\beta_i\}_{i=1}^{2}$. Repeating on similar steps, the following general expressions for the third and fourth orders can be derived, respectively,

$$\mathcal{B}_3(\theta) = \epsilon_0 + \epsilon_1\cos\theta + \epsilon_2\cos^2\theta + \epsilon_3\cos^3\theta + \epsilon_4\sin\theta\cos\theta + \epsilon_5\sin\theta + \epsilon_6\sin^3\theta \tag{21}$$

and

$$\mathcal{B}_4(\theta) = \eta_0 + \eta_1\cos\theta + \eta_2\cos^2\theta + \eta_3\cos^3\theta + \eta_4\cos^4\theta + \eta_5\sin\theta\cos\theta + \eta_6\sin^3\theta\cos\theta + \eta_7\sin\theta + \eta_8\sin^3\theta. \tag{22}$$

Based on the last results, we can obtain the Nth-order asymmetric CDMA beampattern with the mainlobe steered to θ_{s}:

$$\mathcal{B}_N(\theta-\theta_{\mathrm{s}}) = \sum_{n=0}^{N}\xi_n\cos^n(\theta-\theta_{\mathrm{s}}) + \sum_{n=0}^{\lfloor\frac{N-1}{2}\rfloor}\mu_n\sin^{2n+1}(\theta-\theta_{\mathrm{s}}) + \sum_{n=1}^{\lfloor\frac{N}{2}\rfloor}\zeta_n\cos(\theta-\theta_{\mathrm{s}})\sin^{2n-1}(\theta-\theta_{\mathrm{s}}), \tag{23}$$

which is a trigonometric polynomial of power N with $2N$ roots. Note that (23) is a general expression for the beampattern which can be reduced to the traditional symmetric beampattern (9) by setting the coefficients $\{\zeta_n,\mu_n\}_n$ to zero.

In order to prove that (23) is indeed the general theoretical expression for all possible beampatterns of CDMAs of order N, we may refer to the Fourier theorem stating that each function $f(\theta) \in \mathbb{F}$, where $\mathbb{F}$ is the space of continuous functions in $[-\pi,\pi]$, can be represented by the infinite series:

$$f(\theta) = \sum_{n=0}^{\infty}\left[a_n\cos(n\theta) + b_n\sin(n\theta)\right], \tag{24}$$

where

$$a_n = \frac{1}{\pi}\int_{-\pi}^{\pi} f(\theta)\cos(n\theta)\,d\theta, \quad n = 0,1,2,... \tag{25}$$

$$b_n = \frac{1}{\pi}\int_{-\pi}^{\pi} f(\theta)\sin(n\theta)\,d\theta, \quad n = 0,1,2,... \tag{26}$$

Let $f_N(\theta) \in \mathbb{F}_N \subset \mathbb{F}$, where $\mathbb{F}_N$ is a subspace of all the continuous functions in $[-\pi,\pi]$, which can be represented by the following finite series:

$$f_N(\theta) = \sum_{n=0}^{N}\left[a_n\cos(n\theta) + b_n\sin(n\theta)\right]. \tag{27}$$

In the Appendix, we show that every function $f_N(\theta) \in \mathbb{F}_N$ can also be represented by (23). Actually, we show that the space of functions specified by (27) is equivalent to the space of functions specified by (23) for each N. This equivalence ensures that for an Nth-order beampattern, only the basis functions $\{\cos(n\theta),\sin(n\theta)\}_{n=0}^{N}$ are required. Since it is true for each N and particularly when $N \to \infty$, it is obvious that (23) is the general expression for any Nth-order asymmetric beampattern. Therefore, we can express (23) more compactly as

$$\mathcal{B}_N(\theta-\theta_{\mathrm{s}}) = \sum_{n=0}^{N}a_n\cos\left[n(\theta-\theta_{\mathrm{s}})\right] + \sum_{n=1}^{N}b_n\sin\left[n(\theta-\theta_{\mathrm{s}})\right]. \tag{28}$$

Note that (28) is a trigonometric polynomial with $2N+1$ coefficients, which implies that at least $2N+1$ sensors are required in order to implement Nth-order asymmetric CDMAs, as will be discussed in Section V. In contrast, the traditional symmetric beampattern (9) is a trigonometric polynomial with $N+1$ coefficients, which implies that only $N+1$ sensors are required for implementing symmetric Nth-order DMAs.

While this is true for the linear geometry, for the circular geometry, still at least $2N$ sensors are required as presented in [33].

In the next subsections, we develop the equivalent hypercardioid and the equivalent supercardioid optimal patterns for the case of asymmetric CDMAs. For convenience, we use (28) instead of (23).

B. Optimal Asymmetric Hypercardioid

The most common directivity patterns in the context of microphone arrays are the dipole, cardioid, hypercardioid, and supercardioid, which were obtained via optimization with respect to various criteria. For example, the hypercardioid was designed to maximize the DF of the array which is the gain in signal-to-noise ratio (SNR) for the case of diffuse noise. These patterns, originally developed for the linear geometry, are traditionally symmetric with respect to the steering angle, $\theta_{\rm s}$.

The proposed analytical model for the asymmetric beampattern of CDMAs (28) can be used to produce several beampatterns which can be controlled by the adjustment of its coefficients. In this section, we derive the equivalent asymmetric hypercardioid, i.e., the beampattern that maximizes the DF, which is defined as (see for example [35, ch.2])

$$\mathcal{D}=\frac{\mathcal{B}^2\left(\theta_{\rm s},\phi_{\rm s}\right)}{\frac{1}{4\pi}\int_0^{2\pi}\int_0^{\pi}\mathcal{B}^2\left(\theta,\phi\right)\sin\phi d\phi d\theta}, \tag{29}$$

where $\mathcal{B}\left(\theta,\phi\right)$ is a 3D beampattern and $(\theta_{\rm s},\phi_{\rm s})$ specifies the steering direction. In our study, we are concentrating on the 2D scenario for which the beampattern is a function of only the azimuthal angle, θ, i.e.,

$$\mathcal{B}_N\left(\theta-\theta_{\rm s}\right)=\mathcal{B}\left(\theta-\theta_{\rm s},\phi=\pi/2\right), \tag{30}$$

and (29) is actually the DF for the cylindrical noise field model. A cylindrical noise field model is often assumed for scenarios where the reflections from the floor or the ceiling of the room are negligible. Without loss of generality, we assume that $\theta_{\rm s}=0^\circ$. It is obvious that

$$\mathcal{D}^{-1}=\frac{1}{2\pi}\int_0^{2\pi}\mathcal{B}_N^2\left(\theta\right)d\theta. \tag{31}$$

From Fourier Theorem it is known that the basis functions $\{\cos(n\theta),\sin(n\theta)\}_{n=0}^{\infty}$ that appear in (28) form a complete orthonormal system, therefore it is straightforward to show that

$$\int_0^{2\pi}\mathcal{B}_N^2\left(\theta\right)d\theta=\mathbf{c}^T\mathbf{\Gamma}_{\rm h}\mathbf{c}, \tag{32}$$

where

$$\mathbf{c}=\left[a_0,a_1,...,a_N,b_1,...,b_N\right]^T \tag{33}$$

is a vector of length $2N+1$ containing the coefficients of the asymmetric beampattern (28), and the matrix $\mathbf{\Gamma}_{\rm h}$ is diagonal of size $(2N+1)\times(2N+1)$, where its diagonal elements are

$$\left[\mathbf{\Gamma}_{\rm h}\right]_{n,n}=\begin{cases}\int_0^{2\pi}\cos^2\left(n\theta\right)d\theta, & n=0,1,...,N\\ \int_0^{2\pi}\sin^2\left[(n-N)\theta\right]d\theta, & n=N+1,...,2N.\end{cases} \tag{34}$$

Calculation of (34) yields the following compact expression:

$$\mathbf{\Gamma}_{\rm h}=\pi{\rm diag}\left(\left[2,\mathbf{1}_{2N}^T\right]^T\right), \tag{35}$$

where ${\rm diag}(\mathbf{x})$ is a diagonal matrix with the elements of the vector $\mathbf{x}$ on its diagonal, and $\mathbf{1}_{2N}$ is a $2N\times 1$ column vector with all elements equal to one.

According to (31), maximizing the DF is equivalent to minimizing (32). Yet, minimizing (32) without any constraints will obviously lead to the trivial solution $\mathbf{c}=\mathbf{0}$. Therefore, at least one directional constraint should be imposed, either for the symmetric design or the asymmetric design, namely the distortionless constraint:

$$\mathcal{B}_N\left(\theta_{\rm s}=0^\circ\right)=1, \tag{36}$$

which leads to

$$\sum_{n=0}^{N}a_n=1. \tag{37}$$

One can see that (37) constrains the coefficients $\{a_n\}_{n=0}^N$ to each other, but still the coefficients $\{a_n\}_{n=0}^N$ and $\{b_n\}_{n=1}^N$ are independent by the diagonality of $\mathbf{\Gamma}_{\rm h}$. Thus, the circular geometry provides additional degrees of freedom in the design of optimal patterns such as the hypercardioid, which can be exploited to achieve higher performance when it is desirable to impose additional directional constraints. In that case, we can add up to $L\leq 2N$ attenuation constraints of the form:

$$\mathcal{B}_N\left(\theta=\theta_l\right)=g_l,\quad l=1,2,...,L, \tag{38}$$

where $0\leq g_l\leq 1$. We formulate these constraints as

$$\mathbf{H}_{\rm c}\mathbf{c}=\mathbf{g}, \tag{39}$$

where $\mathbf{H}_{\rm c}$ is the constraint matrix of size $(L+1)\times(2N+1)$. The vector $\mathbf{g}$ of length $L+1$ contains the coefficients g_l, $l=1,2,...,L$, and a single unity entry satisfying (36).

The optimization problem for the asymmetric hypercardioid beampattern can be formulated as

$$\min_{\mathbf{c}}\quad\mathbf{c}^T\mathbf{\Gamma}_{\rm h}\mathbf{c}\quad\text{ subject to }\quad\mathbf{H}_{\rm c}\mathbf{c}=\mathbf{g}. \tag{40}$$

Using the method of Lagrange multipliers, we get the following closed-form expression:

$$\mathbf{c}_{\rm opt}=\mathbf{\Gamma}_{\rm h}^{-1}\mathbf{H}_{\rm c}^T\left[\mathbf{H}_{\rm c}\mathbf{\Gamma}_{\rm h}^{-1}\mathbf{H}_{\rm c}^T\right]^{-1}\mathbf{g}. \tag{41}$$

This solution yields the optimal asymmetric hypercardioid CDMA for a cylindrical noise field. Note that even though we can add up to $2N$ constraints, it is obvious that a lower number of attenuation constraints leads to more flexibility and higher DF. Specifically, if we add exactly $2N$ attenuation constraints, (40) has no meaning and (39) should be solved directly. Moreover, if no additional constraints except (36) are imposed, (41) reduces to the solution of the symmetric unconstrained hypercardioid in [6]. In Section VI-A, two design examples of a second-order asymmetric hypercardioid are presented and compared to the symmetric design.

C. Optimal Asymmetric Supercardioid

In this section, we develop the asymmetric version of the supercardioid for CDMAs. The supercardioid pattern maximizes the FBR of an array [6], which is defined as the ratio between the directional gain of the microphone to signals propagating to the front of the microphone relative to signals propagating to the rear. For a cylindrical noise field, the FBR is defined as

$$\mathcal{F} = \frac{\int_{-\pi/2}^{\pi/2} \mathcal{B}_N^2(\theta)\, d\theta}{\int_{\pi/2}^{3\pi/2} \mathcal{B}_N^2(\theta)\, d\theta}, \tag{42}$$

where we assume, without loss of generality, that the steering angle is $\theta_{\mathrm{s}} = 0^{\circ}$. Similarly to the hypercardioid, it can be shown that

$$\int_{-\pi/2}^{\pi/2} \mathcal{B}_N^2(\theta)\, d\theta = \mathbf{c}^T \mathbf{\Gamma}_{\mathrm{f}} \mathbf{c} \tag{43}$$

and

$$\int_{\pi/2}^{3\pi/2} \mathcal{B}_N^2(\theta)\, d\theta = \mathbf{c}^T \mathbf{\Gamma}_{\mathrm{b}} \mathbf{c}, \tag{44}$$

where the vector $\mathbf{c}$ is defined in (33), and the matrices $\mathbf{\Gamma}_{\mathrm{f}}$ and $\mathbf{\Gamma}_{\mathrm{b}}$ are diagonal, with

$$[\mathbf{\Gamma}_{\mathrm{f}}]_{n,n} = \begin{cases} \int_{-\pi/2}^{\pi/2} \cos^2(n\theta)\, d\theta, & n = 0, 1, ..., N \\ \int_{-\pi/2}^{\pi/2} \sin^2[(n-N)\theta]\, d\theta, & n = N+1, ..., 2N \end{cases} \tag{45}$$

and

$$[\mathbf{\Gamma}_{\mathrm{b}}]_{n,n} = \begin{cases} \int_{\pi/2}^{3\pi/2} \cos^2(n\theta)\, d\theta, & n = 0, 1, ..., N \\ \int_{\pi/2}^{3\pi/2} \sin^2[(n-N)\theta]\, d\theta, & n = N+1, ..., 2N. \end{cases} \tag{46}$$

Similarly to $\mathbf{\Gamma}_{\mathrm{h}}$, both $\mathbf{\Gamma}_{\mathrm{f}}$ and $\mathbf{\Gamma}_{\mathrm{b}}$ can be expressed in a compact form as

$$\mathbf{\Gamma}_{\mathrm{f}} = \mathbf{\Gamma}_{\mathrm{b}} = \frac{\pi}{2} \mathrm{diag}\left(\left[2, \mathbf{1}_{2N}^T \right]^T \right). \tag{47}$$

Like in the previous case of the hypercardioid, we can add the linear directional constraints specified by (39) in order to achieve some benefits from the asymmetric framework. Now we can formulate the optimization problem which provides the asymmetric supercardioid beampattern:

$$\max_{\mathbf{c}} \quad \frac{\mathbf{c}^T \mathbf{\Gamma}_{\mathrm{f}} \mathbf{c}}{\mathbf{c}^T \mathbf{\Gamma}_{\mathrm{b}} \mathbf{c}} \qquad \text{subject to} \quad \mathbf{H}_{\mathrm{c}} \mathbf{c} = \mathbf{g}. \tag{48}$$

Rather than solving (48), we solve the equivalent problem:

$$\max_{\hat{\mathbf{c}}} \frac{\hat{\mathbf{c}}^T \hat{\mathbf{\Gamma}}_{\mathrm{f}} \hat{\mathbf{c}}}{\hat{\mathbf{c}}^T \hat{\mathbf{\Gamma}}_{\mathrm{b}} \hat{\mathbf{c}}} \quad \text{subject to } \hat{\mathbf{H}}_{\mathrm{c}} \hat{\mathbf{c}} = \mathbf{0}, \tag{49}$$

where

$$\hat{\mathbf{c}} = \begin{bmatrix} \mathbf{c} \\ -1 \end{bmatrix}, \hat{\mathbf{H}}_{\mathrm{c}} = \begin{bmatrix} \mathbf{H}_{\mathrm{c}} & \mathbf{g} \end{bmatrix}, \hat{\mathbf{\Gamma}}_{\mathrm{f}} = \begin{bmatrix} \mathbf{\Gamma}_{\mathrm{f}} & \mathbf{0} \\ \mathbf{0}^T & 0 \end{bmatrix}, \hat{\mathbf{\Gamma}}_{\mathrm{b}} = \begin{bmatrix} \mathbf{\Gamma}_{\mathrm{b}} & \mathbf{0} \\ \mathbf{0}^T & 0 \end{bmatrix}. \tag{50}$$

Let $\mathbf{D}$ be a null-space matrix of $\hat{\mathbf{H}}_{\mathrm{c}}$ (i.e., $\hat{\mathbf{H}}_{\mathrm{c}} \mathbf{D} = \mathbf{0}$) of size $(2N+2) \times (2N+1-L)$ and rank of $2N+1-L$, which contains $2N+1-L$ basis vectors in its columns, and let $\hat{\mathbf{c}} = \mathbf{D}\tilde{\mathbf{c}}$. Note that the matrices $\mathbf{D}^T \hat{\mathbf{\Gamma}}_{\mathrm{f}} \mathbf{D}$ and $\mathbf{D}^T \hat{\mathbf{\Gamma}}_{\mathrm{b}} \mathbf{D}$ are full-rank even though $\hat{\mathbf{\Gamma}}_{\mathrm{f}}$ and $\hat{\mathbf{\Gamma}}_{\mathrm{b}}$ are not full rank since the product matrices $\mathbf{D}^T \hat{\mathbf{\Gamma}}_{\mathrm{f}} \mathbf{D}$ and $\mathbf{D}^T \hat{\mathbf{\Gamma}}_{\mathrm{b}} \mathbf{D}$ are of size $(2N+1-L) \times (2N+1-L)$ with a rank of $(2N+1-L)$, i.e, full-rank matrices. Thus, we transform (49) to the following unconstrained optimization problem [36], [37]:

$$\max_{\tilde{\mathbf{c}}} \frac{\tilde{\mathbf{c}}^T \mathbf{D}^T \hat{\mathbf{\Gamma}}_{\mathrm{f}} \mathbf{D} \tilde{\mathbf{c}}}{\tilde{\mathbf{c}}^T \mathbf{D}^T \hat{\mathbf{\Gamma}}_{\mathrm{b}} \mathbf{D} \tilde{\mathbf{c}}}. \tag{51}$$

The solution to (51) is the generalized eigenvector of $\mathbf{D}^T \hat{\mathbf{\Gamma}}_{\mathrm{f}} \mathbf{D}$ and $\mathbf{D}^T \hat{\mathbf{\Gamma}}_{\mathrm{b}} \mathbf{D}$ that corresponds to the maximal generalized eigenvalue, i.e.,

$$\mathbf{D}^T \hat{\mathbf{\Gamma}}_{\mathrm{f}} \mathbf{D} \tilde{\mathbf{c}}_{\mathrm{opt}} = \lambda_{\max} \mathbf{D}^T \hat{\mathbf{\Gamma}}_{\mathrm{b}} \mathbf{D} \tilde{\mathbf{c}}_{\mathrm{opt}}. \tag{52}$$

Finally, we reconstruct $\mathbf{c}$ from $\tilde{\mathbf{c}}_{\mathrm{opt}}$.

Similarly to the previous case of the hypercardioid, if no additional constraints except (36) are imposed, (52) reduces to the solution of the symmetric unconstrained supercardioid in [6].

In Section VI-B, two design examples of a third-order asymmetric supercardioid are presented and compared to the symmetric design.

The theoretical framework of the asymmetric CDMAs which has been developed in this section, may provide much more flexible design of broadband beamformers based on CDMAs with improved performance level. In the next section, we present a general framework for a practical implementation of Nth-order asymmetric CDMAs, whose inputs are the analytical optimal asymmetric beampatterns derived in this section.

V. Practical Design for Asymmetric CDMAs

In this section, we present a general framework for a practical implementation of asymmetric CDMAs. One way to implement CDMAs is by the conventional time-domain approach [6]. This approach is limited by some aspects like the flexibility to forming different patterns and the ability to handle white noise amplification. Instead, we may employ here a more general approach in the frequency domain as described in details in [14], [33]. The major advantages of the frequency-domain design with respect to the traditional time-domain design are the following. 1) It is easier to design different patterns by using only the null and attenuation information. 2) The high-pass response of the time-domain implementation is inherently compensated by the design in the frequency domain. 3) It enables to apply a minimum-norm approach that can maximize the WNG with a given number of sensors, i.e., the frequency-domain framework is suitable for any number of sensors, while the traditional approach is suitable only for the case of $M = N+1$. 4) It is well-known that frequency-domain processing of broadband signals has several advantages with respect to time-domain broadband processing by means of lower computational complexity and high convergence rate [38], and in some applications, beamforming will serve as a pre-processing stage followed by a second adaptive processing stage implemented more efficiently in the frequency-domain (e.g., de-reverberation, speech enhancement). Due to all these reasons, we propose to implement asymmetric CDMAs by the following approach.

The solutions for the optimal asymmetric hypercardioid and supercardioid, derived in the previous section, yield the vector $\mathbf{c}$ which is used to build the corresponding theoretical beampattern (28), which is a trigonometric polynomial with $2N$ zeros. Recall that during the design of the asymmetric hypercardioid and the asymmetric supercardioid we impose in (38) up to $L \leq 2N$ directional attenuation constraints denoted by $\{\theta_l\}_{l=1}^{L}$. We use these L directions to the following processing, and calculate $2N-L$ additional null directions of the beampattern, by numerical standard methods of finding roots. At the end of this process we have the column vector:

$$\boldsymbol{\theta} = [\theta_1, ..., \theta_{2N}]^T \tag{53}$$

of length $2N$, where these directions are with respect to a steering angle of $\theta_{\mathrm{s}} = 0^\circ$. The next step is to implement the beamformer with the attenuation directions specified by the vector $\boldsymbol{\theta}$. Note that the rotation to any different steering angle is straightforward.

The following design generalizes the derivation of CDMAs proposed in [33]. The main contribution of [33] is a symmetric design of CDMAs for the angle $\theta = 0^\circ$ which can be steered directly to each of the other sensor angles, $\psi_m,\ m = 2, ..., M$, without any change in the properties of the beamformer. Herein, we present a general asymmetric design which enables to steer to all azimuthal directions without any change in the beampattern, WNG, DF, or FBR. This solution coincides with the solution in [33] for the case of symmetric design and steering to one of the sensors directions, $\psi_m,\ m = 1, 2, ..., M$, therefore the solution proposed in [33] is considered as a particular case.

Nth-order asymmetric CDMAs can be designed with at least $2N+1$ microphones for the general case where the steering angle can be each of the azimuthal directions [33]. This is because in the general Nth-order design we enforce $2N$ attenuation constraints and one distortionless constraint. For the case of symmetric design with steering to $\psi_m,\ m = 1, 2, ..., M$, only $2N$ microphones are sufficient because the symmetry constraint enables to reduce the total number of the attenuation constraints.

In order to design the asymmetric CDMAs, we have to apply the distortionless constraint in the desired signal direction, θ_{s}, i.e.,

$$\mathbf{d}^H(\omega, \theta_{\mathrm{s}})\, \mathbf{h}(\omega) = 1, \tag{54}$$

where

$$\mathbf{h}(\omega) = [H_1(\omega) \quad H_2(\omega) \quad \cdots \quad H_M(\omega)]^T \tag{55}$$

is a vector containing the complex weights of the beamformer, and $\mathbf{d}(\omega, \theta)$ is the steering vector (6). Then, we have $2N$ additional directional constraints of the form

$$\mathbf{d}^H(\omega, \theta_{\mathrm{s}} + \theta_i)\, \mathbf{h}(\omega) = \nu_i, \quad i = 1, ..., 2N, \tag{56}$$

where $\nu_i,\ i = 1, 2, \ldots, 2N$, are the attenuation parameters, with $0 \leq \nu_i \leq 1$, and $\theta_i \in \boldsymbol{\theta},\ i = 1, 2, \ldots, 2N$, with $\theta_1 \neq \theta_2 \neq \cdots \neq \theta_{2N}$, are the corresponding directions where the attenuations are desired ($\nu_l = g_l, \forall l = 1, ..., L$, and $\nu_l = 0, \forall l = L+1, ..., 2N$). Combining these $2N+1$ constraints together, we get the following linear system to solve

$$\mathbf{D}_{N,M}(\omega, \theta_{\mathrm{s}}, \boldsymbol{\theta})\mathbf{h}(\omega) = \boldsymbol{\nu}, \tag{57}$$

where

$$\mathbf{D}_{N,M}(\omega, \theta_{\mathrm{s}}, \boldsymbol{\theta}) = \begin{bmatrix} \mathbf{d}^H(\omega, \theta_{\mathrm{s}}) \\ \mathbf{d}^H(\omega, \theta_{\mathrm{s}} + \theta_1) \\ \vdots \\ \mathbf{d}^H(\omega, \theta_{\mathrm{s}} + \theta_{2N}) \end{bmatrix} \tag{58}$$

is a $(2N+1) \times M$ matrix and the vector $\boldsymbol{\nu}$ is

$$\boldsymbol{\nu} = \begin{bmatrix} 1 & \nu_1 & \nu_2 & \cdots & \nu_{2N} \end{bmatrix}^T. \tag{59}$$

Practically, it is desired to add a constraint on the squared norm of the solution vector $\mathbf{h}(\omega)$, which is inversely proportional to the WNG and minimizes the objective function

$$J(\mathbf{h}(\omega)) = \|\boldsymbol{\nu} - \mathbf{D}_{N,M}(\omega, \theta_{\mathrm{s}}, \boldsymbol{\theta})\mathbf{h}(\omega)\|_2^2 + \eta \|\mathbf{h}(\omega)\|_2^2, \tag{60}$$

where $||\cdot||_2$ is ℓ_2-norm. The small positive parameter η is usually set according to the desired WNG, where the WNG is given by [33]

$$\mathcal{W}[\mathbf{h}(\omega)] = \frac{\left|\mathbf{h}^H(\omega)\, \mathbf{d}(\omega, \theta_{\mathrm{s}})\right|^2}{\mathbf{h}^H(\omega)\, \mathbf{h}(\omega)}, \tag{61}$$

which is a measure indicating the array gain in the presence of uncorrelated white noise. It also indicates the sensitivity of the array to model mismatch errors [35].

Assuming $M \geq 2N+1$, and using the method of Lagrange multipliers we can obtain the regularized pseudo-inverse solution:

$$\mathbf{h}(\omega) = \mathbf{P}^{\dagger}_{\mathbf{D}_{N,M}}(\omega, \theta_{\mathrm{s}}, \boldsymbol{\theta})\boldsymbol{\nu}, \tag{62}$$

where

$$\mathbf{P}^{\dagger}_{\mathbf{X}} = \left[\mathbf{X}^H\mathbf{X} + \eta\mathbf{I}\right]^{-1}\mathbf{X}^H \tag{63}$$

is the pseudo-inverse of a matrix $\mathbf{X}$, and $\mathbf{I}$ is the identity matrix with the same dimensions as the matrix $\mathbf{X}^H\mathbf{X}$.

Although (62) depends on frequency and its structure is different from the traditional time-domain DMAs [6], it indeed leads to an equivalent implementation of differential beamforming with frequency-invariant beampatterns as presented in [14] for the linear symmetric case, and in [33] for the circular case. Specifically, the authors of [14] show analytically that for each ω satisfying the DMAs model assumption (7), the beampattern obtained by the frequency domain design is very similar to the theoretical one obtained by the time-domain design. Moreover, the simulations presented in the next section support this claim. Therefore, as both the frequency- and time-domain designs are equivalent, the proposed frequency-domain design yields a frequency-invariant differential beamformer.

Notice that for a design of beampatterns with multiple nulls in the same directions like dipole and cardioid, $\mathbf{D}_{N,M}(\omega, \theta_{\mathrm{s}}, \boldsymbol{\theta})$ becomes singular. In order to overcome this singularity, we can add constraints on the derivatives of the steering vector in directions of the multiple nulls. Derivative constraints are known in the literature and have recently also been applied to DMAs [39].

VI. Simulations

In this section, we demonstrate some of the benefits of the asymmetric design with respect to the traditional symmetric one. We start with two examples demonstrating how to design optimal second-order asymmetric hypercardioid according to Section IV-B, and optimal third-order asymmetric supercardioid according to Section IV-C. Then, we proceed to present two more examples of a practical design of CDMAs according to Section V. The first practical design example is for the simple case of a first-order asymmetric design, and the second example is for higher order.

A. An Optimal Second-Order Asymmetric Hypercardioid

Figure 2 shows beampatterns of two design examples for the second-order asymmetric hypercardioid, obtained by the calculation of (41). In the first example (a), we choose two null directions at $\theta_1 = 60°$ and $\theta_2 = 110°$. Three beampatterns are compared. The first is the asymmetric beampattern (blue solid line), the second is the corresponding symmetric version beampattern (black dashed line), i.e., the beampattern obtained by enforcing the above two null directions plus the symmetry constraint. The third beampattern is the second-order unconstrained symmetric hypercardioid (red circles line) which is obtained by maximization of the DF without any constraints on the null directions [6]. The symmetric design achieves slightly narrower mainbeam but much higher sidelobes with respect to the asymmetric design and the unconstrained symmetric design. In the second example (b), we choose two null directions at $\theta_1 = 120°$, and $\theta_2 = 295°$. Table I shows the DF (31) obtained by each of the designs for both examples. One can see that while in the asymmetric design, the DF approaches the optimal value, the symmetric design achieves much lower DF with respect to the theoretical upper bound associated with the unconstrained symmetric design. In both examples we choose $\theta_s = 0°$, yet, the modification to any direction is straightforward.

TABLE I: Directivity Factor Achieved by Each of the Designs of a Second-Order Hypercardioid.

$\mathcal{D}$[dB]	(a)	(b)
Asymmetric	6.22	6.70
Symmetric	2.63	5.50
Unconstrained symmetric	6.98	6.98

B. An Optimal Third-Order Asymmetric Supercardioid

Figure 3 shows beampatterns of two design examples for the third-order asymmetric supercardioid, obtained by the calculation of (52). In the first example (a), we choose three null directions at $\theta_1 = 80°$, $\theta_2 = 120°$, and $\theta_3 = 155°$. Three beampatterns are compared. The first is the asymmetric beampattern (blue solid line), the second is the corresponding symmetric version beampattern (black dashed line), i.e., the beampattern obtained by enforcing the above three null directions plus the symmetry constraint. The third beampattern is the third-order unconstrained symmetric supercardioid (red circles line) which is obtained by maximization of the FBR without any constraints on the null directions [6]. The symmetric design achieves slightly narrower mainbeam but much higher sidelobes with respect to the asymmetric design and the unconstrained symmetric design. In the second example (b), we choose three null directions at $\theta_1 = 75°$, $\theta_2 = 105°$, and $\theta_3 = 240°$. Table II shows the FBR (42) obtained by each of the designs in each example. One can see that while in the asymmetric design, the FBR approaches the optimal value, the symmetric design achieves much lower FBR with respect to the unconstrained symmetric design. These examples show that the proposed asymmetric design achieves superior results with respect to the symmetric design, as more flexibility is allowed in the null directions. We now demonstrate two examples of a practical design of asymmetric CDMAs, based on what we have presented in Section V.

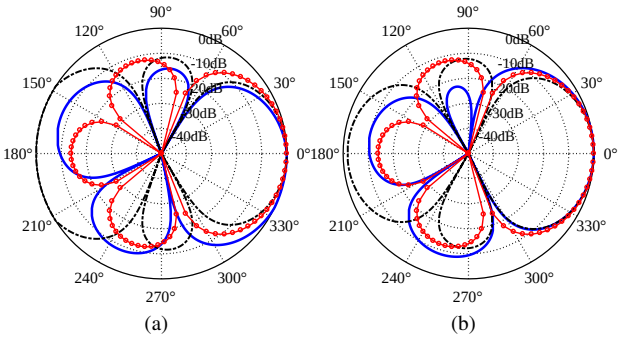

Fig. 2: Beampatterns for the second-order asymmetric hypercardioid CDMAs (blue solid line) and its symmetric version (black dashed line). The red circles line is the second-order unconstrained symmetric hypercardioid [6]. (a) $\theta_1 = 60°$, $\theta_2 = 110°$. (b) $\theta_1 = 120°$, $\theta_2 = 295°$.

TABLE II: Front-to-Back-Ratio Achieved by Each of the Designs of a Third-Order Supercardioid.

$\mathcal{F}$[dB]	(a)	(b)
Asymmetric	35.0	33.8
Symmetric	29.7	19.8
Unconstrained symmetric	40.6	40.6

C. Asymmetric Implementation of First-Order CDMAs

Herein, we present a design example of a first-order asymmetric hypercardioid and compare it to the symmetric design. We choose the radius of the array to be $r = 0.75$ cm and $M = 3$ which leads to a sensor spacing of $\delta \approx 1.3$ cm. For this choice of parameters, we get a small value of $\varpi \approx 0.15 \ll M$ justifying the approximation on (13). Let us assume that the steering angle is $\theta_s = 0°$ and we would like to null signals arriving from $\theta_1 = 95°$. Substituting these constraints into (39), and solving (41), we get the optimal coefficients vector, $\mathbf{c}$ (33), used to calculate the analytical first-order asymmetric beampattern (28):

$$\mathcal{B}_1(\theta) = 0.261 + 0.738\cos\theta - 0.1977\sin\theta, \qquad (64)$$

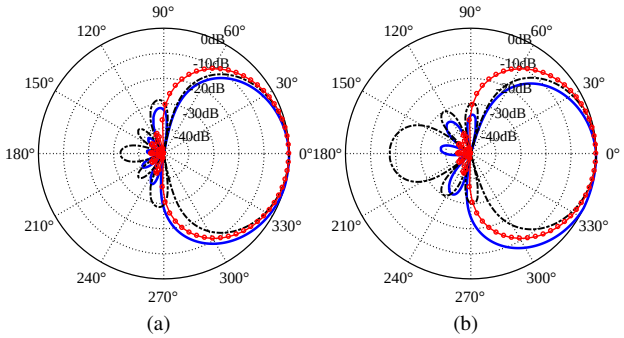

Fig. 3: Beampatterns for the third-order asymmetric supercardioid CDMAs (blue solid line) and its symmetric version (black dashed line). The red circles line is the third-order unconstrained symmetric supercardioid [6]. (a) $\theta_1 = 80°$, $\theta_2 = 120°$, $\theta_3 = 155°$. (b) $\theta_1 = 75°$, $\theta_2 = 105°$, $\theta_3 = 220°$.

which is a first-order trigonometric polynomial with two roots. The second root is $\theta_2 = 235°$. Figure 4 shows the analytical beampattern of the first-order asymmetric design (blue solid line), the symmetric version (black dashed line), i.e., the beampattern for the case that $\theta_1 = 95°$ and $\theta_2 = 265°$, and also the first-order unconstrained symmetric hypercardioid (red circles line), which was obtained in [6] for a null at $\theta_1 = 120°$. The asymmetric design leads to the desired beampattern which is similar to the unconstrained hypercardioid but with a slight bias in the azimuth in order to satisfy both the distortionless and the null constraints. In contrast to the asymmetric design, the symmetric design achieves a beampattern with a much wider and higher sidelobe.

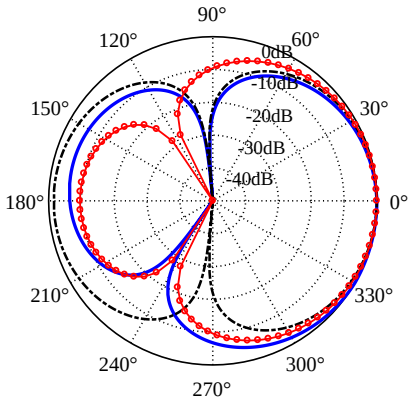

Fig. 4: A first-order asymmetric hypercardioid beampattern (blue solid line) obtained by (28) and a symmetric beampattern (black dashed line) obtained by imposing symmetry, for the case of $M = 3$ sensors, and desired null at $\theta_1 = 95°$. The red circles line is the first-order unconstrained hypercardioid [6].

The null directions calculated from (28) are then used to design the first-order asymmetric CDMA filter vector $\mathbf{h}(\omega)$ according to (62), where we used the regularization parameter $\eta = 10^{-8}$. We calculate the designed beampattern defined as

$$\begin{aligned}\mathcal{B}\left[\mathbf{h}(\omega),\theta\right] &= \mathbf{h}^H(\omega)\mathbf{d}(\omega,\theta) \\ &= \sum_{m=1}^{M} H_m^*(\omega)e^{j\varpi\cos(\theta-\psi_m)},\end{aligned} \tag{65}$$

where $\mathbf{d}(\omega,\theta)$ is the steering vector (6). While (65) is the designed beampattern, (28) is the theoretical asymmetric beampattern.

Figure 5 shows $\mathcal{B}\left[\mathbf{h}(\omega),\theta\right]$ for the first-order asymmetric hypercardioid (a)-(b), the symmetric hypercardioid (c)-(d), and the first-order unconstrained hypercardioid (e)-(f), for different frequencies and steering angles. The black dashed line is the designed beampattern (65), while the blue circles line is the analytical beampattern (28). One can see that the beampatterns in both cases are frequency-invariant and also rotation-invariant in the azimuthal axis. These properties make the circular geometry very suitable to processing broadband signals which can come from any azimuthal direction.

Note that when the steering angle coincides with one of the other sensors' directions (i.e., ψ_2, ψ_3), the filter coefficients vector, $\mathbf{h}(\omega)$ (62) is a permutation of the vector designed for the case of $\theta_s = \psi_1 = 0°$. This observation implies that the proposed solution is general, which includes also the previous solution [33] as a particular case, as this property is satisfied also by the solution derived in [33].

Figure 6 shows the WNG and DF as a function of frequency for the practical design of a first-order asymmetric hypercardioid (blue solid line), the symmetric hypercardioid (black dashed line), and the first-order unconstrained symmetric hypercardioid (red circles line). The DF for the case of a cylindrically diffuse noise is calculated similarly to (31) as

$$\mathcal{D}\left[\mathbf{h}(\omega)\right] = \frac{2\pi}{\int_0^{2\pi} |\mathcal{B}\left[\mathbf{h}(\omega),\theta\right]|^2 d\theta}. \tag{66}$$

The performance of the asymmetric design is very close to that of the unconstrained symmetric hypercardioid, while the non-optimal symmetric design achieves lower DF. The WNG of all three considered methods has similar behavior and is quite poor in low frequencies which is a drawback of DMAs. In the next subsection, we show how a higher-order asymmetric design can be exploited to achieve better WNG, and discuss about other ways to improve it even further.

The results presented in this section demonstrate the benefit of the asymmetric design, which can be exploited for the circular geometry. For this simple first-order example, it is obvious that higher DF can be obtained with respect to the standard symmetric design for a given required null direction.

D. Second-Order CDMAs With More Than Two Imposed Nulls

In this section, we present a design example for the second-order hypercardioid and exemplify another advantage of the asymmetric framework. Traditionally, in the Nth-order DMAs symmetric design up to N distinct nulls could be imposed. Herein, we show that the proposed asymmetric design may enable more than N imposed nulls for order N. This is an important property of the asymmetric design as it enables to

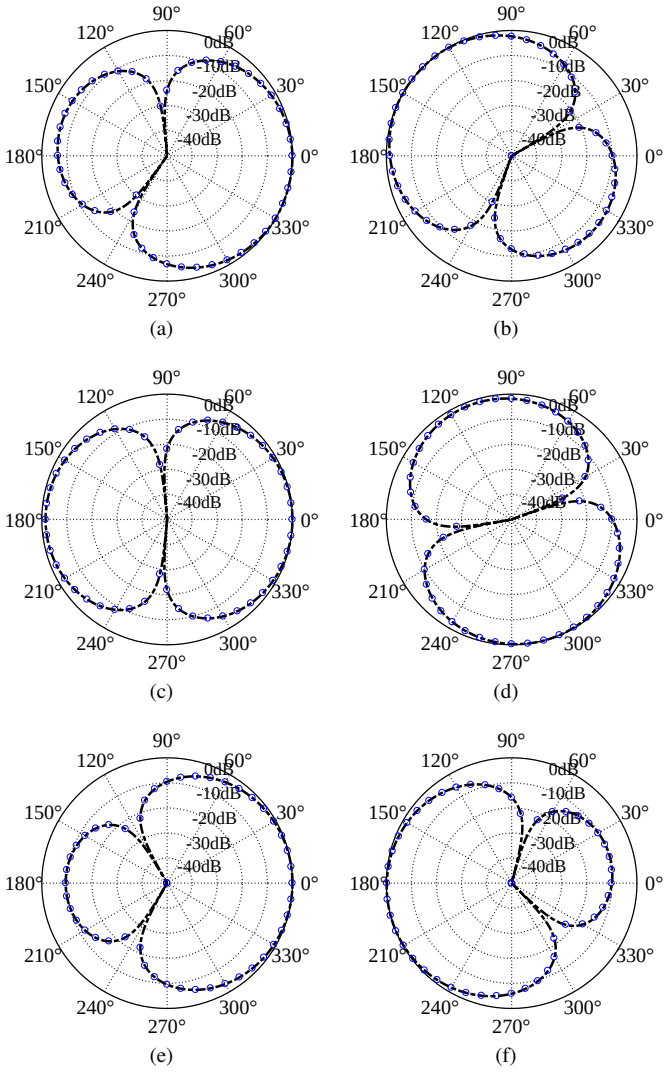

Fig. 5: Beampatterns of the first-order asymmetric hypercardioid using CDMAs with $M = 3$ sensors for different steering angles and frequencies: (a) $\theta_s = 0°$, $f = 600$ Hz, (b) $\theta_s = 155°$, $f = 2400$ Hz. Beampatterns of the corresponding first-order symmetric design: (c) $\theta_s = 0°$, $f = 1000$ Hz, (d) $\theta_s = 285°$, $f = 3200$ Hz . Beampatterns of the first-order unconstrained symmetric hypercardioid: (e) $\theta_s = 0°$, $f = 900$ Hz, (f) $\theta_s = 195°$, $f = 2100$ Hz . The black dashed line is the designed beampattern (65), while the blue circles line is the analytical beampattern (28).

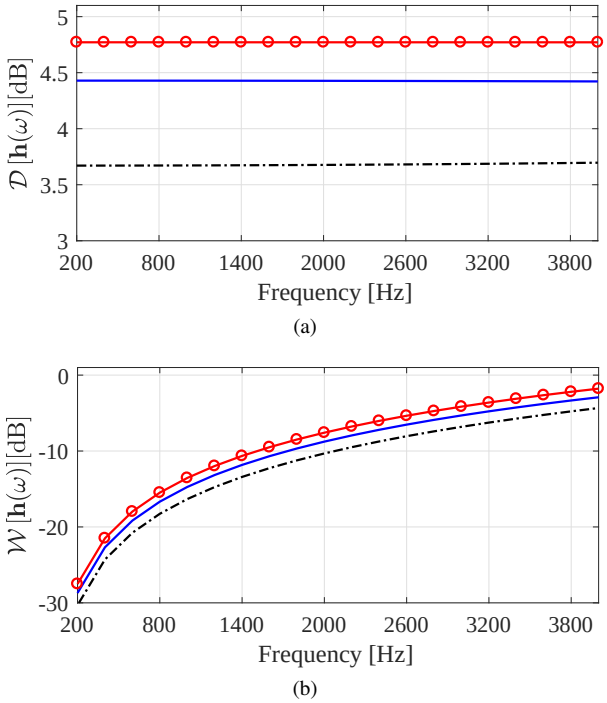

Fig. 6: DF (a) and WNG (b) vs. frequency for the first-order asymmetric hypercardioid (blue solid line), the optimal unconstrained symmetric hypercardioid (red circles line), and the symmetric design (black dashed line) with $M = 3$ sensors.

design reduced-order CDMAs for a given number of nulls and achieve a much larger WNG with respect to the symmetric design. Note that one of the effective ways to improve the WNG is by increasing the number of microphones [15], which is limited in some practical applications. Therefore, the following example is of a great relevance for real-world applications.

Let us assume that we are limited only to $M = 5$ microphones and we are interested to impose three nulls at $\theta_1 = 60°$, $\theta_2 = 190°$, and $\theta_3 = 275°$. We choose the radius of the array to be $r = 0.75$ cm which leads to a sensor spacing of $\delta \approx 0.88$ cm. While for the asymmetric design, five microphones are sufficient, for the traditional symmetric design, we need at least third-order CDMA and seven microphones, therefore, for the symmetric design, we use $M = 7$ sensors and keep the value of $r = 0.75$ cm which leads to $\delta \approx 0.65$ cm. We compare between the second-order asymmetric design and the third-order symmetric design.

First, we need to find an expression for the analytical beampattern for asymmetric hypercardioid with the above directions by using (41). From (41), we get the optimal coefficients vector, $\mathbf{c}$ (33), and substitute it into the analytical asymmetric beampattern (28). We get the following second-order asymmetric beampattern:

$$\mathcal{B}_2(\theta) = 0.16 + 0.482\cos\theta + 0.358\cos(2\theta) - 0.13\sin\theta - 0.126\sin(2\theta), \quad (67)$$

which is a second-order trigonometric polynomial with four roots. The fourth root is $\theta_2 = 156°$. Figure 7 shows the analytical beampattern of the second-order asymmetric design (blue solid line), the corresponding third-order symmetric design (black dashed line) which enforces nulls in the above directions, and the second-order unconstrained symmetric hypercardioid (red circles line), which was obtained for nulls at $\theta_1 = 72°$, and $\theta_2 = 144°$, and their corresponding symmetric directions. The symmetric design has narrower mainbeam as it is a third-order design while the asymmetric design is a second-order design.

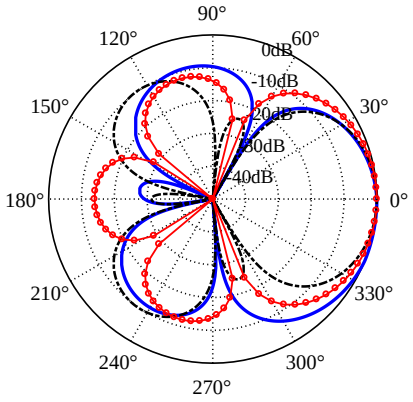

Fig. 7: An asymmetric second-order hypercardioid beampattern (blue solid line) obtained by (28) for the case of three imposed nulls and $M = 5$ microphones. Also presented the corresponding third-order symmetric beampattern (black dashed line) for the case of $M = 7$ sensors, and desired nulls at $\theta_1 = 60°$, $\theta_2 = 190°$, and $\theta_3 = 275°$. The red circles line is the second-order unconstrained hypercardioid [6].

We can now use these outputs in order to design the practical second-order asymmetric CDMA using (62), with the same regularization parameter $\eta = 10^{-8}$. Figure 8 shows the beampattern of the second-order asymmetric hypercardioid (a)-(b), the third-order symmetric hypercardioid (c)-(d), and the second-order unconstrained symmetric hypercardioid, for different frequencies and steering angles. The black dashed line is the designed beampattern (65), while the blue circles line is the analytical beampattern (28).

Figure 9 shows the WNG and the DF as a function of frequency for the second-order asymmetric hypercardioid (blue solid line), the third-order symmetric design (black dashed line), and the second-order unconstrained symmetric hypercardioid (red circles line). Two more designs are presented for comparison. The first is the third-order symmetric design for the case of $M = 15$ and $\delta = 0.65$ cm, leading to $r = 1.57$ cm (magenta diamonds line), and a larger array. The second (green triangles line) is for the case of $M = 20$ microphones and the radius is $r = 0.75$ cm, meaning that the array is more dense but of the same size like the original one. As expected, while the third-order symmetric design achieves higher directivity by less than 1dB with respect to the other second-order designs, the second-order design achieves superior WNG of up to 15dB with respect to the third-order design. Moreover, comparing the performances of the asymmetric design and the second-order unconstrained design, the loss in performance is negligible even though three nulls were imposed instead of two. Regarding the third-order symmetric design with larger M, we can see that increasing only the number of sensors (green triangles line) provides a small improvement, but still far from the performance of the second-order designs. The other case of a larger array (magenta diamonds line), yields better performance, but at the price of a larger physical array which can be problematic in some scenarios where strong limitations on the available space exist. Therefore, we conclude that the proposed asymmetric design can be used to

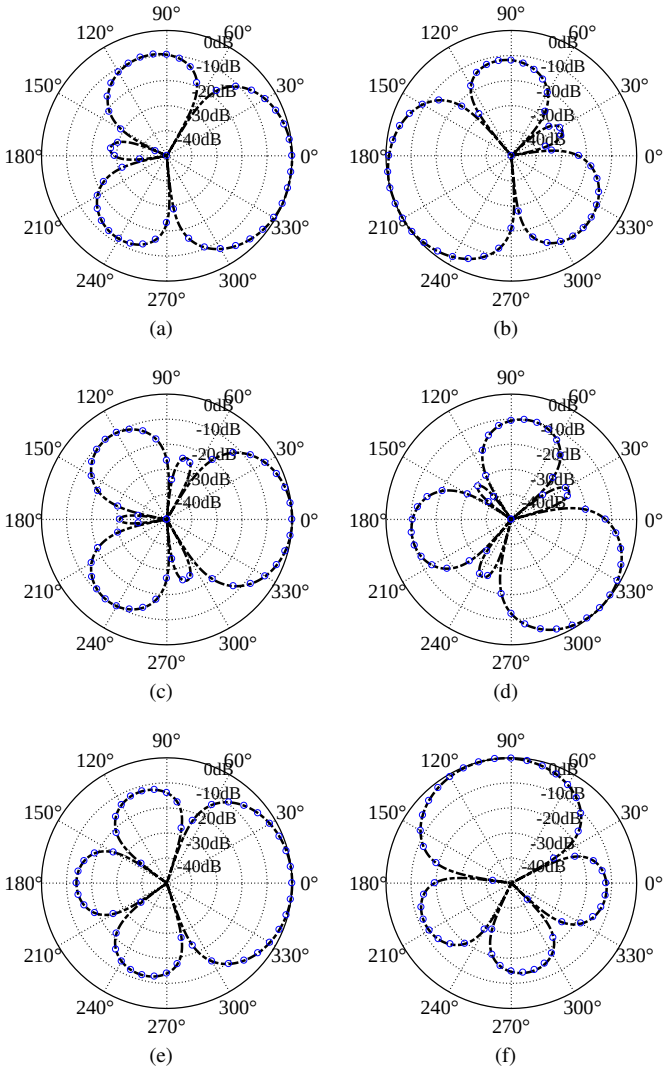

Fig. 8: Beampatterns of the second-order asymmetric hypercardioid CDMAs with $M = 5$ sensors and three imposed nulls for different steering angles and frequencies: (a) $\theta_s = 0°$, $f = 800$ Hz, (b) $\theta_s = 215°$, $f = 1800$ Hz. Beampatterns of the corresponding third-order symmetric design with $M = 7$ sensors: (c) $\theta_s = 0°$, $f = 200$ Hz, (d) $\theta_s = 315°$, $f = 1900$ Hz. Beampatterns of the second-order unconstrained symmetric hypercardioid: (e) $\theta_s = 0°$, $f = 1300$ Hz, (f) $\theta_s = 100°$, $f = 3500$ Hz. The black dashed line is the designed beampattern (65), while the blue circles line is the analytical beampattern (28).

resolve the trade-off between high directivity and robustness associated with the design of CDMAs.

Note that even the improved results of the asymmetric design presented in Fig. 9 are inadequate for real scenarios, as the WNG at low frequencies is much lower. Further improvement of the WNG involves methods which are based either on increasing the number of sensors [14] or more advanced regularization methods [35], [40], where the regularization parameter depends on frequency. We did not include such improvements, which can be applied either for the asymmetric

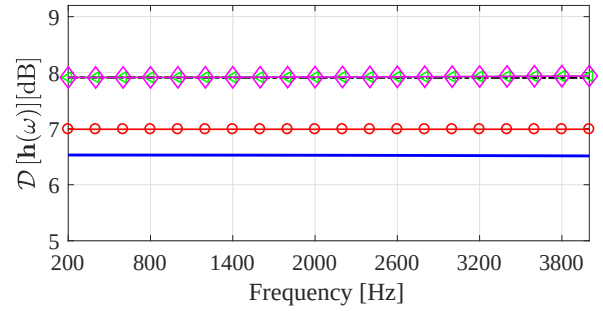

(a)

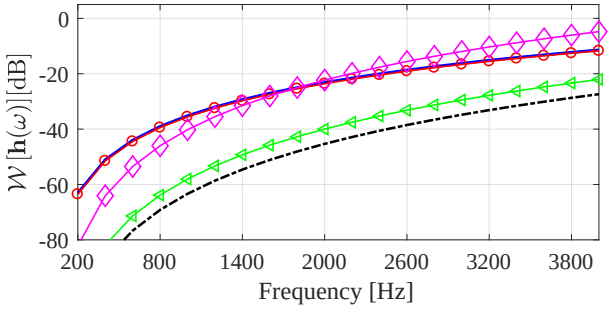

(b)

Fig. 9: DF (a) and WNG (b) vs. frequency for the second-order asymmetric hypercardioid (blue solid line), the second-order unconstrained symmetric hypercardioid (red circles line) with $M = 5$ sensors, and the third-order symmetric design (black dashed line) with $M = 7$ sensors. Also presented the third-order symmetric design (magenta diamonds line) with $M = 15$ sensors and larger array (element spacing, $\delta = 0.65$ cm), and the third-order symmetric design (green triangles line) with $M = 20$ sensors and the same size of original array ($r = 0.75$ cm).

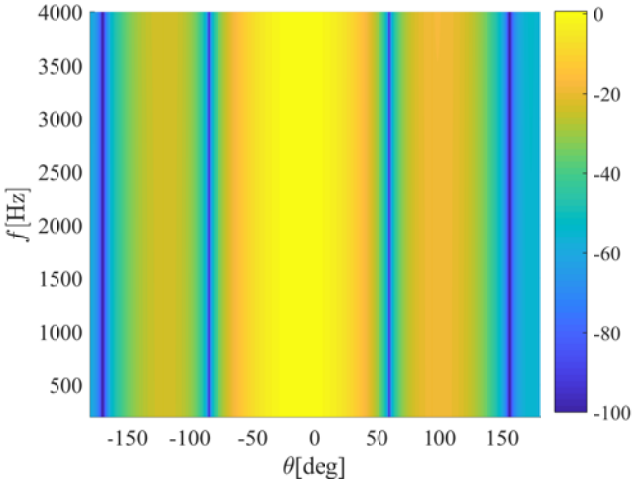

Fig. 10: A top view of the beampattern versus frequency and θ for the asymmetric second-order hypercardioid CDMA implemented in Section VI-D.

design or the traditional symmetric one, in the scope of this paper since we have concentrated on the improvement obtained by the utilization of the asymmetric model rather than the symmetric one.

Finally, Fig. 10 shows from a top view the beampattern versus frequency and θ for the asymmetric second-order hypercardioid CDMA designed in this subsection. As expected, the frequency-invariance property can be clearly seen. One can identify the main lobe and the two dominant sidelobes in accordance with Fig. 8 (a)-(b), which presents up to azimuthal rotation, two slices of Fig. 10 corresponding to frequencies $f_1 = 800$Hz and $f_2 = 1800$Hz.

The examples presented in this section illustrate the benefits of the proposed asymmetric model to achieve better performance and control of the null directions during the design process of CDMAs.

VII. Conclusions

We have presented an analytical model for asymmetric CDMAs, which includes the traditional symmetric model as a particular case. This model includes the derivation of the analytical Nth-order asymmetric beampattern, and asymmetric versions of two commonly-used optimal beampatterns, namely the hypercardioid and the supercardioid. A simple general Nth-order asymmetric practical design in the frequency-domain for any number of microphones is also presented. Simulation results demonstrate some of the benefits achieved by the asymmetric model with respect to the traditional symmetric model for DMAs. Specifically, the asymmetric model allows more degrees of freedom which can be exploited to achieve better performance in terms of WNG, DF, and FBR. Moreover, for a given number of desired null directions, the asymmetric model may allow reduced order of CDMAs with respect to the symmetric model leading to an improved robustness to array imperfections. Therefore, this concept is of a great importance for some real-world CDMAs based beamforming applications since it allows smaller and more robust designs with respect to the regular symmetric design.

Appendix
Proof of the equivalence between (23) and (28)

In order to prove the equivalence, we may use the formula:

$$\sin(N\theta) = \sum_{k=0}^{N} \binom{N}{k} \cos^k\theta \sin^{N-k}\theta \sin\left[\frac{(N-k)\,\pi}{2}\right], \tag{68}$$

which can be obtained from Euler Formula and the Binomial theorem. We consider the following four cases:

Case 1: N and k are both even. Thus, $N - k = 2l$ is also even and l is an integer number. In that case, the coefficient of each term in (68) is

$$\sin\left[\frac{(N-k)\,\pi}{2}\right] = \sin\left[\frac{(2l)\,\pi}{2}\right] \equiv 0. \tag{69}$$

Case 2: N and k are both odd. Thus, $N - k = 2l$ is even. In that case we also get that each term in (68) is equal to zero.

Case 3: N is even and k is odd. Thus, $N-k$ is also odd. In that case:

$$\begin{aligned}\cos^k\theta\sin^{N-k}\theta &= \cos\theta\cos^{k-1}\theta\sin^{N-k}\theta \\ &= \cos\theta\left(\cos^2\theta\right)^{\frac{k-1}{2}}\sin\theta\left(\sin^2\theta\right)^{\frac{N-k-1}{2}} \\ &= \cos\theta\left(1-\sin^2\theta\right)^{\frac{k-1}{2}}\sin\theta\left(\sin^2\theta\right)^{\frac{N-k-1}{2}} \\ &= \cos\theta\sin\theta\mathcal{P}_{\frac{N-2}{2}}\left(\sin^2\theta\right) \\ &= \cos\theta\sin\theta\left(p_0+p_1\sin^2\theta+\right. \\ &\quad \left. p_2\sin^4\theta+...+p_{\frac{N-2}{2}}\sin^{N-2}\right) \\ &= \cos\theta\left(p_0\sin\theta+p_1\sin^3\theta+\right. \\ &\quad \left. p_2\sin^5\theta+...+p_{\frac{N-2}{2}}\sin^{N-1}\theta\right), \end{aligned} \tag{70}$$

where $\mathcal{P}_\alpha(x)$ is a polynomial in x of degree α.

Case 4: N is odd and k is even. Thus, $N-k$ is also odd. In that case:

$$\begin{aligned}\cos^k\theta\sin^{N-k}\theta &= \left(1-\sin^2\theta\right)^{\frac{k}{2}}\sin^{N-k}\theta \\ &= \mathcal{P}_{\frac{k}{2}}\left(\sin^2\theta\right)\sin\theta\mathcal{P}_{\frac{N-k-1}{2}}\left(\sin^2\theta\right) \\ &= \sin\theta\mathcal{P}_{\frac{N-1}{2}}\left(\sin^2\theta\right) \\ &= p_0\sin\theta+p_1\sin^3\theta+ \\ &\quad p_2\sin^5\theta+...+p_{\frac{N-2}{2}}\sin^N\theta. \end{aligned} \tag{71}$$

From (70) and (71), one can see that all the terms required to express $\sin(N\theta)$ are exactly the terms at the second and third summations of (23).

Regarding the terms $\cos(N\theta)$. It is well known that

$$\cos(N\theta) = T_N(\cos\theta), \tag{72}$$

where $T_N(\cdot)$ is the Nth Chebyshev polynomial of the first kind [41], which has the recurrence relation:

$$T_{N+1}(\cos\theta) = 2\cos\theta\times T_N(\cos\theta) - T_{N-1}(\cos\theta), \tag{73}$$

with

$$T_0(\cos\theta)=1, \quad T_1(\cos\theta)=\cos\theta. \tag{74}$$

Thus, $\cos(N\theta)$ can be expressed as a sum of powers of $\cos\theta$, which is exactly the terms at the first summation of (23). Therefore, we can conclude that (23) and (28) are both equivalent for all N.

REFERENCES

[1] H. Cox, R. M. Zeskind, and T. Kooij, "Practical supergain," *IEEE Trans. Acoust., Speech, Signal Processing*, vol. ASSP-34, no. 3, pp. 393–398, June 1986.

[2] M. Crocco and A. Trucco, "Design of robust superdirective arrays with a tunable tradeoff between directivity and frequency-invariance," *IEEE Trans. Signal Process.*, vol. 59, no. 5, pp. 2169–2181, May 2011.

[3] H. H. Olson, "Gradient microphones," *J. Acoust. Soc. Amer.*, vol. 17, pp. 192–198, Jan. 1946.

[4] G. M. Sessler and J. E. West, "Directional transducers," *IEEE Trans. Audio Electroacoustic.*, vol. 19, pp. 19–23, Mar. 1971.

[5] G. W. Elko and A. T. N. Pong, "A simple adaptive first-order differential microphone," in *Proc. IEEE Workshop Applicat. Signal Process. Audio Acoust. (WASPAA)*, 1995, pp. 169–172.

[6] G. W. Elko, "Superdirectional microphone arrays," in *Acoustic Signal Processing for Telecommunication*, S. L. Gay and J. Benesty, Eds. Boston, MA: Kluwer Academic Publishers, 2000, ch. 10, pp. 181–237.

[7] ——, "Differential microphone arrays," in *in Audio Signal Processing for Next-Generation Multimedia Communication Systems*, Y. Huang and J. Benesty, Eds. Norwell, MA: Kluwer, 2004, ch. 2, pp. 11–65.

[8] T. D. Abhayapala and A. Gupta, "Higher order differential-integral microphone arrays," *J. Acoust. Soc. Amer.*, vol. 127, pp. 227–233, May 2010.

[9] M. Kolundžija, C. Faller, and M. Vetterli, "Spatiotemporal gradient analysis of differential microphone arrays," *J. Audio Eng. Soc.*, vol. 59, pp. 20–28, Feb. 2011.

[10] M. Buck, "Aspects of first-order differential microphone arrays in the presence of sensor imperfections," *European Trans. Telecommunications*, vol. 13, pp. 115–122, Mar. 2002.

[11] R. M. M. Derkx and K. Janse, "Theoretical analysis of a first-order azimuth-steerable superdirective microphone array," *IEEE Trans. Audio, Speech, Language Process.*, vol. 17, pp. 150–162, Jan. 2009.

[12] H. Teutsch and G. W. Elko, "First- and second-order adaptive differential microphone arrays," in *Darmstadt, Germany: 7th International Workshop on Acoustic Echo and Noise Control*, 2001, pp. 57–60.

[13] E. De Sena, H. Hacihabiboğlu, and Z. Cavetković, "On the design and implementation of higher order differential microphones," *IEEE Trans. Audio, Speech, Language Process.*, vol. 20, no. 1, pp. 162–174, Jan. 2012.

[14] J. Benesty and J. Chen, *Study and Design of Differential Microphone Arrays*. Berlin, Germany: Springer-Verlag, 2012.

[15] L. Zhao, J. Benesty, and J. Chen, "Design of robust differential microphone arrays," *IEEE Trans. Audio, Speech, Language Process.*, vol. 22, no. 10, pp. 1455–1464, Oct. 2014.

[16] C. Pan, J. Benesty, and J. Chen, "Design of robust differential microphone arrays with orthogonal polynomials," *J. Acoust. Soc. Amer.*, vol. 138, no. 2, pp. 1079–1089, Aug. 2015.

[17] H. Zhang, J. Chen, and J. Benesty, "Study of nonuniform linear differential microphone arrays with the minimum-norm filter," *Applied Acoustics*, vol. 98, pp. 62–69, May 2015.

[18] C. Pan, J. Chen, and J. Benesty, "Theoretical analysis of differential microphone array beamforming and an improved solution," *IEEE Trans. Audio, Speech, Language Process.*, vol. 23, no. 11, pp. 2093–2105, Nov. 2015.

[19] Y. Buchris, I. Cohen, and J. Benesty, "First-order differential microphone arrays from a time-domain broadband perspective," in *International Workshop on Acoustic Echo and Noise Control (IWAENC) 2016 conf.*

[20] G. Huang, J. Benesty, and J. Chen, "Design of robust concentric circular differential microphone arrays," *The Journal of the Acoustical Society of America*, vol. 141, no. 5, pp. 3236–3249, 2017.

[21] C. Pan, J. Chen, and J. Benesty, "Performance study of the mvdr beamformer as a function of the source incident angle," *IEEE/ACM Trans. Audio, Speech, Language Process.*, vol. 22, no. 1, pp. 67–79, Jan. 2014.

[22] H. Teutsch and W. Kellerman, "Acoustic source detection and localization based on wavefield decomposition using circular microphone arrays," *J. Acoust. Soc. Amer.*, vol. 120, no. 5, pp. 2724–2736, Nov. 2006.

[23] M. Wax and J. Sheinvald, "Direction finding of coherent signals via spatial smoothing for uniform circular arrays," *IEEE Trans. Antennas. Propag.*, vol. 42, no. 5, pp. 613–620, May 1994.

[24] C. P. Mathews and M. D. Zoltowski, "Eigenstructure techniques for 2-D angle estimation with uniform circular arrays," *IEEE Trans. Signal Process.*, vol. 42, no. 9, pp. 2395–2407, Sep. 1994.

[25] E. Tiana-Roig, F. Jacobsen, and E. F. Grande, "Beamforming with a circular microphone array for localization of environmental noise sources," *J. Acoust. Soc. Am.*, vol. 128, pp. 3535–3542, 2010.

[26] B. Friedlander, "The MVDR beamformer for circular arrays," in *Proc. 34th Asilomar Conf. Signals, Systems, Computers*, vol. 1, Nov. 2000, pp. 25–29.

[27] P. Ioannides and C. A. Balanis, "Uniform circular and rectangular arrays for adaptive beamforming applications," *IEEE Antennas Wireless Propagat. Lett.*, vol. 4, pp. 351–354, 2005.

[28] Y. L. Ma, Y. Yang, Z. He, K. Yang, C. Sun, and Y. Wang, "Theoretical and practical solutions for high-order superdirectivity of circular sensor arrays," *IEEE Trans. Ind. Electron.*, vol. 60, pp. 203–209, 2013.

[29] S. C. Chan and K. S. Pun, "On the design of digital broadband beamformer for uniform circular array with frequency invariant characteristics," in *Proc. IEEE Int. Symp. Circuits Systems (ISCAS), Phoenix, AZ*, vol. 1, May 2002, pp. 693–696.

[30] H. H. Chen, S. C. Chan, and K. L. Ho, "Adaptive beamforming using frequency invariant uniform concentric circular arrays," *IEEE Trans.Circuits Syst. I, Reg. Papers*, vol. 54, no. 9, pp. 1938–1949, Sept. 2007.

[31] S. C. Chan and H. H. Chen, "Uniform concentric circular arrays with frequency-invariant characteristics - theory, design, adaptive beamforming and doa estimation," *IEEE Trans. Signal Process.*, vol. 55, no. 1, pp. 165–177, Jan. 2007.
[32] X. Zhang, W. Ser, Z. Zhang, and A. K. Krishna, "Selective frequency invariant uniform circular broadband beamformer," *EURASIP Journal on Advances in Signal Processing*, pp. 1–11, 2010.
[33] J. Benesty, J. Chen, and I. Cohen, *Design of Circular Differential Microphone Arrays*. Berlin, Germany: Springer-Verlag, 2015.
[34] Y. Buchris, I. Cohen, and J. Benesty, "Analysis and design of time-domain first-order circular differential microphone arrays," in *the 22nd International Congress on Acoustics (ICA)*, 2016.
[35] H. L. Van-trees, *Detection, Estimation and Modulation Theory, Part IV - Optimum Array Processing*. New York: Wiley Interscience, 2002.
[36] S. Doclo and M. Moonen, "Design of far-field and near-field broadband beamformers using eigenfilters," *Signal Process.*, vol. 83, pp. 2641–2673, Dec. 2003.
[37] S. C. Pei and C. C. Tseng, "A new eigenfilter based on total least squares error criterion," *IEEE Trans. Circuits Syst. I*, vol. 48, pp. 699–709, June 2001.
[38] Y. Avargel and I. Cohen, "System identification in the short-time Fourier transform domain with crossband filtering," *IEEE Trans.Audio, Speech, Language Process.*, vol. 15, no. 4, pp. 1305–1319, May 2007.
[39] C. Pan, J. Benesty, and J. Chen, "Design of directivity patterns with a unique null of maximum multiplicity," *IEEE/ACM Trans.Audio, Speech, Language Process.*, vol. 24, no. 2, pp. 226–235, Feb. 2016.
[40] R. Berkun, I. Cohen, and J. Benesty, "Combined beamformers for robust broadband regularized superdirective beamforming," *IEEE/ACM Trans. Audio, Speech, Language Process.*, vol. 23, no. 5, pp. 877–886, May 2015.
[41] M. Abramowitz and I. A. Stegun, *Handbook of Mathematical Functions with Formulas, Graphs, and Mathematical Tables*. New York: Dover, 1970.

Chapter 5

Incoherent Synthesis of Sparse Arrays for Frequency-Invariant Beamforming

This chapter contains the following manuscript:

Y. Buchris, A. Amar, I. Cohen, and J. Benesty, "Incoherent Synthesis of Sparse Arrays for Frequency-Invariant Beamforming," IEEE/ACM Transactions on Audio, Speech, and Language Processing, vol. 27, no. 3, pp. 482–495, (2019).

Incoherent Synthesis of Sparse Arrays for Frequency-Invariant Beamforming

Yaakov Buchris, *Member, IEEE*, Alon Amar, *Member, IEEE*, Jacob Benesty, and Israel Cohen, *Fellow, IEEE*

***Abstract*—Frequency-invariant beamformers are used to prevent signal waveform distortions in real world applications like audio, underwater acoustics, and radar. Most of existing methods assume uniform arrays, and only few consider sparse designs, which may lead to higher performance in terms of robustness and directivity factor. We propose an incoherent approach that first determines for each frequency bin a sparse set of sensors positions. Subsequently, by using tools of dimensionality reduction and clustering, these selections are merged together yielding the optimal sensors on a sparse array layout. We present design examples of sparse linear and planar superdirective array designs. We show that the proposed incoherent sparse design obtains superior performance in terms of white noise gain, directivity factor, and computational load compared to a uniform array design and compared to a coherent sparse approach, where the sensors' locations and the beamformer coefficients are optimized simultaneously for all frequencies.**

***Index terms*—** Frequency-invariant beamformer, sparse design, superdirective beamformers, differential microphone arrays.

I. Introduction

Design of nearly frequency-invariant (FI) broadband beamformers for several real-world applications like audio, communication, and sonar systems [1]–[3], is important as such beamformers can recover the signals of interest while reducing some artifacts caused by beamforming. Classical approaches of FI beamforming are based on constrained optimization [4]–[10], analytical solutions [11], [12], and coherent subspace methods [13]–[15]. Another concept is based on differential microphone arrays (DMAs) [16]–[23] and superdirective beamformers [24]. In all these former works, it was assumed that the sensors are located either uniformly or nonuniformly in a given aperture which can be linear, planar, or arbitrary. Yet, optimizing the number of sensors and/or their locations was not considered, and only the beamformer coefficients were optimized according to certain design constraints.

The shortcomings of the previous design opens a window of opportunities for a class of sparse methods which optimize also the number of sensors and their positions. In sparse arrays, also termed as aperiodic, random, thinned or space tapered arrays, the nonuniform design of the sensors' locations enables to obtain arrays where part of their adjacent sensors have spacing larger than half the wavelength. Yet, the harmful effects of grating lobes can be completely mitigated. Thus, arrays with a greater aperture and better robustness to array imperfections, but with a smaller number of sensors than in the uniform design, can be designed using the sparse approach. In the context of FI beamformers, sparsity may lead to more flexibility and better design in terms of satisfying constraints on a wider range of frequencies. Practically, sparse arrays can be integrated into several real-world applications where strong limitations are imposed on the weight, size, and cost of sensors.

While for the narrowband design many advanced techniques have been presented for the synthesis of sparse arrays [25]–[36], less work has been done for the sparse design of FI broadband beamformers. One simple sparse structure of FI beamforming is based on the concept of harmonic nested arrays [37], [38] where the total array is composed from several uniform subarrays, each matched to a different frequency subband. Yet, the locations of the sensors are set only according to the spatial sampling constraint in the relevant subband, and are not optimized according to some design constraints like robustness to mismatch errors.

Analytical approaches for optimization of the sensors positions in order to obtain FI beampattern can be found in [39], [40]. However, in these approaches no consideration regarding issues like robustness to noise has been done. This restricts to some extent the feasibility of such approaches in cases of small size arrays. Crocco and Trucco [41] proposed a FI sparse design by joint-optimization of the sensors positions and the beamformer coefficients, using simulated annealing optimization, while assuming a given a-priori number of sensors on the sparse array. In [42], a genetic algorithm combined with a gradient-based method was applied to find a global minimum for the optimization of the cost function. A design of FI beampattern for linear arrays based on the generalized matrix pencil method can be found in [43].

Recently, both Hawes and Liu [44], and Liu et al. [45] proposed sparse designs for broadband beamformers based on an iterative weighted ℓ_1-norm minimization under multiple convex constraints. One of the imposed constraints is a joint-sparsity constraint [46] aimed to ensure that the chosen sensors are joint for all frequency bins in the relevant bandwidth. In other words, the same sensors are used to build the beamformers coefficient vectors in all frequency bins. As the optimization of sensors positions and beamformer coefficients is performed simultaneously over all frequency bins in the relevant bandwidth, we may refer to this design approach as a coherent sparse design. While good results were reported, this method is limited when the number of candidate sensors is an order of magnitude of hundreds or more.

In this paper, we propose a new incoherent sparse array design for nearly FI beamforming. The main idea is to split

This research was supported by the Israel Science Foundation (grant no. 576/16), the ISF-NSFC joint research program (grant No. 2514/17) and MAFAAT-Israel Ministry of Defense.

an ℓ_1-optimization problem with a large number of constraints like in the coherent approach, into several smaller optimization subproblems, each matched to a different frequency bin with a smaller number of constraints. In the first step, an ℓ_1-norm constrained optimization problem is solved for each frequency bin separately, yielding a sparse vector containing the indices of the optimal sensors. All these sparse vectors are then arranged in a matrix, on which the principal component analysis (PCA) algorithm is applied to reduce its dimension. The reduced set of data is then clustered in the third step which determines the joint sparse vector containing the dominant sensors positions, i.e., the chosen sensors are common to all frequency bins in the bandwidth of interest. The chosen sensors are used in the synthesis step to obtain the FI joint sparse beampattern. As the ℓ_1-norm optimization is performed for each frequency bin separately, we may refer to this approach as the incoherent sparse design. We also present a modified version of the coherent approach [45], which is compared to the proposed incoherent design later in the simulation section. Note that in this paper the terms coherent and incoherent refer to whether or not we optimize the entire bandwidth simultaneously, and have no relation to the phases of the complex frequency-domain beamformer coefficient vectors.

Though the proposed scheme is general, our focus is on superdirective beamformers and DMAs, since we are interested in FI broadband beamformers which also provide high performance level like directivity factor (DF). These families are characterized as small size, dense arrays with high directivity. According to the model of the superdirective beamformers, it is assumed that the element spacing is much smaller than the wavelength of the incoming signal in order to achieve supergain effect [24].

Therefore, in the simulation section, we present two design examples illustrating the benefits of the proposed incoherent sparse design with respect to the coherent one and also to the uniform array design. The first example considers the case of sparse DMAs design with linear geometry, and the second example considers a 2D planar superdirective beamformer. In the first example, both the coherent and the incoherent sparse design approaches obtain similar performance levels but the computation runtime of the incoherent design was shorter by almost two orders of magnitude than that of the coherent design. Also, it is shown that the sparse designs constitute a good compromise between robustness to array imperfections and prevention of grating lobes. For the second example, the coherent design was infeasible using a standard hardware, while the incoherent design was still feasible and maintained the aforementioned advantages with respect to the uniform design approaches. These results demonstrate that the incoherent sparse design is more practical for applications involving large arrays with hundreds of candidate sensors. Moreover, in some applications adaptive versions of the incoherent sparse design may be also of a great interest. In such applications, the potential sensors physically exist on the array but it is desired to adaptively choose a sparse subset of sensors and preserve some system resources like energy, processing time, storage, and more.

II. Signal Model and Problem Formulation

Consider $\mathcal{B}_{\mathrm{d}}(\boldsymbol{\rho})$, where $\boldsymbol{\rho}=(\theta,\phi)$ specifies the azimuth θ and the elevation ϕ, to be a desired far-field FI beampattern in the bandwidth of interest Ω.

We are given an array in the q-dimensional space ($q=1,2,3$ in the case of a linear, planar, or volumetric aperture, respectively) with M possible positions for locating the sensors, where the mth position is denoted by $\mathbf{p}_m,\ m=1,2,\ldots,M$. In its general form, the beampattern of such an array for the angular frequency ω is defined as

$$\mathcal{B}\left(\mathbf{h}(\omega)\right)=\mathbf{h}^{H}(\omega)\mathbf{d}\left(\mathbf{k}_{\omega}\left(\boldsymbol{\rho}\right)\right), \tag{1}$$

where the superscript ^{H} denotes the conjugate-transpose operator,

$$\mathbf{h}(\omega)=\left[H_1(\omega),H_2(\omega),\ldots,H_M(\omega)\right]^{T} \tag{2}$$

is a vector containing the beamformer complex gains in the frequency ω, and the superscript ^{T} denotes the transpose operator. The vector:

$$\mathbf{k}_{\omega}\left(\boldsymbol{\rho}\right)=-\frac{\omega}{c}\begin{bmatrix}\cos\theta\sin\phi\\ \sin\theta\sin\phi\\ \cos\phi\end{bmatrix} \tag{3}$$

is the wavenumber vector at frequency ω and direction $\boldsymbol{\rho}$ associated with the $M\times 1$ steering vector

$$\mathbf{d}\left(\mathbf{k}_{\omega}\left(\boldsymbol{\rho}\right)\right)=\left[e^{-\jmath\mathbf{k}_{\omega}^{T}(\boldsymbol{\rho})\mathbf{p}_0},e^{-\jmath\mathbf{k}_{\omega}^{T}(\boldsymbol{\rho})\mathbf{p}_1},\ldots,e^{-\jmath\mathbf{k}_{\omega}^{T}(\boldsymbol{\rho})\mathbf{p}_M}\right]^{T}, \tag{4}$$

where $\jmath=\sqrt{-1}$, and c is the waveform's speed.

Assume that we select a subset of $K\ll M$ position candidates $\{\mathbf{p}_{i_k}\}_{k=1}^{K}$, where $\{i_k\}_{k=1}^{K}\in[1,2,\ldots,M]$ are their indices, which will determine the K spatio-temporal beampatterns for each frequency $\omega\in\Omega$, that is,

$$\mathcal{B}\left(\mathbf{h}(\omega),\mathbf{T}_{\mathrm{sc}}\left(\mathbf{i}_K\right)\right)=\mathbf{h}^{H}(\omega)\mathbf{T}_{\mathrm{sc}}^{T}\left(\mathbf{i}_K\right)\mathbf{T}_{\mathrm{sc}}\left(\mathbf{i}_K\right)\mathbf{d}\left(\mathbf{k}_{\omega}\left(\boldsymbol{\rho}\right)\right), \tag{5}$$

where $\mathbf{i}_K=\left[i_1,i_2,\ldots,i_K\right]^{T}$ and $\mathbf{T}_{\mathrm{sc}}\left(\mathbf{i}_K\right)$ is a $K\times M$ FI selection matrix, i.e., containing K rows of an $M\times M$ identity matrix corresponding to the indices $\{i_k\}_{k=1}^{K}$. Note that the following property is satisfied: $\mathbf{T}_{\mathrm{sc}}\left(\mathbf{i}_M\right)=\mathbf{I}_M$ where $\mathbf{i}_M=[1,2,\ldots,M]^{T}$ and $\mathbf{I}_M$ is the $M\times M$ identity matrix.

Our goal is stated as follows: we want to select a set of K positions out of the M candidate positions such that the synthesized beampattern $\mathcal{B}\left(\mathbf{h}(\omega),\mathbf{T}_{\mathrm{sc}}\left(\mathbf{i}_K\right)\right),\forall\omega\in\Omega$ will be FI but at the same time will be as close as possible to the desired power beampattern, $\mathcal{B}_{\mathrm{d}}\left(\boldsymbol{\rho}\right)$ (in the mean square error sense), under some design constraints to be specified below.

III. Typical Design Constraints

We now present several design constraints which are supposed to ensure FI broadband beampattern. Given the reference beampattern $\mathcal{B}_{\mathrm{d}}\left(\boldsymbol{\rho}\right)$, we can use the LS error constraint to get the desired FI beampattern, generally defined as

$$\int_{\Omega}\int_{\Theta}\left\|\mathcal{B}_{\mathrm{d}}\left(\boldsymbol{\rho}\right)-\mathbf{h}^{H}(\omega)\mathbf{d}\left(\mathbf{k}_{\omega}(\boldsymbol{\rho})\right)\right\|_2^2 d\omega d\boldsymbol{\rho}\leq\epsilon_{\mathrm{t}}, \tag{6}$$

where Ω and Θ denote the frequency and angle range of interest, respectively, $||\cdot||_2$ is the ℓ_2-norm, and $\epsilon_{\rm t}$ is a small positive tolerance parameter indicating the total overall allowed error. Despite its generality, by using (6) directly we cannot take into consideration that there is a difference in the ability to obtain FI beampattern in different frequencies and also that there are spatial regions that are more important than others, e.g., the mainlobe region is more important than the sidelobe regions. Therefore, we uniformly discretize both the frequency and angle spaces and introduce J frequency bins $\{\omega_j\}_{j=1}^{J} \in \Omega$, and P directions $\left\{\boldsymbol{\rho}_p\right\}_{p=1}^{P} \in \Theta$ that cover the entire beampattern. We set L out of the P directions that cover the mainlobe region $\Theta_{\rm m}$, and define $\boldsymbol{K}_j^{\rm m}$ to be the set containing these directions on frequency ω_j, i.e.,

$$\boldsymbol{K}_j^{\rm m} = \left\{\mathbf{k}_{\omega_j}(\boldsymbol{\rho}_1), \mathbf{k}_{\omega_j}(\boldsymbol{\rho}_2), \ldots, \mathbf{k}_{\omega_j}(\boldsymbol{\rho}_L)\right\}, \tag{7}$$

where the superscript m stands for mainlobe. Similarly, we define the set $\boldsymbol{K}_j^{\rm s}$ containing $P-L$ directions that cover the sidelobe region $\Theta_{\rm s}$ as

$$\boldsymbol{K}_j^{\rm s} = \left\{\mathbf{k}_{\omega_j}(\boldsymbol{\rho}_{L+1}), \mathbf{k}_{\omega_j}(\boldsymbol{\rho}_{L+2}), \ldots, \mathbf{k}_{\omega_j}(\boldsymbol{\rho}_P)\right\}, \tag{8}$$

where the superscript s stands for sidelobe.

We can reformulate (6) as

$$\begin{aligned}
&\int_{\Omega}\int_{\Theta} \left\|\mathcal{B}_{\rm d}\left(\boldsymbol{\rho}\right) - \mathbf{h}^H(\omega)\mathbf{d}\left(\mathbf{k}_{\omega}(\boldsymbol{\rho})\right)\right\|_2^2 d\omega d\boldsymbol{\rho} \\
\approx\ & C\sum_{\omega_j\in\Omega}\sum_{\boldsymbol{\rho}_p\in\Theta_{\rm m}} \left\|\mathcal{B}_{\rm d}\left(\boldsymbol{\rho}\right) - \mathbf{h}^H(\omega_j)\mathbf{d}\left(\mathbf{k}_{\omega_j}(\boldsymbol{\rho}_p)\right)\right\|_2^2 \\
+\ & C\sum_{\omega_j\in\Omega}\sum_{\boldsymbol{\rho}_p\in\Theta_{\rm s}} \left\|\mathcal{B}_{\rm d}\left(\boldsymbol{\rho}\right) - \mathbf{h}^H(\omega_j)\mathbf{d}\left(\mathbf{k}_{\omega_j}(\boldsymbol{\rho}_p)\right)\right\|_2^2 \qquad (9)\\
=\ & C\sum_{\omega_j\in\Omega}\left\|(\mathbf{b}_{\rm d}^{\rm m})^T - \mathbf{h}^H\left(\omega_j\right)\mathbf{T}_{\rm s}^T\left(\mathbf{i}_K\right)\mathbf{T}_{\rm s}\left(\mathbf{i}_K\right)\mathbf{D}\left(\boldsymbol{K}_j^{\rm m}\right)\right\|_2^2 \\
+\ & C\sum_{\omega_j\in\Omega}\left\|(\mathbf{b}_{\rm d}^{\rm s})^T - \mathbf{h}^H\left(\omega_j\right)\mathbf{T}_{\rm s}^T\left(\mathbf{i}_K\right)\mathbf{T}_{\rm s}\left(\mathbf{i}_K\right)\mathbf{D}\left(\boldsymbol{K}_j^{\rm s}\right)\right\|_2^2,
\end{aligned}$$

where C is a positive constant representing the contribution of the differential $d\omega d\boldsymbol{\rho}$,

$$\mathbf{D}\left(\boldsymbol{K}_j^{\rm m}\right) = \left[\mathbf{d}\left(\mathbf{k}_{\omega_j}\left(\boldsymbol{\rho}_1\right)\right), \mathbf{d}\left(\mathbf{k}_{\omega_j}\left(\boldsymbol{\rho}_2\right)\right), \ldots, \mathbf{d}\left(\mathbf{k}_{\omega_j}\left(\boldsymbol{\rho}_L\right)\right)\right] \tag{10}$$

is an $M \times L$ matrix, and

$$\mathbf{b}_{\rm d}^{\rm m} = \left[\mathcal{B}_{\rm d}\left(\boldsymbol{\rho}_1\right), \mathcal{B}_{\rm d}\left(\boldsymbol{\rho}_2\right), \ldots, \mathcal{B}_{\rm d}\left(\boldsymbol{\rho}_L\right)\right]^T \tag{11}$$

is a vector containing the desired beampattern in the directions covering the mainlobe. The matrix $\mathbf{D}\left(\boldsymbol{K}_j^{\rm s}\right)$ is defined similarly to $\mathbf{D}\left(\boldsymbol{K}_j^{\rm m}\right)$, and the vector $\mathbf{b}_{\rm d}^{\rm s}$ is defined similarly to $\mathbf{b}_{\rm d}^{\rm m}$.

As a mainlobe constraint we can decompose the first summation term of (9) into multiple joint-sparse constraints, that is, $\forall\omega_j \in \Omega$,

$$\mathcal{C}_1: \left\|(\mathbf{b}_{\rm d}^{\rm m})^T - \mathbf{h}^H\left(\omega_j\right)\mathbf{T}_{\rm s}^T\left(\mathbf{i}_K\right)\mathbf{T}_{\rm s}\left(\mathbf{i}_K\right)\mathbf{D}\left(\boldsymbol{K}_j^{\rm m}\right)\right\|_2^2 \le \epsilon_1(\omega_j), \tag{12}$$

where $\epsilon_1(\omega_j)$ is a small positive parameter.

Similarly, for the sidelobe constraint we can decompose the second summation term in (9) into multiple joint-sparse constraints, and write $\forall\omega_j \in \Omega$,

$$\mathcal{C}_2: \left\|(\mathbf{b}_{\rm d}^{\rm s})^T - \mathbf{h}^H\left(\omega_j\right)\mathbf{T}_{\rm s}^T\left(\mathbf{i}_K\right)\mathbf{T}_{\rm s}\left(\mathbf{i}_K\right)\mathbf{D}\left(\boldsymbol{K}_j^{\rm s}\right)\right\|_2^2 \le \epsilon_2(\omega_j), \tag{13}$$

where $\epsilon_2(\omega_j)$ is a small positive parameter. Typically, $\epsilon_1(\omega_j) < \epsilon_2(\omega_j)$ since the mainlobe region has more influence on the performance than the sidelobe region. Note that both $\epsilon_1(\omega_j)$ and $\epsilon_2(\omega_j)$ are frequency-varying parameters as the capability to satisfy either $\mathcal{C}_1$ or $\mathcal{C}_2$ in adequate accuracy depends on frequency. We can also establish the following relationship:

$$C\sum_{\omega_j\in\Omega}\epsilon_1(\omega_j) + C\sum_{\omega_j\in\Omega}\epsilon_2(\omega_j) \le \epsilon_{\rm t}. \tag{14}$$

Clearly, imposing only $\mathcal{C}_1$ and $\mathcal{C}_2$ does not ensure that the array responses $\mathcal{B}\left(\mathbf{h}(\omega_j), \mathbf{T}_{\rm s}\left(\mathbf{i}_K\right)\right),\ \omega_j \in \Omega$ will not distort the signal of interest and especially that they will be robust to array calibration and model mismatch errors. Hence, we include two more constraints. The first is the common distortionless response, stating that, $\forall\omega_j \in \Omega$,

$$\mathcal{C}_3:\ \mathbf{h}^H\left(\omega_j\right)\mathbf{T}_{\rm s}^T\left(\mathbf{i}_K\right)\mathbf{T}_{\rm s}\left(\mathbf{i}_K\right)\mathbf{d}\left(\mathbf{k}_{\omega_j}\left(\boldsymbol{\rho}_{\rm s}\right)\right) = 1, \tag{15}$$

where $\mathbf{k}_{\omega_j}\left(\boldsymbol{\rho}_{\rm s}\right)$ is the wavenumber of the desired signal at frequency ω_j and direction $\boldsymbol{\rho}_{\rm s}$. The second is the limitation of the white noise output power, given as, $\forall\omega_j \in \Omega$,

$$\mathcal{C}_4:\ \mathbf{h}^H\left(\omega_j\right)\mathbf{T}_{\rm s}^T\left(\mathbf{i}_K\right)\mathbf{T}_{\rm s}\left(\mathbf{i}_K\right)\mathbf{h}\left(\omega_j\right) \le \gamma(\omega_j), \tag{16}$$

where $\gamma(\omega_j)$ is a parameter expressing the maximal allowed white noise output power at frequency ω_j. Note that due to the distortionless constraint specified by (15), the formulation of (16) is equivalent to restricting the white noise gain (WNG) of the array to be above a certain threshold value [47, ch.6]. The WNG, given by [17],

$$\mathcal{W}\left(\mathbf{h}(\omega_j)\right) = \frac{\left|\mathbf{h}^H\left(\omega_j\right)\mathbf{d}\left(\mathbf{k}_{\omega_j}\left(\boldsymbol{\rho}\right)\right)\right|^2}{\mathbf{h}^H\left(\omega_j\right)\mathbf{h}\left(\omega_j\right)}, \tag{17}$$

is a measure indicating the array gain in the presence of uncorrelated white noise. It also indicates the sensitivity of the array to model mismatch errors [47].

Combining constraints $\mathcal{C}_1$,$\mathcal{C}_2$,$\mathcal{C}_3$,$\mathcal{C}_4$, we can formulate the general joint-sparse problem of interest as

$$\begin{aligned}
&\text{minimize}\{\text{number of active sensors} - K\} \\
&\text{subject to}\ \ \mathcal{C}_1, \mathcal{C}_2, \mathcal{C}_3, \mathcal{C}_4,\ \forall\omega_j \in \Omega,
\end{aligned} \tag{18}$$

whose solution yields the jointly-sparse filters

$$\mathbf{h}_K\left(\omega_j\right) = \mathbf{T}_{\rm s}\left(\mathbf{i}_K\right)\mathbf{h}\left(\omega_j\right),\ \forall\omega_j \in \Omega. \tag{19}$$

In this work, we propose two approaches to practically solve (18). The first approach, referred to as the coherent approach, is a modified version of what have been presented in [45]. Accordingly, the joint-sparse filters $\{\mathbf{h}_K\left(\omega_j\right)\}_{j=1}^{J}$ are obtained by a direct ℓ_1-norm optimization over all frequencies and directions of interest, simultaneously. We propose a second approach, where the ℓ_1-norm optimization is performed for

each frequency bin $\omega_j \in \Omega$ separately, and based on these selections the joint-sparse sensors are determined. We refer to that proposed approach as the incoherent approach. The advantage of the proposed incoherent approach over the coherent approach is by its reduced computationally which makes the incoherent approach more feasible for practical designs, especially where the number of potential sensors is an order of hundreds.

It is worth noting that both the coherent and the incoherent approaches can be used for either an offline or an online design. In the offline case, once the K chosen sensors are already determined, the corresponding array is constructed using only these sensors. In the online case, all the M candidate sensors physically exist on the array, and a sparse subset of K sensors are adaptively chosen, which are joint to all the frequencies in the relevant bandwidth. We do not consider here the case where different subsets of K sensors are adaptively chosen for each frequency bin. We now describe in details both these approaches.

IV. Coherent design of FI sparse arrays

This approach provides the K sensors by direct optimization over all frequencies. Theoretically, sparse solutions can be obtained by minimizing the ℓ_0-norm of the vector, which is, however, an NP-hard combinatorial optimization problem. A practical alternative is to solve an ℓ_1-norm optimization problem instead [48]. Our problem is more complicated since another essential constraint should be imposed. This is the joint-sparsity constraint which insures that all the filters $\{\mathbf{h}_K(\omega_j)\}_{j=1}^J$ have the same sparse pattern, i.e., the sensors positions which are chosen out of all the potential positions are common over all the frequencies in the signal's bandwidth of interest Ω. The way to insert such a constraint is by minimizing the ℓ_{12}-norm instead of the ℓ_1-norm [49]. It is defined as the following: suppose we have the vectors $\mathbf{x}_i, i = 1, 2, \ldots, n$, of length M, and define $\mathbf{X} = [\mathbf{x}_1, \mathbf{x}_2, \ldots, \mathbf{x}_n]$ to be a matrix containing these vectors in its columns, then the ℓ_{12}-norm of the matrix $\mathbf{X}$ is defined as [46]

$$\|\mathbf{X}\|_{12} \triangleq \sum_{m=1}^{M} \left(\sum_{i=1}^{n} |\mathbf{X}[m,i]|^2 \right)^{\frac{1}{2}}, \tag{20}$$

where $\mathbf{X}[m,i]$ being the entry corresponds to the mth row and the ith column of $\mathbf{X}$. Herein, we present the optimization problem yielding the required joint-sparse filters. It is a modified version of what have been presented in [45], that is,

$$\begin{aligned}
\underset{\{\mathbf{h}(\omega_j)\}_{j=1}^J}{\text{minimize}} \quad & \sum_{m=1}^{M} \alpha_m^k \eta_m \\
\text{subject to} \quad & \eta_m \geq \left\|\bar{\mathbf{h}}_m\right\|_2, \\
\text{and} \quad \forall \omega_j \in \Omega \quad & \\
& \mathbf{h}^H(\omega_j)\, \mathbf{d}\left(\mathbf{k}_{\omega_j}(\boldsymbol{\rho}_{\mathrm{s}})\right) = 1 \\
& \mathbf{h}^H(\omega_j)\, \mathbf{h}(\omega_j) \leq \gamma(\omega_j) \\
& \left\| (\mathbf{b}_{\mathrm{d}}^{\mathrm{m}})^T - \mathbf{h}^H(\omega_j)\, \mathbf{D}\left(\boldsymbol{K}_j^{\mathrm{m}}\right) \right\|_2^2 \leq \epsilon_1(\omega_j) \\
& \left\| (\mathbf{b}_{\mathrm{d}}^{\mathrm{s}})^T - \mathbf{h}^H(\omega_j)\, \mathbf{D}\left(\boldsymbol{K}_j^{\mathrm{s}}\right) \right\|_2^2 \leq \epsilon_2(\omega_j),
\end{aligned} \tag{21}$$

where

$$\bar{\mathbf{h}}_m = [H_m(\omega_1), H_m(\omega_2), \ldots, H_m(\omega_J)]^T, \quad m = 1, 2, \ldots, M, \tag{22}$$

$\alpha_m^k = 1/\left(\eta_m^{k-1} + \epsilon\right)$ for $k > 1$ and $\alpha_m^1 = 1$, η_m^{k-1} is the result obtained from the $(k-1)$th iteration, and ϵ is a regularization parameter. We run this algorithm iteratively until

$$\Delta\boldsymbol{\eta} \triangleq \frac{\left\|\boldsymbol{\eta}^k - \boldsymbol{\eta}^{k-1}\right\|_2}{\|\boldsymbol{\eta}^k\|_2} \leq \epsilon_\eta, \tag{23}$$

where $\boldsymbol{\eta}^k = \left[\eta_1^k, \eta_2^k, ..., \eta_M^k\right]^T$, and ϵ_η is a small positive parameter. This iterative algorithm yields a sparse solution which is a good approximation to the ℓ_0-norm solution. As the optimization problem in (21) is convex, it can be solved by convex optimization methods (e.g. CVX toolbox [50]).

Both the vectors $\boldsymbol{\eta}^k$ and $\{\mathbf{h}(\omega_j)\}_{j=1}^J$ are iteratively updated using (21) until (23) is satisfied. The K sensors corresponding to the K largest entries of the vector $\boldsymbol{\eta}^k$ will determine the support S of the filters $\{\mathbf{h}(\omega_j)\}_{j=1}^J$, from which the desired sparse filters $\{\mathbf{h}_K(\omega_j)\}_{j=1}^J$ satisfying $\mathcal{C}_1$,$\mathcal{C}_2$,$\mathcal{C}_3$,$\mathcal{C}_4$ are obtained.

V. Incoherent design of FI sparse arrays

In the previous section, the optimization problem in (21) is solved over the entire bandwidth. It may be very inefficient and sometimes infeasible when a large number of candidate sensors is assumed. In this section, we propose a four-step algorithm which separates between the analysis step of determining the support S of the filters $\{\mathbf{h}(\omega_j)\}_{j=1}^J$ and the synthesis step where the actual filters, $\{\mathbf{h}_K(\omega_j)\}_{j=1}^J$, are calculated. This separation enables to solve the optimization problem much more efficiently and also facilitates design of arrays with a large number of candidate sensors.

Note that the parameter K can be determined in the coherent design from (23). However, in the incoherent design it is not trivial and less intuitive to determine analytically the value of K. In this work, we do not address this problem, and solve a slightly different problem from what has been defined in (18), assuming that K is given but satisfies $K \ll M$. In the simulations, we may take the same value obtained by the coherent approach, in order to concentrate on the comparison between the incoherent and coherent design. Yet, a method

for determining the optimal parameter K for the incoherent design is an important problem to be addressed in a future research. Practically, K can be determined by a line search over this parameter. Later, in the simulation section we present the performance of the incoherent design for different values of K. In the following subsections, we describe each of these steps.

A. Analysis

As a first step, we would like to solve separately $\forall \omega_j \in \Omega$ the following ℓ_1-norm optimization problem:

$$\begin{aligned} \underset{\mathbf{h}(\omega_j)}{\text{minimize}} \quad & \sum_{m=1}^{M} |H_m(\omega_j)| \\ \text{subject to} \quad & \\ & \mathbf{h}^H(\omega_j)\,\mathbf{d}\left(\mathbf{k}_{\omega_j}(\boldsymbol{\rho}_{\mathrm{s}})\right) = 1 \\ & \mathbf{h}^H(\omega_j)\,\mathbf{h}(\omega_j) \le \gamma(\omega_j) \\ & \left\| (\mathbf{b}_{\mathrm{d}}^{\mathrm{m}})^T - \mathbf{h}^H(\omega_j)\,\mathbf{D}\left(\boldsymbol{K}_j^{\mathrm{m}}\right) \right\|_2^2 \le \epsilon_1(\omega_j) \\ & \left\| (\mathbf{b}_{\mathrm{d}}^{\mathrm{s}})^T - \mathbf{h}^H(\omega_j)\,\mathbf{D}\left(\boldsymbol{K}_j^{\mathrm{s}}\right) \right\|_2^2 \le \epsilon_2(\omega_j). \end{aligned} \tag{24}$$

Similarly to the coherent optimization approach, both the objective function and the constraints in (24) are convex, therefore, (24) can be solved by convex optimization methods (e.g., using CVX toolbox [50]).

We solve (24) $\forall \omega_j \in \Omega$ separately, and get the sparse vectors, $\mathbf{h}_{\mathrm{A}}(\omega_j)$, $j = 1, 2, \ldots, J$ of length M, where the subscript A stands for analysis. Each of these vectors has different support which influenced by the frequency. Specifically, as the frequency increases, the support becomes smaller. Let us define the data matrix $\mathbf{H}_{\mathrm{A}}$ of size $M \times J$ containing the vectors $\{\mathbf{h}_{\mathrm{A}}(\omega_j)\}_{j=1}^{J}$ in its columns, i.e.,

$$\mathbf{H}_{\mathrm{A}} = \left[\mathbf{h}_{\mathrm{A}}(\omega_1), \mathbf{h}_{\mathrm{A}}(\omega_2), \ldots, \mathbf{h}_{\mathrm{A}}(\omega_J)\right]. \tag{25}$$

Similarly to the coherent approach where the solution for (21) yields K sensors jointly used for all the frequencies, we would like also for the incoherent approach to make an elegant decision regarding the best choice of K sensors jointly used during the array synthesis process.

The problem of determining the K most dominant sensors positions where K is given, can be viewed as a clustering problem whose solution may yield K clusters of sensors. Therefore, we treat the matrix $\mathbf{H}_{\mathrm{A}}$ as a measurements matrix of M observations, each with J features. In other words, each of the M potential microphones is represented by a feature vector in $\mathbb{C}^J$.

B. Dimensionality Reduction

As the matrix $\mathbf{H}_{\mathrm{A}}$ was obtained by an ℓ_1-norm optimization, it consists of the sparse vectors $\{\mathbf{h}_{\mathrm{A}}(\omega_j)\}_{j=1}^{J}$ in its columns, and thus effectively a rank-deficient matrix with a decaying singular values spectrum. Figure 1 presents a typical example of the absolute value of $\mathbf{H}_{\mathrm{A}}$ on a logarithmic scale. The parameters for this example are specified later in Section VII-A. One can see that this matrix is sparse: For each frequency five to ten sensors are required. Furthermore, as the frequency increases, the energy of the selected sensors is spread over a smaller array aperture. This structure stems from the fact that in each frequency the spatial sampling constraint should be satisfied, meaning that the element spacing should be smaller than half the wavelength at that frequency.

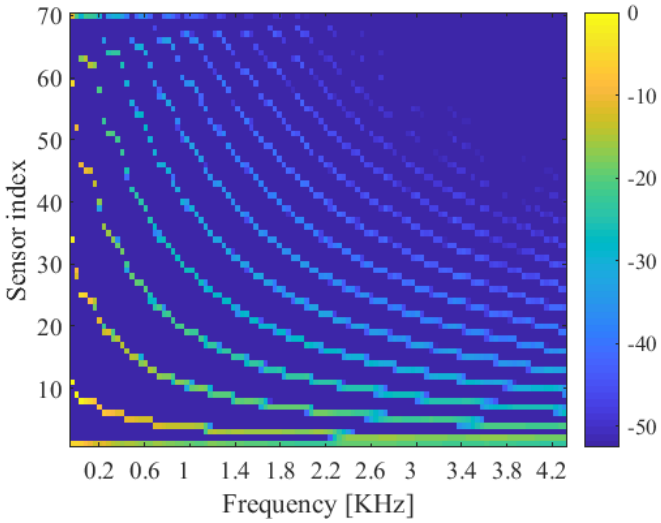

Fig. 1: Absolute values of the elements of the matrix $\mathbf{H}_{\mathrm{A}}$ on a logarithmic scale.

In order to show that $\mathbf{H}_{\mathrm{A}}$ is indeed effectively a rank-deficient matrix, we may look at the sampled correlation matrix of $\mathbf{H}_{\mathrm{A}}$:

$$\mathbf{R}_{\mathrm{A}} = \mathbf{H}_{\mathrm{A}}^H \mathbf{H}_{\mathrm{A}} \tag{26}$$

of size $J \times J$.

The jth diagonal element of $\mathbf{R}_{\mathrm{A}}$ is simply the squared-norm of the filter vector $\mathbf{h}_{\mathrm{A}}(\omega_j)$. As the frequency increases, the coefficient energy of a superdirective beamformer usually decreases, as can be seen in Fig. 1. Due to the sparseness of the matrix $\mathbf{H}_{\mathrm{A}}$ the off-diagonal entries of $\mathbf{R}_{\mathrm{A}}$ are very close to zero since two different columns of $\mathbf{H}_{\mathrm{A}}$ are uncorrelated. These considerations lead to a conclusion that $\mathbf{R}_{\mathrm{A}}$ is effectively a rank-deficient matrix as observed from Fig. 2 where the absolute value of $\mathbf{R}_{\mathrm{A}}$ on a logarithmic scale is presented.

The effective low rank of the matrix $\mathbf{R}_{\mathrm{A}}$, which results in a decaying eigenvalues spectrum as will be shown later, implies also the same property for the matrix $\mathbf{H}_{\mathrm{A}}$, because of the well-known relation between the singular values of both matrices: Let $\{\sigma_i\}_{i=1}^{r}$ be the singular values of the matrix $\mathbf{H}_{\mathrm{A}}$ where r denotes its rank, then $\left\{\lambda_i = \sigma_i^2\right\}_{i=1}^{r}$ are the eigenvalues of the matrix $\mathbf{R}_{\mathrm{A}}$.

Therefore, we may assume that the matrix $\mathbf{H}_{\mathrm{A}}$ contains some redundancy, as its high dimensional feature vectors are not spread across the entire space, but rather concentrated on a significantly lower dimension. Thus, prior to the clustering step, we apply a pre-processing step of dimensionality reduction to the matrix $\mathbf{H}_{\mathrm{A}}$. In this work, we use the principal component analysis (PCA) algorithm [51] commonly used for dimensionally reduction, which is a linear algorithm.

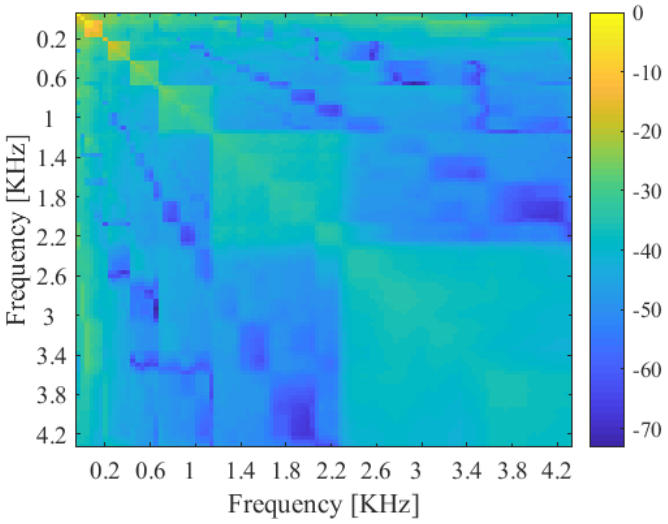

Fig. 2: Absolute values of the elements of the matrix $\mathbf{R}_{\mathrm{A}}$ on a logarithmic scale.

Of course, other linear and non-linear dimension reduction techniques can be used and are part of a future research.

The input to the PCA algorithm is the data matrix $\mathbf{H}_{\mathrm{A}}$ of size $M \times J$ defined above. Define the matrix $\overline{\mathbf{H}}_{\mathrm{A}}$ to be a centralized version of $\mathbf{H}_{\mathrm{A}}$, i.e., the sampled mean of each column of $\mathbf{H}_{\mathrm{A}}$ has been shifted to zero. The output of the PCA algorithm yields the compact data representation matrix:

$$\mathbf{H}_{\mathrm{R}} = \overline{\mathbf{H}}_{\mathrm{A}} \overline{\mathbf{U}}, \tag{27}$$

where $\overline{\mathbf{U}}$ is a matrix of size $J \times i$ contains i eigenvectors corresponding to the i largest eigenvalues, and the subscript R stands for reduced.

The column dimension i of the matrix $\overline{\mathbf{U}}$ is set according to the following criteria: let $\lambda_1 \geq \lambda_2 \geq \cdots \geq \lambda_J$ be the eigenvalues of the matrix $\mathbf{R}_{\mathrm{A}}$, then we choose the first $i \ll J$ eigenvalues which satisfy

$$\Sigma_i \triangleq \frac{\sum_{j=1}^{i} \lambda_j}{\sum_{j=1}^{J} \lambda_j} \leq \alpha, \tag{28}$$

where typically $0.6 \leq \alpha \leq 0.9$.

C. Clustering

The next step is to apply a clustering algorithm on the rows of $\mathbf{H}_{\mathrm{R}}$ in order to determine the most dominant microphones. Herein, we use the k-means algorithm [52] to divide all the M sensors into K clusters. The k-means algorithm is a two-step iterative algorithm, where in each iteration the first step is to assign each observation to the cluster whose mean yields the least within-cluster sum of squares. Then, an update step is applied where updated mean values are calculated to be the centroids of the observations in the new clusters. The algorithm also includes an initialization step by choosing a set of K mean values. The k-means algorithm is heuristic, and convergence to the global minimum is not assured, meaning that the result may depend on the initial clusters. Therefore, it is common to run it multiple times (typically 10-20 times) with different initial conditions, and choose the best solution, i.e., the one that yields the minimal within-cluster sums of points-to-centroid distances. Finally, we choose one representative microphone from each of the K chosen clusters, which is closest to the corresponding centroid. We denote by $\{\mathbf{p}_{i_k}\}_{k=1}^{K}$ the positions of the chosen sensors.

Note that in this work we employ separately a dimensionally reduction based PCA stage and a clustering k-means based stage. A different approach that combines both these stages together is presented in [53]. Considering such an approach for the selection of the K candidate sensors is a subject for a future research.

D. Synthesis

In Section V-A the goal is to determine the minimal number of the active sensors, K, which fulfill the constraints, and consequently, the objective function was the ℓ_1-norm of the filters $\{\mathbf{h}(\omega_j)\}_{j=1}^{J}$. In the synthesis step, where the K indices $\{i_k\}_{k=1}^{K}$ of the sensors used to build the FI beampattern are already determined, there is no need to solve an ℓ_1-norm optimization problem and instead we may solve an optimization problem whose objective function is related to the four $\mathcal{C}_1$,$\mathcal{C}_2$,$\mathcal{C}_3$,$\mathcal{C}_4$ constraints presented in Section III. A reasonable choice is to minimize the noise output power (i.e., $\mathcal{C}_4$), subject to the remaining constraints, $\mathcal{C}_1$,$\mathcal{C}_2$, and $\mathcal{C}_3$. Therefore, we can formulate it as follows: $\forall \omega_j \in \Omega$, solve

$$\begin{aligned} \underset{\mathbf{h}_K(\omega_j)}{\text{minimize}} \quad & \left\|\mathbf{h}_K^H(\omega_j)\right\|_2^2 \\ \text{subject to} \quad & \\ & \mathbf{h}_K^H(\omega_j)\, \mathbf{d}_K\left(\mathbf{k}_{\omega_j}(\boldsymbol{\rho}_{\mathrm{s}})\right) = 1 \\ & \left\|(\mathbf{b}_{\mathrm{d}}^{\mathrm{m}})^T - \mathbf{h}_K^H(\omega_j)\, \mathbf{D}_K\left(\boldsymbol{K}_j^{\mathrm{m}}\right)\right\|_2^2 \leq \epsilon_1(\omega_j) \\ & \left\|(\mathbf{b}_{\mathrm{d}}^{\mathrm{s}})^T - \mathbf{h}_K^H(\omega_j)\, \mathbf{D}_K\left(\boldsymbol{K}_j^{\mathrm{s}}\right)\right\|_2^2 \leq \epsilon_2(\omega_j), \end{aligned} \tag{29}$$

where $\mathbf{d}_K\left(\mathbf{k}_{\omega_j}(\boldsymbol{\rho}_{\mathrm{s}})\right) = \mathbf{T}_{\mathrm{s}}(\mathbf{i}_K)\, \mathbf{d}\left(\mathbf{k}_{\omega_j}(\boldsymbol{\rho}_{\mathrm{s}})\right)$, $\mathbf{D}_K\left(\boldsymbol{K}_j^{\mathrm{m}}\right) = \mathbf{T}_{\mathrm{s}}(\mathbf{i}_K)\, \mathbf{D}\left(\boldsymbol{K}_j^{\mathrm{m}}\right)$, and $\mathbf{D}_K\left(\boldsymbol{K}_j^{\mathrm{s}}\right) = \mathbf{T}_{\mathrm{s}}(\mathbf{i}_K)\, \mathbf{D}\left(\boldsymbol{K}_j^{\mathrm{s}}\right)$. The resulting filters $\{\mathbf{h}_K(\omega_j)\}_{j=1}^{J}$ correspond to the sensors located in the indices $\{\mathbf{p}_{i_k}\}_{k=1}^{K}$. This fact is important since it means that we can use only K out of M sensors and still obtain adequate results as presented later in the simulations section.

VI. Parameters Adjustment

In both the coherent and incoherent approaches several parameters must be chosen properly in order to get optimal performance. While for the incoherent approach a simple procedure to initialize these parameters will be offered in the following, for the coherent approach, searching for the appropriate parameters may be a much more exhaustive task as it should be done over all the frequency bins, simultaneously. Therefore, we may concentrate on the incoherent design.

The most important parameters to be determined are the number of active sensors, K, and the tolerance parameters $\{\epsilon_1(\omega_j)\}_{j=1}^{J}$, $\{\epsilon_2(\omega_j)\}_{j=1}^{J}$, and $\{\gamma(\omega_j)\}_{j=1}^{J}$. Other parameters

like ϵ and ϵ_η are set once, and are not changed with frequency. We propose the following procedure for the initialization and adjustment of these parameters.

As noted before, determining the number of active sensors, K, is an open question, and we assume it is given. In the next section, an example illustrating the influence of this parameter on the performance is presented. Practically, a very rough line search over K will be sufficient to get a reasonable value for this parameter. In the next section, we use the same value obtained by the coherent approach for comparison.

In order to determine properly initial values for the tolerance parameters $\{\epsilon_1(\omega_j)\}_{j=1}^J$, $\{\epsilon_2(\omega_j)\}_{j=1}^J$, and $\{\gamma(\omega_j)\}_{j=1}^J$, we may conduct a two-dimensional grid search of $\epsilon_1(\omega_1)$ and $\gamma(\omega_1)$. We set $\epsilon_2(\omega_1) = \beta\epsilon_1(\omega_1)$, where $\beta > 1$ is fixed and not changed at all. We set a uniform grid for possible values of $\{\epsilon_1(\omega_j)\}_{j=1}^J$ and $\{\gamma(\omega_j)\}_{j=1}^J$. In some cases, like the one presented in Section VII-A, $\{\gamma(\omega_j)\}_{j=1}^J$ can be modeled and bounded by lower and upper limits corresponding to the worst case and the best case of output noise power. In these cases, we may apply a grid of possible values between the worst case and the best case.

The above two-dimensional search provides the optimal set of parameters $\{\epsilon_1(\omega_1), \epsilon_2(\omega_1), \gamma(\omega_1)\}$. We use this set for the next frequency bins where in each one we adaptively increase $\epsilon_1(\omega_j)$ and $\epsilon_2(\omega_j)$ by a factor of g_1 each time the CVX solver do not yield a feasible solution to (24), meaning that we increase the maximal allowed tolerance of $\mathcal{C}_1$ and $\mathcal{C}_2$. Once we find appropriate values of $\epsilon_1(\omega_j)$ and $\epsilon_2(\omega_j)$, we decrease $\gamma(\omega_j)$ by a factor of g_2, and solve the optimization problem. If a feasible solution is accepted, then $\gamma(\omega_j)$ is updated to its new value.

The above parameters initialization and adjustment procedure is a part of the analysis step. The obtained values for these parameters may be also suitable for the synthesis step. Yet, fine-tuning of these parameters may still be required because in the synthesis step, we are restricted to use only K sensors. Such a fine-tuning process can be done similarly to the process described above, used for the analysis step.

VII. Numerical Simulations

The proposed incoherent approach is demonstrated for two classes of superdirective beamformers. The first example shows a sparse design of DMAs with a linear geometry, and the second example considers a sparse design of a superdirective beamformer with a planar geometry. The performance of the incoherent sparse design is compared to that of the coherent design presented in Section IV, and also to the performance of a uniform array design.

A. One-dimensional Array Design

We consider a sparse design of linear DMAs, which refer to arrays that combine closely spaced sensors to respond to the spatial derivatives of the acoustic pressure field. These small-size arrays yield nearly FI beampatterns, and include the well-known superdirective beamformer as a particular case. Due to the linear geometry, the directivity pattern depends only on the azimuth θ and we can treat the case of two-dimensional beampattern where $\phi = 90^\circ$, i.e., the plane where the array is laid. For the 2D case, the FI beampattern of an Nth-order DMA is given by [18]

$$\mathcal{B}_N(\theta) = \sum_{n=0}^{N} a_{N,n} \cos^n \theta, \tag{30}$$

where $\{a_{N,n}\}_{n=0}^N$ are real coefficients, and the desired signal arrives from the endfire direction, i.e., from $\theta = 0^\circ$. For this example $\mathcal{B}_N(\theta)$ is considered to be the desired beampattern, i.e., $\mathcal{B}_\mathrm{d}(\boldsymbol{\rho}) = \mathcal{B}_N(\theta)$. It is also assumed that the element spacing, δ, is much smaller than the wavelength of the incoming signal, i.e,

$$\forall \omega \in \Omega: \quad \delta \ll \lambda = \frac{2\pi c}{\omega} \;\Rightarrow \delta \ll \frac{2\pi c}{\omega_{\max}}, \tag{31}$$

in order to approximate the spatial differential of the pressure signal, where $\omega_{\max}$ is the angular frequency corresponding to the highest frequency in the bandwidth of interest, Ω, and $c = 340$ m/sec.

In spite of their benefits, traditional DMAs suffer from noise amplification, especially at low frequencies. For that, we apply a sparse approach for designing robust DMAs with relatively smaller number of sensors.

We compare between four approaches for design of linear arrays. The first one is our proposed incoherent sparse design presented in the previous section. The second is the coherent sparse design presented in Section IV. The third approach is based on minimum-norm design for Nth-order DMAs presented in [16], where K closely uniformly spaced microphones were used to obtain a desired directivity pattern. We refer to this approach as the minimum-norm (MN) approach. The fourth design is similar to the third, but with the only difference that the K sensors are spread uniformly over the entire possible aperture of M sensors. We refer to this approach as the minimum-norm extended array (MNE) approach.

We apply the four approaches to designing a FI broadband beampattern for the range of frequencies between $f_{\mathrm{low}} = 200$ Hz and $f_{\mathrm{high}} = 4480$ Hz. Assuming a typical duration of $T = 25$ msec for the window analysis used for the corresponding time-domain received signal, the frequency resolution is $\Delta f = 1/T = 40$ Hz. Thus, the number of bins J can be calculated as $J = \frac{f_{\mathrm{high}} - f_{\mathrm{low}}}{\Delta f} = 108$. For the sparse approaches, an initial array of $M = 70$ potential microphones, with element spacing of $\delta = 1$ cm $\ll \frac{2\pi c}{\omega_{\max}} \approx 7.6$ cm between two adjacent sensors is assumed.

We design a third-order hypercardioid pattern (i.e., $N = 3$) which maximizes the DF, whose theoretical beampattern is given according to (30) as

$$\mathcal{B}_N^{\mathrm{HC}}(\theta) = -0.14 - 0.57\cos\theta + 0.57\cos^2\theta + 1.15\cos^3\theta. \tag{32}$$

For this case we set $\boldsymbol{\rho}_L = \theta_L = 60^\circ$, i.e., the mainlobe region in the azimuthal axis is $-60^\circ \le \theta \le 60^\circ$.

For the MN and MNE approaches, we impose three null directions at $\theta_1 = 51^\circ$, $\theta_2 = 103^\circ$, and $\theta_3 = 154^\circ$, according to the theoretical beampattern of a third-order hypercardioid [18], and distortionless constraint at $\theta = 0^\circ$.

We set the parameter $\gamma(\omega_j)$ to be

$$\gamma(\omega_j) = \alpha(\omega_j)\gamma_{\mathrm{MN}}(\omega_j) + [1-\alpha(\omega_j)]\,\gamma_{\mathrm{MNE}}(\omega_j), \qquad (33)$$

where $\gamma_{\mathrm{MN}}(\omega_j) = \mathbf{h}_{\mathrm{MN}}^H(\omega_j)\mathbf{h}_{\mathrm{MN}}(\omega_j)$ is the white noise output power for the case of the MN approach, which yields the maximal white noise output power for the case of K sensors. The other quantity $\gamma_{\mathrm{MNE}}(\omega_j) = \mathbf{h}_{\mathrm{MNE}}^H(\omega_j)\mathbf{h}_{\mathrm{MNE}}(\omega_j)$ is the white noise output power of the MNE approach which yields the lowest white noise output power for the case of K sensors. The frequency-dependent weighting parameter $\alpha(\omega_j)$ is used to get more flexibility in regions where the noise output power is high. As explained in Section VI, a two dimensional grid search is performed in order to find optimal values for $\epsilon_1(\omega_1)$ and $\gamma(\omega_1)$. In this example, we perform a grid of possible values for $\alpha(\omega_1)$, instead. We choose a uniform grid between 0 to 1 with a spacing of 0.1. The meaning of (33) is that we confine the output noise power of the sparse design to a moderate value between the best achievable one and the worst-case value.

In order to build the matrices $\mathbf{D}\left(\boldsymbol{K}_j^{\mathrm{m}}\right)$ and $\mathbf{D}\left(\boldsymbol{K}_j^{\mathrm{s}}\right)$ we uniformly discretize the angular axis with $\Delta\theta = 2^\circ$. We choose the parameters $\epsilon = 10^{-4}$, $\epsilon_\eta = 5\cdot 10^{-3}$, $\beta = 4$, and $g_1 = g_2 = 1.25$. We set a uniform grid between 0.1 to 2 with a spacing of 0.2 for the line search of $\epsilon_1(\omega_1)$.

For the proposed incoherent approach, we run the first step of analysis presented in Section V-A, with the parameters adjustment procedure presented in Section VI. We get the initial optimal values of $\epsilon_1(\omega_1) = 0.3$, $\epsilon_2(\omega_1) = 1.2$, and $\alpha(\omega_1) = 0.2$. The final values of these parameters were $\epsilon_1(\omega_J) \approx 0.5$, $\epsilon_2(\omega_J) \approx 1.8$, and $\alpha(\omega_J) = 0.4$. We get the $M \times 1$ filter vectors $\mathbf{h}_{\mathrm{A}}(\omega_j)$, $\forall \omega_j \in \Omega$, which are used to construct the matrix $\mathbf{H}_{\mathrm{A}}$ (25) of size $M \times J$, presented in Fig. 1.

We use the matrix $\mathbf{H}_{\mathrm{A}}$ as an input to the PCA algorithm described in Section V-B. In Fig. 3 the eigenvalues of $\mathbf{R}_{\mathrm{A}}$(26) are presented in an ascending order (blue solid line), normalized by the maximal eigenvalue, and also presented is the cumulative function, Σ_i (28) (red dashed line). We observe a rapid decay rate of the eigenvalues which motivates the choice to take a much smaller number of eigenvalues in order to construct the matrix $\mathbf{H}_{\mathrm{R}}$ (27).

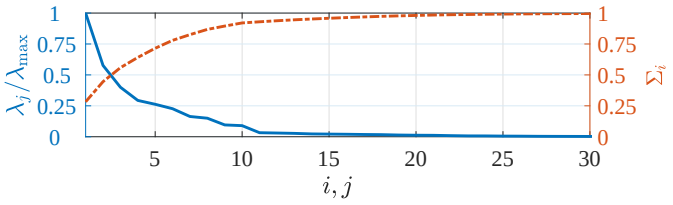

Fig. 3: The spectrum $\lambda_j/\lambda_{\max}, j = 1, 2, ..., J$ of the correlation matrix $\mathbf{R}_{\mathrm{A}}$ (blue solid line), and the quantity Σ_i (28) vs. j (red dashed line) for the third-order asymmetric hypercardioid obtained by the incoherent sparse design.

The value of $\alpha = 0.6$ in (28) was chosen yielding $i = 3$ (i.e., the first three dominant eigenvalues where selected), as it obtains the best results with respect to other choices of the parameter α. Although non-negligible energy exists also in the remaining eigenvalues, it is expected that only part of them will obtain the optimal results since they may carry most of the variability of the sensors features vectors.

In the next step, we apply the k-means algorithm to the matrix $\mathbf{H}_{\mathrm{R}}$ to obtain K clusters, and in the fourth step, the synthesis was performed using the K sensors according to Section V-D.

We run the coherent approach by solving (21) using the CVX software [50], where we used the optimal values of the tolerance parameters $\{\epsilon_1(\omega_j)\}_{j=1}^J$, $\{\epsilon_2(\omega_j)\}_{j=1}^J$, and $\{\gamma(\omega_j)\}_{j=1}^J$, obtained by the incoherent design. After 7 iterations, we get $\Delta\boldsymbol{\eta} < \epsilon_\eta$ and $K = 10$ dominant sensors were identified, while all the rest are close to zero, meaning that both $\boldsymbol{\eta}$ and the filters $\{\mathbf{h}(\omega_j)\}_{j=1}^J$ are sparse vectors with $K = 10$ active sensors. The number of selected elements remains the same even if more iterations are used. We finally obtain the filters $\{\mathbf{h}_K(\omega_j)\}_{j=1}^J$ using (19).

Figure 4 presents the array layout for each of the four approaches. The incoherent approach yields the sensors marked by the black stars, while the coherent approach yields the red diamond. One can see that both approaches lead to a similar array layout. Also presented the sensor positions obtained by the MN and MNE approaches, where for these both approaches, the sensors positions are set a-priori. The MN approach achieves the smallest array aperture, yet, it suffers from white noise amplification as will be discussed later.

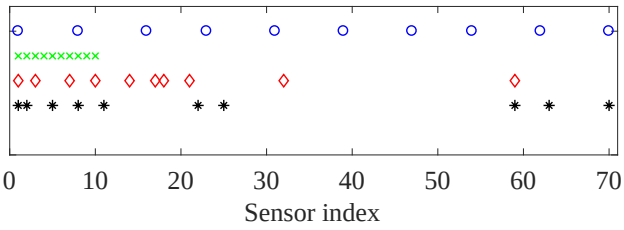

Fig. 4: Array layout for each of the compared design approaches. The black stars line is for the incoherent design. The red diamond line is for the coherent design. The green 'x' line is for the MN approach, and the blue circles line is for the MNE approach.

Figure 5 illustrates the beampattern (1) of a third-order hypercardioid for a specific frequency of $f = 2500$ Hz, obtained by each of the four approaches (blue dotted line). Also presented is the theoretical beampattern (32) of a third-order hypercardioid (black dashed line). One can see that the MN approach obtains the beampattern which is the most similar to the theoretical value while the MNE has much higher sidelobes due to the spatial aliasing. Both the coherent sparse approach and the incoherent sparse approach obtain beampatterns with similar characteristics.

Figure 6 shows the WNG (17) and the DF (34) as a function of the frequency obtained by the incoherent sparse design (black dashed line), the coherent sparse design (red circles line), the MNE design (blue triangles line), and the MN design (green diamonds line). Also presented is the theoretical DF of a third-order hypercardioid (magenta stars line). The DF of the

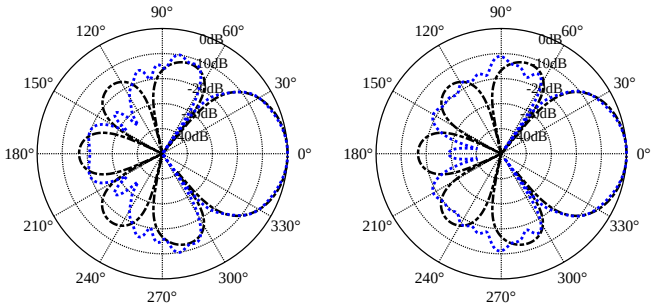

(a) incoherent sparse design (b) coherent sparse design

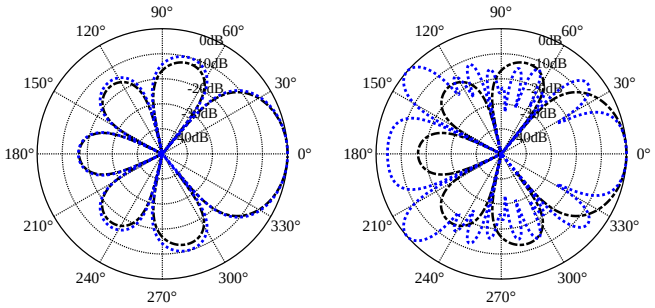

(c) MN design (d) MNE design

Fig. 5: Beampatterns of a third-order hypercardioid (blue dotted line) for $f = 2500$ Hz, obtained by various approaches. Also presented is the theoretical beampattern of a third-order hypercardioid (black dashed line).

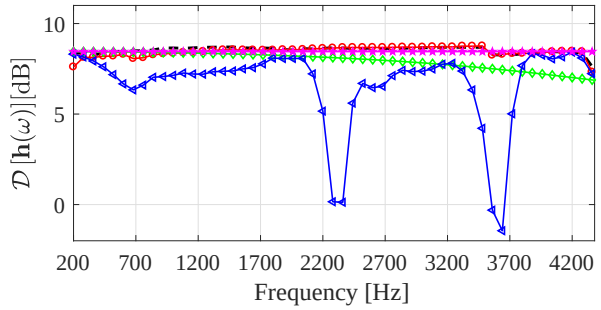

(a)

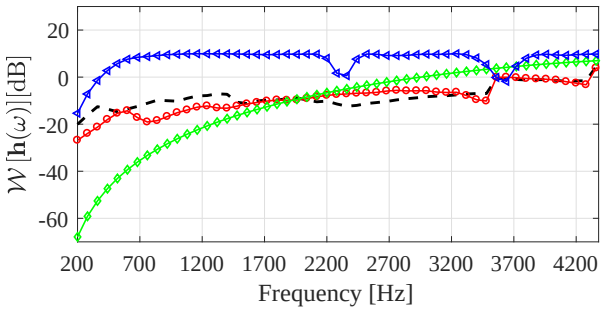

(b)

Fig. 6: (a) DF and (b) WNG vs. frequency for the incoherent sparse design (black dashed line), the coherent sparse design (red circles line), the MNE design (blue triangles line), and the MN design (green diamonds line). Also presented is the theoretical DF of a third-order hypercardioid (magenta stars line).

array is the gain in signal-to-noise ratio (SNR) for the case of a spherical diffuse noise, i.e. [16]:

$$\mathcal{D}\left(\mathbf{h}(\omega_j)\right) = \frac{\left|\mathbf{h}^H\left(\omega_j\right)\mathbf{d}\left(\mathbf{k}_{\omega_j}\left(\boldsymbol{\rho}\right)\right)\right|^2}{\mathbf{h}^H\left(\omega_j\right)\boldsymbol{\Gamma}_{\mathrm{dn}}\left(\omega_j\right)\mathbf{h}\left(\omega_j\right)}, \tag{34}$$

where

$$\left[\boldsymbol{\Gamma}_{\mathrm{dn}}\left(\omega_j\right)\right]_{il} = \mathrm{sinc}\left(\frac{\omega_j\delta}{c}(l-i)\right) \tag{35}$$

is an $M \times M$ pseudo-coherence matrix of the diffuse noise field. As expected, both coherent and incoherent sparse approaches obtain similar results in terms of WNG and DF. The main difference is the processing time for each approach. Both approaches were run on an i7-5600U CPU @ 2.6 GHz of INTEL with 12 GB ram. While the incoherent approach takes about 5 minutes of running including the adjustment procedure, the coherent approach run for almost 160 minutes, which is almost two order of magnitudes more than the incoherent approach. Moreover, as written before, we used the values of the tolerance parameters obtained by incoherent approach also for the coherent design. The consequence of adjusting such parameters directly using the coherent design is that such design may take much more time than 160 seconds. Note also that for the coherent approach, an iterative algorithm is required in order to get adequate approximation of ℓ_0-norm. For the incoherent approach, such an iterative algorithm is not required at all, and a good approximation of the ℓ_0-norm is obtained by a single iteration. Yet, both PCA and K-means are iterative algorithms.

The MN obtains nearly FI optimal DF implying on its FI beampattern, but achieves poor WNG, especially for low frequencies, which is a well-known problem of superdirective beamformers in general, and of DMAs in particular. On the contrary, the MNE approach yields superior WNG, but for frequencies above 2000 Hz the DF fluctuates due to the presence of grating lobes, which may appear when $f \geq c/\left(2\delta_{\mathrm{MNE}}\right)$, where $\delta_{\mathrm{MNE}} = (M-1)\delta/(K-1)$ is the element spacing for the extended uniform array. Substituting the values in this formula we get that for $f \geq 2300$ Hz grating lobes may appear, in accordance with the results presented in this figure.

The synthesized FI beampatterns versus frequency are shown in Fig. 7 for the (a) incoherent approach, (b) the coherent approach, (c) the MN approach, and (d) the MNE approach. This figure reflects the trends inspected by the DF plot. Specifically, for both the coherent and incoherent sparse approaches the beampattern is almost FI, especially in the mainlobe region and less in the sidelobes regions, as dictated by the constraints $\mathcal{C}_1$ and $\mathcal{C}_2$. The MN approach achieves the clearest and most perfect FI beampattern, and in the MNE one can see the grating lobes starting from approximately $f = 2000$ Hz.

As specified before, it is assumed that for the incoherent design, K is given. We now present the influence of this parameter on the performance of the incoherent design. Figure 8 shows the WNG (17) and the DF (34) as a function of the frequency obtained by the incoherent sparse design

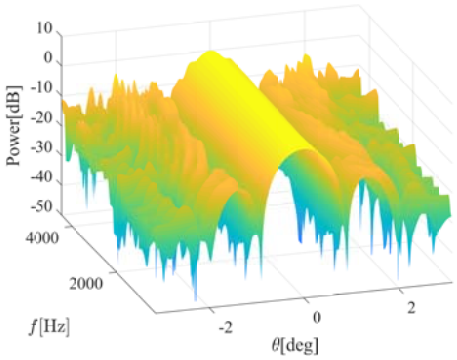

(a) incoherent sparse design

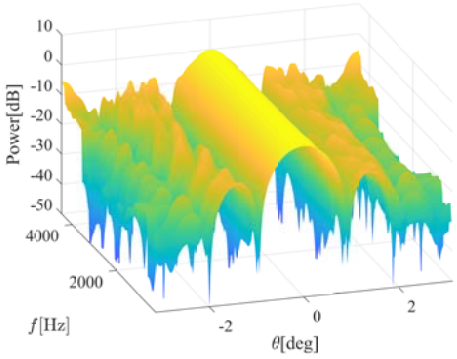

(b) coherent sparse design

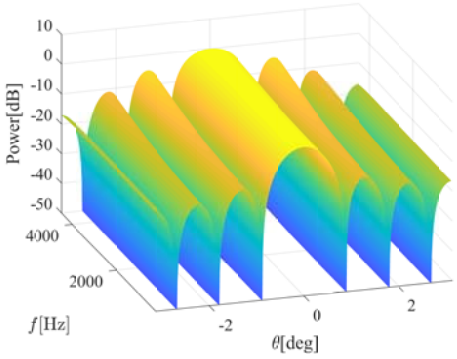

(c) MN design

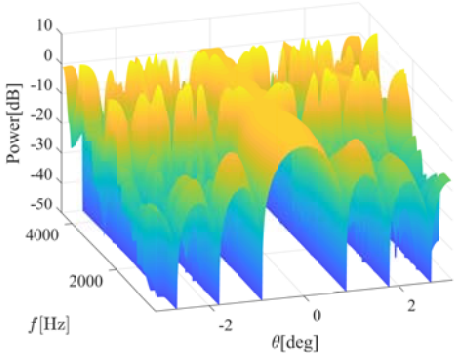

(d) MNE design

Fig. 7: Beampatterns versus frequency for the four examined design approaches.

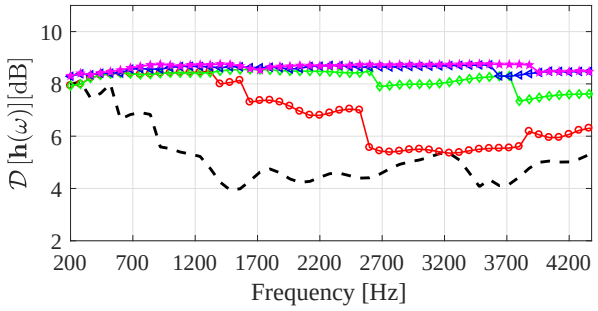

(a)

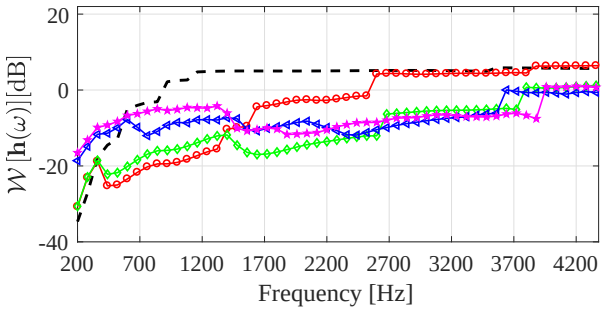

(b)

Fig. 8: (a) DF and (b) WNG vs. frequency obtained by the incoherent sparse design for the case that $K = 4$ (black dashed line), $K = 6$ (red circles line), $K = 8$ (green diamonds line), $K = 10$ (blue triangles line), and $K = 12$ (magenta stars line).

for $K = 4, 6, 8, 10,$ and 12. One can see the influence of a proper choice of K on the performance, especially on the ability to obtain nearly constant and superior DF. One can see that $K = 10$ and $K = 12$ obtain similar performances. Thus, a practical procedure to set K is to design the beamformer for several values of K, and choose the one that yields the optimal performance. Note that for $K = 4$ and $K = 6$, superior WNG for high frequencies was obtained due to larger tolerance values of ϵ_1 and ϵ_2, but at the expense of much lower DF.

Figure 9 shows the WNG and the DF as a function of frequency obtained by the incoherent sparse design for $\alpha = 0.45, 0.6, 0.7, 0.8,$ and 0.9. One can see that the choice of $\alpha = 0.6$ yields a good compromise between the WNG and the DF.

B. Sparse Superdirective Planar Array

Let us now consider the problem of synthesizing a sparse planar array of sensors used for implementation of FI superdirective beamformer. Such a beamformer can be used for several applications like underwater acoustic sonar arrays. Herein, we focus only on the proposed incoherent design approach since for such a high number of potential sensors and frequency bins, the coherent processing is infeasible when using standard hardware while the proposed approach still yields results with a reasonable computational complexity.

We apply the design for the frequency range between $f_{\mathrm{low}} = 400$ Hz and $f_{\mathrm{high}} = 6000$ Hz. Assuming a typical duration

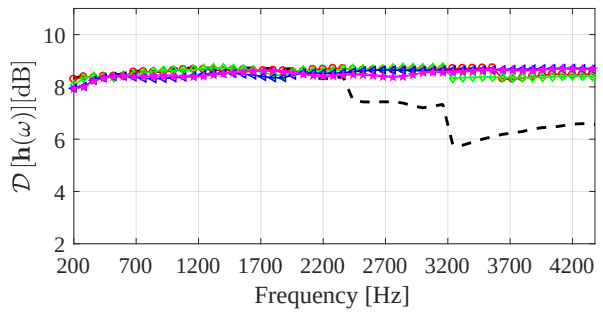

(a)

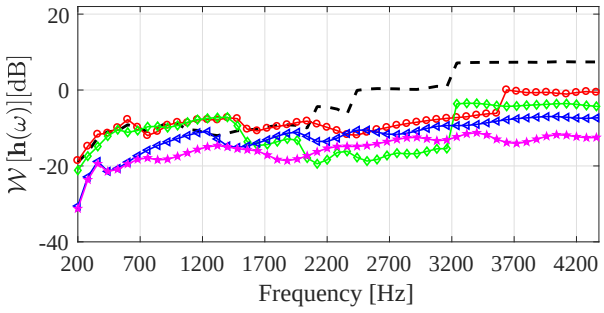

(b)

Fig. 9: (a) DF and (b) WNG vs. frequency obtained by the incoherent sparse design for the case that $\alpha = 0.45$ (black dashed line), $\alpha = 0.6$ (red circles line), $\alpha = 0.7$ (green diamonds line), $\alpha = 0.8$ (blue triangles line), and $\alpha = 0.9$ (magenta stars line).

of $T = 10$ msec for the window used for the analysis of underwater acoustic signals, the frequency resolution is $\Delta f = 1/T = 100$ Hz. Thus, the number of bins J can be calculated as $J = \frac{f_{\text{high}} - f_{\text{low}}}{\Delta f} = 58$. For the incoherent sparse approach, an initial square array of 16×16 potential sensors (i.e., $M = 256$), with an element spacing of $\delta = 1.5$ cm $\ll \frac{2\pi c}{\omega_{\max}} \approx 5.5$ cm between two adjacent sensors is assumed.

We uniformly discretize the angular axis and the elevation axis with $\Delta\theta = 4^\circ$ and $\Delta\phi = 4^\circ$, respectively. Under the assumption that the plane of the array consolidates with the x-y plane, the wavenumber is

$$\mathbf{k}_{\omega_j}(\boldsymbol{\rho}) = -\frac{\omega_j}{c}\left[\cos\theta\sin\phi \quad \sin\theta\sin\phi\right]^T. \tag{36}$$

The analytical expression of the superdirective beamformer is obtained by maximizing the DF (34) subject to the distortionless constraint in the desired signal direction, $\boldsymbol{\rho}_{\text{s}}$, and for a given ω_j is [24]

$$\mathbf{h}_{\text{SD}}(\omega_j) = \frac{\boldsymbol{\Gamma}^{-1}_{\text{dn},\epsilon}(\omega_j)\mathbf{d}\left(\mathbf{k}_{\omega_j}(\boldsymbol{\rho}_{\text{s}})\right)}{\mathbf{d}^H\left(\mathbf{k}_{\omega_j}(\boldsymbol{\rho}_{\text{s}})\right)\boldsymbol{\Gamma}^{-1}_{\text{dn},\epsilon}(\omega_j)\mathbf{d}\left(\mathbf{k}_{\omega_j}(\boldsymbol{\rho}_{\text{s}})\right)}, \tag{37}$$

where $\boldsymbol{\Gamma}_{\text{dn},\epsilon}(\omega_j)$ is a regularized version of $\boldsymbol{\Gamma}_{\text{dn}}(\omega_j)$ (35), i.e.,

$$\boldsymbol{\Gamma}_{\text{dn},\epsilon}(\omega_j) = \boldsymbol{\Gamma}_{\text{dn}}(\omega_j) + \epsilon\mathbf{I}_M, \tag{38}$$

with the regularization parameter $\epsilon = 10^{-4}$.

We set the frequency $f_0 = 400$ Hz to be the reference frequency of the desired beampattern, i.e.,

$$\mathcal{B}_{\text{d}}(\boldsymbol{\rho}) = \mathcal{B}(\mathbf{h}(\omega_0)) = \mathbf{h}^H(\omega_0)\mathbf{d}\left(\mathbf{k}_{\omega_0}(\boldsymbol{\rho})\right), \tag{39}$$

where $\omega_0 = 2\pi f_0$. Figure 10 (a) presents in a logarithmic scale, the three-dimensional desired beampattern, $\mathcal{B}_{\text{d}}(\boldsymbol{\rho})$, matched to the reference frequency of $f_0 = 400$ Hz . Note that even-though $\mathcal{B}_{\text{d}}(\boldsymbol{\rho})$ has two mainlobes in opposite directions, practically it contains only one mainlobe steered towards the broadside while the opposite direction is blocked by the array plane and there is a negligible radiation in this direction.

We set empirically the number of sensors for the incoherent sparse design to be $K = 36$ sensors, and compare the incoherent approach with two uniform design approaches. In the first one, all the $K = 36$ sensors are placed in the center of the allowed aperture with an element spacing of $\delta = 1.5$ cm. Similarly to the linear case, very good FI and DF can be obtained at the expense of poor WNG. Therefore, the beamformer coefficients vector for that case was obtained by minimizing $\mathcal{C}_4$ (16) subject to $\mathcal{C}_1, \mathcal{C}_2, \mathcal{C}_3$ (12)-(15). We refer to this approach as the small aperture planar (SAP) array approach. The second uniform design approach may use the $K = 36$ sensors spread over the entire allowable aperture. The trends for this design are the opposite: high WNG but inferior DF, especially at high frequencies. Therefore, for this design we minimize $\mathcal{C}_1$ (12) subject to $\mathcal{C}_2, \mathcal{C}_3, \mathcal{C}_4$ (13)-(16). We refer to this approach as the large aperture planar (LAP) array.

Similarly to the previous example, we apply the parameters adjustment procedure proposed in Section VI to set the tolerance parameters. We get the initial values $\epsilon_1(\omega_1) = 0.6$, $\epsilon_2(\omega_1) = 2$, and $\gamma(\omega_1) \approx 3$, and the final values of $\epsilon_1(\omega_J) = 1.8$, $\epsilon_2(\omega_J) = 6$, and $\gamma(\omega_J) \approx 0.1$.

For simplicity, we may concentrate on beampatterns whose mainbeams are at the broadside, i.e., corresponding to $\phi_{\text{s}} = 0^\circ$. Sparse designs of beampatterns steered to other directions are topics for future research. For this case, it is reasonable to assume that the beampatterns have symmetry with respect to the axes $x = 0$ and $y = 0$, i.e., all the four quarters combining the plane of the array are identical. Therefore, after the first analysis step, we use the PCA algorithm to find only $K/4 = 9$ sensors in one of the quarters, and duplicate it to the three remaining quarters. Figure 11 presents the array layout of the incoherent sparse approach (black stars), the SAP uniform design with small spacing (green squares), and the LAP design approach (blue circles).

In order to get more intuition regarding the sensors selected by the incoherent sparse design, we calculate the total energy of the coefficients of each sensor, that is

$$\mathcal{E}_m = \|\mathbf{H}_{\text{A}}(m,:)\|_2^2, \ m = 1, 2, ..., M, \tag{40}$$

where $\mathbf{H}_{\text{A}}(m,:)$ is the mth row of the matrix $\mathbf{H}_{\text{A}}$. We define the log-ratio

$$\mathcal{L}_m = 10\log_{10}\frac{\mathcal{E}_m}{\max\limits_m \{\mathcal{E}_m\}_{m=1}^M}, \tag{41}$$

indicating how much dominant is the mth-sensor with respect to the other sensors by terms of the total energy it contains across the bandwidth of interest Ω, and define a threshold parameter T_0 such that sensors whose log-ratio satisfy $\mathcal{L}_m \leq T_0$ are ignored. In Fig. 12 one can see the selected sensors for the choice of (a) $T_0 = -5$ dB, (b) $T_0 = -7$ dB, (c)

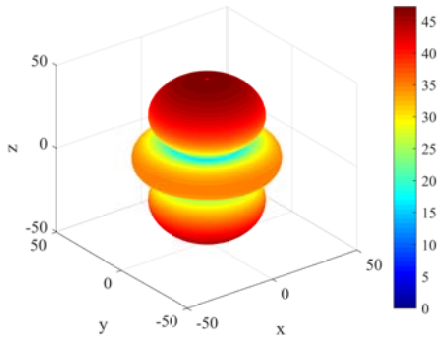

(a) Desired beampattern

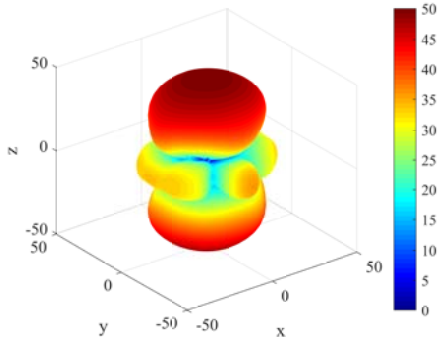

(b) Incoherent sparse design

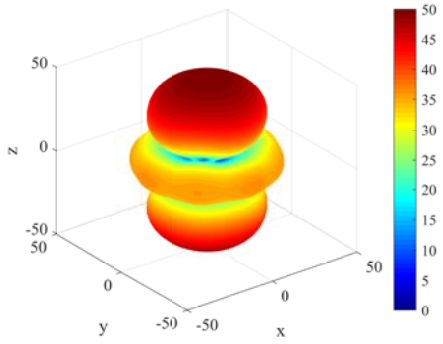

(c) SPA design

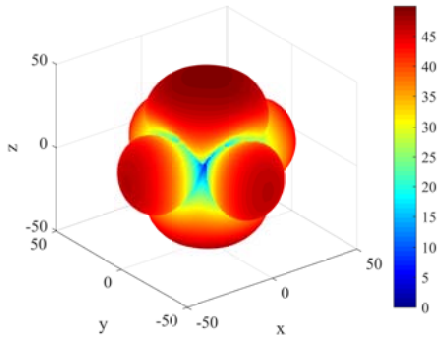

(d) LPA design

Fig. 10: Synthesized FI beampatterns for $f = 5100$ Hz using various approaches. Also presented is the desired beampattern, $\mathcal{B}_{\mathrm{d}}(\boldsymbol{\rho})$ matched to the reference frequency of $f_0 = 400$ Hz.

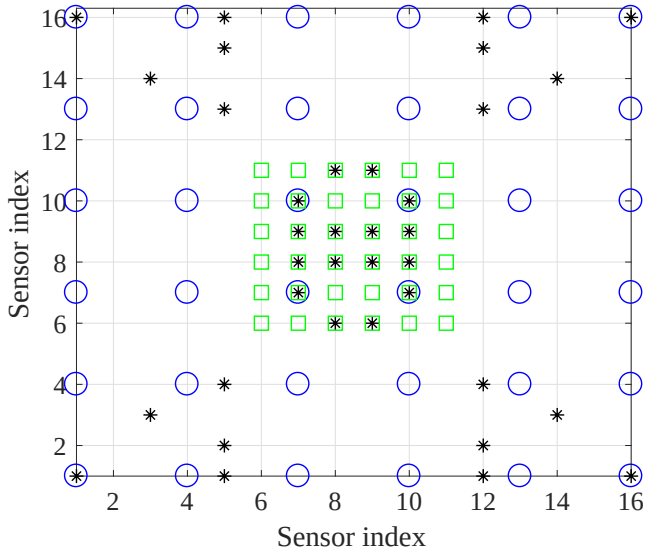

Fig. 11: The array layout of the planar array obtained by the incoherent proposed approach (black stars), the SAP uniform approach (green squares), and the LAP approach (blue circles).

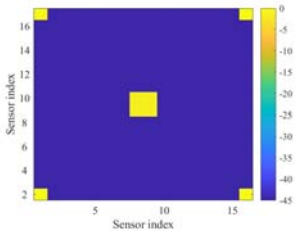

(a) $T_0 = -5$ dB

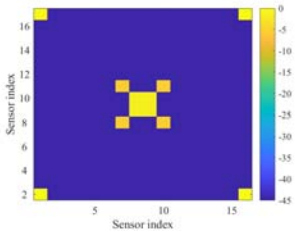

(b) $T_0 = -7$ dB

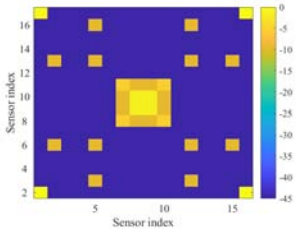

(c) $T_0 = -10$ dB

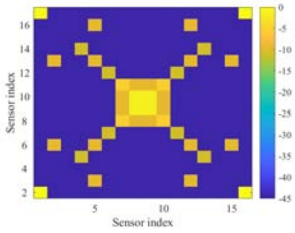

(d) $T_0 = -12$ dB

Fig. 12: Sensors chosen for different values of the threshold value T_0.

$T_0 = -10$ dB, and (d) $T_0 = -12$ dB. We can see from (a) that the most dominant sensors lay in the center and in the distant corners. As we decrease T_0, more sensors are added as illustrated in (b)-(d).

Figure 13 shows the WNG (17) and the DF (34) as a function of the frequency obtained by the incoherent sparse design (black dashed line), the LAP design (blue triangles line), and the SAP design (green diamonds line). Also presented is the DF of the desired beampattern (magenta stars line). Like in the previous example, the incoherent sparse design is a good solution and optimal in terms of WNG and DF.

Figures 10(b)-(d) show synthesized FI beampatterns for $f = 5100$ Hz using the incoherent approach, the SPA approach, and

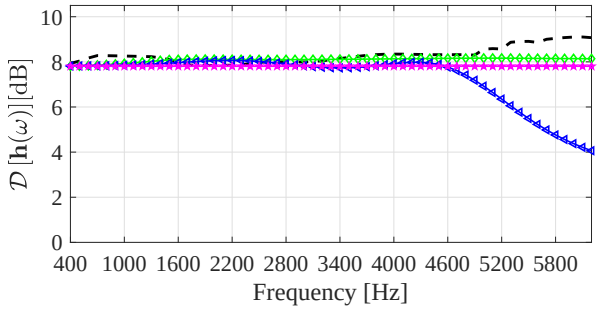

(a)

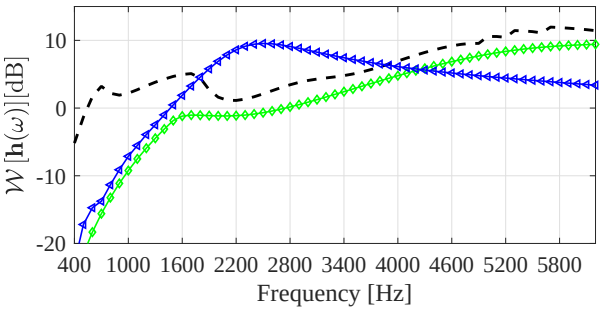

(b)

Fig. 13: (a) DF and (b) WNG vs. frequency obtained by the incoherent sparse design (black dashed line), the LAP design (blue triangles line), and the SAP design (green diamonds line). Also presented is the DF of the desired beampattern (magenta stars line).

the LPA approach.

The above design examples demonstrate the feasibility and the advantages of the incoherent approach compared to the coherent sparse design approach and to the uniform design approaches.

Note that for both the coherent and incoherent designs, it was assumed that the direction of the source, ρ_s, is given and the design depends on it, meaning that once the source direction is changed, the design is not valid anymore. A more sophisticated sparse design for geometries such as circular and concentric arrays, that can be steered in multiple directions, is currently under research.

VIII. Conclusion

We have presented an incoherent approach for a sparse design of FI beamformers, where the sensors positions are sparsely selected for each frequency bin separately, and subsequently a fusion mechanism is applied in order to determine the sensors used jointly for all frequencies in order to synthesize the FI beamformer. The proposed approach was applied to design robust superdirective FI beamformers with minimal number of sensors. It was compared to the coherent approach where optimization is performed simultaneously over all directions and frequencies of interest, and also to uniform design approaches. Simulations show that the proposed incoherent sparse design is a good compromise between robustness and directivity and obtains FI beamformer with significantly reduced computational complexity. Moreover, for scenarios where a large number of potential sensors and frequency bins is assumed, the coherent approach is infeasible while the incoherent design provides results with a reasonable computation time. Future research may focus on different array geometries, applying nonlinear dimension reduction techniques, as well as greedy-based algorithms for sparse design.

References

[1] M. Branstein and D. B. Ward, Eds, *Microphone Arrays: Signal Processing Techniques and Applications*. Berlin, Germany: Springer-Verlag, 2001.

[2] J. Benesty, J. Chen, Y. Huang, and J. Dmochowski, "On microphone-array beamforming from a MIMO acoustic signal processing perspective," *IEEE Trans. Audio, Speech, Language Process.*, vol. 15, no. 3, pp. 1053–1065, Mar. 2007.

[3] J. Benesty, J. Chen, and Y. Huang, *Microphone Array Signal Processing*. Berlin, Germany: Springer-Verlag, 2008.

[4] S. Yan, "Optimal design of FIR beamformer with frequency invariant patterns," *Appl. Acoust.*, vol. 67, pp. 511–528, 2006.

[5] E. Mabande, A. Schad, and W. Kellermann, "Design of robust superdirective beamformer as a convex optimization problem," in *Proc. IEEE Int. Conf. Acoust. Specch Signal Process. (ICASSP), Taipei, Taiwan*, 2009, pp. 77–80.

[6] H. H. Chen, S. C. Chan, and K. L. Ho, "Adaptive beamforming using frequency invariant uniform concentric circular arrays," *IEEE Trans.Circuits Syst. I, Reg. Papers*, vol. 54, no. 9, pp. 1938–1949, Sept. 2007.

[7] S. C. Chan and H. H. Chen, "Uniform concentric circular arrays with frequency-invariant characteristics - theory, design, adaptive beamforming and doa estimation," *IEEE Trans. Signal Process.*, vol. 55, no. 1, pp. 165–177, Jan. 2007.

[8] W. Liu and S. Weiss, *Wideband Beamforming: Concepts and Techniques*. Chichester, U.K.: Wiley, 2010.

[9] M. Crocco and A. Trucco, "Design of robust superdirective arrays with a tunable tradeoff between directivity and frequency-invariance," *IEEE Trans. Signal Process.*, vol. 59, no. 5, pp. 2169–2181, May 2011.

[10] B. D. Van Veen and K. V. Buckley, "Beamforming: A versatile approach to spatial filtering," *IEEE Mag. Acoust., Speech, Signal Process.*, vol. 5, pp. 4–24, Apr. 1988.

[11] W. Liu and S. Weiss, "Design of frequency invariant beamformers for broadband arrays," *IEEE Trans. Signal Process.*, vol. 56, no. 2, pp. 855–860, Feb. 2008.

[12] T. Do-Hong and P. Russer, "Spatial signal processing for wideband beamforming," in *Proc.VII International Symposium on Theoretical Electrical Engineering*, 2003, pp. 73–76.

[13] H. Hung and M. Kaveh, "Focusing matrices for coherent signal subspace processing," *IEEE Trans. Acoust. Speech Signal Process.*, vol. 36, no. 8, pp. 1272–1281, Aug 1988.

[14] M. A. Doron and A. Nevet, "Robust wavefield interpolation for adaptive wideband beamforming," *Signal Process.*, vol. 80, pp. 1579–1594, 2008.

[15] Y. Buchris, I. Cohen, and M. A. Doron, "Bayesian focusing for coherent wideband beamforming," *IEEE Trans. Audio, Speech, Language Process.*, vol. 20, no. 4, pp. 1282–1295, May 2012.

[16] J. Benesty and J. Chen, *Study and Design of Differential Microphone Arrays*. Berlin, Germany: Springer-Verlag, 2012.

[17] J. Benesty, J. Chen, and I. Cohen, *Design of Circular Differential Microphone Arrays*. Berlin, Germany: Springer-Verlag, 2015.

[18] G. W. Elko, "Superdirectional microphone arrays," in *Acoustic Signal Processing for Telecommunication*, S. L. Gay and J. Benesty, Eds. Boston, MA: Kluwer Academic Publishers, 2000, ch. 10, pp. 181–237.

[19] H. Teutsch and G. W. Elko, "First- and second-order adaptive differential microphone arrays," in *Darmstadt, Germany: 7th International Workshop on Acoustic Echo and Noise Control*, 2001, pp. 57–60.

[20] M. Buck, "Aspects of first-order differential microphone arrays in the presence of sensor imperfections," *European Trans. Telecommunications*, vol. 13, pp. 115–122, Mar. 2002.

[21] E. De Sena, H. Hacihabiboğlu, and Z. Cavetković, "On the design and implementation of higher order differential microphones," *IEEE Trans. Audio, Speech, Language Process.*, vol. 20, no. 1, pp. 162–174, Jan. 2012.

[22] L. Zhao, J. Benesty, and J. Chen, "Design of robust differential microphone arrays," *IEEE Trans. Audio, Speech, Language Process.*, vol. 22, no. 10, pp. 1455–1464, Oct. 2014.

[23] C. Pan, J. Benesty, and J. Chen, "Design of robust differential microphone arrays with orthogonal polynomials," *J. Acoust. Soc. Amer.*, vol. 138, no. 2, pp. 1079–1089, Aug. 2015.

[24] H. Cox, R. M. Zeskind, and T. Kooij, "Practical supergain," *IEEE Trans. Acoust., Speech, Signal Processing*, vol. ASSP-34, no. 3, pp. 393–398, June 1986.

[25] M. I. Skolnik, G. Nemhauser, and J. W. Sherman III, "Dynamic programming applied to unequally spaced arrays," *IEEE Trans. Antennas Propagat.*, vol. AP-12, pp. 35–43, Jan. 1964.

[26] O. M. Bucci, M. D'Urso, T. Isernia, P. Angeletti, and G. Toso, "Deterministic synthesis of uniform amplitude sparse arrays via new density taper techniques," *IEEE Trans. Antennas Propagat.*, vol. 58, no. 6, pp. 1949–1958, Jun. 2010.

[27] O. Quevedo-Teruel and E. Rajo-Iglesias, "Ant colony optimization in thinned array synthesis with minimum sidelobe level," *IEEE Trans. Antennas Wireless Propag. Lett.*, vol. 5, pp. 349–352, Jun. 2006.

[28] A. Trucco, E. Omodei, and P. Repetto, "Synthesis of sparse planar arrays," *Electron. Lett.*, vol. 33, no. 22, pp. 1834–1835, Oct. 1997.

[29] R. M. Leahy and B. D. Jeffs, "On the design of maximally sparse beamforming arrays," *IEEE Trans. Antennas Propagat.*, vol. 39, no. 8, pp. 1178–1187, Aug. 1991.

[30] Y. Liu, Q. H. Liu, and Z. Nie, "Reducing the number of elements in the synthesis of shaped-beam patterns by the forward-backward matrix pencil method," *IEEE Trans. Antennas Propagat.*, vol. 58, no. 2, pp. 604–608, Feb. 2010.

[31] W. Zhang, L. Li, and F. Li, "Reducing the number of elements in linear and planar antenna arrays with sparseness constrained optimization," *IEEE Trans. Antennas Propagat.*, vol. 59, no. 8, pp. 3106–3111, Feb. 2011.

[32] G. Oliveri, E. T. Bekele, F. Robol, and A. Massa, "Sparsening conformal arrays through a versatile bcs-based method," *IEEE Trans. Antennas Propagat.*, vol. 62, no. 4, pp. 1681–1689, Apr. 2014.

[33] B. Fuchs, "Synthesis of sparse arrays with focused or shaped beampattern via sequential convex optimizations," *IEEE Trans. Antennas Propagat.*, vol. 60, no. 7, pp. 3499–3503, Jul. 2012.

[34] M. D'Urso, G. Prisco, and R. M. Tumolo, "Maximally sparse, steerable, and nonsuperdirective array antennas via convex optimizations," *IEEE/ACM Trans. Antennas Propag.*, vol. 64, no. 9, pp. 800–815, Sep. 2016.

[35] S. E. Nai, W. Ser, Z. L. Yu, and H. Chen, "Beampattern synthesis for linear and planar arrays with antenna selsction by convex optimization," *IEEE Transactions on Antennas and Propagation*, vol. 58, no. 12, pp. 3923–3930, Dec. 2010.

[36] M. Crocco and A. Trucco, "Design of superdirective planar arrays with sparse aperiodic layouts for processing broadband signals via 3-d beamforming," *IEEE/ACM Trans. Audio, Speech, Language Process.*, vol. 22, no. 4, pp. 800–815, Apr. 2014.

[37] T. Chou, "Frequency-independent beamformer with low response error," in *Proc. IEEE Int. Conf. Acoust. Specch Signal Process. (ICASSP), Detroit, MI*, May 1995, pp. 2995–2998.

[38] Y. R. Zheng, R. A. Goubran, and M. El-Tanany, "Experimental evaluation of a nested microphone array with adaptive noise cancellers," *IEEE Trans. Instrum. Meas.*, vol. 53, pp. 777–786, June 2004.

[39] I. J. H. Doles and F. D. Benedict, "Broad-band array design using the asymptotic theory of unequally spaced arrays," *IEEE Trans. Antennas Propagat.*, vol. 36, pp. 27–33, Jan. 1988.

[40] D. B. Ward, R. A. Kennedy, and R. C. Williamson, "Theory and design of broadband sensor arrays with frequency invariant farfield beampatterns," *J. Acoust. Soc. Amer.*, vol. 97, no. 2, pp. 1023–1034, Feb. 1995.

[41] M. Crocco and A. Trucco, "Stochastic and analytic optimization of sparse aperiodic arrays and broadband beamformers with robust superdirective patterns," *IEEE Trans. Audio, Speech, Language Process.*, vol. 20, no. 9, pp. 2433–2447, Nov. 2012.

[42] Z. Li, K. F. Cedric Yiu, and Z. Fen, "A hybrid descent method with genetic algorithm for microphone array placement design," *Appl. soft Comput.*, vol. 13, pp. 1486–1490, 2013.

[43] Y. Liu, L. Zhang, C. Zhu, and Q. H. Liu, "Synthesis of nonuniformly spaced linear arrays with frequency-invariant patterns by the generalized matrix pencil methods," *IEEE Trans. Antennas Propagat.*, vol. 63, no. 4, pp. 1614–1625, Apr. 2015.

[44] M. B. Hawes and W. Liu, "Sparse array design for wideband beamforming with reduced complexity in tapped delay-lines," *IEEE/ACM Transactions on Audio, Speech and Language Processing (TASLP)*, vol. 22, no. 8, pp. 1236–1247, 2014.

[45] Y. Liu, L. Zhang, L. Ye, Z. Nie, and Q. H. Liu, "Synthesis of sparse arrays with frequency-invariant-focused beam patterns under accurate sidelobe control by iterative second-order cone programming," *IEEE Trans. Antennas Propagat.*, vol. 63, no. 12, pp. 5826–5832, Dec. 2015.

[46] S. F. Cotter, B. D. Rao, K. Engan, and K. Kreutz-Delgado, "Sparse solutions to linear inverse problems with multiple measurement vectors," *IEEE Transactions on Signal Processing*, vol. 53, no. 7, pp. 2477–2488, July 2005.

[47] H. L. Van-trees, *Detection, Estimation and Modulation Theory, Part IV - Optimum Array Processing*. New York: Wiley Interscience, 2002.

[48] E. J. Candès, M. B. Wakin, and S. P. Bond, "Enhancing sparsity by reweighted ℓ_1 minimization," *J. Fourier Analy. Appl.*, vol. 14, pp. 877–905, Dec. 2008.

[49] P. T. Boufounosa, P. Smaragdisb, and B. Rajc, "Joint sparsity models for wideband array processing," in *SPIE Optical Engineering+ Applications*. International Society for Optics and Photonics, 2011, pp. 81 380–K.

[50] M. Grant, S. Boyd, and Y. Ye, "CVX: Matlab software for disciplined convex programming," 2008.

[51] I. Jolliffe, *Principal Component Analysis*. Springer Series in Statistics. Springer, New York, NY, 1986.

[52] J. A. Hartigan and M. A. Wong, "Algorithm as 136: A k-means clustering algorithm," *Journal of the Royal Statistical Society. Series C (Applied Statistics)*, vol. 28, no. 1, pp. 100–108, 1979.

[53] C. Ding and X. He, "K-means clustering via principal component analysis," in *Proceedings of the twenty-first international conference on Machine learning*. ACM, 2004, p. 29.

Chapter 6

Joint Sparse Concentric Array Design for Frequency and Rotationally Invariant Beampattern

This chapter contains the following manuscript:

Y. Buchris, I. Cohen, J. Benesty, and A. Amar, "Joint Sparse Concentric Array Design for Frequency and Rotationally Invariant Beampattern," submitted to IEEE/ACM Transactions on Audio, Speech, and Language Processing.

Joint Sparse Concentric Array Design for Frequency and Rotationally Invariant Beampattern

Yaakov Buchris, *Member, IEEE*, Israel Cohen, *Fellow, IEEE*, Jacob Benesty, and Alon Amar, *Member, IEEE*

***Abstract*—Frequency-invariant concentric arrays are fundamental components in some real-world applications, like teleconferencing, voice service devices, underwater acoustics, and others, where the azimuthal arrival direction of the desired signal is changeable. The fact that the demand for limited hardware and computational resources in such applications is typically essential, motivates the use of a sparse design which can optimize both the number of the required sensors and the beamformer gain vectors. Herein, we propose a new greedy based joint-sparse design of frequency and rotationally invariant concentric arrays which preserves the properties of the designed directivity pattern for different azimuthal directions of steering. Simulation results show that the greedy sparse design, compared to uniform and random designs, obtains superior performance in terms of array gain, and frequency and rotationally invariant beampattern, with a reasonable computational and hardware resources.**

***Index terms*—** Concentric arrays, frequency-invariant beamformer, rotationally-invariant beamformer, greedy joint sparse, superdirective beamformers.

I. Introduction

Practical applications requiring variable steering direction of the mainlobe while preserving similar performance in terms of array gain and directivity pattern, e.g., circular and concentric arrays integrated in video conference systems and some voice service devices, nowadays become more and more an essential part of human life [1]–[3]. In particular, concentric arrays that contain one or more rings of sensors in different radii and provide similar and steerable beampattern for 360° azimuthal coverage, are advantageous also for broadband beamformers as they enable robust and frequency-invariant (FI) beampatterns over a wide range of frequencies [4]. Among several classical approaches for FI beamformer design which were extensively explored during the last decades [5]–[18], the class of sparse design approaches of FI beamformers is of a great interest, since both the beamformer gains as well as the entire number of sensors and their positions are optimized [19]–[23].

Previous work on sparse concentric array design includes stochastic optimization methods, such as genetic algorithm (GA) [24]–[26], modified particle swarm optimization (MPSO) [27], and biogeographybased optimization (BBO) [28]. These approaches take advantage from the stochastic optimization mechanism which mitigates problems of local minima convergence and have a good numerical stability, yielding sparse concentric arrays with lower sidelobes level (SLL), fewer elements, and nearly rotationally-invariant azimuthal coverage. Chatterjee et al. [29] apply a differential evolution (DE) algorithm in order to optimize both the radii and the element spacing of each ring, resulting in an array layout with reduced SLL and a smaller number of elements with respect to a uniform array. In [30] an iterative perturbation algorithm is applied in order to get a sparse planar array with a desired beampattern and directivity. Zhao et al. [31] propose a hybrid approach which combines both convex optimization and deterministic one in order to determine the number of concentric rings, the ring radii, and the current ring excitations satisfying the requirements on the directivity pattern. Other deterministic design approaches for sparse concentric arrays can be found in [32]–[34]. The main limitation of all these works is that the design was focused mainly on the narrowband case and/or optimization only of the ring radii, each with sensors arranged uniformly along it.

To the best of the authors' knowledge, in contrast to the narrowband case, broadband sparse designs of FI concentric arrays have almost not been addressed in previous works. In [35]–[37] various design approaches for the synthesis of broadband rotationally symmetric sparse concentric arrays are presented. These approaches optimize the suppression of the peak SLL across the bandwidth of interest, yet they are not considered as FI arrays, and they adapted only to a broadside reception of signals. Li et al. [38] propose an analytical approach for synthesis of FI directivity pattern of concentric arrays over a certain frequency band. In that approach the ring radii and their weights are determined analytically, matched to a specific frequency satisfying a desired beampattern. Then, for each different frequency some connections are established used to calculate different sets of coefficients that yield the same directivity pattern. The main shortcomings of that approach is that it does not provide enough frequency range coverage over which the beampattern is nearly FI, and it does not optimize the total number of sensors in the array layout.

Motivated by the aforementioned shortcomings of previous approaches, in this paper, we extend our recent work on joint-sparse design of FI beamforming [39], and propose a new greedy based joint-sparse design for FI concentric arrays, which optimizes both the number of sensors and the number of rings while taking into consideration the requirement regarding the rotationally-invariant property. Therefore, the obtained sparse array layout may allow to get a similar array response for different azimuthal directions of steering. Moreover, it also supports the case that one is interested on a similar array response only for an azimuthal range or for a discrete number of azimuthal directions. The proposed approach is more general with respect to [39] as it allows more than a one fixed steering direction. Note that in this work we focus

This research was supported by the Israel Science Foundation (grant no. 576/16), and the ISF-NSFC joint research program (grant No. 2514/17).

on the two-dimensional (2D) scenario where both the array and the incoming signals are on the same plane. Such a model approximates real scenarios where most of the reflected signals arrive from the walls and less from the floor and the ceiling, e.g., a concentric array in a video conference room. The more general three-dimensional (3D) scenario is out of the scope of this work.

As a first step of the proposed design, a modified Orthogonal Matching Pursuit (OMP) [40], [41] greedy based iterative algorithm is applied aiming to determine the array layout for a case of steering to a fixed direction. In each iteration, it seeks for the sensors that mostly contribute to the residual signal. As a stopping criterion, the selected set of sensors up to the current iteration, which are joint to all the frequency bins in the bandwidth of interest, are used to construct the array layout steered to the fixed direction while fulfilling several desired constraints. In the next step, the array layout is symmetrically duplicated into additional azimuthal directions in order to obtain nearly rotationally-invariant beampattern. As the duplicated array layout contains some redundancy, an ℓ_{12}-optimization problem is solved in order to attain a more compact array layout which is joint sparse both in the number of rings and in the number of sensors, used in the final synthesis step to obtain the rotationally-invariant FI beampattern. Reducing also the number of rings may contribute to the rotationally-invariant property of the sparse array. The fact that the array layout is a joint-sparse implies on the desired property of hardware consuming since the selected sensors are joint for all the frequencies in the bandwidth of interest.

Simulation results compare between the proposed greedy sparse design, a uniform array design and a random array design. It is shown that the greedy sparse design yields an FI rotationally-invariant beamformer with high robustness to array imperfections and high directivity. In contrast, the uniform designs suffer from high SLL and sensitivity to noise, while the random design provides unstable and fluctuated results. In addition, the sparse design requires reasonable resource consumption leading to a practical design for applications involving large arrays with hundreds of candidate sensors.

II. Signal Model and Problem Formulation

Assume a 2D scenario during which signals are propagating towards a concentric array composed from G rings, where the gth ring is characterized by its radii, $r_g,\ g = 1, 2, ..., G$, and the number of candidate positions for locating the sensors, M_g, as illustrated in Fig. 1. The total number of candidate positions is $M = \sum_{g=1}^{G} M_g$. The center of the concentric array coincides with the first ring having $r_1 = 0$ and M_1=1. The direction of arrival of signals towards the array is denoted by the azimuth θ, measured anti-clockwise from the x axis, i.e., at $\theta = 0°$, and sensor 1 of each ring is placed on the x axis, i.e., at $\theta = 0°$. The direction of arrival of the desired source signal to the array is denoted by the azimuth angle $\theta_{\rm s}$.

Let Ω and Θ denote the frequency and angle range of interest, respectively. We uniformly discretize both the frequency and angle spaces and introduce J frequency bins

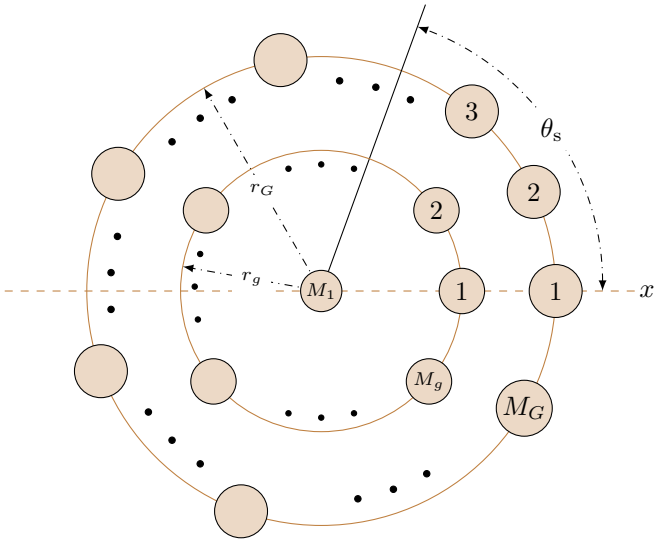

Fig. 1: Illustration of a concentric circular array with G rings, where the gth ($g = 1, 2, ..., G$) ring, with a radius of r_g, consists of M_g omnidirectional microphones, with $\theta_{\rm s}$ being the source incidence angle.

$\{\omega_j\}_{j=1}^{J} \in \Omega$, and P directions $\{\theta_p\}_{p=1}^{P} \in \Theta$ that cover the entire beampattern, i.e., $\Theta \in [-\pi, \pi]$.

The beampattern of such an array for the angular frequency $\omega_j \in \Omega$ and azimuth $\theta_p \in \Theta$ can be expressed as

$$\mathcal{B}\left(\omega_j, \theta_p\right) = \text{Trace}\left[\mathbf{H}^H(\omega_j)\mathbf{D}\left(\omega_j, \theta_p\right)\right], \tag{1}$$

where the superscript ^{H} denotes the conjugate-transpose operator, the matrix

$$\mathbf{H}(\omega) = \begin{bmatrix} H_{1,1}(\omega_j) & \cdots & H_{1,g}(\omega_j) & \cdots & H_{1,G}(\omega_j) \\ H_{2,1}(\omega_j) & \cdots & H_{2,g}(\omega_j) & \cdots & H_{2,G}(\omega_j) \\ \vdots & \cdots & H_{3,g}(\omega_j) & \cdots & H_{3,G}(\omega_j) \\ H_{M_1,1}(\omega_j) & \cdots & \vdots & \cdots & H_{4,G}(\omega_j) \\ 0 & \cdots & H_{M_g,g}(\omega_j) & \cdots & \vdots \\ 0 & \cdots & 0 & \cdots & H_{M_G,G}(\omega_j) \end{bmatrix} \tag{2}$$

is an $M_G \times G$ matrix containing in its gth column the beamformer coefficients of the sensors located on the gth ring of the array, while we assume that M_G is the maximal number of sensors on a single ring. The matrix $\mathbf{D}(\omega_j, \theta_p)$ is an $M_G \times G$ steering matrix whose gth column is given by

$$\mathbf{d}_g(\omega_j, \theta_p) = \begin{bmatrix} e^{\jmath \frac{\omega_j r_g}{c} \cos(\theta_p - \psi_{g,1})} \\ e^{\jmath \frac{\omega_j r_g}{c} \cos(\theta_p - \psi_{g,2})} \\ \vdots \\ e^{\jmath \frac{\omega_j r_g}{c} \cos(\theta_p - \psi_{g,M_g})} \\ 0 \\ 0 \end{bmatrix} \tag{3}$$

where

$$\psi_{g,m} = \frac{2\pi(m-1)}{M_g},\ m = 1, 2, ..., M_g \tag{4}$$

is the angular position of the mth array element of the gth ring, $\jmath = \sqrt{-1}$, and c is the waveform's speed.

Assume that we select a subset of $K \ll M$ sensors, concentrated in $G' < G$ rings, used to synthesize the K spatio-temporal beampatterns for each frequency $\omega_j \in \Omega$, that is,

$$\mathcal{B}_K(\omega_j, \theta_p) = \mathcal{Q}\{\mathbf{H}(\omega_j); \mathbf{A}_K(\mathbf{i}_{G'})\}^H \mathcal{Q}\{\mathbf{D}(\omega_j, \theta_p); \mathbf{A}_K(\mathbf{i}_{G'})\}, \tag{5}$$

where $\mathcal{Q}\{\cdot\}$ is a FI selection operator defined as follows: for matrices $\mathbf{X}_1$ and $\mathbf{X}_2$ of size $m \times n$, $\mathcal{Q}\{\mathbf{X}_1; \mathbf{X}_2\}$ returns a column vector with all the entries in $\mathbf{X}_1$ for which the corresponding entries in the binary matrix $\mathbf{X}_2$ are equal to '1'. The matrix $\mathbf{A}_K(\mathbf{i}_{G'})$ of size $M_G \times G$ contains K nonzero elements which spread across only G' columns, whose indexes are specified by the $G' \times 1$ vector $\mathbf{i}_{G'}$. Note that for the particular case that $\mathcal{Q}\{\cdot\}$ operates on vectors $\mathbf{x}_1$ and $\mathbf{x}_2$ of size n, where the binary vector $\mathbf{x}_2$ contains $n' \leq n$ nonzero elements, we simply get that

$$\mathcal{Q}\{\mathbf{x}_1; \mathbf{x}_2\} = \mathbf{T}_{\mathrm{s}}(\mathbf{i}_{n'}(\mathbf{x}_2))\, \mathbf{x}_1, \tag{6}$$

where the vector $\mathbf{i}_{n'}(\mathbf{x}_2)$ of length n' contains the indexes of the nonzero entries of the vector $\mathbf{x}_2$, and $\mathbf{T}_{\mathrm{s}}(\mathbf{i}_{n'}(\mathbf{x}_2))$ is an $n' \times n$ FI selection matrix, i.e., containing n' rows of an $n \times n$ identity matrix corresponding to the nonzero indices of the vector $\mathbf{x}_2$. Note that the following property is satisfied: $\mathbf{T}_{\mathrm{s}}(\mathbf{i}_n) = \mathbf{I}_n$ where $\mathbf{i}_n = [1, 2, \ldots, n]^T$ and $\mathbf{I}_n$ is the $n \times n$ identity matrix.

Let the function $\mathcal{B}_{\mathrm{d}}(\theta, \theta_{\mathrm{s}}), \theta, \theta_{\mathrm{s}} \in \Theta$, be a desired far-field FI beampattern in the bandwidth of interest Ω, with a mainlobe steered to θ_{s}. Our goal is stated as follows: we want that the synthesized beampattern $\mathcal{B}_K(\omega_j, \theta_p), \forall \omega_j \in \Omega$, with the structure specified by (5), will be FI but at the same time will be as close as possible to the desired power beampattern, $\mathcal{B}_{\mathrm{d}}(\theta, \theta_{\mathrm{s}})$ (in the mean square error sense), under some design constraints to be specified below. Additionally, the K selected sensors should also support the rotational-invariant property of circular arrays in general, and of concentric arrays in particular, meaning that approximately similar response can be obtained for different values of the steering direction, θ_{s}. For example, assume that the K selected sensors are used to synthesize the beampattern $\mathcal{B}_K^{(1)}(\omega_j, \theta_p), \forall \omega_j \in \Omega, \forall \theta_p \in \Theta$ being similar to $\mathcal{B}_{\mathrm{d}}(\theta, \theta_{\mathrm{s}})$ with the following overall error

$$\sum_{j=1}^{J} \sum_{p=1}^{P} |\mathcal{B}_{\mathrm{d}}(\theta_p, \theta_{\mathrm{s}}) - \mathcal{B}_K^{(1)}(\omega_j, \theta_p)|^2 \leq \epsilon_{\mathrm{t}}^2, \tag{7}$$

where ϵ_{t} is a small positive parameter, then the same K sensors can be used to synthesize also $\mathcal{B}_K^{(2)}(\omega_j, \theta_p), \forall \omega_j \in \Omega, \forall \theta_p \in \Theta$ being similar to $\mathcal{B}_{\mathrm{d}}(\theta, \theta_{\mathrm{s}} + \Delta\theta_{\mathrm{s}})$ with similar accuracy (i.e., similar ϵ_{t}^2), while $\mathcal{B}_{\mathrm{d}}(\theta, \theta_{\mathrm{s}} + \Delta\theta_{\mathrm{s}})$ is a shifted version of $\mathcal{B}_{\mathrm{d}}(\theta, \theta_{\mathrm{s}})$ by $\Delta\theta_{\mathrm{s}}$ degrees.

The structure of the synthesized beampattern $\mathcal{B}_K(\omega_j, \theta_p)$ with the K sensors concentrated in $G' < G$ rings may contribute to obtain the rotationally-invariant property by minimizing also G'. The intuition for this constraint is as follows: consider the case that the array layout obtained by the K sensors is linear and a second case where all the sensors are concentrated in a single ring. In the first case where all the rings are used, the linear geometry can provide sparse robust design as presented in [39], yet it clearly does not support the rotationally-invariant property. In the second case, we get nearly rotationally-invariant circular array but may obtain limited performance in terms of robust FI beampattern. The intermediate cases with a small number of rings used to construct the array layout are expected to yield a compromise between robustness and rotationally-invariance. Therefore, in the proposed design we also require that the K selected sensors will be concentrated on $G' < G$ rings.

III. Typical Design Constraints

Herein, we present several constraints that should be taken into consideration while designing concentric FI beamformer. Denote the vector $\mathbf{h}(\omega_j)$ of length M containing the nonzero elements of the matrix $\mathbf{H}(\omega_j)$ arranged in a column vector of length M, that is,

$$\mathbf{h}(\omega_j) = [H_{1,1}(\omega_j) \cdots H_{1,M_1}(\omega_j)\ H_{2,1}(\omega_j) \cdots H_{2,M_2}(\omega_j) \cdots\ H_{G,1}(\omega_j) \cdots H_{G,M_G}(\omega_j)]^T, \tag{8}$$

where the superscript ^{T} denotes the transpose operator, and the mth element corresponds to the mth candidate sensor whose position is denoted by $\mathbf{p}_m,\ m = 1, 2, \ldots, M$, given as

$$\{\mathbf{p}_m\}_{m=1}^{M} \in \left\{ \begin{bmatrix} r_g \cos(\psi_{g,m_g}) \\ r_g \sin(\psi_{g,m_g}) \end{bmatrix} \right\}, m_g = 1, ..., M_g, g = 1, ..., G. \tag{9}$$

Similarly, define also the vector $\mathbf{d}(\omega_j, \theta_p)$ of length M containing the nonzero elements of the matrix $\mathbf{D}(\omega_j, \theta_p)$ arranged in a column vector. We set $P' < P$ directions that cover the mainlobe region Θ_{m}, where the superscript m stands for mainlobe, and the remaining $P - P'$ directions that cover the sidelobe region Θ_{s} where the superscript s stands for sidelobe.

The first constraint is a mainlobe constraint formulated as multiple joint-sparse constraints, that is, $\forall \omega_j \in \Omega$,

$$\mathcal{C}_1 : \left\| (\mathbf{b}_{\mathrm{d}}^{\mathrm{m}}(\theta_{\mathrm{s}}))^T - \mathbf{h}^H(\omega_j) \mathbf{T}_{\mathrm{s}}^T(\mathbf{i}_K) \mathbf{T}_{\mathrm{s}}(\mathbf{i}_K) \mathbf{D}_{M,\Theta_{\mathrm{m}}}(\omega_j) \right\|_2^2 \leq \epsilon_1(\omega_j), \tag{10}$$

where $\mathbf{i}_K = [i_1, i_2, ..., i_K]^T$ is a vector containing the indexes of the K chosen sensors located at $\{\mathbf{p}_{i_k}\}_{k=1}^{K}$, $\epsilon_1(\omega_j)$ is a small positive parameter, $||\cdot||_2$ is the ℓ_2-norm,

$$\mathbf{D}_{M,\Theta_{\mathrm{m}}}(\omega_j) = [\mathbf{d}(\omega_j, \theta_1), \mathbf{d}(\omega_j, \theta_2), \ldots, \mathbf{d}(\omega_j, \theta_{P'})] \tag{11}$$

is an $M \times P'$ matrix, and

$$\mathbf{b}_{\mathrm{d}}^{\mathrm{m}}(\theta_{\mathrm{s}}) = [\mathcal{B}_{\mathrm{d}}(\theta_1, \theta_{\mathrm{s}}), \mathcal{B}_{\mathrm{d}}(\theta_2, \theta_{\mathrm{s}}), \ldots, \mathcal{B}_{\mathrm{d}}(\theta_{P'}, \theta_{\mathrm{s}})]^T \tag{12}$$

is a vector containing samples of the desired beampattern in the directions covering the mainlobe.

Similarly, for the sidelobe constraint we can obtain multiple joint-sparse constraints, and write $\forall \omega_j \in \Omega$,

$$\mathcal{C}_2 : \left\| (\mathbf{b}_{\mathrm{d}}^{\mathrm{s}}(\theta_{\mathrm{s}}))^T - \mathbf{h}^H(\omega_j) \mathbf{T}_{\mathrm{s}}^T(\mathbf{i}_K) \mathbf{T}_{\mathrm{s}}(\mathbf{i}_K) \mathbf{D}_{M,\Theta_{\mathrm{s}}}(\omega_j) \right\|_2^2 \leq \epsilon_2(\omega_j), \tag{13}$$

where $\epsilon_2(\omega_j)$ is a small positive parameter. The matrix $\mathbf{D}_{M,\Theta_{\mathrm{s}}}(\omega_j)$ is defined similarly to $\mathbf{D}_{M,\Theta_{\mathrm{m}}}(\omega_j)$, and the vector $\mathbf{b}_{\mathrm{d}}^{\mathrm{s}}(\theta_{\mathrm{s}})$ is defined similarly to $\mathbf{b}_{\mathrm{d}}^{\mathrm{m}}(\theta_{\mathrm{s}})$.

Clearly, imposing only $\mathcal{C}_1$ and $\mathcal{C}_2$ does not ensure that the array responses $\mathcal{B}_K\left(\omega_j,\theta_p\right)$, $\omega_j\in\Omega$ will not distort the signal of interest and especially that they will be robust to array calibration and model mismatch errors. Hence, we include additional constraints. The first is the well known distortionless response constraint, stating that, $\forall\omega_j\in\Omega$,

$$\mathcal{C}_3:\ \mathbf{h}^H\left(\omega_j\right)\mathbf{T}_{\mathrm{s}}^T\left(\mathbf{i}_K\right)\mathbf{T}_{\mathrm{s}}\left(\mathbf{i}_K\right)\mathbf{d}\left(\omega_j,\theta_{\mathrm{s}}\right)=1, \tag{14}$$

and the second is the limitation of the white noise output power, given as, $\forall\omega_j\in\Omega$,

$$\mathcal{C}_4:\ \mathbf{h}^H\left(\omega_j\right)\mathbf{T}_{\mathrm{s}}^T\left(\mathbf{i}_K\right)\mathbf{T}_{\mathrm{s}}\left(\mathbf{i}_K\right)\mathbf{h}\left(\omega_j\right)\leq\gamma(\omega_j), \tag{15}$$

where $\gamma(\omega_j)$ is a parameter expressing the maximal allowed white noise output power at frequency ω_j. Note that due to the distortionless constraint specified by (14), the formulation of (15) is equivalent to restricting the white noise gain (WNG) of the array to be above a certain threshold value [42, ch.6]. The WNG for the general case of a beamformer coefficient vector $\mathbf{h}(\omega_j)$ [43],

$$\mathcal{W}\left(\mathbf{h}(\omega_j)\right)=\frac{\left|\mathbf{h}^H\left(\omega_j\right)\mathbf{d}\left(\omega_j,\theta_{\mathrm{s}}\right)\right|^2}{\mathbf{h}^H\left(\omega_j\right)\mathbf{h}\left(\omega_j\right)}, \tag{16}$$

is a measure indicating the array gain in the presence of uncorrelated white noise. It also indicates the sensitivity of the array to model mismatch errors [42].

In the framework of sparse design of concentric arrays we may define two additional constraints. The first is a symmetry of the designed beampattern with respect to the steering direction, θ_{s}. The motivation to such constraint is as explained above that we would like the final array layout to include as less as possible rings, thus, it may lead to a better rotational-invariant response.

Assuming $\theta_{\mathrm{s}}=0^\circ$, we may arrange all the candidate sensors in symmetric pairs, while sensors that lay on the main axis (i.e., the x axis presented in Fig. 1) are symmetric to themselves, that is, we have $M'\leq M$ symmetric pairs. Without loss of generality, we assume that $M''\leq M'$ are pairs of sensors that do not lay on the main axis, while the remaining $M'-M''$ sensors correspond to the sensors on the main axis.

Let the matrix $\mathbf{S}$ be a matrix of size $M'\times M$ where each of its first M'' rows contain zeros except two entries of '1's corresponding to the indexes of the mth symmetric pair $(m=1,2,...,M'')$. The entries of the remaining $M'-M''$ sensors laying on the main axis, are equal to '2'. As a simple example to illustrate the structure of the matrix $\mathbf{S}$, we consider a concentric array with two rings, the inner ring has four sensors locating in the azimuthal directions $\psi_{1,1}=0^\circ,\psi_{1,2}=90^\circ,\psi_{1,3}=180^\circ$, and $\psi_{1,4}=270^\circ$. The external ring has five sensors locating in the azimuthal directions $\psi_{2,1}=0^\circ,\psi_{2,2}=72^\circ,\psi_{2,3}=144^\circ,\psi_{2,4}=216^\circ$ and $\psi_{2,5}=288^\circ$. Therefore, three pairs of symmetric sensors lay on the main axis, while three more pairs do not lay on the main axis. Consequently, the corresponding matrix is

$$\mathbf{S}=\begin{bmatrix}0&1&0&1&0&0&0&0&0\\0&0&0&0&0&1&0&0&1\\0&0&0&0&0&0&1&1&0\\2&0&0&0&0&0&0&0&0\\0&0&2&0&0&0&0&0&0\\0&0&0&0&2&0&0&0&0\end{bmatrix}. \tag{17}$$

The symmetry constraint is formulated as, $\forall\omega_j\in\Omega$,

$$\mathcal{C}_5:\left\|\mathbf{S}(1:M'',:)\mathbf{h}\left(\omega_j\right)\right\|_2^2\leq\epsilon_3(\omega_j), \tag{18}$$

where $\epsilon_3(\omega_j)$ is a small positive parameter. Note that we take only the rows of pairs that do not lay on the main axis. We later use all the rows of the matrix $\mathbf{S}$.

The second additional constraint relates to the desired property of rotationally-invariant beampattern. As discussed before we would like to get a similar response for different values of the steering direction, θ_{s}. Thus, we may formulate the following rotationally-invariant constraint as $\forall\theta_{\mathrm{s}}\in\Theta$

$$\mathcal{C}_6:\sum_{j=1}^{J}\sum_{p=1}^{P}\left|\mathcal{B}_{\mathrm{d}}\left(\theta_p,\theta_{\mathrm{s}}\right)-\mathcal{B}_K\left(\omega_j,\theta_p\right)\right|^2\leq\epsilon_{\mathrm{t}}^2. \tag{19}$$

Combining constraints $\mathcal{C}_1$,$\mathcal{C}_2$,$\mathcal{C}_3$,$\mathcal{C}_4$,$\mathcal{C}_5$,$\mathcal{C}_6$, we can formulate the general joint-sparse rotational-invariant problem of interest as

$$\begin{aligned}&\text{minimize}\{K,G'\}\\&\text{subject to}\ \ \mathcal{C}_1,\mathcal{C}_2,\mathcal{C}_3,\mathcal{C}_4,\mathcal{C}_5,\mathcal{C}_6,\ \forall\omega_j\in\Omega,\end{aligned} \tag{20}$$

whose solution yields the jointly-sparse filters

$$\mathbf{h}_K\left(\omega_j\right)=\mathbf{T}_{\mathrm{s}}\left(\mathbf{i}_K\right)\mathbf{h}\left(\omega_j\right),\ \forall\omega_j\in\Omega. \tag{21}$$

In this work, we solve (20) by extending our recent incoherent sparse FI design [39], and propose a greedy-based sparse approach to design of concentric arrays. Based on a joint sparse version of the OMP algorithm [44]–[46], $K'\leq K$ joint-sparse sensors are selected, which comply constraints $\mathcal{C}_1$-$\mathcal{C}_5$. In order to comply $\mathcal{C}_6$, the obtained array layout is duplicated and an additional ℓ_{12} optimization is performed aiming to obtain an array layout which is sparse both in the number of sensors and in the number of rings. The proposed approach has much lower computational burden, which makes it more feasible for practical designs, especially where the number of candidate sensors is an order of hundreds or more.

IV. A GREEDY BASED DESIGN OF FI SPARSE CONCENTRIC ARRAYS

In this section, we present a four-step greedy based approach for solving (20) and obtain a sparse design of an FI concentric beamformer. Note that while in our previous incoherent design the task of determining the parameter K was not trivial, in the proposed greedy design it may be much more intuitive and straightforward. In the following subsections, we describe each of these steps.

A. Determine the array layout for steering from endfire

The first step includes a greedy search of the best $K' \leq K$ sensors over all the candidate sensors that fulfill the above constraints. We may assume that the desired signal arrives from the endfire direction (i.e. $\theta_{\rm s} = 0^\circ$), while other interfering signals arrive from different arbitrary directions. As we are looking for an FI beampattern, the problem should be formulated as a joint-sparse greedy search one. One of the popular tools for implementing greedy-based search algorithms is the OMP. Applying the OMP directly to our problem is not a trivial task and some manipulations should be applied.

Let us consider the matrix $\mathbf{D}_j$, of size $P \times M$, to be the concatenation of the matrices $\mathbf{D}^H_{M,\Theta_{\rm m}}(\omega_j)$ and $\mathbf{D}^H_{M,\Theta_{\rm s}}(\omega_j)$, i.e.,

$$\mathbf{D}_j = \begin{bmatrix} \mathbf{D}^H_{M,\Theta_{\rm m}}(\omega_j) \\ \mathbf{D}^H_{M,\Theta_{\rm s}}(\omega_j) \end{bmatrix}. \tag{22}$$

We treat the matrix $\mathbf{D}_j$ as a dictionary containing in each column one word of length P, also called an atom, which corresponds to one of the M candidate sensors. It is desired to express $\mathcal{B}_{\rm d}(\theta, \theta_{\rm s})$ with atoms from the dictionary by finding a vector $\mathbf{h}^{\rm uc}(\omega_j) \in \mathbb{C}^M$ which solves the following problem

$$\mathbf{D}_j \mathbf{h}^{\rm uc}(\omega_j) = \mathbf{b}_{\rm d}(\theta_{\rm s}), \tag{23}$$

where

$$\mathbf{b}_{\rm d}(\theta_{\rm s}) = \begin{bmatrix} \mathbf{b}^{\rm m}_{\rm d}(\theta_{\rm s}) \\ \mathbf{b}^{\rm s}_{\rm d}(\theta_{\rm s}) \end{bmatrix} \tag{24}$$

is the desired beampattern, and the superscript $\rm uc$ stands for unconstrained.

Since typically $\mathbf{D}_j$ is an under-determined matrix, (23) has infinite solutions. Among them, the class of sparse solutions with few nonzero elements is of a great interest because it means that practically small number of sensors is required to construct the desired beampattern.

Mathematically, the solution with the fewest nonzero elements can be found by solving the NP-hard ℓ_0-norm problem

$$\min \|\mathbf{h}^{\rm uc}(\omega_j)\|_0 \ \text{ subject to } \mathbf{D}_j \mathbf{h}^{\rm uc}(\omega_j) = \mathbf{b}_{\rm d}(\theta_{\rm s}), \tag{25}$$

where $\|\mathbf{x}\|_0$ is the number of nonzero elements in the vector $\mathbf{x}$. One way to solve (25) is by modifying it to the ℓ_1-norm optimization problem [47]

$$\min \|\mathbf{h}^{\rm uc}(\omega_j)\|_1 \ \text{ subject to } \mathbf{D}_j \mathbf{h}^{\rm uc}(\omega_j) = \mathbf{b}_{\rm d}(\theta_{\rm s}). \tag{26}$$

Instead of solving (25) by an ℓ_1 optimization like in [39], it can be solved using the OMP algorithm which finds $\mathbf{h}^{\rm uc}(\omega_j)$ element by element in the step-by-step iterative greedy manner. In other words, we would like to find greedily an approximation to the P length vector $\mathcal{B}_{\rm d}(\theta)$ using as small as possible number of atoms from the dictionary matrix, $\mathbf{D}_j$. In order to solve (25) using OMP, it is useful to consider the mutual coherence of the matrix, $\mathbf{D}_j$, defined as [48]

$$\mu(\mathbf{D}_j) = \max_{k \neq l} \frac{|\mathbf{d}^H_{j_l} \mathbf{d}_{j_k}|}{\|\mathbf{d}_{j_l}\|_2 \|\mathbf{d}_{j_k}\|_2} \tag{27}$$

where $\mathbf{d}_{j_l}$ is the lth column of the matrix $\mathbf{D}_j$. The following theorem [49] indicate whether a sparse signal can be recovered uniquely by the OMP algorithm.

Theorem: Let $\mathbf{x} \in \mathbb{C}^n$ being a k-sparse vector, meaning that it has up to k nonzero elements. For the model $\mathbf{A}\mathbf{x} = \mathbf{b}$, where $\mathbf{b} \in \mathbb{C}^m$, $\mathbf{A} \in \mathbb{C}^{m \times n}$, $n \gg m$ are given, $\mathbf{x}$ can be recovered uniquely by the OMP algorithm if $\mathbf{A}$ and $\mathbf{x}$ satisfy

$$\mu(\mathbf{A}) < \frac{1}{2k-1}. \tag{28}$$

Equivalently, if

$$k < \frac{1}{2}\left(\frac{1}{\mu(\mathbf{A})} - 1\right), \tag{29}$$

then $\mathbf{x}$ can be recovered uniquely from a given $\mathbf{A}$ and $\mathbf{b}$ using the OMP algorithm.

In the appendix we derive the mutual coherence of the matrix $\mathbf{D}_j$ to be

$$\mu(\mathbf{D}_j) = \max_{k \neq l} \left| I_0\left(\sqrt{-\frac{\omega_j^2}{c^2}\left[r^2(\mathbf{p}_l) + r^2(\mathbf{p}_k) - \mathbf{p}_l^T \mathbf{p}_k\right]}\right)\right|, \tag{30}$$

where $r(\mathbf{p}_m)$ denotes the radius the mth sensor located at $\mathbf{p}_m$, and $I_0(\cdot)$ is the modified Bessel function of the first kind. Substituting typical values to the parameters appeared in (30) like those presented later in the Simulation Section, one may sees that (29) does not hold for $k > 0$, meaning that the matrix $\mathbf{D}_j$ does not satisfy the above theorem. This can be explained since in our setup the desired beampattern is indeed not a pure sparse vector but an approximated one, which has a non-unique sparse representation. Therefore, our dictionary has high mutual coherence implying that it has some redundancy which will be exploited to obtain higher performance. In the following we may obtain an approximated sparse version of the beampattern. In order to mitigate the influence of the high mutual coherence, we employ a mask in order to reduce the possibility to chose different atoms with high similarity.

The joint-sparse OMP algorithm contains the following steps:

1) Initialization: Initialize $\forall \omega_j \in \Omega$ the vectors

$$\mathbf{r}^{(0)}(\omega_j) = \mathbf{b}_{\rm d}(\theta_{\rm s}) \tag{31}$$

of length P to be a residual vector which supposed to approach iteratively to a zero vector, and initialize the sparse vector

$$\mathbf{b}^{(0)}_{\rm g}(\omega_j) = \mathbf{0}_P \tag{32}$$

which stores the desired beampattern after the iterative algorithm converges, where $\mathbf{0}_P$ is a zeros vector of length P. We also initialize the vector $\mathbf{i}^{(0)}_{K'}$ which stores the indexes of the selected sensors in each iteration.

2) An iterative greedy algorithm: Initialize the $M' \times M'$ diagonal weighting matrix $\mathbf{W}^{(0)} = \mathbf{I}_{M'}$, used to assign a low weighting to sensors already chosen in previous iteration and to their neighbors by multiplying the corresponding indexes by a mask vector, $\mathbf{m}$, of length $L_{\mathbf{m}}$.

In each iteration of a standard OMP algorithm, it is desired to find the next atom which has the most contribution in the reconstruction of the desired vectors, $\mathbf{b}^{(l)}_{\rm g}(\omega_j)$, $\omega_j \in \Omega$. It is done by projecting the residual signals, $\mathbf{r}^{(l)}(\omega_j)$, $\omega_j \in \Omega$, over all the remaining atoms in the current iteration. For

the narrowband case the atom with the most contribution maximizes the following term

$$m_l^{\mathrm{NB}} = \underset{m=1,2,\ldots,M}{\operatorname{argmax}} \left[|\mathbf{D}_j \mathbf{r}^{(l)}(\omega_j)| \right]_m, \tag{33}$$

where $[\mathbf{x}]_i$ denotes the ith element of the vector $\mathbf{x}$, and the superscript NB stands for narrowband. As we are interested to obtain a sparse array layout which is joint $\forall \omega_j \in \Omega$, we have to take it into consideration when we are searching for the sensors that have the largest contribution in the lth iteration. One way to do so, is to sum the contributions over all the frequencies, i.e., to solve the following joint sparse problem [44]–[46]

$$m_l^{\mathrm{BB}} = \underset{m=1,2,\ldots,M}{\operatorname{argmax}} \left[\sum_{j=1}^{J} |\mathbf{D}_j \mathbf{r}^{(l)}(\omega_j)| \right]_m, \tag{34}$$

where the superscript BB stands for broadband. The dimension of the inner product in the last equations is a vector of length M, where each entry contains a positive value which express the contribution of the corresponding sensor to the residual signal. As discussed before, it is desired to obtain a symmetric solution with respect to the endfire direction, therefore, for the lth iteration we may find the symmetric pair of sensors out of M' that maximizes the function:

$$m_l^{\mathrm{JSBB}} = \underset{m=1,2,\ldots,M'}{\operatorname{argmax}} \left[\mathbf{W}^{(l-1)} \mathbf{S} \sum_{j=1}^{J} |\mathbf{D}_j \mathbf{r}^{(l)}(\omega_j)| \right]_m, \tag{35}$$

where the superscript JSBB stands for joint symmetric broad band. The meaning of (35) is that we find the pair of symmetric sensors with the largest projection over the desired beampattern across the entire bandwidth.

3) Update: Update the following $L^{(l)} \times 1$ vector

$$\mathbf{i}_{K'}^{(l)} = \left[\left(\mathbf{i}_{K'}^{(l-1)} \right)^T \quad \left(\mathbf{i}(m_l^{\mathrm{JSBB}}) \right)^T \right]^T, \tag{36}$$

where $\mathbf{i}(m_l^{\mathrm{JSBB}})$ contains the indexes of the sensors whose entries are not equal to zero in the corresponding rows of the matrix $\mathbf{S}$.

Let $\mathbf{D}_j(\mathbf{i}_{K'}^{(l)})$ be a matrix of size $L^{(l)} \times P$ containing only the rows of $\mathbf{D}_j$ whose indices are specify by $\mathbf{i}_{K'}^{(l)}$, i.e.,

$$\mathbf{D}_j(\mathbf{i}_{K'}^{(l)}) = \mathbf{T}_{\mathrm{s}} \left(\mathbf{i}_{K'}^{(l)} \right) \mathbf{D}_j, \tag{37}$$

where $\mathbf{T}_{\mathrm{s}} \left(\mathbf{i}_{K'}^{(l)} \right)$ is an $L^{(l)} \times M$ selection matrix.

We can calculate, $\forall \omega_j \in \Omega$, the projection vector of size $L^{(l)} \times 1$ of the desired beampattern over the chosen atoms up to the lth iteration as

$$\mathbf{h}_{L^{(l)}}^{\mathrm{uc}}(\omega_j) = \left[\mathbf{D}_j^H(\mathbf{i}_{K'}^{(l)}) \mathbf{D}_j(\mathbf{i}_{K'}^{(l)}) \right]^{-1} \mathbf{D}_j^H(\mathbf{i}_{K'}^{(l)}) \mathbf{b}_{\mathrm{d}}(\theta_{\mathrm{s}}), \tag{38}$$

which is used to update the following vectors $\forall \omega_j \in \Omega$:

$$\mathbf{b}_{\mathrm{g}}^{(l)}(\omega_j) = \mathbf{D}_j^H(\mathbf{i}_{K'}^{(l)}) \mathbf{h}_{L^{(l)}}^{\mathrm{uc}}(\omega_j), \tag{39}$$

and

$$\mathbf{r}^{(l)}(\omega_j) = \mathbf{r}^{(l-1)}(\omega_j) - \mathbf{b}_{\mathrm{g}}^{(l)}(\omega_j). \tag{40}$$

Finally we update the masking matrix ,$\mathbf{W}^{(l)}$, to be

$$\mathbf{W}^{(l)} = \mathbf{W}^{(l-1)} \mathrm{diag}\left([\mathbf{1}_{L_1}^T \ \mathbf{m}^T \ \mathbf{1}_{L_2}^T]^T \right), \tag{41}$$

where $\mathrm{diag}[\mathbf{x}]$ is a diagonal matrix whose nonzero elements are the entries of the vector $\mathbf{x}$. The vectors $\mathbf{1}_{L_1}$ and $\mathbf{1}_{L_2}$ are vectors of ones of length L_1 and L_2, respectively, where

$$L_1(l) = m_l^{\mathrm{JSBB}} - \frac{L_{\mathbf{m}} - 1}{2}, \tag{42}$$

and

$$L_2(l) = M' - m_l^{\mathrm{JSBB}} - \frac{L_{\mathbf{m}} - 1}{2}, \tag{43}$$

while $L_{\mathbf{m}}$ is assumed to be odd.

4) Check compliance to the constraints: As a stopping criteria, we check whether or not the chosen sensors up to the lth iteration comply the constraints specified in the previous section. To do so, we may solve the following optimization problems, $\forall \omega_j \in \Omega$:

$$\begin{aligned} \underset{\mathbf{h}_{L^{(l)}}(\omega_j)}{\text{minimize}} \quad & \|\mathbf{h}_{L^{(l)}}(\omega_j)\|_2^2 \\ \text{subject to} \quad & \\ & \mathbf{h}_{L^{(l)}}^H(\omega_j) \mathbf{d}_{L^{(l)}}(\omega_j, \theta_{\mathrm{s}}) = 1 \\ & \left\| (\mathbf{b}_{\mathrm{d}}^{\mathrm{m}}(\theta_{\mathrm{s}}))^T - \mathbf{h}_{L^{(l)}}^H(\omega_j,) \mathbf{D}_{L^{(l)},\Theta_{\mathrm{m}}}(\omega_j) \right\|_2^2 \leq \epsilon_1(\omega_j) \\ & \left\| (\mathbf{b}_{\mathrm{d}}^{\mathrm{s}}(\theta_{\mathrm{s}}))^T - \mathbf{h}_{L^{(l)}}^H(\omega_j) \mathbf{D}_{L^{(l)},\Theta_{\mathrm{s}}}(\omega_j) \right\|_2^2 \leq \epsilon_2(\omega_j), \end{aligned} \tag{44}$$

where $\mathbf{d}_{L^{(l)}}(\omega_j, \theta_{\mathrm{s}}) = \mathbf{T}_{\mathrm{s}} \left(\mathbf{i}_{K'}^{(l)} \right) \mathbf{d}(\omega_j, \theta_{\mathrm{s}})$, $\mathbf{D}_{L^{(l)},\Theta_{\mathrm{m}}}(\omega_j) = \mathbf{T}_{\mathrm{s}} \left(\mathbf{i}_{K'}^{(l)} \right) \mathbf{D}_{M,\Theta_{\mathrm{m}}}^H(\omega_j)$, $\mathbf{D}_{L^{(l)},\Theta_{\mathrm{s}}}(\omega_j) = \mathbf{T}_{\mathrm{s}} \left(\mathbf{i}_{K'}^{(l)} \right) \mathbf{D}_{M,\Theta_{\mathrm{s}}}^H(\omega_j)$, and the vector $\mathbf{h}_{L^{(l)}}(\omega_j)$ is a constrained version of the vector $\mathbf{h}_{L^{(l)}}^{\mathrm{uc}}(\omega_j)$. If we get a valid solution to (44) and also $\|\mathbf{h}_{L^{(l)}}(\omega_j)\|_2^2 \leq \gamma(\omega_j)$, $\forall \omega_j \in \Omega$, then we finish, otherwise, we may go back to the second step to choose additional symmetric pair of sensors. As both the objective function and the constraints in (44) are convex, (44) can be solved by convex optimization methods (e.g., using CVX toolbox [50]).

B. Duplicating the array layout

The previous step yields the $K' \leq K$ indices $\{i_k\}_{k=1}^{K'}$ of sensors that can be used to construct the sparse array layout of a concentric array steered to the endfire direction, i.e., $\theta_{\mathrm{s}} = 0^\circ$. Yet, the main motivation to consider concentric array instead of a more simple geometry like the linear one was due to the rotational-invariant attribute of concentric arrays. Therefore, we add two more steps to the design. We first duplicate the obtained array layout to $Q-1$ additional directions, meaning that we add a rotated version of the array layout in the following directions: $\frac{2\pi}{Q}, 2\frac{2\pi}{Q}, \ldots, (Q-1)\frac{2\pi}{Q}$. We now have $Z \leq QK'$ sensors in the array layout, whose indices are denoted by $\{i_z\}_{z=1}^{Z} \in \mathbf{i}_Z$. This step produces redundancy in both the number of required sensors and the number of required rings. Thus, the next step may apply an optimization in order to obtain a sparse array both in the number of rings, G', and in the total number of sensors, K. Note that, we can use this algorithm also for cases where only a range of angles is desired and not all the azimuthal directions.

C. Optimizing number of rings

As it is assumed that $QK' \ll M$, it is feasible to optimize G' and K for all the relevant bandwidth simultaneously. Moreover, we can save some hardware resources by decimating the number of frequencies by a factor of $J_{\rm d}$, i.e., the following optimization may be performed over the $J' = J/J_{\rm d}$ frequencies $\left\{\omega'_j\right\}_{j=1}^{J'} = \{\omega_j \mid j \bmod J_{\rm d} = 0\} \in \Omega$, since the main purpose of this step is to determine the final array layout.

Similarly to the joint-sparse constraint in the greedy part optimization problem (35), a similar constraint should be embedded also to the ℓ_1 optimization problem of that step, insuring that all the filters $\left\{\mathbf{h}_K\left(\omega_j\right)\right\}_{j=1}^{J}$ have the same sparse pattern, i.e., the sensors positions which are chosen out of all the candidate positions are common over all the frequencies in the signal's bandwidth of interest Ω. The way to insert such a constraint is by minimizing the ℓ_{12}-norm instead of the ℓ_1-norm [51]. It is defined as the following: suppose we have the vectors $\mathbf{x}_i, i = 1, 2, \ldots, n$, of length M, and define $\mathbf{X} = [\mathbf{x}_1, \mathbf{x}_2, \ldots, \mathbf{x}_n]$ to be a matrix containing these vectors in its columns, then the ℓ_{12}-norm of the matrix $\mathbf{X}$ is defined as [52]

$$\|\mathbf{X}\|_{12} \triangleq \sum_{m=1}^{M} \sqrt{\left(\sum_{i=1}^{n} |\mathbf{X}(m,i)|^2\right)}, \tag{45}$$

where $\mathbf{X}(m,i)$ being the entry corresponds to the mth row and the ith column of the matrix $\mathbf{X}$.

Define $\mathbf{h}_Z(\omega'_j) = [H_{i_1}(\omega'_j), H_{i_2}(\omega'_j), ..., H_{i_Z}(\omega'_j)]^T, \omega'_j \in \Omega$ to be vectors of length Z, whose each one of their entries is mapped to one of the Z sensors of the original vector $\mathbf{h}(\omega_j)$ (8) whose indexes are specified by the vector $\mathbf{i}_Z$. Define $\bar{\mathbf{h}}_p,\ p = 1, ..., P$ being vectors containing all the entries of $\mathbf{h}_Z(\omega'_j)$ locating on the pth ring $\forall \omega'_j \in \Omega$ as

$$\bar{\mathbf{h}}_p = \left\{ \left\{ \left\{H_{i_z}(\omega'_j)\right\}_{z=1}^{Z} \right\}_{j=1}^{J'} \in \ p\text{th ring} \right\},\ p = 1, 2, ..., P. \tag{46}$$

Employing the concept of the ℓ_{12}-norm introduced by (45), we may define the following iterative optimization problem

$$\begin{aligned}
\underset{\{\mathbf{h}_Z(\omega'_j)\}}{\text{minimize}} \quad & \sum_{p=1}^{P} \alpha_p^k \eta_p \\
\text{subject to} \quad & \eta_p \geq \left\|\bar{\mathbf{h}}_p\right\|_2, \\
\text{and} \quad \forall \omega'_j \in \Omega \quad & \\
& \mathbf{h}_Z^H\left(\omega'_j\right) \mathbf{d}_{L_Z}\left(\omega'_j, \theta'_{\rm s}\right) = 1 \\
& \mathbf{h}_Z^H\left(\omega'_j\right) \mathbf{h}_Z\left(\omega'_j\right) \leq \gamma(\omega'_j) \\
& \left\|(\mathbf{b}_{\rm d}^{\rm m}(\theta_{\rm s}))^T - \mathbf{h}_Z^H\left(\omega'_j\right) \mathbf{D}_{L_Z,\Theta'_{\rm m}}(\omega'_j)\right\|_2^2 \leq \epsilon_1(\omega'_j) \\
& \left\|(\mathbf{b}_{\rm d}^{\rm s}(\theta_{\rm s}))^T - \mathbf{h}_Z^H\left(\omega'_j\right) \mathbf{D}_{L_Z,\Theta'_{\rm s}}\left(\omega'_j\right)\right\|_2^2 \leq \epsilon_2(\omega'_j),
\end{aligned} \tag{47}$$

where $\alpha_m^k = 1/\left(\eta_m^{k-1} + \epsilon\right)$ for $k > 1$ and $\alpha_m^1 = 1$, η_m^{k-1} is the result obtained from the $(k-1)$th iteration, ϵ is a regularization parameter, $\mathbf{d}_{L_Z}\left(\omega'_j, \theta'_{\rm s}\right) = \mathbf{T}_{\rm s}\left(\mathbf{i}_Z\right) \mathbf{d}\left(\omega'_j, \theta'_{\rm s}\right)$, $\mathbf{D}_{L_Z,\Theta'_{\rm m}}\left(\omega'_j\right) = \mathbf{T}_{\rm s}\left(\mathbf{i}_Z\right) \mathbf{D}_{M,\Theta'_{\rm m}}\left(\omega'_j\right)$, and $\mathbf{D}_{L_Z,\Theta'_{\rm s}}\left(\omega'_j\right) = \mathbf{T}_{\rm s}\left(\mathbf{i}_Z\right) \mathbf{D}_{M,\Theta'_{\rm s}}\left(\omega'_j\right)$. The last equation can be interpreted as a weighted ℓ_1-optimization of the vector $\boldsymbol{\eta}^k = \left[\eta_1^k, \eta_2^k, ..., \eta_P^k\right]^T$, whose pth entry contains the energy of all the selected sensors located on the pth ring, thus, a sparse solution both in the rings and in the sensors is obtained. The optimization is performed for directions $\theta'_{\rm s} = \theta_{\rm s} + \frac{\pi}{Q}$, $\Theta'_{\rm m} = \Theta_{\rm m} + \frac{\pi}{Q}$, and $\Theta'_{\rm s} = \Theta_{\rm s} + \frac{\pi}{Q}$, meaning that the steering direction is exactly between the endfire direction and the direction of the first duplication since this direction is considered to be the worst case scenario. Therefore, it insures that steering to other directions would be also of a high quality.

We run this algorithm iteratively until

$$\Delta\boldsymbol{\eta} \triangleq \frac{\left\|\boldsymbol{\eta}^k - \boldsymbol{\eta}^{k-1}\right\|_2}{\left\|\boldsymbol{\eta}^k\right\|_2} \leq \epsilon_\eta, \tag{48}$$

where ϵ_η is a small positive parameter. Both the vectors $\boldsymbol{\eta}^k$ and $\left\{\mathbf{h}_Z(\omega'_j)\right\}_{j=1}^{J'}$ are iteratively updated using (47) until (48) is satisfied. The dominant entries of the vector $\boldsymbol{\eta}^k$ (i.e., non-zero elements) determine the G' active rings to be used during the synthesis process. The sensors belong to these rings are the K sensors used to construct the desired sparse filters $\left\{\mathbf{h}_K\left(\omega_j\right)\right\}_{j=1}^{J}$ satisfying $\mathcal{C}_1$,$\mathcal{C}_2$,$\mathcal{C}_3$,$\mathcal{C}_4$, $\mathcal{C}_5$, and $\mathcal{C}_6$. The outcome of this iterative algorithm is a joint sparse array layout, both in the number of selected rings, G', and in the total number of selected sensors, K.

D. Synthesis

The goal of the previous steps was to determine the minimal number of the active sensors, K, in a minimal number of rings, G', which fulfill the constraints, using greedy search and ℓ_{12}-norm optimization tools. In the synthesis step, where the K indices $\{i_k\}_{k=1}^{K}$ of the sensors used to build the FI beampattern were already determined, there is no need to solve an ℓ_1-norm optimization problem and instead we may solve an optimization problem whose objective function is related to constraints $\mathcal{C}_1$,$\mathcal{C}_2$,$\mathcal{C}_3$,$\mathcal{C}_4$,$\mathcal{C}_5$,$\mathcal{C}_6$ presented in Section III. A reasonable choice is to minimize the noise output power (i.e., $\mathcal{C}_4$), subject to the constraints, $\mathcal{C}_1$,$\mathcal{C}_2$, and $\mathcal{C}_3$. Constraints $\mathcal{C}_5$ and $\mathcal{C}_6$ are already embedded in the previous steps. Therefore, we can formulate it as follows: $\forall \omega_j \in \Omega$, solve

$$\begin{aligned}
\underset{\mathbf{h}_K(\omega_j)}{\text{minimize}} \quad & \left\|\mathbf{h}_K^H\left(\omega_j\right)\right\|_2^2 \\
\text{subject to} \quad & \\
& \mathbf{h}_K^H\left(\omega_j\right) \mathbf{d}_K\left(\omega_j, \theta_{\rm s}\right) = 1 \\
& \left\|(\mathbf{b}_{\rm d}^{\rm m}(\theta_{\rm s}))^T - \mathbf{h}_K^H\left(\omega_j\right) \mathbf{D}_{K,\Theta_{\rm m}}\left(\omega_j\right)\right\|_2^2 \leq \epsilon_1(\omega_j) \\
& \left\|(\mathbf{b}_{\rm d}^{\rm s}(\theta_{\rm s}))^T - \mathbf{h}_K^H\left(\omega_j\right) \mathbf{D}_{K,\Theta_{\rm s}}\left(\omega_j\right)\right\|_2^2 \leq \epsilon_2(\omega_j),
\end{aligned} \tag{49}$$

where $\mathbf{d}_K\left(\omega_j, \theta_{\rm s}\right) = \mathbf{T}_{\rm s}\left(\mathbf{i}_K\right) \mathbf{d}\left(\omega_j, \theta_{\rm s}\right)$, $\mathbf{D}_{K,\Theta_{\rm m}}\left(\omega_j\right) = \mathbf{T}_{\rm s}\left(\mathbf{i}_K\right) \mathbf{D}_{\Theta_{\rm m}}\left(\omega_j\right)$, and $\mathbf{D}_{K,\Theta_{\rm s}}\left(\omega_j\right) = \mathbf{T}_{\rm s}\left(\mathbf{i}_K\right) \mathbf{D}_{\Theta_{\rm s}}\left(\omega_j\right)$. The resulting filters $\left\{\mathbf{h}_K\left(\omega_j\right)\right\}_{j=1}^{J}$ contain the sensors located in the indices $\left\{\mathbf{p}_{i_k}\right\}_{k=1}^{K}$. This fact is important since it means that we can use only K out of M sensors and still obtain adequate results as presented later in the simulations section.

The proposed design involves the adjustment of several parameters, like the tolerance parameters. In [39], we established a procedure for initialization and adjustment of these parameters, which is also relevant to the proposed design.

Note that the proposed design focuses on the two-dimensional (2D) scenario meaning that it takes into consideration the beampattern in the plane where the array is laid and not across the entire 3D space. Such scenario may lead to simpler solutions with higher performance. Yet, extension of the derivations presented in this work for the 3D scenario is a subject to a future research.

V. Numerical Simulations

We consider a sparse design of concentric differential microphone arrays (CCDMAs) [4], originally designed with a linear geometry, which combines closely spaced sensors to respond to the spatial derivatives of the acoustic pressure field. These small-size arrays yield nearly FI beampatterns, and include the well-known superdirective beamformer as a particular case [18]. As discussed before, we confine ourselves to the case of a 2D beampattern where $\phi = 90^\circ$, i.e., the plane where the array is laid. For that case, the general theoretical expression for the FI beampattern of an Nth-order DMA is given by [43]

$$\mathcal{B}_{\rm d}\left(\theta,\theta_{\rm s}\right) = \mathcal{B}_N(\theta_{\rm s}-\theta) = \sum_{n=0}^{N} a_{N,n}\cos^n(\theta_{\rm s}-\theta), \qquad (50)$$

where $\{a_{N,n}\}_{n=0}^{N}$ are real coefficients, and the desired signal arrives from the direction $\theta_{\rm s}$. For this example $\mathcal{B}_N(\theta_{\rm s}-\theta)$ is considered to be the desired beampattern. It is assumed that the element spacing, δ, is much smaller than the wavelength of the incoming signal, i.e,

$$\forall\omega\in\Omega: \quad \delta \ll \lambda = \frac{2\pi c}{\omega} \;\Rightarrow \delta \ll \frac{2\pi c}{\omega_{\max}}, \qquad (51)$$

in order to approximate the spatial differential of the pressure signal, where $\omega_{\max}$ is the angular frequency corresponding to the highest frequency in the bandwidth of interest, Ω, and $c = 340$ m/sec.

In spite of their benefits, traditional differential microphone arrays (DMAs) suffer from noise amplification, especially at lower frequencies, and also confined to steering from the endfire for linear geometry. For that, we apply a sparse approach for designing robust DMAs of concentric geometry with relatively smaller number of sensors, and nearly rotationally-invariant beampattern.

We assume an initial array geometry consisting of $G = 15$ rings, where the radius of the gth ring is $r_g = (g-1)\delta,\ g = 1,2,...,G$. We choose uniformly the number of candidate sensors on the gth ring to be

$$M_g = \begin{cases} \frac{\pi}{\arcsin\left(\frac{\sqrt{g-1}\delta}{2r_g}\right)}, & g = 2,...,G \\ 1, & g = 1, \end{cases} \qquad (52)$$

meaning that the element spacing between two adjacent sensors in the gth ring is $\sqrt{g-1}\delta$. Such a choice of sensor positions leads to a lower density of sensors as the radii of the ring is increased, which is reasonable because sensors from inner rings may contribute to the higher frequencies, while the contribution of sensors from the outer rings is mainly for the lower frequencies, obtaining higher WNG and robustness for the overall FI beampattern. The total number of candidate sensors according to (52) is $M = \sum_{g=1}^{G} M_g = 234$.

We compare between four design approaches. The first one is our proposed greedy sparse design presented in the previous section. The second approach is a uniform one, where K closely uniformly spaced microphones are used to obtain a desired directivity pattern by solving (49). We refer to this approach as the small aperture concentric (SAC) array approach. The third design approach is similar to the second, but with the only difference that the K sensors are spread uniformly over the entire possible concentric aperture of the M candidate sensors. We refer to this approach as the large aperture concentric (LAC) approach. The fourth approach is a random approach, i.e., we choose randomly the K sensors out of M candidate sensors, and solve (49). For that approach, we may average over several realizations in order to get a more representative performance level.

We apply the four approaches to designing a FI broadband beampattern for the range of frequencies between $f_{\rm low} = 200$ Hz and $f_{\rm high} = 8200$ Hz. Assuming a typical duration of $T = 25$ msec for the window analysis used for the corresponding time-domain received signal, the frequency resolution is $\Delta f = 1/T = 40$ Hz. Thus, the number of bins can be calculated as $J = \frac{f_{\rm high}-f_{\rm low}}{\Delta f} = 202$. Note that for such a high number of candidate sensors and frequencies, the proposed greedy sparse design is much more feasible than coherent based sparse design [53], where optimization is performed simultaneously over all frequencies. We choose the element spacing to be $\delta = 1$ cm $\ll \frac{2\pi c}{\omega_{\max}} \approx 4.3$ cm.

We design a third-order hypercardioid pattern (i.e., $N = 3$) which maximizes the directivity factor (DF), whose theoretical beampattern is given according to (50) as [15]

$$\mathcal{B}_N^{\rm HC}(\theta) = -0.14 - 0.57\cos\theta + 0.57\cos^2\theta + 1.15\cos^3\theta, \qquad (53)$$

while we assume that $\theta_{\rm s} = 0^\circ$. In order to build the matrices $\mathbf{D}_{M,\Theta_{\rm m}}(\omega_j)$ and $\mathbf{D}_{M,\Theta_{\rm s}}(\omega_j)$, we uniformly discretize the angular axis with $\Delta\theta = 2^\circ$. For that case we set $\theta_{P'} = 60^\circ$, i.e., the mainlobe region in the azimuthal axis is $-60^\circ \le \theta \le 60^\circ$.

We set initial values for the tolerance parameters $\{\epsilon_1(\omega_j)\}_{j=1}^{J}$, $\{\epsilon_2(\omega_j)\}_{j=1}^{J}$, and $\{\gamma(\omega_j)\}_{j=1}^{J}$, by applying the parameters adjustment procedure introduced in [39]. We also choose the parameters $\epsilon = 10^{-4}$, and $\epsilon_\eta = 5\cdot 10^{-3}$.

For the proposed incoherent greedy sparse approach, we choose the following mask vector, $\mathbf{m}$, of length $L_{\mathbf{m}} = 5$:

$$\mathbf{m} = [0.9, 0.75, 0, 0.75, 0.9]^T, \qquad (54)$$

which ensures that already selected sensors will not be chosen again, while their neighboring sensors will get lower priority.

We run the first step of the greedy search in order to find a sparse array layout which yields the desired FI beampattern, while complying the constraints specified in Section III according to the algorithm presented in Section IV-A for the case of steering from the endfire. The array layout obtained by

the greedy search, consists of $K' = 26$ sensors, spread over most of the rings, is presented in Fig 2.

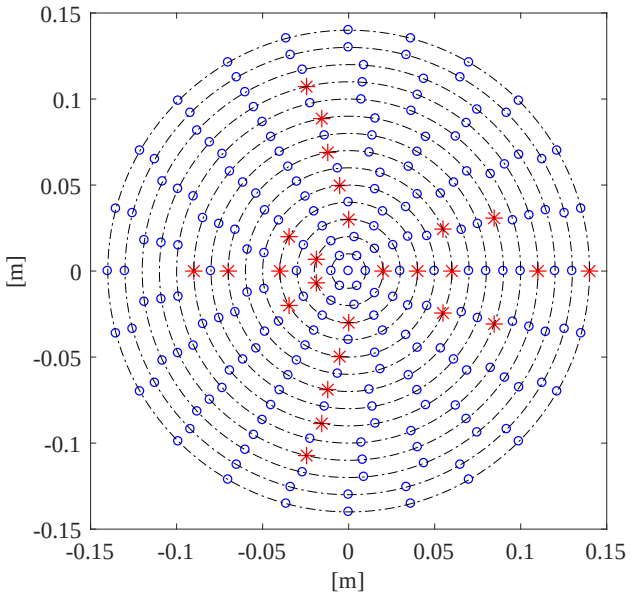

Fig. 2: The array layout obtained by the greedy search. It consists of $K' = 26$ sensors, spread over most of the rings. The blue circles are all the candidate sensors, while the red stars are the selected sensors.

The next step is to duplicate the array layout presented in Fig. 2 by a factor of $Q = 3$, meaning that we get a reflected image of the array layout in two more additional directions: $\frac{2\pi}{Q}$ and $\frac{4\pi}{Q}$. Figure 3 presents the duplicated array layout which composed from $Z = 72$ sensors.

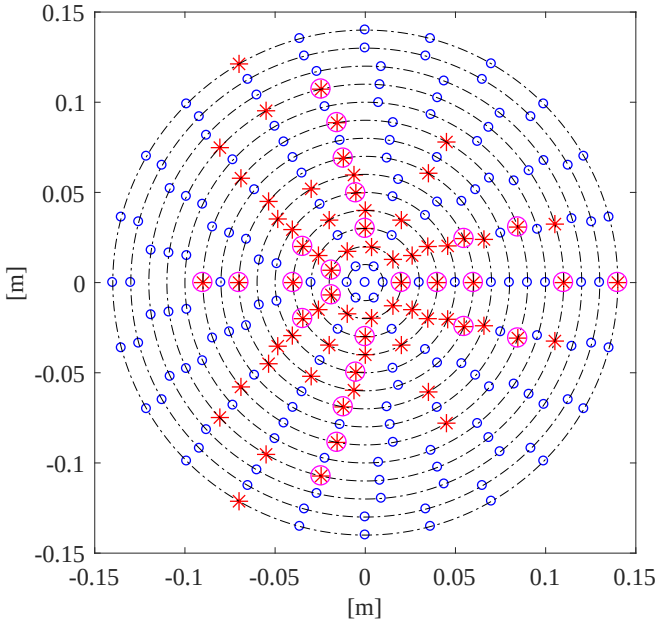

Fig. 3: The array layout after duplication. It consists of $Z = 72$ sensors, spread over most of the rings. The blue circles are all the candidate sensors, the red stars are the selected sensors after duplication, and the pink circles are the sensors obtained by the greedy algorithm of the previous step.

On that step much more sensors were selected while part of them is unnecessary. Therefore, we apply an ℓ_{12}-norm optimization as presented in Section IV-C, using the CVX software [50]. We set the decimation parameter to be $J_{\mathrm{d}} = 5$. After 5 iterations, we get $\Delta\boldsymbol{\eta} < \epsilon_\eta$ and $K = 33$ dominant sensors over $G' = 4$ rings were identified, while all the rest are close to zero, meaning that both $\boldsymbol{\eta}$ and the filters $\left\{\mathbf{h}_Z(\omega_j')\right\}_{j=1}^{J'}$ are sparse vectors with $K = 33$ active elements, concentrated in $G' = 4$ rings. The number of selected elements remains the same even if more iterations are used. This iterative optimization problem yields the final array layout presented in Fig. 4. We finally obtain the filters $\{\mathbf{h}_K(\omega_j)\}_{i=1}^{J}$ by solving

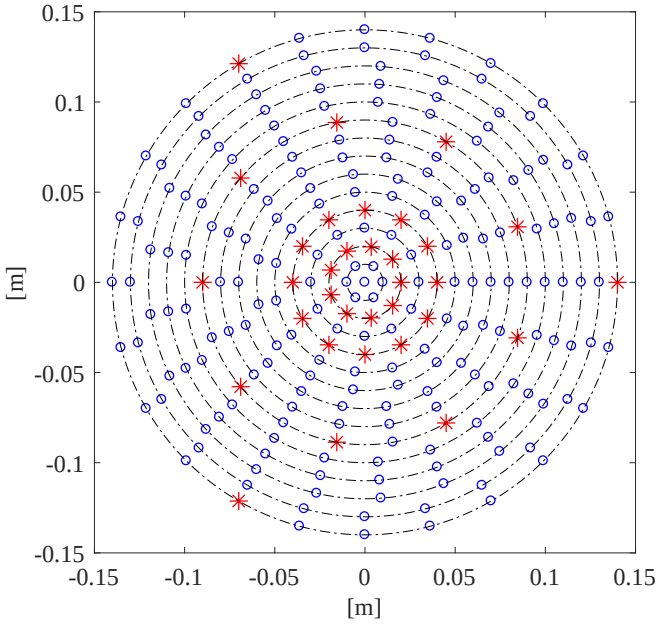

Fig. 4: The array layout of the concentric DMAs obtained by the ring optimization procedure presented on Section IV-C. It consists of $K = 33$ sensors, spread over $G' = 4$ rings. The blue circles are all the candidate sensors, while the red stars are the selected sensors.

(49), according to Section IV-D.

Figure 5 presents the array layout for each of the three remaining approaches. The black squares are the array layout of the LAC approach, while the pink pentagrams are the array layout obtained by the SAC design. One realization of a random design is presented by the green diamonds. For these three approaches, the sensors positions are set a-priori. The SAC approach achieves the smallest array aperture, yet, it suffers from white noise amplification as will be discussed later. Note that comparing the array layout of Fig 4 obtained by the sparse design and the array layout obtained by other approaches as presented in Fig. 5, one can see that the sparse design offers some kind of compromise between high and low frequencies and panoramic design.

Figure 6 illustrates the designed beampattern (1) of a third-order hypercardioid for a specific frequency of $f = 6280$ Hz, obtained by each of the four approaches for the case of steering for $\theta_{\mathrm{s}} = 70°$. Also presented is the theoretical beampattern (53) of a third-order hypercardioid (blue dotted line) for the

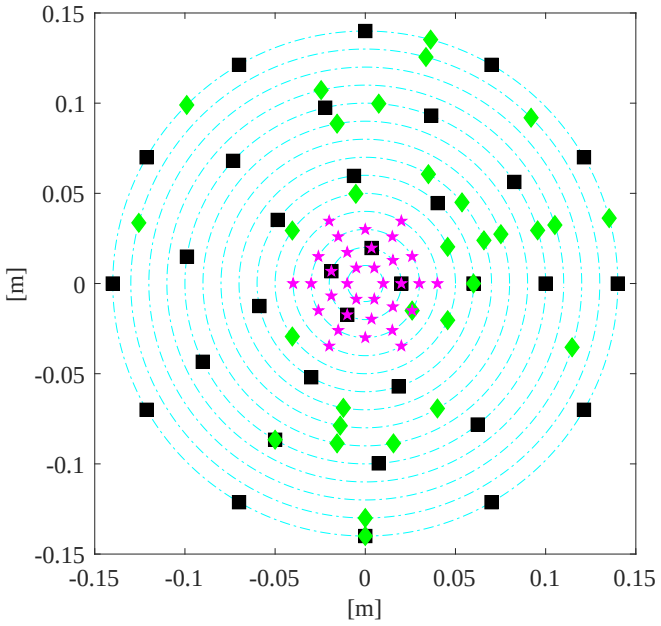

Fig. 5: The array layout of the CCDMAs obtained by uniform and random designs. The black squares are the array layout of the LAC approach, while the pink pentagrams are the array layout obtained by the SAC design. One realization of a random design is presented by the green diamonds.

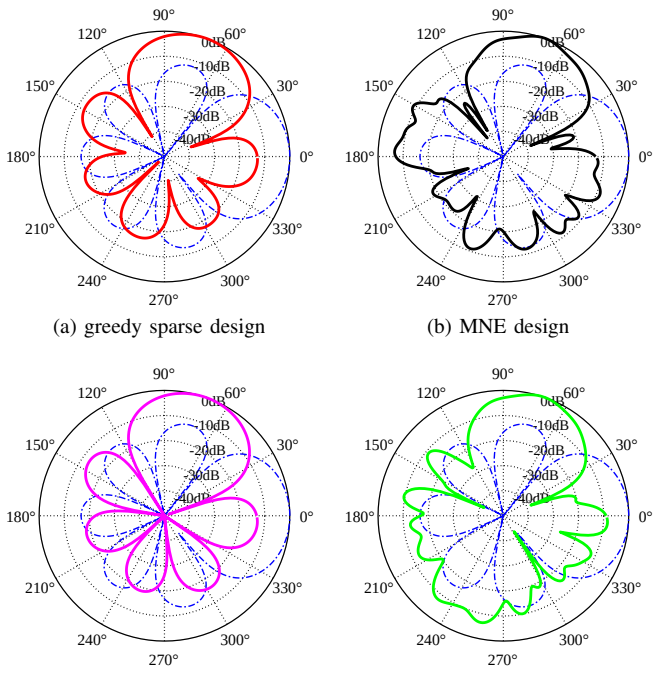

(a) greedy sparse design (b) MNE design

(c) MN design (d) random design

Fig. 6: Beampatterns of a third-order hypercardioid for $f = 6280$ Hz, steered to $\theta_{\mathrm{s}} = 70°$, obtained by the sparse design (red line), the LAC approach (black line), the SAC approach (pink line), and the random design (green line). Also presented is the theoretical beampattern of a third-order hypercardioid (blue dotted line), steered to $\theta_{\mathrm{s}} = 0°$.

case of $\theta_{\mathrm{s}} = 0°$. One can see that the SAC approach obtains the beampattern which is the most similar to the theoretical value while the LAC and the random design have much higher sidelobes due to the spatial aliasing. The proposed greedy sparse approach obtain beampattern which is quite similar to the theoretical one.

Figure 7 shows the WNG (16), the DF (55), and the SLL (57) as a function of frequency obtained by the greedy sparse design (red stars line), the LAC design (black squares line), the SAC design (pink pentagrams line), the random design (green diamonds line), and the theoretical DF of a third-order hypercardioid (blue dashed line). The DF of an array is the gain in signal-to-noise ratio (SNR) for the case of a spherical diffuse noise, i.e. [42]:

$$\begin{aligned}\mathcal{D}\left(\mathbf{h}(\omega_j)\right) &= \frac{\left|\mathcal{B}\left(\mathbf{h}(\omega),\theta_0,\phi_0\right)\right|^2}{\frac{1}{4\pi}\int_0^{2\pi}\int_0^{\pi}\left|\mathcal{B}\left(\mathbf{h}(\omega),\theta,\phi\right)\right|^2\sin\phi d\phi d\theta} \\ &= \frac{\left|\mathbf{h}^H\left(\omega_j\right)\mathbf{d}\left(\omega_j,\theta_{\mathrm{s}}\right)\right|^2}{\mathbf{h}^H\left(\omega_j\right)\mathbf{\Gamma}_{\mathrm{dn}}\left(\omega_j\right)\mathbf{h}\left(\omega_j\right)},\end{aligned} \tag{55}$$

where $\mathcal{B}\left(\mathbf{h}(\omega),\theta,\phi\right)$ is the synthesized 3D directivity pattern,

$$\left[\mathbf{\Gamma}_{\mathrm{dn}}\left(\omega_j\right)\right]_{il} = \mathrm{sinc}\left(\frac{\omega_j}{c}d_{i,j}\right) \tag{56}$$

is an $M \times M$ pseudo-coherence matrix of the diffuse noise field, and $d_{i,j}$ is the distance between the ith sensor and the jth sensor. As we focus on the 2D scenario and optimize only the 2D directivity pattern, the presented DF is for the case that the integral in (55) was calculated for the case that $\phi = \frac{\pi}{2}$.

We also define the SLL as the integral of the square of the beampattern over the region of the sidelobes, i.e., Θ_{s}, that is:

$$\mathcal{S}\left(\mathbf{h}(\omega_j)\right) = \int_{\theta\in\Theta_{\mathrm{s}}}\left|\mathcal{B}\left(\mathbf{h}(\omega),\theta,\phi=\frac{\pi}{2}\right)\right|^2 d\theta. \tag{57}$$

One can see that the greedy sparse design obtains superior results in terms of WNG, DF, and SLL with respect to the other approaches. The SAC obtains nearly FI optimal DF implying on its FI beampattern, but achieves poor WNG, especially for low frequencies, which is a well-known problem of superdirective beamformers in general, and of DMAs in particular. The LAC approach obtains higher level of sidelobes in high frequencies, which is reasonable because of the effect of grating lobes which start to appear. Note that the effect of grating lobes in the concentric geometry is much weaker with respect to the case of linear or plannar geometry because in the concentric geometry the sensors in the inner rings are close each other to prevent or at least to reduce the effect of grating lobes.

The synthesized FI beampatterns versus frequency are shown in Fig. 8 for the (a) greedy sparse design, (b) the LAC design, (c) the SAC design, and (d) the random design. This figure reflects the trends inspected by the DF and the SLL plots. Specifically, for the greedy sparse approach the beampattern is almost FI, especially in the mainlobe region and less in the sidelobes regions, as dictated by the constraints $\mathcal{C}_1$ and $\mathcal{C}_2$. The SAC approach achieves the clearest and most

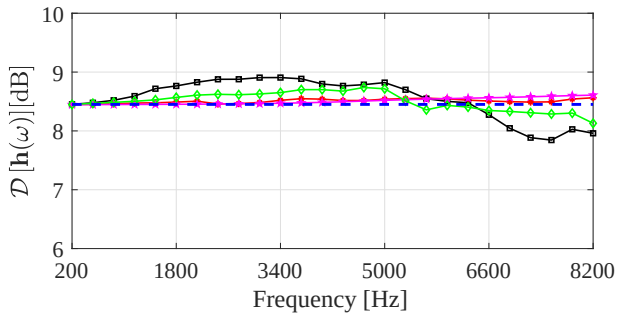

(a)

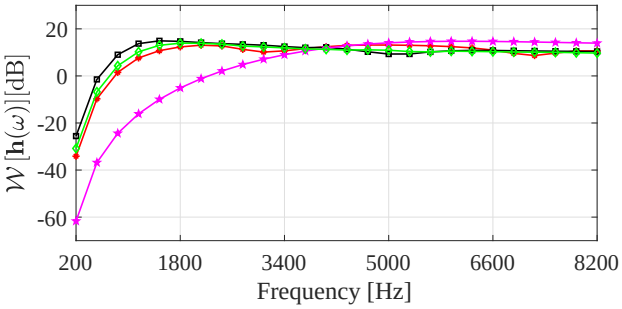

(b)

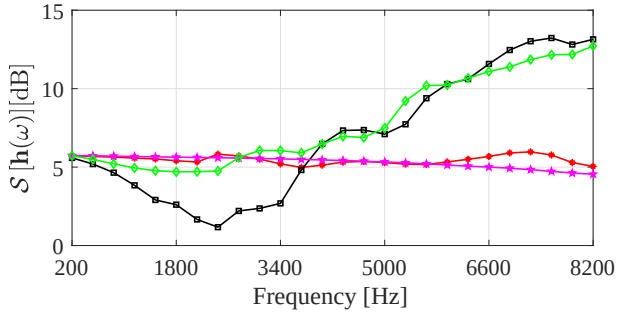

(c)

Fig. 7: (a) DF , (b) WNG, and SLL vs. frequency for the greedy sparse design (red circles line), the LAC design (black squares line), the SAC design (pink pentagrams line), and the random design (green diamonds line). Also presented is the theoretical DF of a third-order hypercardioid (blue dashed line).

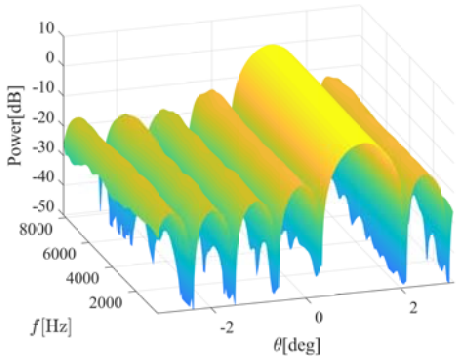

(a) greedy sparse design

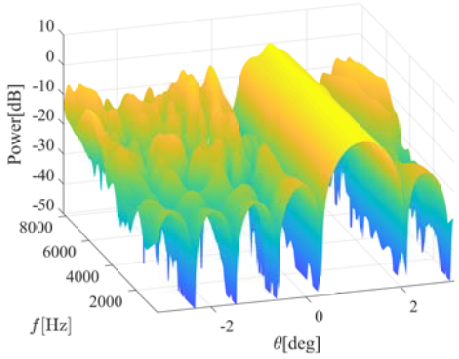

(b) LAC design

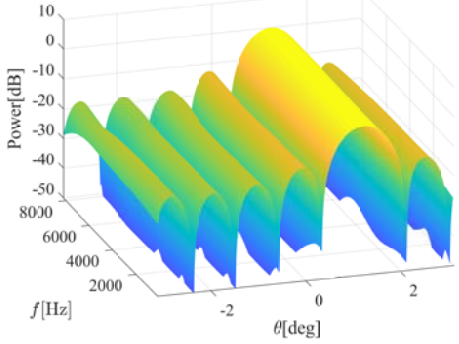

(c) SAC design

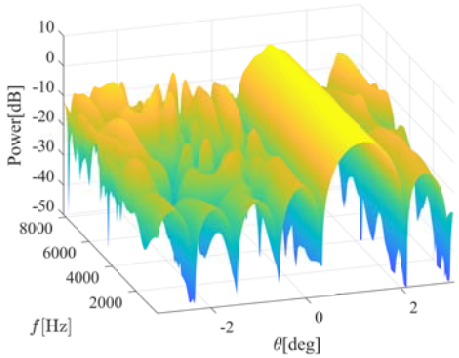

(d) random design

Fig. 8: Beampatterns versus frequency for the four examined design approaches.

perfect FI beampattern, and in the LAC and random designs one can see higher level of sidelobes.

The above design example demonstrate the feasibility and the advantages of the greedy sparse approach compared to the uniform and random design approaches.

VI. Conclusions

A greedy sparse design for FI concentric arrays was derived, which supports also the rotationally-invariant property, meaning that almost the same directivity pattern can be designed for different azimuthal directions of steering using the same sparse array layout. The proposed design extends our recent work on incoherent sparse design of FI beamformers where the obtained sparse array layout was not steerable but designed for a fixed steering direction. Moreover, the proposed greedy

approach offers more natural and intuitive way to set the number of required sensors in the sparse array layout, which was one of the shortcomings of our previous design. The proposed approach was applied to design a third-order FI robust superdirective DMA with a minimal number of sensors. It was compared to a uniform design and to a random design. Simulations show that the proposed greedy sparse design offers a good compromise between robustness and directivity and obtains rotationally-invariant FI beamformer with a reasonable computational complexity. Future research may focus on different array geometries, extension to the 3D scenario, other sparse algorithms, and adaptive versions of sparse FI design.

VII. Appendix: Calculation of $\mu(\mathbf{D}_j)$ (30)

It can be shown that the mth column of the matrix $\mathbf{D}_j$ $(m = 1, ..., M)$ has the form of

$$\mathbf{d}_{j_m} = \Big[e^{-\jmath \frac{\omega_j r(\mathbf{p}_m)}{c} \cos(\theta_1 - \psi(\mathbf{p}_m))} \dots \\ e^{-\jmath \frac{\omega_j r(\mathbf{p}_m)}{c} \cos(\theta_P - \psi(\mathbf{p}_m))} \Big]^T, \quad (58)$$

where $r(\mathbf{p}_m)$ and $\psi(\mathbf{p}_m)$ denote the radius and angle of the mth sensor located at $\mathbf{p}_m$.

We start by deriving the numerator of (27) as

$$\begin{aligned} |\mathbf{d}_{j_l}^H \mathbf{d}_{j_k}| &= \sum_{p=1}^{P} e^{\jmath \frac{\omega_j r(\mathbf{p}_l)}{c} \cos(\theta_p - \psi(\mathbf{p}_l))} e^{-\jmath \frac{\omega_j r(\mathbf{p}_k)}{c} \cos(\theta_p - \psi(\mathbf{p}_k))} \\ &= \sum_{p=1}^{P} e^{\jmath \frac{\omega_j r(\mathbf{p}_l)}{c} [\cos(\theta_p)\cos(\psi(\mathbf{p}_l)) + \sin(\theta_p)\sin(\psi(\mathbf{p}_l))]} \\ &\qquad e^{-\jmath \frac{\omega_j r(\mathbf{p}_k)}{c} [\cos(\theta_p)\cos(\psi(\mathbf{p}_k)) + \sin(\theta_p)\sin(\psi(\mathbf{p}_k))]} \\ &= \sum_{p=1}^{P} e^{\alpha \cos(\theta_p) + \beta \sin(\theta_p)}, \end{aligned} \quad (59)$$

where

$$\alpha \triangleq \jmath \frac{\omega_j r(\mathbf{p}_l)}{c} \cos(\psi(\mathbf{p}_l)) - \jmath \frac{\omega_j r(\mathbf{p}_k)}{c} \cos(\psi(\mathbf{p}_k)) \quad (60)$$

and

$$\beta \triangleq \jmath \frac{\omega_j r(\mathbf{p}_l)}{c} \sin(\psi(\mathbf{p}_l)) - \jmath \frac{\omega_j r(\mathbf{p}_k)}{c} \sin(\psi(\mathbf{p}_k)). \quad (61)$$

Using the following well-known identity

$$\int_0^{2\pi} e^{\alpha \cos(\theta) + \beta \sin(\theta)} d\theta = 2\pi I_0(\sqrt{\alpha^2 + \beta^2}) \quad (62)$$

where $I_0(\cdot)$ is the modified Bessel function of the first kind, (59) can be reduced to

$$\sum_{p=1}^{P} e^{\alpha \cos(\theta_p) + \beta \sin(\theta_p)} \approx \frac{2\pi}{\Delta\theta} I_0(\sqrt{\alpha^2 + \beta^2}), \quad (63)$$

where $\Delta\theta$ is the resolution of the azimuthal direction, θ. Therefore,

$$I_0(\sqrt{\alpha^2 + \beta^2}) = I_0 \left(\sqrt{-\frac{\omega_j^2}{c^2} \left[r^2(\mathbf{p}_l) + r^2(\mathbf{p}_k) - \mathbf{p}_l \cdot \mathbf{p}_k \right]} \right), \quad (64)$$

where $\mathbf{p}_l \cdot \mathbf{p}_k = r(\mathbf{p}_l) r(\mathbf{p}_k) \cos(\psi(\mathbf{p}_l) - \psi(\mathbf{p}_k)) = \mathbf{p}_l^T \mathbf{p}_k$ and $\cdot$ denotes the scalar product. Finally, we can obtain the following result

$$\mu(\mathbf{D}_j) = \max_{k \neq l} \left| I_0 \left(\sqrt{-\frac{\omega_j^2}{c^2} \left[r^2(\mathbf{p}_l) + r^2(\mathbf{p}_k) - \mathbf{p}_l^T \mathbf{p}_k \right]} \right) \right|. \quad (65)$$

References

[1] J. Benesty, J. Chen, and Y. Huang, *Microphone Array Signal Processing*. Berlin, Germany: Springer-Verlag, 2008.

[2] M. Branstein and D. B. Ward, Eds, *Microphone Arrays: Signal Processing Techniques and Applications*. Berlin, Germany: Springer-Verlag, 2001.

[3] J. Benesty, J. Chen, Y. Huang, and J. Dmochowski, "On microphone-array beamforming from a MIMO acoustic signal processing perspective," *IEEE Trans. Audio, Speech, Language Process.*, vol. 15, no. 3, pp. 1053–1065, Mar. 2007.

[4] G. Huang, J. Benesty, and J. Chen, "Design of robust concentric circular differential microphone arrays," *The Journal of the Acoustical Society of America*, vol. 141, no. 5, pp. 3236–3249, 2017.

[5] S. Yan, "Optimal design of FIR beamformer with frequency invariant patterns," *Appl. Acoust.*, vol. 67, pp. 511–528, 2006.

[6] E. Mabande, A. Schad, and W. Kellermann, "Design of robust superdirective beamformer as a convex optimization problem," in *Proc. IEEE Int. Conf. Acoust. Specch Signal Process. (ICASSP), Taipei, Taiwan*, 2009, pp. 77–80.

[7] S. C. Chan and H. H. Chen, "Uniform concentric circular arrays with frequency-invariant characteristics - theory, design, adaptive beamforming and doa estimation," *IEEE Trans. Signal Process.*, vol. 55, no. 1, pp. 165–177, Jan. 2007.

[8] W. Liu and S. Weiss, *Wideband Beamforming: Concepts and Techniques*. Chichester, U.K.: Wiley, 2010.

[9] M. Crocco and A. Trucco, "Design of robust superdirective arrays with a tunable tradeoff between directivity and frequency-invariance," *IEEE Trans. Signal Process.*, vol. 59, no. 5, pp. 2169–2181, May 2011.

[10] B. D. Van Veen and K. V. Buckley, "Beamforming: A versatile approach to spatial filtering," *IEEE Mag. Acoust., Speech, Signal Process.*, vol. 5, pp. 4–24, Apr. 1988.

[11] W. Liu and S. Weiss, "Design of frequency invariant beamformers for broadband arrays," *IEEE Trans. Signal Process.*, vol. 56, no. 2, pp. 855–860, Feb. 2008.

[12] H. Hung and M. Kaveh, "Focusing matrices for coherent signal subspace processing," *IEEE Trans. Acoust. Speech Signal Process.*, vol. 36, no. 8, pp. 1272–1281, Aug 1988.

[13] Y. Buchris, I. Cohen, and M. A. Doron, "Bayesian focusing for coherent wideband beamforming," *IEEE Trans. Audio, Speech, Language Process.*, vol. 20, no. 4, pp. 1282–1295, May 2012.

[14] J. Benesty and J. Chen, *Study and Design of Differential Microphone Arrays*. Berlin, Germany: Springer-Verlag, 2012.

[15] G. W. Elko, "Superdirectional microphone arrays," in *Acoustic Signal Processing for Telecommunication*, S. L. Gay and J. Benesty, Eds. Boston, MA: Kluwer Academic Publishers, 2000, ch. 10, pp. 181–237.

[16] M. Buck, "Aspects of first-order differential microphone arrays in the presence of sensor imperfections," *European Trans. Telecommunications*, vol. 13, pp. 115–122, Mar. 2002.

[17] E. De Sena, H. Hacihabiboğlu, and Z. Cavetković, "On the design and implementation of higher order differential microphones," *IEEE Trans. Audio, Speech, Language Process.*, vol. 20, no. 1, pp. 162–174, Jan. 2012.

[18] H. Cox, R. M. Zeskind, and T. Kooij, "Practical supergain," *IEEE Trans. Acoust., Speech, Signal Processing*, vol. ASSP-34, no. 3, pp. 393–398, June 1986.

[19] I. J. H. Doles and F. D. Benedict, "Broad-band array design using the asymptotic theory of unequally spaced arrays," *IEEE Trans. Antennas Propagat.*, vol. 36, pp. 27–33, Jan. 1988.

[20] D. B. Ward, R. A. Kennedy, and R. C. Williamson, "Theory and design of broadband sensor arrays with frequency invariant farfield beampatterns," *J. Acoust. Soc. Amer.*, vol. 97, no. 2, pp. 1023–1034, Feb. 1995.

[21] M. Crocco and A. Trucco, "Stochastic and analytic optimization of sparse aperiodic arrays and broadband beamformers with robust superdirective patterns," *IEEE Trans. Audio, Speech, Language Process.*, vol. 20, no. 9, pp. 2433–2447, Nov. 2012.

[22] Z. Li, K. F. Cedric Yiu, and Z. Fen, "A hybrid descent method with genetic algorithm for microphone array placement design," *Appl. soft Comput.*, vol. 13, pp. 1486–1490, 2013.

[23] B. P. Kumar and G. Branner, "Generalized analytical technique for the synthesis of unequally spaced arrays with linear, planar, cylindrical or spherical geometry," *IEEE Transactions on Antennas and Propagation*, vol. 53, no. 2, pp. 621–634, 2005.

[24] R. L. Haupt, "Optimized element spacing for low sidelobe concentric ring arrays," *IEEE Transactions on Antennas and Propagation*, vol. 56, no. 1, pp. 266–268, 2008.

[25] C. Liu, J. Cai, Z. Huang, X. Wang, and S. Chen, "Pattern synthesis of sparse concentric circular array based on the niche genetic algorithm," in *2017 IEEE 9th International Conference on Communication Software and Networks (ICCSN)*. IEEE, 2017, pp. 906–911.

[26] K. Chen, H. Chen, L. Wang, and H. Wu, "Modified real ga for the synthesis of sparse planar circular arrays," *IEEE Antennas and Wireless Propagation Letters*, vol. 15, pp. 274–277, 2015.

[27] N. N. Pathak, G. K. Mahanti, S. K. Singh, J. K. Mishra, and A. Chakraborty, "Synthesis of thinned planar circular array antennas using modified particle swarm optimization," *Progress In Electromagnetics Research*, vol. 12, pp. 87–97, 2009.

[28] U. Singh and T. Kamal, "Synthesis of thinned planar concentric circular antenna arrays using biogeography-based optimisation," *IET microwaves, antennas & propagation*, vol. 6, no. 7, pp. 822–829, 2012.

[29] A. Chatterjee, G. Mahanti, and P. R. S. Mahapatra, "Optimum ring spacing and interelement distance for sidelobe reduction of a uniform concentric ring array antenna using differential evolution algorithm," in *2010 IEEE International Conference on Communication Systems*. IEEE, 2010, pp. 254–258.

[30] T. N. Kaifas, D. G. Babas, and J. N. Sahalos, "Design of planar arrays with reduced nonuniform excitation subject to constraints on the resulting pattern and the directivity," *IEEE Transactions on Antennas and Propagation*, vol. 57, no. 8, pp. 2270–2278, 2009.

[31] X. Zhao, Q. Yang, and Y. Zhang, "A hybrid method for the optimal synthesis of 3-d patterns of sparse concentric ring arrays," *IEEE Transactions on Antennas and Propagation*, vol. 64, no. 2, pp. 515–524, 2015.

[32] A. F. Morabito and P. G. Nicolaci, "Optimal synthesis of shaped beams through concentric ring isophoric sparse arrays," *IEEE Antennas and Wireless Propagation Letters*, vol. 16, pp. 979–982, 2016.

[33] L. Zhang, Y.-C. Jiao, and B. Chen, "Optimization of concentric ring array geometry for 3d beam scanning," *International Journal of Antennas and Propagation*, vol. 2012, 2012.

[34] P. Angeletti, G. Toso, and G. Ruggerini, "Array antennas with jointly optimized elements positions and dimensions part ii: Planar circular arrays," *IEEE Transactions on Antennas and Propagation*, vol. 62, no. 4, pp. 1627–1639, 2013.

[35] L. Zhang, Y.-C. Jiao, B. Chen, and Z.-B. Weng, "Design of wideband concentric-ring arrays with three-dimensional beam scanning based on the optimization of array geometry," *Electromagnetics*, vol. 32, no. 6, pp. 305–320, 2012.

[36] R.-Q. Wang and Y.-C. Jiao, "Synthesis of wideband rotationally symmetric sparse circular arrays with multiple constraints," *IEEE Antennas and Wireless Propagation Letters*, vol. 18, no. 5, pp. 821–825, 2019.

[37] M. D. Gregory, F. A. Namin, and D. H. Werner, "Exploiting rotational symmetry for the design of ultra-wideband planar phased array layouts," *IEEE Transactions on Antennas and Propagation*, vol. 61, no. 1, pp. 176–184, 2012.

[38] Y. Li, K. Ho, and C. Kwan, "3-d array pattern synthesis with frequency invariant property for concentric ring array," *IEEE Transactions on signal processing*, vol. 54, no. 2, pp. 780–784, 2006.

[39] Y. Buchris, A. Amar, J. Benesty, and I. Cohen, "Incoherent synthesis of sparse arrays for frequency-invariant beamforming," *IEEE/ACM Transactions on Audio, Speech, and Language Processing*, vol. 27, no. 3, pp. 482–495, 2019.

[40] Y. C. Pati, R. Rezaiifar, and P. S. Krishnaprasad, "Orthogonal matching pursuit: Recursive function approximation with applications to wavelet decomposition," in *Proceedings of 27th Asilomar conference on signals, systems and computers*. IEEE, 1993, pp. 40–44.

[41] S. G. Mallat and Z. Zhang, "Matching pursuits with time-frequency dictionaries," *IEEE Transactions on signal processing*, vol. 41, no. 12, pp. 3397–3415, 1993.

[42] H. L. Van-trees, *Detection, Estimation and Modulation Theory, Part IV - Optimum Array Processing*. New York: Wiley Interscience, 2002.

[43] J. Benesty, J. Chen, and I. Cohen, *Design of Circular Differential Microphone Arrays*. Berlin, Germany: Springer-Verlag, 2015.

[44] J. A. Tropp, A. C. Gilbert, and M. J. Strauss, "Algorithms for simultaneous sparse approximation. part i: Greedy pursuit," *Signal processing*, vol. 86, no. 3, pp. 572–588, 2006.

[45] J. D. Blanchard, M. Cermak, D. Hanle, and Y. Jing, "Greedy algorithms for joint sparse recovery," *IEEE Transactions on Signal Processing*, vol. 62, no. 7, pp. 1694–1704, 2014.

[46] S. Sarvotham, D. Baron, M. Wakin, M. F. Duarte, and R. G. Baraniuk, "Distributed compressed sensing of jointly sparse signals," in *Asilomar conference on signals, systems, and computers*, 2005, pp. 1537–1541.

[47] E. J. Candès, M. B. Wakin, and S. P. Bond, "Enhancing sparsity by reweighted ℓ_1 minimization," *J. Fourier Analy. Appl.*, vol. 14, pp. 877–905, Dec. 2008.

[48] J. A. Tropp, "Just relax: Convex programming methods for identifying sparse signals in noise," *IEEE transactions on information theory*, vol. 52, no. 3, pp. 1030–1051, 2006.

[49] ——, "Greed is good: Algorithmic results for sparse approximation," *IEEE Transactions on Information theory*, vol. 50, no. 10, pp. 2231–2242, 2004.

[50] M. Grant, S. Boyd, and Y. Ye, "CVX: Matlab software for disciplined convex programming," 2008.

[51] P. T. Boufounosa, P. Smaragdisb, and B. Rajc, "Joint sparsity models for wideband array processing," in *SPIE Optical Engineering+ Applications*. International Society for Optics and Photonics, 2011, pp. 81 380–K.

[52] S. F. Cotter, B. D. Rao, K. Engan, and K. Kreutz-Delgado, "Sparse solutions to linear inverse problems with multiple measurement vectors," *IEEE Transactions on Signal Processing*, vol. 53, no. 7, pp. 2477–2488, July 2005.

[53] Y. Liu, L. Zhang, L. Ye, Z. Nie, and Q. H. Liu, "Synthesis of sparse arrays with frequency-invariant-focused beam patterns under accurate sidelobe control by iterative second-order cone programming," *IEEE Trans. Antennas Propagat.*, vol. 63, no. 12, pp. 5826–5832, Dec. 2015.

Chapter 7

Discussion and Conclusions

7.1 Discussion and Conclusions

In this thesis, we considered several important issues regarding DMAs and superdirective beamformers. Such arrays have compact physical dimensions while obtaining high directivity and frequency-invariant (FI) directivity pattern. Therefore, they are highly suitable for some real-world applications involving broadband signals like audio and speech. In such applications, desired signals as well as interfering signals propagate towards array of microphones from various directions. Consequently, the received signals are mixtures of both desired and undesired parts of interferences and noise. Array processing and beamforming techniques are widely used to recover the signals of interest while rejecting undesired components of signals and obtain spatial diversity gain. As the signals are broadband, the standard narrowband model of beamforming cannot be applied directly, and FI beamformers should be used instead. Beamformers with FI directivity patterns allow to obtain signals in their outputs which do not suffer from artifacts and distortions due to a different beamwidth of the mainbeam in different frequencies. Among several concepts of FI beamforming, DMAs which inherently have FI directivity pattern, can be applied. These arrays combine closely spaced sensors to respond to the spatial derivatives of the acoustic field, and in-

clude the well-known superdirective beamformer as a particular case. In spite of their some desired properties, DMAs suffer from inferior WNG, especially in low frequencies, meaning that DMAs are non robust and much vulnerable to model mismatch errors and array imperfections.

We addressed this problem by using tools of convex optimization and data mining in order to determine an optimal sparse array layout in terms of FI, directivity, robustness, and computationally. Specifically, we develop an incoherent sparse design which first optimizes the array layout for each frequency bin in the bandwidth of interest. Then, all the decisions are fused together using some data mining tools yielding a joint sparse array layout used in the synthesis step. We also generalize this concept and propose a greedy sparse design for more complicated array geometries like concentric arrays, which supports a flexible steering direction of the desired signal.

We also explored and proposed two extensions to the traditional model of DMAs which contribute to the robustness and to a more simple and flexible implementation of DMAs. The first is a time-domain equivalent model which is important in some applications where minimal delay is required, such as real-time audio communications. We analytically represent in the time domain the array input signal, the FI beampattern of DMAs, the performance measures and the beamformer coefficient vector. We also show the convergence of the proposed time-domain model to the traditional model of DMAs. The second extension is an asymmetric model for DMAs which contributes to much more flexible and robust implementations of DMAs. The common to all of the methods developed in this research is that they take the traditional performance of DMAs one step further and provide more robust and flexible design. Specifically, the main conclusions of this research are as follows:

1) A framework for a time-domain implementation of DMAs was derived in Chapter 3, which includes also a closed-form solution for temporal DMAs filters of any order and any number of sensors as well as equivalent time-domain performance measures. It was shown that the proposed model converges to the

classical DMAs model due to the convergence of the time-domain beampattern to the theoretical beampattern. Several design examples were presented in the simulation part demonstrating the equivalence of the time- and frequency- domain implementations. Since each of the possible implementations involves some benefits and shortcomings, choosing time- or frequency- domain implementation for a specific system, is of a great importance because it provides flexibility in the design considerations of several real-world applications involving DMAs.

2) The asymmetric model for DMAs derived in Chapter 4, offers more degrees of freedom with respect to the traditional symmetric model which can be exploited to achieve better performance in terms of WNG, DF, and FBR. Moreover, for a given number of desired null directions, the asymmetric model may allows reduced order of CDMAs with respect to the symmetric model leading to an improved robustness to array imperfections. Therefore, this concept is of a great importance for some real-world CDMAs based beamforming applications since it allows smaller and more robust designs with respect to the regular symmetric design.

3) The proposed incoherent sparse design approach, derived in Chapter 5, was applied to design robust superdirective FI beamformers with minimal number of sensors. It was compared to the coherent approach where optimization is performed simultaneously over all directions and frequencies of interest, and also to uniform design approaches. Simulations show that the proposed incoherent sparse design is a good compromise between robustness and directivity and obtains a FI beamformer with significantly reduced computational complexity. Moreover, for scenarios where a large number of candidate sensors and frequency bins is assumed, the coherent approach is infeasible while the incoherent design provides results with a reasonable computation time.

4) The extension of the incoherent sparse design approach presented in Chapter 6 is important for geometries like concentric arrays where multiple different azimuthal directions are required. Specifically, a greedy sparse design for FI concentric arrays was derived, which supports also the rotationally-invariant property,

meaning that almost the same directivity pattern can be designed for different azimuthal directions of steering using the same sparse array layout. The proposed greedy approach offers a more natural and intuitive way to set the number of required sensors in the sparse array layout, which was one of the shortcomings of our previous design. The proposed approach was applied to design a third-order FI robust superdirective DMA with a minimal number of sensors. It was compared to a uniform design and to a random design. Simulations show that the proposed greedy sparse design offers a good compromise between robustness and directivity and obtains FI beamformer with a reasonable computational complexity.

7.2 Future Research Directions

Throughout this thesis, we developed various approaches to obtained better DMAs design in terms of robustness, directivity, design flexibility, and computational complexity. Although superior performance were obtained as reflected from the simulations, there are still other issues for a future research which are expected to take the obtained performance one step further:

1) Along all this research we focused on a 2D design, meaning that we optimize quantities like directivity pattern only in the same plane where the array is laid. While for the linear geometry such an optimization actually yields a 3D optimized solutions due to the symmetry in the elevation, in other geometries like circular and concentric arrays, the 2D approximation provides simplicity with a payment of accuracy and more. For example, in the sparse incoherent design, the constraints about the ℓ_2-norm optimization of the error between the design beampattern and the desired one, yield small errors only in the plane of the array, while some higher sidelobes are exist in different elevations. Therefore, future research may focuses on extending the 2D model and approaches derived in this research to the general 3D model where signals may arrive to the array also from different elevations.

2) Following on from the previous section, we would like to expand our ap-

proaches also for the setup of volumetric arrays, where sensors can be located not only in a 2D plain but also for the 3D case. Volumetric arrays may have more degrees of freedom which can be used to obtain higher performance with respect to 2D arrays.

3) Along the third and fourth parts of this research, we consider several data mining tools in order to find an optimal joint-sparse array layout. This was accomplished by either dimensionality reduction algorithms and clustering or by using a greedy based iterative approach. Yet, in both approaches there is no unique solution, meaning that other algorithms may yield more optimal results. Future work may explore for other tools and algorithms of data fusion that can obtain more superior and optimal performance.

4) Along the third and forth parts of this research where we propose sparse approaches, we consider the case of a uniform distance between two adjacent sensors and also uniform gaps between two bins in the frequency domain. As in several acoustic systems the logarithmic scale is preferred since the human ear has a logarithmic scale, it is of a great interest to assimilate such apriori knowledge in the sparse design, which is expected to lead to a better fitting of the optimization solution.

5) Finally, aspects of adaptive versions of DMAs used for more complicated scenarios like reverberations should also be explored in future research. While along the entire of this research, an isotropic free space medium was assumed, in real indoor scenarios like rooms, there are some reflections from the walls, the floor and the ceilings. This problem is even worsen in the case of DMAs and superdirective beamformers as their mainbeam is wider than the case of traditional arrays, meaning that part of the reflections enter into the mainbeam. Thus, the spatial filtering of the beamformer is not sufficient to mitigate this artifacts, and more sophisticated dereverberations approaches should be applied.

Bibliography

[1] J. Benesty, J. Chen, and Y. Huang, *Microphone array signal processing*. Berlin, Germany: Springer-Verlag, 2008, vol. 1.

[2] J. Benesty and J. Chen, *Study and Design of Differential Microphone Arrays*. Berlin, Germany: Springer-Verlag, 2012.

[3] J. Benesty, J. Chen, Y. Huang, and J. Dmochowski, "On microphone-array beamforming from a MIMO acoustic signal processing perspective," *IEEE Trans. Audio, Speech, Language Process.*, vol. 15, no. 3, pp. 1053–1065, Mar. 2007.

[4] M. Branstein and D. B. Ward, Eds, *Microphone Arrays: Signal Processing Techniques and Applications*. Berlin, Germany: Springer-Verlag, 2001.

[5] H. L. Van-trees, *Detection, Estimation and Modulation Theory, Part IV - Optimum Array Processing*. New York: Wiley Interscience, 2002.

[6] M. Crocco and A. Trucco, "Design of robust superdirective arrays with a tunable tradeoff between directivity and frequency-invariance," *IEEE Trans. Signal Process.*, vol. 59, no. 5, pp. 2169–2181, May 2011.

[7] ——, "Stochastic and analytic optimization of sparse aperiodic arrays and broadband beamformers with robust superdirective patterns," *IEEE Trans. Audio, Speech, Language Process.*, vol. 20, no. 9, pp. 2433–2447, Nov. 2012.

[8] J. Flangan, D. Berkeley, G. Elko, J. West, and M. Sondhi, "Autodirective microphone systems," *Acustica*, vol. 73, pp. 58–71, 1991.

[9] I. J. H. Doles and F. D. Benedict, "Broad-band array design using the asymptotic theory of unequally spaced arrays," *IEEE Trans. Antennas Propagat.*, vol. 36, pp. 27–33, Jan. 1991.

[10] D. B. Ward, R. A. Kennedy, and R. C. Williamson, "Theory and design of broadband sensor arrays with frequency invariant farfield beam-patterns," *J. Acoust. Soc. Amer.*, vol. 97, no. 2, pp. 1023–1034, Feb. 1995.

[11] S. C. Chan and H. H. Chen, "Uniform concentric circular arrays with frequency-invariant characteristics - theory, design, adaptive beamforming and doa estimation," *IEEE Trans. Signal Process.*, vol. 55, pp. 165–177, Jan. 2007.

[12] W. Liu and S. Weiss, "Design of frequency invariant beamformers for broadband arrays," *IEEE Trans. Signal Process.*, vol. 56, no. 2, pp. 855–860, Feb. 2008.

[13] S. Doclo and M. Moonen, "Design of broadband beamformers robust against gain and phase errors in the microphone array characteristics," *IEEE Trans. Signal Process.*, vol. 51, no. 10, pp. 2511–2526, Oct. 2003.

[14] B. D. Van Veen and K. V. Buckley, "Beamforming: A versatile approach to spatial filtering," *IEEE Mag. Acoust., Speech, Signal Process.*, vol. 5, pp. 4–24, Apr. 1988.

[15] E. Mabande, A. Schad, and W. Kellermann, "Design of robust superdirective beamformer as a convex optimization problem," in *Proc. IEEE Int. Conf. Acoust. Specch Signal Process. (ICASSP), Taipei, Taiwan*, 2009, pp. 77–80.

[16] T. Do-Hong and P. Russer, "Spatial signal processing for wideband beamforming," in *Proc.VII International Symposium on Theoretical Electrical Engineering*, 2003, pp. 73–76.

[17] T. Chou, "Frequency-independent beamformer with low response error," in *Proc. IEEE Int. Conf. Acoust. Specch Signal Process. (ICASSP), Detroit, MI*, May 1995, pp. 2995–2998.

[18] Y. R. Zheng, R. A. Goubran, and M. El-Tanany, "Experimental evaluation of a nested microphone array with adaptive noise cancellers," *IEEE Trans. Instrum. Meas.*, vol. 53, pp. 777–786, June 2004.

[19] Y. Buchris, I. Cohen, and M. Doron, "Bayesian focusing for coherent wideband beamforming," *IEEE Trans. Audio, Speech, Language Process.*, vol. 20, no. 4, pp. 1282–1295, May 2012.

[20] H. Cox, R. M. Zeskind, and T. Kooij, "Practical supergain," *IEEE Trans. Acoust., Speech, Signal Processing*, vol. ASSP-34, no. 3, pp. 393–398, June 1986.

[21] H. F. Olson, "Gradient microphones," *J. Acoust. Soc. Amer.*, vol. 17, pp. 192–198, Jan. 1946.

[22] G. M. Sessler and J. E. West, "Directional transducers," *IEEE Trans. Audio Electroacoustic.*, vol. 19, pp. 19–23, Mar. 1971.

[23] G. W. Elko and A. T. N. Pong, "A simple first-order differential microphone," in *Proc. IEEE Workshop Applicat. Signal Process. Audio Acoust. (WASPAA)*, 1995, pp. 169–172.

[24] G. W. Elko, "Superdirectional microphone arrays," in *Acoustic Signal Processing for Telecommunication*, S. L. Gay and J. Benesty, Eds. Boston, MA: Kluwer Academic Publishers, 2000, ch. 10, pp. 181–237.

[25] ——, "Differential microphone arrays," in *in Audio Signal Processing for Next-Generation Multimedia Communication Systems*, Y. Huang and J. Benesty, Eds. Norwell, MA: Kluwer, 2004, ch. 2, pp. 11–65.

[26] T. D. Abhayapala and A. Gupta, "Higher order differential-integral microphone arrays," *J. Acoust. Soc. Amer.*, vol. 127, pp. 227–233, May 2010.

[27] M. Kolundžija, C. Faller, and M. Vetterli, "Spatiotemporal gradient analysis of differential microphone arrays," *J. Audio Eng. Soc.*, vol. 59, pp. 20–28, Feb. 2011.

[28] M. Buck, "Aspects of first-order differential microphone arrays in the presence of sensor imperfections," *European Trans. Telecommunications*, vol. 13, pp. 115–122, Mar. 2002.

[29] R. M. M. Derkx and K. Janse, "Theoretical analysis of a first-order azimuth-steerable superdirective microphone array," *IEEE Trans. Audio, Speech, Language Process.*, vol. 17, pp. 150–162, Jan. 2009.

[30] H. Teutsch and G. W. Elko, "First- and second-order adaptive differential microphone arrays," in *Darmstadt, Germany: 7th International Workshop on Acoustic Echo and Noise Control*, 2001, pp. 57–60.

[31] E. De Sena, H. Hacihabibğlu, and Z. Cavetković, "On the design and implementation of higher order differential microphones," *IEEE Trans. Audio, Speech, Language Process.*, vol. 20, no. 1, pp. 162–174, Jan. 2012.

[32] L. Zhao, J. Benesty, and J. Chen, "Design of robust differential microphone arrays," *IEEE Trans. Audio, Speech, Language Process.*, vol. 22, no. 10, pp. 1455–1464, Oct. 2014.

[33] P. Chao, J. Benesty, and J. Chen, "Design of robust differential microphone arrays with orthogonal polynomials," *The Journal of the Acoustical Society of America*, vol. 138, no. 2, pp. 1079–1089, Aug. 2015.

[34] H. Zhang, J. Chen, and J. Benesty, "Study of nonuniform linear differential microphone arrays with the minimum-norm filter," *Applied Acoustics*, vol. 98, pp. 62–69, May 2015.

[35] P. Chao, J. Chen, and J. Benesty, "Theoretical analysis of differential microphone array beamforming and an improved solution," *IEEE Trans. Audio, Speech, Language Process.*, vol. 23, no. 11, pp. 2093–2105, Nov. 2015.

[36] Y. Buchris, I. Cohen, and J. Benesty, "First-order differential microphone arrays from a time-domain broadband perspective," in *International Workshop on Acoustic Echo and Noise Control (IWAENC) 2016 conf.*

[37] G. Huang, J. Benesty, and J. Chen, "Design of robust concentric circular differential microphone arrays," *The Journal of the Acoustical Society of America*, vol. 141, no. 5, pp. 3236–3249, 2017.

[38] L. C. Godara, "Application of the fast fourier transform to broadband beamforming," *J. Acoust. Soc. Amer.*, vol. 98, no. 1, pp. 230–240, July 1995.

[39] R. T. Compton, "The relationship between tapped delay-line and FFT processing in adaptive arrays," *IEEE Trans. Antennas and Propagation.*, vol. 36, no. 1, pp. 15–26, Jan. 1988.

[40] M. I. Skolnik, G. Nemhauser, and J. W. Sherman III, "Dynamic programming applied to unequally spaced arrays," *IEEE Trans. Antennas Propagat.*, vol. AP-12, pp. 35–43, Jan. 1964.

[41] O. M. Bucci, M. D'Urso, T. Isernia, P. Angeletti, and G. Toso, "Deterministic synthesis of uniform amplitude sparse arrays via new density taper techniques," *IEEE Trans. Antennas Propagat.*, vol. 58, no. 6, pp. 1949–1958, Jun. 2010.

[42] O. Quevedo-Teruel and E. Rajo-Iglesias, "Ant colony optimization in thinned array synthesis with minimum sidelobe level," *IEEE Trans. Antennas Wireless Propag. Lett.*, vol. 5, pp. 349–352, Jun. 2006.

[43] A. Trucco, E. Omodei, and P. Repetto, "Synthesis of sparse planar arrays," *Electron. Lett.*, vol. 33, no. 22, pp. 1834–1835, Oct. 1997.

[44] R. M. Leahy and B. D. Jeffs, "On the design of maximally sparse beamforming arrays," *IEEE Trans. Antennas Propagat.*, vol. 39, no. 8, pp. 1178–1187, Aug. 1991.

[45] Y. Liu, Q. H. Liu, and Z. Nie, "Reducing the number of elements in the synthesis of shaped-beam patterns by the forward-backward matrix pencil method," *IEEE Trans. Antennas Propagat.*, vol. 58, no. 2, pp. 604–608, Feb. 2010.

[46] W. Zhang, L. Li, and F. Li, "Reducing the number of elements in linear and planar antenna arrays with sparseness constrained optimization," *IEEE Trans. Antennas Propagat.*, vol. 59, no. 8, pp. 3106–3111, Feb. 2011.

[47] G. Oliveri, E. T. Bekele, F. Robol, and A. Massa, "Sparsening conformal arrays through a versatile bcs-based method," *IEEE Trans. Antennas Propagat.*, vol. 62, no. 4, pp. 1681–1689, Apr. 2014.

[48] B. Fuchs, "Synthesis of sparse arrays with focused or shaped beampattern via sequential convex optimizations," *IEEE Trans. Antennas Propagat.*, vol. 60, no. 7, pp. 3499–3503, Jul. 2012.

[49] M. D'Urso, G. Prisco, and R. M. Tumolo, "Maximally sparse, steerable, and nonsuperdirective array antennas via convex optimizations," *IEEE/ACM Trans. Antennas Propag.*, vol. 64, no. 9, pp. 800–815, Sep. 2016.

[50] S. E. Nai, W. Ser, Z. L. Yu, and H. Chen, "Beampattern synthesis for linear and planar arrays with antenna selsction by convex optimization," *IEEE Transactions on Antennas and Propagation*, vol. 58, no. 12, pp. 3923–3930, Dec. 2010.

[51] M. Crocco and A. Trucco, "Design of superdirective planar arrays with sparse aperiodic layouts for processing broadband signals via 3-d beamforming," *IEEE/ACM Trans. Audio, Speech, Language Process.*, vol. 22, no. 4, pp. 800–815, Apr. 2014.

[52] Z. Li, K. F. Cedric Yiu, and Z. Fen, "A hybrid descent method with genetic algorithm for microphone array placement design," *Appl. soft Comput.*, vol. 13, pp. 1486–1490, 2013.

[53] Y. Liu, L. Zhang, C. Zhu, and Q. H. Liu, "Synthesis of nonuniformly spaced linear arrays with frequency-invariant patterns by the generalized matrix pencil methods," *IEEE Trans. Antennas Propagat.*, vol. 63, no. 4, pp. 1614–1625, Apr. 2015.

[54] M. B. Hawes and W. Liu, "Sparse array design for wideband beamforming with reduced complexity in tapped delay-lines," *IEEE/ACM Transactions on Audio, Speech and Language Processing (TASLP)*, vol. 22, no. 8, pp. 1236–1247, 2014.

[55] Y. Liu, L. Zhang, L. Ye, Z. Nie, and Q. H. Liu, "Synthesis of sparse arrays with frequency-invariant-focused beam patterns under accurate sidelobe control by iterative second-order cone programming," *IEEE Trans. Antennas Propagat.*, vol. 63, no. 12, pp. 5826–5832, Dec. 2015.

[56] S. F. Cotter, B. D. Rao, K. Engan, and K. Kreutz-Delgado, "Sparse solutions to linear inverse problems with multiple measurement vectors," *IEEE Transactions on Signal Processing*, vol. 53, no. 7, pp. 2477–2488, July 2005.

[57] Y. Buchris, A. Amar, J. Benesty, and I. Cohen, "Incoherent synthesis of sparse arrays for frequency-invariant beamforming," *IEEE/ACM Transactions on Audio, Speech, and Language Processing*, vol. 27, no. 3, pp. 482–495, 2019.

[58] Y. C. Pati, R. Rezaiifar, and P. S. Krishnaprasad, "Orthogonal matching pursuit: Recursive function approximation with applications to wavelet decomposition," in *Proceedings of 27th Asilomar conference on signals, systems and computers*. IEEE, 1993, pp. 40–44.

[59] S. G. Mallat and Z. Zhang, “Matching pursuits with time-frequency dictionaries,” *IEEE Transactions on signal processing*, vol. 41, no. 12, pp. 3397–3415, 1993.

Appendices

Appendix I:

This appendix contains the following manuscript:

Y. Buchris, I. Cohen, and J. Benesty, "First-order differential microphone arrays from a time-domain broadband perspective," in Proc. IEEE International Workshop on Acoustic Signal Enhancement (IWAENC 2016).

FIRST-ORDER DIFFERENTIAL MICROPHONE ARRAYS FROM A TIME-DOMAIN BROADBAND PERSPECTIVE

Yaakov Buchris and Israel Cohen

Technion, Israel Institute of Technology
Technion City, Haifa 32000, Israel
{bucris@tx, icohen@ee}.technion.ac.il

Jacob Benesty

INRS-EMT, University of Quebec
800 de la Gauchetiere Ouest, Suite 6900
Montreal, QC H5A 1K6, Canada
benesty@emt.inrs.ca

ABSTRACT

Differential microphone arrays (DMAs) have a great potential to overcome some of the problems of additive arrays and provide high spatial gain relative to their small size. In this work, we present a time-domain formulation for implementing first-order DMAs, which is very important for some applications in which minimal delay is required, such as real-time communications. We present a design example for first-order DMAs illustrating some of the fundamental properties of the time-domain implementation as well as the equivalence to the frequency-domain implementation.

Index Terms— Microphone arrays, differential microphone arrays (DMAs), time-domain broadband beamforming.

1. INTRODUCTION

Differential microphone arrays (DMAs) can be integrated into several real-world beamforming applications involving speech signals, e.g., hands-free telecommunication. DMAs are characterized as superdirective [3] in general, small-size arrays, whose beampattern is almost frequency invariant, leading to greatly intelligible speech signals even in heavy reverberant and noisy environments. Due to these benefits, DMAs have attracted a significant amount of interest in the field of broadband microphone array processing during the past decade (see [4] - [11] and the references therein).

Broadband array processing algorithms can be implemented both in the time and frequency domains. Design in the time domain is important for applications that require small delays such as real-time communications [13]. Second, processing in the time domain circumvents the edge effects between successive snapshots of the incoming signals. Furthermore, in some cases the implementation of time-domain filters is computationally more efficient than the equivalent frequency-domain filters, especially when short filters are sufficient. The advantage of frequency-domain implementation is mainly due to the ability to implement some frequency dependent processing algorithms, like frequency-selective null-steering and efficient calculation of the sample matrix inversion (SMI) [12] used in several adaptive array processing applications.

In this work, we present a framework for a broadband time-domain implementation of first-order DMAs. First, the input array signals are manipulated and represented in a separable form as a product between a desired signal dependent term and a second term which depends only on the array geometry. This representation is beneficial because it enables to apply several array processing algorithms, originally developed in the frequency domain, into broadband time-domain DMAs. We derive a closed-form solution for time-domain first-order DMAs for any given number of sensors. Due to the DMA assumption, the derived solution is very simple with respect to other methods usually employed in the design of general arrays where some constraints that ensure the frequency invariance should be imposed. We also establish the equivalent time-domain expressions for several commonly-used quality measures like the beampattern, white noise gain (WNG), and directivity factor (DF). Finally, we evaluate the performance of the time-domain DMAs and compare it with that of the frequency-domain implementation recently proposed by Benesty et al. [5].

2. SIGNAL MODEL

We consider a broadband source signal, $s(n)$, in the far-field, where n is the discrete-time index, that propagates in an anechoic acoustic environment at the speed of sound, i.e., $c = 340$ m/s, and impinges on a uniform linear sensor array consisting of M omnidirectional microphones, where the distance between two successive sensors is equal to δ. The direction of the source signal to the array is parameterized by the angle θ, where $\theta = 0^\circ$ corresponds to the endfire direction. In the rest, microphone 1 is chosen as the reference sensor. In this scenario, the signal measured at the mth microphone is

This Research was supported by Qualcomm Research Fund and MAFAAT-Israel Ministry of Defense.

978-1-5090-2007-2/16/$31.00 2016 IEEE

given by

$$y_m(n) = s\left[n - \Delta - f_s\tau_m(\theta)\right] + v_m(n), \quad (1)$$

where Δ is the propagation time from the position of the source $s(t)$ to sensor 1, f_s is the sampling frequency, $\tau_m(\theta) = (m-1)\frac{\delta\cos\theta}{c}$ is the delay between the first and the mth microphone which can be either positive or negative, and $v_m(n)$ is the noise picked up by the mth sensor. We can also express (1) as

$$y_m(n) = \mathbf{g}_m^T(\theta)\mathbf{s}\left(n-\Delta\right) + v_m(n), \quad (2)$$

where the superscript ^{T} is the transpose operator, and $\mathbf{g}_m(\theta)$ is a vector containing causal fractional delay filter coefficients [14] with a maximum value in the location suitable to the delay between the mth sensor and the reference sensor. The length of the vector $\mathbf{g}_m(\theta)$ is $L_g = 2L_{\mathrm{D}} + L_{\mathrm{fd}} + 1$ where L_{fd} is the length of the causal fractional delay filter, and $L_{\mathrm{D}} = \lceil\frac{(M-1)\delta f_s}{c}\rceil$ is the maximal delay between the reference sensor and the extreme sensor. Note also that we introduce non-causality to the vector $\mathbf{g}_m(\theta)$ in order to support the scenario of signals that propagate from directions in which the signal arrives to the sensors before it arrives to the reference sensor. The signal vector $\mathbf{s}\left(n-\Delta\right)$ is a vector containing L_g successive samples of the signal $s\left(n-\Delta\right)$.

By considering L_h successive time samples of the mth microphone signal, (2) becomes a vector of length L_h:

$$\mathbf{y}_m(n) = \mathbf{G}_m(\theta)\mathbf{s}_L\left(n-\Delta\right) + \mathbf{v}_m(n), \quad (3)$$

where $\mathbf{G}_m(\theta)$ is a Sylvester matrix of size $L_h \times L$ created from the vector $\mathbf{g}_m(\theta)$, with $L = L_g + L_h - 1$, the vector $\mathbf{s}_L\left(t-\Delta\right)$ is the signal vector of length L containing the signal samples, and $\mathbf{v}_m(n)$ is a vector of length L_h containing the noise samples.

Now, by concatenating the observations from the M microphones, we get a vector of length ML_h:

$$\begin{aligned}\underline{\mathbf{y}}(n) &= \left[\begin{array}{cccc}\mathbf{y}_1^T(n) & \mathbf{y}_2^T(n) & \cdots & \mathbf{y}_M^T(n)\end{array}\right]^T \\ &= \underline{\mathbf{G}}(\theta)\mathbf{s}_L\left(n-\Delta\right) + \underline{\mathbf{v}}(n), \end{aligned} \quad (4)$$

where

$$\underline{\mathbf{G}}(\theta) = \left[\begin{array}{c}\mathbf{G}_1(\theta)\\ \mathbf{G}_2(\theta)\\ \vdots \\ \mathbf{G}_M(\theta)\end{array}\right] \quad (5)$$

is a matrix of size $ML_h \times L$ and

$$\underline{\mathbf{v}}(n) = \left[\begin{array}{cccc}\mathbf{v}_1^T(n) & \mathbf{v}_2^T(n) & \cdots & \mathbf{v}_M^T(n)\end{array}\right]^T \quad (6)$$

is a vector of length ML_h.

Like in DMAs, we assume that δ is much small with respect to the wavelength of the signal, and the desired signal propagates at the endfire, so that the observations are

$$\underline{\mathbf{y}}(t) = \underline{\mathbf{G}}(0)\mathbf{s}_L\left(t-\Delta\right) + \underline{\mathbf{v}}(t). \quad (7)$$

Then, our objective is to design all kind of broadband DMAs, where the main lobe is at the angle $\theta = 0$, with a real-valued spatiotemporal filter of length ML_h:

$$\underline{\mathbf{h}} = \left[\begin{array}{cccc}\mathbf{h}_1^T & \mathbf{h}_2^T & \cdots & \mathbf{h}_M^T\end{array}\right]^T, \quad (8)$$

where $\mathbf{h}_m,\ m = 1,\ldots,M$ are temporal filters of length L_h.

3. BROADBAND BEAMFORMING

By applying the filter $\underline{\mathbf{h}}$ to the observation vector $\underline{\mathbf{y}}(n)$, we obtain the output of the broadband beamformer:

$$z(n) = \sum_{m=1}^{M}\mathbf{h}_m^T\mathbf{y}_m(n) = \underline{\mathbf{h}}^T\underline{\mathbf{y}}(n) = x_{\mathrm{fd}}(n) + v_{\mathrm{rn}}(n), \quad (9)$$

where

$$\begin{aligned}x_{\mathrm{fd}}(n) &= \sum_{m=1}^{M}\mathbf{h}_m^T\mathbf{G}_m(0)\mathbf{s}_L\left(n-\Delta\right) \\ &= \underline{\mathbf{h}}^T\underline{\mathbf{G}}(0)\mathbf{s}_L\left(n-\Delta\right)\end{aligned} \quad (10)$$

is the filtered desired signal and

$$v_{\mathrm{rn}}(n) = \sum_{m=1}^{M}\mathbf{h}_m^T\mathbf{v}_m(n) = \underline{\mathbf{h}}^T\underline{\mathbf{v}}(n) \quad (11)$$

is the residual noise. We see from (10) that our desired signal is $s\left(n-\Delta\right)$. Therefore, the distortionless constraint is

$$\underline{\mathbf{h}}^T\underline{\mathbf{G}}(0) = \mathbf{i}^T, \quad (12)$$

where $\mathbf{i}$ is a column vector of length L with all its elements equal to zero except for the (L_D+1)th element. This constraint is always required in the design of DMAs.

4. DESIGN OF FIRST-ORDER DMAS

It is well known that the design of a first-order DMA requires at least $M \geq 2$ microphones [5], [6]. For first-order design, we have two constraints to fulfill; the distortionless one given in (12) and a constraint with a null in the direction $\theta_1 \in \left[\frac{\pi}{2}, \pi\right]$, i.e.,

$$\underline{\mathbf{h}}^T\underline{\mathbf{G}}(\theta_1) = \mathbf{0}^T, \quad (13)$$

where $\mathbf{0}$ is a zero vector of length L. Combining these two constraints together, we get the following linear system:

$$\left[\begin{array}{cccc}\mathbf{G}_1^T(0) & \mathbf{G}_2^T(0) & \cdots & \mathbf{G}_M^T(0)\\ \mathbf{G}_1^T(\theta_1) & \mathbf{G}_2^T(\theta_1) & \cdots & \mathbf{G}_M^T(\theta_1)\end{array}\right]\underline{\mathbf{h}} = \underline{\mathbf{i}}_1, \quad (14)$$

or, equivalently,

$$\mathbf{C}_{1,M}(\boldsymbol{\theta})\underline{\mathbf{h}} = \underline{\mathbf{i}}_1, \quad (15)$$

where $\mathbf{C}_{1,M}(\boldsymbol{\theta})$ is a matrix of size $2L \times ML_h$, and

$$\underline{\mathbf{i}}_1 \triangleq \begin{bmatrix} \mathbf{i} \\ \mathbf{0} \end{bmatrix} \tag{16}$$

is a vector of length $2L$. We can solve (15) using the pseudo-inverse of $\mathbf{C}_{1,M}(\boldsymbol{\theta})$:

$$\underline{\mathbf{h}} = \mathbf{P}^{\dagger}_{\mathbf{C}_{1,M}}(\boldsymbol{\theta})\underline{\mathbf{i}}_1, \tag{17}$$

where

$$\mathbf{P}^{\dagger}_{\mathbf{C}_{1,M}}(\boldsymbol{\theta}) = \left[\mathbf{C}^T_{1,M}(\boldsymbol{\theta})\mathbf{C}_{1,M}(\boldsymbol{\theta}) + \lambda\mathbf{I}\right]^{-1}\mathbf{C}^T_{1,M}(\boldsymbol{\theta}) \tag{18}$$

is the pseudo-inverse of the matrix $\mathbf{C}_{1,M}(\boldsymbol{\theta})$ and the scalar λ is a regularization small parameter which provide stable inversion of the matrix. Later, in the simulation section we show that this simple solution yields a frequency-invariant beampattern although no specific constraints were imposed. This is due to the fact that we deal with the DMA model which inherently provide the frequency-invariance property.

5. PERFORMANCE MEASURES

Herein, we establish some measures which we use in the simulation section in order to assess the performance. Assuming microphone 1 to be the reference sensor, the gain in signal-to-noise ratio (SNR) is

$$\mathcal{G}\left(\underline{\mathbf{h}}\right) = \frac{\mathrm{oSNR}\left(\underline{\mathbf{h}}\right)}{\mathrm{iSNR}} = \frac{\underline{\mathbf{h}}^T\underline{\mathbf{G}}(0)\underline{\mathbf{G}}^T(0)\underline{\mathbf{h}}}{\underline{\mathbf{h}}^T\boldsymbol{\Gamma}_{\underline{\mathbf{v}}}\underline{\mathbf{h}}}. \tag{19}$$

where $\boldsymbol{\Gamma}_{\underline{\mathbf{v}}} = \frac{\mathbf{R}_{\underline{\mathbf{v}}}}{\sigma^2_{v_1}}$ is the pseudo-correlation matrix of $\underline{\mathbf{v}}(t)$.

The WNG is obtained by taking $\boldsymbol{\Gamma}_{\underline{\mathbf{v}}} = \mathbf{I}_{ML_h}$, where $\mathbf{I}_{ML_h}$ is the $ML_h \times ML_h$ identity matrix, i.e.,

$$\mathcal{W}\left(\underline{\mathbf{h}}\right) = \frac{\underline{\mathbf{h}}^T\underline{\mathbf{G}}(0)\underline{\mathbf{G}}^T(0)\underline{\mathbf{h}}}{\underline{\mathbf{h}}^H\underline{\mathbf{h}}}. \tag{20}$$

We can also define the broadband beampattern or broadband directivity pattern as

$$\left|\mathcal{B}\left(\underline{\mathbf{h}},\theta\right)\right|^2 = \underline{\mathbf{h}}^T\underline{\mathbf{G}}(\theta)\underline{\mathbf{G}}^T(\theta)\underline{\mathbf{h}}. \tag{21}$$

Finally, we define the DF of the array which is the gain in SNR for the case of spherical diffuse noise. One way to calculate the DF is to use (19) and substitute the time-domain version of $\boldsymbol{\Gamma}_{\underline{\mathbf{v}}}$ for diffuse noise. Yet, an explicit expression for $\boldsymbol{\Gamma}_{\underline{\mathbf{v}}}$ in the time domain is unavailable. Instead, we can use directly the definition of the DF (see for example [15, ch.2]):

$$\mathcal{D}\left(\underline{\mathbf{h}}\right) = \frac{2}{\int_0^{\pi}\left|\mathcal{B}\left(\underline{\mathbf{h}},\theta\right)\right|^2\sin\theta d\theta}, \tag{22}$$

where $\mathcal{B}\left(\underline{\mathbf{h}},\theta\right)$ is defined in (21).

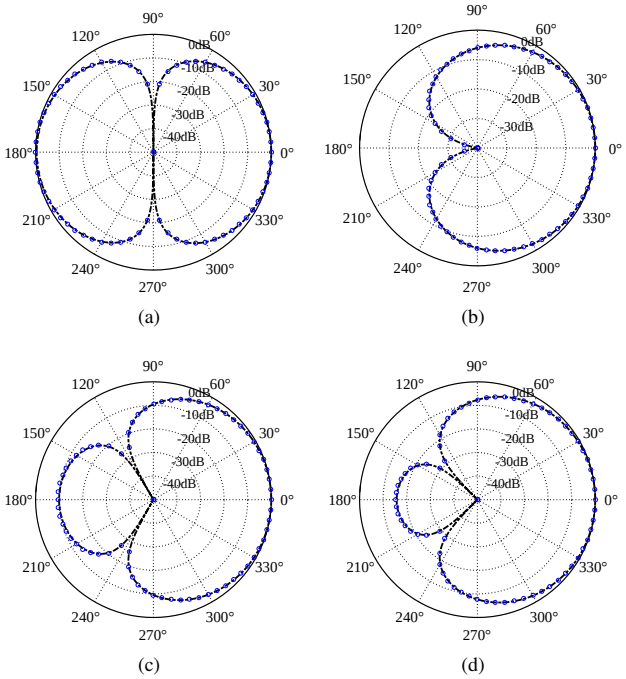

Fig. 1: Beampatterns for the four basic shapes of first-order DMAs produced by the time-domain implementation (dark dashed line): (a) dipole, (b) cardioid, (c) hypercardioid, and (d) supercardioid. The theoretical patterns are also presented (blue circles line).

6. A DESIGN EXAMPLE

In this section, we study the design of first-order standard DMA directivity patterns: dipole, cardioid, hypercardioid, and supercardioid, each with one distinct null in the following directions: $\theta_{\mathrm{Dp}} = \frac{\pi}{2}, \theta_{\mathrm{Cd}} = \pi, \theta_{\mathrm{Hc}} = \frac{2\pi}{3}$, and $\theta_{\mathrm{Sc}} = \frac{3\pi}{4}$. We choose a sensor spacing of $\delta = 1$cm and examine the case of $M = 2$ sensors. We choose $L_{\mathrm{fd}} = 7$ taps and get $L_g = 10$ taps. We choose the filter length $L_h = 12$ taps and the sampling frequency to be $f_{\mathrm{s}} = 8000$ Hz. The regularization parameter is set to be $\lambda = 10^{-3}$.

Figure 1 shows a comparison between the broadband beampattern of the time-domain implementation (21) (dark dashed line), to the theoretical beampattern [5, ch.2] (blue circles line). These patterns were also achieved by the frequency-domain implementation in [5, ch.3]. Comparing both patterns, one can obviously notice the equivalence between the time-domain and frequency-domain implementations.

The obtained filters were tested by simulating a white noise signal impinging towards the DMA and received by the sensors according to the model presented at (3). The received vector was fed into the temporal filters (17). Figure 2 shows

the time-domain waveform (dark blue line) of the signals arrived from the endfire direction, null direction, and arbitrary direction of 88°. It also shows the waveforms of the recovered signals in the output of the DMA (light red line). One can see that the derived filters provide perfect recovery of the desired endfire signal while suppressing the signal coming from the null direction. For signals impinging from an arbitrary direction which the DMA was not designed to suppress at all, the output signal is reasonably suppressed as compared to the input signal.

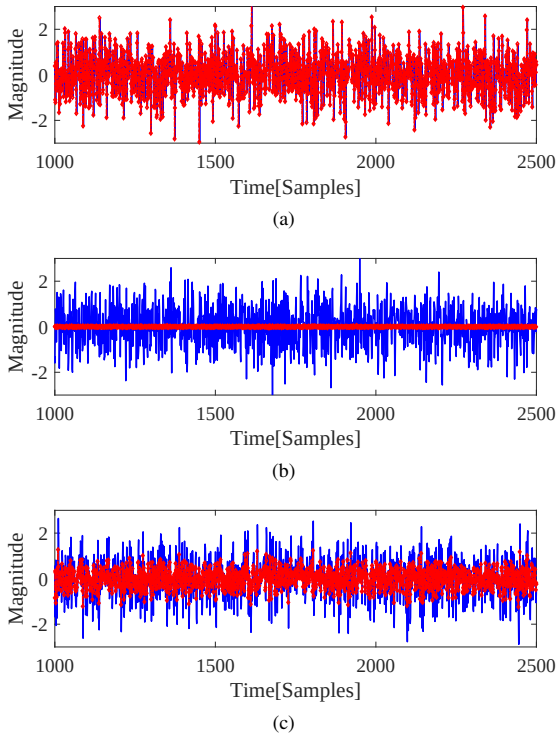

Fig. 2: Time-domain waveforms of the original signals (dark blue line) and output recovered signals (light red line) for the supercardioid: (a) source in the endfire direction, (b) source in the null direction, and (c) source in an arbitrary direction of 88°.

We also plot in Fig. 3 the time-domain WNG and the time-domain DF as a function of the number of sensors, M, for the case of a first-order hypercardioid. One can see that the WNG increases with the number of sensors, while the DF is slightly above the value of 6 dB and does not vary at all. This result is expected since from theoretical point of view, we know that the directivity index is proportional to $(N+1)^2$, where N is the order. In addition, from this figure we can see that one of the effective ways to increase the robustness of the beamformer is to increase the number of sensors.

The results presented in this section show equivalence between time-domain and frequency-domain implementations of DMAs. Moreover, testing the time-domain filters with actual broadband signals confirms that the desired endfire signal is perfectly recovered while undesired signals, even if not arriving from null directions, are significantly suppressed.

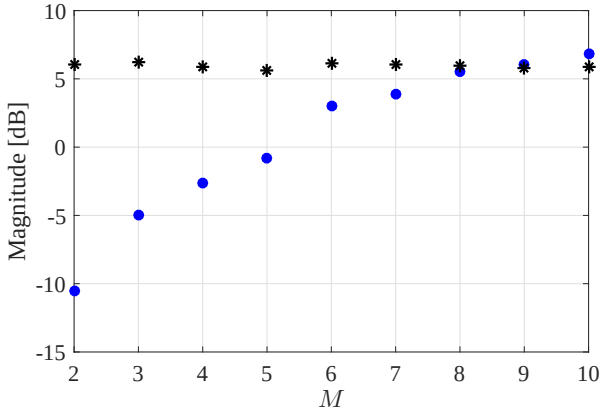

Fig. 3: WNG (circles) and DF (stars) vs. M, for the case of a first-order hypercardioid.

7. CONCLUSIONS

We have presented a framework for time-domain implementation of first-order DMAs, which is desirable in some applications such as real-time communications. Due to the DMA assumption, we get a very simple solution that provides a frequency-invariant beampattern. The quality measures widely used for assessment of beamformers were also defined in the time domain. Simulation results of the proposed implementation demonstrate that it is equivalent to the frequency-domain implementation, while providing more flexibility in the design considerations of practical systems employing DMAs.

8. REFERENCES

[1] H. H. Olson,"Gradient Microphones," *J. Acoust. Soc. Amer.*, vol. 17, pp. 192–198, Jan. 1946.

[2] J. Benesty, J. Chen, and Y. Huang, *Microphone Array Signal Processing*. Berlin, Germany: Springer-Verlag, 2008.

[3] G. W. Elko and J. Meyer, *Microphone arrays*, in Springer Handbook of Speech Processing, J. Benesty, M. M. Sondhi, and Y. Huang, Eds. Berlin, Germany: Springer-Verlag, 2008, Chapter 50, Part I, pp. 1021-1041.

[4] J. Benesty, M. Souden, and Y. Huang, "A perspective on differential microphone arrays in the context of noise

reduction," *IEEE Trans. Audio, Speech, Language Process.*, vol. 20, no. 2, pp. 699-704, Feb. 2012.

[5] J. Benesty and J. Chen, *Study and Design of Differential Microphone Arrays*. Berlin, Germany: Springer-Verlag, 2012.

[6] G. W. Elko, "Superdirectional microphone arrays," in *Acoustic Signal Processing for Telecommunication*, S. L. Gay and J. Benesty, Eds. Boston, MA: Kluwer Academic Publishers, 2000, Chapter 10, pp. 181–237.

[7] G. W. Elko and A. T. N. Pong, "A simple first-order differential microphone,", in *Proc. IEEE Workshop Applicat. Signal Process. Audio Acoust. (WASPAA)*, Oct. 1995, pp. 169-172.

[8] G. W. Elko and A. T. N. Pong, "A steerable and variable firstorder differential microphone array," in *Proc. ICASSP*, 1997, pp.223-226.

[9] R. M. M. Derkx and K. Janse, "Theoretical analysis of a first-order azimuth-steerable superdirective microphone array," *IEEE Trans. Audio, Speech, Lang. Process.*, vol. 17, pp. 150-162, Jan. 2009.

[10] J. Chen and J. Benesty, "A general approach to the design and implementation of linear differential microphone arrays," in *Signal and Information Processing Association Annual Summit and Conference (APSIPA)*, Oct, 2013 Asia-Pacific, pp. 1–7.

[11] L. Zhao, J. Benesty, and J. Chen,"Design of robust differential microphone arrays," *IEEE Trans. Audio, Speech, Language Process.*, vol. 22, no. 10, pp. 1455-1464, Oct. 2014.

[12] R. T. Compton, "The relationship between tapped delayline and FFT processing in adaptive arrays," *IEEE Trans. Antennas and Propagation*, vol. 36, no. 1, pp. 15–26, Jan. 1988

[13] L. C. Godara, "Application of the fast Fourier transform to broadband beamforming," *J. Acoust. Soc. Amer.*, vol. 98, no. 1, pp. 230-240, July 1995.

[14] T. I. Laakso, V. Välimäki, M. Karjalainen and U. K. Laine, "Splitting the unit delay," *IEEE Signal Processing Mag.*, vol. 13, pp. 30–60, Jan. 1996.

[15] H. L. Van-trees, *Detection, Estimation and Modulation Theory, Part IV - Optimum Array Processing*. New York: Wiley Interscience, 2002.

Appendix II:

This appendix contains the following manuscript:

Y. Buchris, I. Cohen, and J. Benesty, "Analysis and design of time-domain first-order circular differential microphone arrays," in Proc. the 22nd International Congress on Acoustics (ICA 2016).

ANALYSIS AND DESIGN OF TIME-DOMAIN FIRST-ORDER CIRCULAR DIFFERENTIAL MICROPHONE ARRAYS

Yaakov Buchris and Israel Cohen

Technion, Israel Institute of Technology
Technion City, Haifa 32000, Israel
{bucris@campus, icohen@ee}.technion.ac.il

Jacob Benesty

INRS-EMT, University of Quebec
800 de la Gauchetiere Ouest, Suite 6900
Montreal, QC H5A 1K6, Canada
benesty@emt.inrs.ca

ABSTRACT

circular differential microphone arrays (CDMAs) are characterized as compact superdirective beamformers whose beampatterns are almost frequency invariant. In contrast to linear differential microphone arrays (LDMAs) where the optimal steering direction is at the endfire, CDMAs provide almost perfect steering for all azimuthal directions. Herein, we present the design of a first-order CDMA in the time domain which is motivated by several aspects. First, time-domain implementation is important in some applications where minimal delay is required, such as real-time communications. Moreover, direct design in the time domain can reduce the computational efforts compared to the frequency-domain design, especially when short filters are sufficient. We present a design example for the time-domain first-order CDMA illustrating some of its fundamental properties as well as the equivalence to the frequency-domain alternative.

Index Terms— Circular differential microphone arrays, time-domain broadband array processing.

1. INTRODUCTION

Differential microphone arrays (DMAs) can be integrated into several real-world beamforming applications involving speech signals, e.g., hands-free telecommunication, mobile phones, and others. DMAs, which is a family of small size-array beamformers and include the well-known superdirective beamformer [1] as a particular case, have beampatterns that are almost frequency invariant, leading to greatly intelligible signals even in heavy reverberant and noisy environments. Due to these benefits, DMAs have attracted a significant amount of interest in the field of broadband microphone array processing during the past decade [2]- [7].

Broadband array processing algorithms can be implemented both in the time and frequency domains. Design in the time domain is important for real-time applications that require small delays [9]. Furthermore, in some cases the implementation of time-domain filters is computationally more efficient than the equivalent frequency-domain filters, especially when short filters are sufficient. The advantage of the frequency-domain implementation is mainly due to the ability to implement some frequency-dependent processing algorithms, like frequency-selective null-steering.

Previous work on DMAs dealt with linear array geometry which is optimal only at the endfire direction. In some applications like teleconferencing and 3D sound recording where the signal of interest may come from any direction, it is necessary for the microphone array to have similar, if not the same response from one direction to another. In this case, circular arrays are often used. Recently, Benesty et al. [8] introduced an innovative approach for the design and implementation of CDMAs. This approach ignores the traditional differential structure of DMAs and develops the fundamental theory and algorithms for broadband frequency-domain CDMAs up to any order from a signal processing perspective. The proposed solution allows perfect steering in the directions of the array sensors. Several examples are presented, showing the equivalence between the traditional design of DMAs and the proposed design.

In this work, we present a framework for a broadband time-domain implementation of first-order CDMAs which enables perfect steering to any azimuthal direction. First, the array input signal is manipulated and represented in a separable form as a product between a desired signal dependent term and a second term which depends only on the array geometry. Then we derive a closed-form solution for time-domain first-order CDMAs. Due to the DMA assumption, the derived solution is very simple with respect to other methods usually employed in the design of general arrays where some constraints that ensure the frequency invariance should be imposed. We also establish the time-domain equivalent of widely used quality measures like the beampattern, the white noise gain (WNG), and the directivity factor (DF). Finally, we evaluate the performance of the time-domain DMAs and compare it with that of the frequency-domain implementation recently proposed by Benesty et al. [3].

The paper is organized as follows. In Section 2, we formulate the signal model. In Section 3, we define a general broadband beamformer and in Section 4, we develop a closed-form solution for the first-order DMA filters. In Section 5, we define some useful performance measures to evaluate time-domain DMAs. In Section 6, we present a design example of the first-order CDMAs along with some simulation results confirming the validity of the developed time-domain solution.

2. SIGNAL MODEL

We consider a broadband source signal, $s\left(n\right)$, in the far-field, where n is the discrete-time index, that propagates in an anechoic acoustic environment at the speed of sound, i.e., $c = 340$ m/s, and impinges on a uniform circular array (UCA) of radius r, consisting of M omnidirectional microphones, where the distance between two

This research was supported by the Israel Science Foundation (grant no. 576/16), Qualcomm Research Fund and MAFAAT-Israel Ministry of Defense.

successive sensors is

$$\delta = 2r \sin\left(\frac{\pi}{M}\right) \approx \frac{2\pi r}{M}. \quad (1)$$

The direction of the source signal to the array is parameterized by the angle θ, where $\theta = 0^\circ$ corresponds to the endfire direction. We assume that the center of the UCA coincides with the origin of the Cartesian coordinate system and serves also as the virtual reference sensor. Assuming a far-field propagation, the time delay between the mth microphone and the center of the array is

$$\tau_m(\theta) = \frac{r}{c}\cos(\theta - \psi_m), \;\; m = 1, 2, ..., M, \quad (2)$$

where

$$\psi_m = \frac{2\pi(m-1)}{M} \quad (3)$$

is the angular position of the mth array element. In this scenario, the signal measured at the mth microphone is given by

$$y_m(n) = s\left[n - \Delta - f_s\tau_m(\theta)\right] + v_m(n), \quad (4)$$

where Δ is the propagation time from the position of the source $s(n)$ to the center of the array, f_s is the sampling frequency, and $v_m(n)$ is the noise picked up by the mth sensor. For the general case where $f_s\tau_m(\theta)$ is not an integer, we may apply the Shannon's sampling theorem [10], which implies that

$$\begin{aligned} y_m(n) &= \sum_{l=-\infty}^{\infty} s\left[n - \Delta - l\right] \mathrm{sinc}\left[l - f_s\tau_m(\theta)\right] + v_m(n) \\ &\approx \sum_{l=-P}^{P+\mu L_h} s\left[n - \Delta - l\right] \mathrm{sinc}\left[l - f_s\tau_m(\theta)\right] + v_m(n), \end{aligned} \quad (5)$$

where $P \gg f_s\tau_m(\theta)$, μ is a fraction, and L_h is the length of the FIR filter to be defined later. Hence, we can also express (4) as

$$y_m(n) = \mathbf{g}_m^T(\theta)\mathbf{s}\left(n - \Delta\right) + v_m(n), \quad (6)$$

where the superscript ^{T} is the transpose operator, the vector $\mathbf{s}\left(n - \Delta\right)$ contains $L = 2P + \mu L_h$ successive samples of the signal $s\left(n - \Delta\right)$, and $\mathbf{g}_m(\theta)$ is a vector containing the coefficients of the interpolation kernel function. By considering L_h successive time samples of the mth microphone signal, (6) becomes a vector of length L_h:

$$\mathbf{y}_m(n) = \mathbf{G}_m(\theta)\mathbf{s}\left(n - \Delta\right) + \mathbf{v}_m(n), \quad (7)$$

where $\mathbf{G}_m(\theta)$ is a Sylvester matrix of size $L_h \times L$ created from the vector $\mathbf{g}_m^T(\theta)$, and $\mathbf{v}_m(n)$ is a vector of length L_h containing the noise samples.

Now, by concatenating the observations from the M microphones, we get a vector of length ML_h:

$$\begin{aligned} \underline{\mathbf{y}}(n) &= \left[\begin{array}{cccc} \mathbf{y}_1^T(n) & \mathbf{y}_2^T(n) & \cdots & \mathbf{y}_M^T(n) \end{array}\right]^T \\ &= \underline{\mathbf{G}}(\theta)\mathbf{s}\left(n - \Delta\right) + \underline{\mathbf{v}}(n), \end{aligned} \quad (8)$$

where

$$\underline{\mathbf{G}}(\theta) = \left[\begin{array}{c} \mathbf{G}_1(\theta) \\ \mathbf{G}_2(\theta) \\ \vdots \\ \mathbf{G}_M(\theta) \end{array}\right] \quad (9)$$

is a matrix of size $ML_h \times L$ and

$$\underline{\mathbf{v}}(n) = \left[\begin{array}{cccc} \mathbf{v}_1^T(n) & \mathbf{v}_2^T(n) & \cdots & \mathbf{v}_M^T(n) \end{array}\right]^T \quad (10)$$

is a vector of length ML_h.

Like in LDMAs, we also assume in CDMAs that δ is small relative to the wavelength. Yet, in contrast to the linear case, herein, we allow the desired signal to arrive from all azimuthal directions and not only from the endfire. We denote the desired signal's direction as θ_d, so that the observations are

$$\underline{\mathbf{y}}(t) = \underline{\mathbf{G}}(\theta_\mathrm{d})\mathbf{s}\left(t - \Delta\right) + \underline{\mathbf{v}}(t). \quad (11)$$

Then, our objective is to design all kind of broadband CDMAs, where the main lobe is at the angle $\theta = \theta_\mathrm{d}$, with a real-valued spatiotemporal filter of length ML_h:

$$\underline{\mathbf{h}} = \left[\begin{array}{cccc} \mathbf{h}_1^T & \mathbf{h}_2^T & \cdots & \mathbf{h}_M^T \end{array}\right]^T, \quad (12)$$

where $\mathbf{h}_m,\ m = 1, \ldots, M$ are temporal filters of length L_h.

3. BROADBAND BEAMFORMING

By applying the filter $\underline{\mathbf{h}}$ to the observation vector $\underline{\mathbf{y}}(n)$, we obtain the output of the broadband beamformer:

$$z(n) = \sum_{m=1}^{M} \mathbf{h}_m^T\mathbf{y}_m(n) = \underline{\mathbf{h}}^T\underline{\mathbf{y}}(n) = x_\mathrm{fd}(n) + v_\mathrm{rn}(n), \quad (13)$$

where

$$\begin{aligned} x_\mathrm{fd}(n) &= \sum_{m=1}^{M} \mathbf{h}_m^T\mathbf{G}_m(\theta_\mathrm{d})\mathbf{s}_L\left(n - \Delta\right) \\ &= \underline{\mathbf{h}}^T\underline{\mathbf{G}}(\theta_\mathrm{d})\mathbf{s}\left(n - \Delta\right) \end{aligned} \quad (14)$$

is the filtered desired signal and

$$v_\mathrm{rn}(n) = \sum_{m=1}^{M} \mathbf{h}_m^T\mathbf{v}_m(n) = \underline{\mathbf{h}}^T\underline{\mathbf{v}}(n) \quad (15)$$

is the residual noise. We see from (14) that the distortionless constraint is

$$\underline{\mathbf{h}}^T\underline{\mathbf{G}}(\theta_\mathrm{d}) = \mathbf{i}^T, \quad (16)$$

where $\mathbf{i}$ is a column vector of length L with all its elements equal to zero except for one element. The decision which element will be non-zero can be made empirically. This constraint is always required in the design of CDMAs.

4. DESIGN OF FIRST-ORDER CDMAS! (CDMAS!)

In order to design first-order CDMAs we need at least $M \geq 3$ (the case of $M = 2$ coincides with the linear case already discussed in [3], [4]). Thus, for first-order CDMAs, we have three constraints to fulfill; the distortionless one given in (16) and two more symmetric constraints with nulls in the directions $\theta_\mathrm{d} + \theta_1$ and $\theta_\mathrm{d} - \theta_1$ where $\theta_1 \in \left[\frac{\pi}{2}, \pi\right]$, i.e.,

$$\underline{\mathbf{h}}^T\underline{\mathbf{G}}(\theta_\mathrm{d} + \theta_1) = \mathbf{0}^T \quad (17)$$

and

$$\underline{\mathbf{h}}^T\underline{\mathbf{G}}(\theta_\mathrm{d} - \theta_1) = \mathbf{0}^T, \quad (18)$$

where $\mathbf{0}$ is a zero vector of length L. Combining all these constraints together, we get the following linear system:

$$\begin{bmatrix} \mathbf{G}_1^T(\theta_\mathrm{d}) & \mathbf{G}_2^T(\theta_\mathrm{d}) & \cdots & \mathbf{G}_M^T(\theta_\mathrm{d}) \\ \mathbf{G}_1^T(\theta_\mathrm{d}+\theta_1) & \mathbf{G}_2^T(\theta_\mathrm{d}+\theta_1) & \cdots & \mathbf{G}_M^T(\theta_\mathrm{d}+\theta_1) \\ \mathbf{G}_1^T(\theta_\mathrm{d}-\theta_1) & \mathbf{G}_2^T(\theta_\mathrm{d}-\theta_1) & \cdots & \mathbf{G}_M^T(\theta_\mathrm{d}-\theta_1) \end{bmatrix} \underline{\mathbf{h}} = \underline{\mathbf{i}}_1, \quad (19)$$

or, equivalently,

$$\mathbf{C}_{1,M}(\boldsymbol{\theta})\underline{\mathbf{h}} = \underline{\mathbf{i}}_1, \quad (20)$$

where $\mathbf{C}_{1,M}(\boldsymbol{\theta})$ is a matrix of size $3L \times ML_h$ and

$$\underline{\mathbf{i}}_1 \triangleq \begin{bmatrix} \mathbf{i} \\ \mathbf{0} \\ \mathbf{0} \end{bmatrix} \quad (21)$$

is a vector of length $3L$. We can solve (20) using the pseudo-inverse of $\mathbf{C}_{1,M}(\boldsymbol{\theta})$:

$$\underline{\mathbf{h}} = \mathbf{P}^\dagger_{\mathbf{C}_{1,M}}(\boldsymbol{\theta})\underline{\mathbf{i}}_1, \quad (22)$$

where

$$\mathbf{P}^\dagger_{\mathbf{C}_{1,M}}(\boldsymbol{\theta}) = \left[\mathbf{C}^T_{1,M}(\boldsymbol{\theta})\mathbf{C}_{1,M}(\boldsymbol{\theta}) + \lambda\mathbf{I}\right]^{-1}\mathbf{C}^T_{1,M}(\boldsymbol{\theta}) \quad (23)$$

is the pseudo-inverse of the matrix $\mathbf{C}_{1,M}(\boldsymbol{\theta})$ and the scalar λ is a regularization parameter. Later, in simulations we show that this simple solution yields a frequency-invariant beampattern although no specific constraints were imposed. This is due to the fact that we deal with the DMA model which inherently provides the frequency-invariance property.

5. PERFORMANCE MEASURES

Herein, we present some useful quality measures which we use in simulations in order to assess the performance. Assuming microphone 1 to be the reference sensor, the gain in signal-to-noise ratio (SNR) is

$$\mathcal{G}(\underline{\mathbf{h}}) = \frac{\mathrm{oSNR}(\underline{\mathbf{h}})}{\mathrm{iSNR}} = \frac{\underline{\mathbf{h}}^T\underline{\mathbf{G}}(\theta_\mathrm{d})\underline{\mathbf{G}}^T(\theta_\mathrm{d})\underline{\mathbf{h}}}{\underline{\mathbf{h}}^T\Gamma_{\underline{\mathbf{v}}}\underline{\mathbf{h}}}, \quad (24)$$

where $\Gamma_{\underline{\mathbf{v}}} = \frac{\mathbf{R}_{\underline{\mathbf{v}}}}{\sigma^2_{v_1}}$ is the pseudo-correlation matrix of $\underline{\mathbf{v}}(t)$.

The WNG is obtained by taking $\Gamma_{\underline{\mathbf{v}}} = \mathbf{I}_{ML_h}$, where $\mathbf{I}_{ML_h}$ is the $ML_h \times ML_h$ identity matrix, i.e.,

$$\mathcal{W}(\underline{\mathbf{h}}) = \frac{\underline{\mathbf{h}}^T\underline{\mathbf{G}}(\theta_\mathrm{d})\underline{\mathbf{G}}^T(\theta_\mathrm{d})\underline{\mathbf{h}}}{\underline{\mathbf{h}}^H\underline{\mathbf{h}}}. \quad (25)$$

We can also define the broadband beampattern or broadband directivity pattern as

$$|\mathcal{B}(\underline{\mathbf{h}}, \theta)|^2 = \underline{\mathbf{h}}^T\underline{\mathbf{G}}(\theta)\underline{\mathbf{G}}^T(\theta)\underline{\mathbf{h}}. \quad (26)$$

Finally, we define the DF of the array which is the gain in SNR for the case of spherical diffuse noise using the direct definition of the DF (see for example [11, ch.2]):

$$\mathcal{D}(\underline{\mathbf{h}}) \approx \frac{2}{\int_{\theta_\mathrm{d}}^{\pi+\theta_\mathrm{d}} |\mathcal{B}(\underline{\mathbf{h}}, \theta)|^2 \sin\theta d\theta}, \quad (27)$$

where $\mathcal{B}(\underline{\mathbf{h}}, \theta)$ is defined in (26). The last definition is a good approximation for small orders of DMAs.

6. A DESIGN EXAMPLE

In this section, we study the design of a first-order hypercardioid circular differential microphone array (CDMA) directivity pattern. For the case of CDMA, the hypercardioid has a distortionless response in the direction θ_d and two more null constraints: the first one is in the direction $\theta_\mathrm{d}+\theta_\mathrm{Hc}$ and the second is in the direction $\theta_\mathrm{d}-\theta_\mathrm{Hc}$, where $\theta_\mathrm{Hc} = \frac{4\pi}{3}$. We choose a sensor spacing of $\delta = 1$cm and examine the case of $M = 3$ sensors. We choose the filter length to be $L_h = 12$ taps and the sampling frequency to be $f_\mathrm{s} = 8000$ Hz. We choose $P = 6$ taps, $\mu = 0.2$, and get $L = 18$ taps. The regularization parameter is set to be $\lambda = 10^{-4}$.

Figure 1 shows the broadband beampattern of the time-domain implementation (26) of a first order hypercardioid for different values of the angle θ_d. These patterns are similar to those obtained with the frequency-domain implementation in [8, ch.3]. One can see that the directivity pattern is identical for each value of the presented steering direction, θ_d. Note also that for the case of $\theta_\mathrm{d} = 120^\circ$, the vectors $\mathbf{h}_i, i = 1, ..., M$ are permutations of the same vectors for the case of $\theta_\mathrm{d} = 0^\circ$. This is because both the angles $\theta_\mathrm{d} = 0^\circ$ and $\theta_\mathrm{d} = 120^\circ$ are the directions of two out of the three array sensors. Therefore, we can exploit this symmetry for scenarios in which only the steering angles of the M sensors' directions are required and calculate the vectors $\mathbf{h}_i, i = 1, ..., M$ only for the endfire direction, then, just permute between filters. This is not the case for the third case of $\theta_\mathrm{d} = 200^\circ$ which is not one of the sensors' directions.

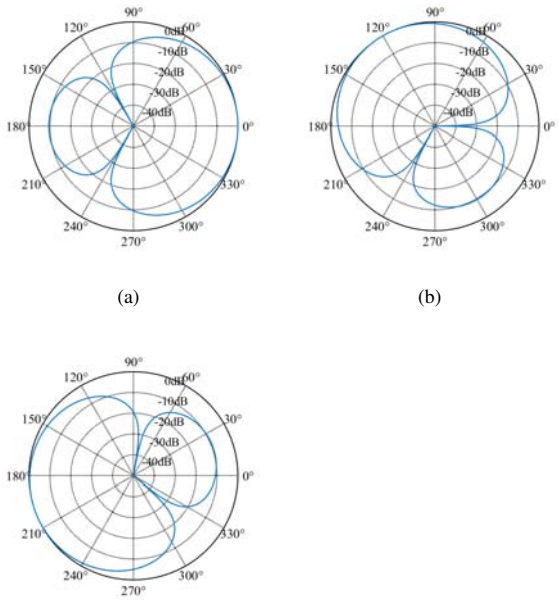

(a) (b)

(c)

Fig. 1: Beampatterns for the time-domain first order hypercardioid CDMA with $M = 3$ sensors in different steering angles: (a) $\theta_\mathrm{d} = 0^\circ$, (b) $\theta_\mathrm{d} = 120^\circ$, and (c) $\theta_\mathrm{d} = 200^\circ$.

We also plot in Fig. 2 the time-domain WNG and the time-domain DF as a function of the number of sensors, M, for the case of a first-order CDMA hypercardioid. One can see that the WNG is increased

with the number of sensors while the DF is slightly above the value of 5 dB and does not vary at all.

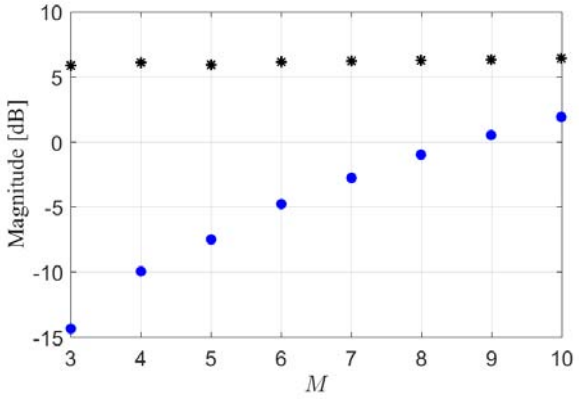

Fig. 2: WNG (circles) and DF (stars) vs. M, for the case of a first-order hypercardioid.

7. CONCLUSIONS

We have presented a framework for time-domain implementation of first-order CDMAs, which is desirable in some applications such as real-time communications. Due to the DMA assumption, we get a very simple solution that provides a frequency-invariant beampattern. The quality measures widely used for assessment of beamformers were also defined in the time domain. Simulation results of the proposed implementation demonstrate that it is equivalent to the frequency-domain implementation, thus providing a large amount of flexibility in the design considerations of practical systems employing CDMAs.

8. REFERENCES

[1] Elko, G. W.; Meyer, J. Microphone arrays, in Springer Handbook of Speech Processing, J. Benesty, M. M. Sondhi, and Y. Huang, Eds. Berlin, Germany: Springer-Verlag, 2008, Chapter 50, Part I, pp. 1021-1041.

[2] Benesty, J.; Souden, M.; Huang, Y. A perspective on differential microphone arrays in the context of noise reduction, IEEE Trans. Audio, Speech, Language Process., vol. 20, no. 2, pp. 699-704, Feb. 2012.

[3] Benesty, J.; Chen, J. Study and Design of Differential Microphone Arrays. Berlin, Germany: Springer-Verlag, 2012.

[4] Elko, G. W. Superdirectional microphone arrays, in Acoustic Signal Processing for Telecommunication, S. L. Gay and J. Benesty, Eds. Boston, MA: Kluwer Academic Publishers, 2000, Chapter 10, pp. 181-237.

[5] Elko, G. W.; Pong, A. T. N. A steerable and variable first-order differential microphone array, in Proc. ICASSP, 1997, pp.223-226.

[6] Chen, J.; Benesty, J. A general approach to the design and implementation of linear differential microphone arrays, in Signal and Information Processing Association Annual Summit and Conference (APSIPA), Oct, 2013, Asia-Pacific, pp. 1-7.

[7] Zhao, L.; Benesty, J.; Chen, J. Design of robust differential microphone arrays, IEEE Trans. Audio, Speech, Language Process., vol. 22, no. 10, pp. 1455-1464, Oct. 2014.

[8] Chen, J.; Benesty, J.; Cohen, I. Design of Circular Differential Microphone Arrays. Berlin, Germany: Springer-Verlag, 2015.

[9] Godara, L. C. Application of the fast Fourier transform to broadband beamforming, J. Acoust. Soc. Amer., vol. 98, no. 1, pp. 230-240, July 1995.

[10] Shannon, C. E. Communications in the presence of noise, Proc. IRE, vol. 37, pp. 1021, 1949.

[11] Van-trees, H. L. Detection, Estimation and Modulation Theory, Part IV - Optimum Array Processing. New York: Wiley Interscience, 2002.

Appendix III:

This appendix contains the following manuscript:

Y. Buchris, I. Cohen, and J. Benesty, "Asymmetric beampatterns with circular differential microphone arrays," in Proc. IEEE Workshop on Applications of Signal Processing to Audio and Acoustics (WASPAA 2017) (pp. 190-194).

ASYMMETRIC BEAMPATTERNS WITH CIRCULAR DIFFERENTIAL MICROPHONE ARRAYS

Yaakov Buchris and Israel Cohen

Technion, Israel Institute of Technology
Technion City, Haifa 32000, Israel
{bucris@campus, icohen@ee}.technion.ac.il

Jacob Benesty

INRS-EMT, University of Quebec
800 de la Gauchetiere Ouest, Suite 6900
Montreal, QC H5A 1K6, Canada
benesty@emt.inrs.ca

ABSTRACT

Circular differential microphone arrays (CDMAs) facilitate compact superdirective beamformers whose beampatterns are nearly frequency invariant, and allow perfect steering for all azimuthal directions. Herein, we eliminate the inherent limitation of symmetric beampatterns associated with a linear geometry, and introduce an analytical asymmetric model for Nth-order CDMAs. We derive the theoretical asymmetric beampattern, and develop the asymmetric supercardioid. In addition, an Nth-order CDMAs design is presented based on the mean-squared-error (MSE) criterion. Experimental results show that the proposed model yields optimal performance in terms of white noise gain, directivity factor, and front-to-back ratio, as well as more flexible nulls design for the interfering signals.

***Index Terms*—** Circular differential microphone arrays, asymmetric beampatterns, broadband beamforming, supercardioid.

1. INTRODUCTION

Differential microphone arrays (DMAs) beamforming constitute a promising solution to some real-world applications involving speech signals, e.g., hands-free telecommunication [1]. DMAs refer to arrays that combine closely spaced sensors to respond to the spatial derivatives of the acoustic pressure field. These small-size arrays yield nearly frequency-invariant beampatterns, and include the superdirective beamformer [2, 3] as a particular case.

The modern concept of DMAs employs pressure microphones, and digital signal processing techniques are used to obtain desired directional response [4–8]. Most of the work on DMAs deals with a linear array geometry, which is preferable in some applications involving small devices. Yet, linear arrays may not have the same response at different directions, and are less suitable for applications like 3D sound recording where signals may come from any direction. In such cases, circular arrays are advantageous [9–13].

Previous works on DMAs, both for linear and circular geometries (e.g., [14, 15]), have considered only the case of symmetric beampatterns, which is an inherent limitation of the linear geometry. Yet, in different array geometries like the circular geometry, asymmetric design may lead to substantial performance improvement.

In this paper, we derive an analytical model for asymmetric circular differential microphone arrays (CDMAs) which includes also the traditional symmetric model as a particular case. It is shown that an asymmetric model achieves higher performances in terms of white noise gain (WNG), directivity factor (DF), and front-to-back-ratio (FBR) due to a more flexible design, which can better take into account the constraints regarding the null directions. We first derive the analytical asymmetric beampattern and then derive an asymmetric version for the supercardioid which is designed to maximize the FBR [4]. Additionally, a mean-squared-error (MSE) solution for an Nth-order CDMA is developed, which enables perfect steering to every azimuthal direction. In the simulations section, we present a third-order asymmetric design and demonstrate its benefits with respect to the symmetric one.

This research was supported by the Israel Science Foundation (grant no. 576/16), Qualcomm Research Fund and MAFAAT-Israel Ministry of Defense.

2. SIGNAL MODEL

We consider an acoustic source signal, $X(\omega)$, that propagates in an anechoic acoustic environment at the speed of sound, i.e., $c \approx 340\ \mathrm{m/s}$, and impinges on a uniform circular array (UCA) of radius r, consisting of M omnidirectional microphones, where the distance between two successive sensors is equal to

$$\delta = 2r \sin\left(\frac{\pi}{M}\right) \approx \frac{2\pi r}{M}. \quad (1)$$

The direction of $X(\omega)$ to the array is denoted by the azimuth angle θ_{s}, measured anti-clockwise from the x axis, i.e., at $\theta = 0^\circ$. Assuming far-field propagation, the time delay between the mth microphone and the center of the array is $\tau_m(\theta_{\mathrm{s}}) = \frac{r}{c}\cos(\theta_{\mathrm{s}} - \psi_m),\ m = 1, 2, ..., M$, where $\psi_m = \frac{2\pi(m-1)}{M}$ is the angular position of the mth array element. The mth microphone signal is

$$Y_m(\omega) = e^{j\varpi\cos(\theta_{\mathrm{s}} - \psi_m)} X(\omega) + V_m(\omega),\ m = 1, 2, ..., M, \quad (2)$$

where $\varpi = \frac{\omega r}{c}$, $j = \sqrt{-1}$, $\omega = 2\pi f$ is the angular frequency, $f > 0$ is the temporal frequency, and $V_m(\omega)$ is the additive noise at the mth microphone. In a vector form, (2) becomes

$$\mathbf{y}(\omega) = [Y_1(\omega)\ \cdots\ Y_M(\omega)]^T = \mathbf{d}\,(\omega, \theta_{\mathrm{s}})\, X(\omega) + \mathbf{v}(\omega), \quad (3)$$

where $\mathbf{d}\,(\omega, \theta_{\mathrm{s}})$ is the steering vector at $\theta = \theta_{\mathrm{s}}$, i.e.,

$$\mathbf{d}\,(\omega, \theta_{\mathrm{s}}) = \left[e^{j\varpi\cos(\theta_{\mathrm{s}} - \psi_1)} \cdots e^{j\varpi\cos(\theta_{\mathrm{s}} - \psi_M)}\right]^T, \quad (4)$$

the superscript ^{T} is the transpose operator, the vector $\mathbf{v}(\omega)$ is defined similarly to $\mathbf{y}(\omega)$, and the acoustic wavelength is $\lambda = c/f$. It is assumed that the element spacing, δ, is much smaller than the wavelength of the incoming signal, i.e, $\delta \ll \lambda$, in order to approximate the differential of the pressure signal.

Assuming a 2D scenario, the frequency-invariant beampattern of an Nth-order DMA is given, for any steering angle $\theta_{\rm s}$, as [4]

$$\mathcal{B}_N(\theta-\theta_{\rm s})=\sum_{n=0}^{N}a_{N,n}\cos^n(\theta-\theta_{\rm s}), \tag{5}$$

where θ is the azimuth, and $\{a_{N,n}\}_{n=0}^{N}$ are real coefficients. The beampattern $\mathcal{B}_N(\theta-\theta_{\rm s})$ is a symmetric function which can properly describe the frequency-invariant beampattern of linear DMAs. Herein, we derive an asymmetric model for Nth-order CDMAs.

3. ASYMMETRIC BEAMPATTERN FOR CDMAs

We start with a simple first-order asymmetric case and then generalize it for any order, N. First-order CDMAs can be designed with at least three microphones, whose positions are $\psi_1=0,\psi_2=\frac{2\pi}{3}$, and $\psi_3=\frac{4\pi}{3}$. Assuming a 2D scenario, the acoustic propagation field received at each sensor is

$$p\left(k,r,\theta,\psi_m\right)=P_0e^{j\varpi\cos(\theta-\psi_m)},\ \ m=1,2,3, \tag{6}$$

where P_0 is the wave amplitude, and $k=\frac{\omega}{c}$ is the wave number. By adding a gain $a_me^{j\omega\tau_m}$ at each sensor, and summing all the sensors, we get the output power:

$$p_{\rm out}\left(k,r,\theta\right)=P_0\sum_{m=1}^{3}a_me^{j\omega\tau_m}e^{j\varpi\cos(\theta-\psi_m)}, \tag{7}$$

where a_m is a real number and τ_m is a temporal delay added to the signal acquired by the mth microphone. Without loss of generality, we assume that $P_0=1$, $a_1=1$, and $\tau_1=0$. Using the approximation $e^x\approx1+x$, and due to the model assumption $\delta\ll\lambda$, (7) becomes

$$\begin{aligned}p_{\rm out}\left(k,r,\theta\right)&\approx1+a_2+a_3\\&\quad+j\omega\sum_{m=1}^{3}a_m\left[\tau_m+\frac{r}{c}\cos(\theta-\psi_m)\right].\end{aligned} \tag{8}$$

In order to simplify (8), we impose $a_2+a_3=-1$, and define

$$\begin{aligned}\alpha_1&=\frac{\sum_{m=1}^{3}a_m\tau_m}{\sum_{m=1}^{3}a_m\left(\tau_m+\frac{r}{c}\cos\psi_m\right)},\\1-\alpha_1&=\frac{\sum_{m=1}^{3}a_m\frac{r}{c}\cos\psi_m}{\sum_{m=1}^{3}a_m\left(\tau_m+\frac{r}{c}\cos\psi_m\right)},\\\beta_1&=\frac{\sum_{m=1}^{3}a_m\frac{r}{c}\sin\psi_m}{\sum_{m=1}^{3}a_m\left(\tau_m+\frac{r}{c}\cos\psi_m\right)}.\end{aligned} \tag{9}$$

Now we can get the normalized response of the first-order asymmetric CDMA:

$$\mathcal{B}_1\left(\theta\right)=\frac{p_{\rm out}\left(k,r,\theta\right)}{p_{\rm out}\left(k,r,0\right)}=\alpha_1+(1-\alpha_1)\cos\theta+\beta_1\sin\theta. \tag{10}$$

The second-order asymmetric CDMA's beampattern can be written as a product of two first-order asymmetric beampatterns terms, i.e.,

$$\mathcal{B}_2\left(\theta\right)=\prod_{i=1}^{2}\left[\alpha_i+(1-\alpha_i)\cos\theta+\beta_i\sin\theta\right], \tag{11}$$

from which, we can easily derive the general form of the second-order asymmetric CDMA:

$$\mathcal{B}_2\left(\theta\right)=\upsilon_0+\upsilon_1\cos\theta+\upsilon_2\cos^2\theta+\upsilon_3\sin\theta\cos\theta+\upsilon_4\sin\theta, \tag{12}$$

where $\{\upsilon_i\}_{i=0}^{4}$ are real coefficients which depend on $\{\alpha_i,\beta_i\}_{i=1}^{2}$. Similarly, the third-order asymmetric beampattern is

$$\begin{aligned}\mathcal{B}_3\left(\theta\right)&=\epsilon_0+\epsilon_1\cos\theta+\epsilon_2\cos^2\theta+\epsilon_3\cos^3\theta\\&\quad+\epsilon_4\sin\theta\cos\theta+\epsilon_5\sin\theta+\epsilon_6\sin^3\theta.\end{aligned} \tag{13}$$

Based on the last results, we can obtain the Nth-order asymmetric CDMAs beampattern with the mainlobe steered to $\theta_{\rm s}$:

$$\begin{aligned}\mathcal{B}_N\left(\theta-\theta_{\rm s}\right)&=\sum_{n=0}^{N}\xi_n\cos^n(\theta-\theta_{\rm s})+\sum_{n=0}^{\lfloor\frac{N-1}{2}\rfloor}\mu_n\sin^{2n+1}(\theta-\theta_{\rm s})\\&\quad+\sum_{n=1}^{\lfloor\frac{N}{2}\rfloor}\zeta_n\cos(\theta-\theta_{\rm s})\sin^{2n-1}(\theta-\theta_{\rm s}),\end{aligned} \tag{14}$$

which is a trigonometric polynomial of power N with $2N$ roots. In fact, (14) can be equivalently expressed as [16]

$$\mathcal{B}_N\left(\theta-\theta_{\rm s}\right)=\sum_{n=0}^{N}a_n\cos\left[n(\theta-\theta_{\rm s})\right]+\sum_{n=1}^{N}b_n\sin\left[n(\theta-\theta_{\rm s})\right]. \tag{15}$$

4. OPTIMAL ASYMMETRIC SUPERCARDIOID

The common directivity patterns in the context of microphone arrays are dipole, cardioid, hypercardioid, and supercardioid. These patterns, originally developed for linear geometry, are traditionally symmetric with respect to the steering angle, $\theta_{\rm s}$.

In this section, we develop an asymmetric version of the supercardioid for CDMAs. The supercardioid pattern maximizes the FBR [4], which is defined for a cylindrical noise field as

$$\mathcal{F}=\frac{\int_{-\pi/2}^{\pi/2}\mathcal{B}_N^2\left(\theta\right)d\theta}{\int_{\pi/2}^{3\pi/2}\mathcal{B}_N^2\left(\theta\right)d\theta}, \tag{16}$$

where we assume, without loss of generality, that the steering angle is $\theta_{\rm s}=0^\circ$. It is easily seen that $\int_{-\pi/2}^{\pi/2}\mathcal{B}_N^2\left(\theta\right)d\theta=\mathbf{c}^T\mathbf{\Gamma}_{\rm f}\mathbf{c}$ and $\int_{\pi/2}^{3\pi/2}\mathcal{B}_N^2\left(\theta\right)d\theta=\mathbf{c}^T\mathbf{\Gamma}_{\rm b}\mathbf{c}$, where

$$\mathbf{c}=\left[a_0,a_1,...,a_N,b_1,...,b_N\right]^T \tag{17}$$

is a vector of length $2N+1$ containing the coefficients of the asymmetric beampattern (15). Matrices $\mathbf{\Gamma}_{\rm f}$ and $\mathbf{\Gamma}_{\rm b}$ are diagonal, with

$$\begin{aligned}\left[\mathbf{\Gamma}_{\rm f}\right]_{n,n}&=\begin{cases}\int_{-\pi/2}^{\pi/2}\cos^2\left(n\theta\right)d\theta, & n=0,1,...,N\\\int_{-\pi/2}^{\pi/2}\sin^2\left[(n-N)\theta\right]d\theta, & n=N+1,...,2N\end{cases}\\\left[\mathbf{\Gamma}_{\rm b}\right]_{n,n}&=\begin{cases}\int_{\pi/2}^{3\pi/2}\cos^2\left(n\theta\right)d\theta, & n=0,1,...,N\\\int_{\pi/2}^{3\pi/2}\sin^2\left[(n-N)\theta\right]d\theta, & n=N+1,...,2N.\end{cases}\end{aligned} \tag{18}$$

The coefficients $\{a_n\}_{n=0}^{N}$ and $\{b_n\}_{n=1}^{N}$ are independent by the diagonality of $\mathbf{\Gamma}_{\rm f}$ and $\mathbf{\Gamma}_{\rm b}$. Thus, the circular geometry provides more degrees of freedom in the design of optimal patterns such as the

supercardioid, and more directional constraints should be imposed. The first one is the distortionless constraint:

$$\mathcal{B}_N\left(\theta_{\mathrm{s}}=0^{\circ}\right)=1, \tag{19}$$

leading to $\sum_{n=0}^{N} a_n = 1$. We can add up to $L \leq 2N$ attenuation constraints of the form:

$$\mathcal{B}_N\left(\theta=\theta_l\right)=g_l, \;\; l=1,2,...,L, \tag{20}$$

where $0 \leq g_l \leq 1$. We formulate these constraints as

$$\mathbf{H}_{\mathrm{c}}\mathbf{c}=\mathbf{g}, \tag{21}$$

where $\mathbf{H}_{\mathrm{c}}$ is the constraint matrix of size $(L+1)\times(2N+1)$, typically non-diagonal. Vector $\mathbf{g}$ of length $L+1$ contains the coefficients $g_l,\ l=1,2,...,L$, and a single unity entry, satisfying (19).

We can now formulate the optimization problem:

$$\max_{\mathbf{c}} \frac{\mathbf{c}^T\mathbf{\Gamma}_{\mathrm{f}}\mathbf{c}}{\mathbf{c}^T\mathbf{\Gamma}_{\mathrm{b}}\mathbf{c}}, \quad \text{subject to } \mathbf{H}_{\mathrm{c}}\mathbf{c}=\mathbf{g}. \tag{22}$$

Rather than solving (22), we solve the equivalent problem:

$$\max_{\hat{\mathbf{c}}} \frac{\hat{\mathbf{c}}^T\hat{\mathbf{\Gamma}}_{\mathrm{f}}\hat{\mathbf{c}}}{\hat{\mathbf{c}}^T\hat{\mathbf{\Gamma}}_{\mathrm{b}}\hat{\mathbf{c}}} \quad \text{subject to } \hat{\mathbf{H}}_{\mathrm{c}}\hat{\mathbf{c}}=\mathbf{0}, \tag{23}$$

where

$$\hat{\mathbf{c}}=\begin{bmatrix}\mathbf{c}\\ -1\end{bmatrix}, \hat{\mathbf{H}}_{\mathrm{c}}=\begin{bmatrix}\mathbf{H}_{\mathrm{c}} & \mathbf{g}\end{bmatrix}, \hat{\mathbf{\Gamma}}_{\mathrm{f}}=\begin{bmatrix}\mathbf{\Gamma}_{\mathrm{f}} & \mathbf{0}\\ \mathbf{0}^T & 0\end{bmatrix}, \hat{\mathbf{\Gamma}}_{\mathrm{b}}=\begin{bmatrix}\mathbf{\Gamma}_{\mathrm{b}} & \mathbf{0}\\ \mathbf{0}^T & 0\end{bmatrix}. \tag{24}$$

Let $\mathbf{D}$ be a null-space matrix of $\hat{\mathbf{H}}_{\mathrm{c}}$ (i.e., $\hat{\mathbf{H}}_{\mathrm{c}}\mathbf{D}=\mathbf{0}$) of size $(2N+2)\times(2N+1-L)$ and rank of $2N+1-L$, which contains $2N+1-L$ basis vectors in its columns, and let $\hat{\mathbf{c}}=\mathbf{D}\tilde{\mathbf{c}}$. Note that the matrices $\mathbf{D}^T\hat{\mathbf{\Gamma}}_{\mathrm{f}}\mathbf{D}$ and $\mathbf{D}^T\hat{\mathbf{\Gamma}}_{\mathrm{b}}\mathbf{D}$ are full-rank even though $\hat{\mathbf{\Gamma}}_{\mathrm{f}}$ and $\hat{\mathbf{\Gamma}}_{\mathrm{b}}$ are not full rank since the product matrices $\mathbf{D}^T\hat{\mathbf{\Gamma}}_{\mathrm{f}}\mathbf{D}$ and $\mathbf{D}^T\hat{\mathbf{\Gamma}}_{\mathrm{b}}\mathbf{D}$ are of size $(2N+1-L)\times(2N+1-L)$ with a rank of $(2N+1-L)$, i.e, full-rank matrices. Thus, we transform (23) to the following unconstrained optimization problem [17]:

$$\max_{\tilde{\mathbf{c}}} \frac{\tilde{\mathbf{c}}^T\mathbf{D}^T\hat{\mathbf{\Gamma}}_{\mathrm{f}}\mathbf{D}\tilde{\mathbf{c}}}{\tilde{\mathbf{c}}^T\mathbf{D}^T\hat{\mathbf{\Gamma}}_{\mathrm{b}}\mathbf{D}\tilde{\mathbf{c}}}. \tag{25}$$

The solution to (25) is the generalized eigenvector of $\mathbf{D}^T\hat{\mathbf{\Gamma}}_{\mathrm{f}}\mathbf{D}$ and $\mathbf{D}^T\hat{\mathbf{\Gamma}}_{\mathrm{b}}\mathbf{D}$ that corresponds to the maximal generalized eigenvalue, i.e.,

$$\mathbf{D}^T\hat{\mathbf{\Gamma}}_{\mathrm{f}}\mathbf{D}\tilde{\mathbf{c}}_{\mathrm{opt}}=\lambda_{\max}\mathbf{D}^T\hat{\mathbf{\Gamma}}_{\mathrm{b}}\mathbf{D}\tilde{\mathbf{c}}_{\mathrm{opt}}, \tag{26}$$

Finally, we reconstruct $\mathbf{c}$ from $\tilde{\mathbf{c}}_{\mathrm{opt}}$.

5. DESIGN FOR ASYMMETRIC CDMAs

We now proceed to design the beamformer. For that, the signal of each microphone is multiplied by a complex gain $H_m(\omega),\ m=1,2,...,M$. Then, all the signals are summed to form the beamformer output. The beampattern is defined as

$$\mathcal{B}\left[\mathbf{h}(\omega),\theta\right]=\mathbf{h}^H(\omega)\mathbf{d}(\omega,\theta), \tag{27}$$

where

$$\mathbf{h}(\omega)=\left[H_1(\omega)\;\; H_2(\omega)\;\; \cdots\;\; H_M(\omega)\right]^T. \tag{28}$$

While (27) is the designed asymmetric beampattern, (15) is the analytical asymmetric beampattern which is considered as the desired beampattern.

Similarly to what have been done in [18], we would like to find a filter $\mathbf{h}(\omega)$, so that $\mathcal{B}\left[\mathbf{h}(\omega),\theta\right]$ is as close as possible to $\mathcal{B}_n\left(\theta\right)$ (15), in the MSE sense. Assuming $\theta_{\mathrm{s}}=0^{\circ}$, we can express (15) as

$$\mathcal{B}_N\left(\theta\right)=\mathbf{t}^T(\theta)\mathbf{a}+\mathbf{s}^T(\theta)\mathbf{b}, \tag{29}$$

where

$$\mathbf{t}(\theta)=\left[1\;\; \cos\theta\;\; \cdots\;\; \cos(N\theta)\right]^T, \tag{30}$$

$$\mathbf{s}(\theta)=\left[0\;\; \sin\theta\;\; \cdots\;\; \sin(N\theta)\right]^T, \tag{31}$$

$$\mathbf{a}=\left[a_0\;\; a_1\;\; \cdots\;\; a_N\right]^T, \tag{32}$$

$$\mathbf{b}=\left[b_0\;\; b_1\;\; \cdots\;\; b_N\right]^T, \tag{33}$$

are vectors of length $N+1$. From now on, it is assumed that θ is a real random variable, which is uniformly distributed in the interval $[0,2\pi]$. We define the MSE criterion between the array beampattern and the desired directivity pattern as

$$\begin{aligned}\mathrm{MSE}\left[\mathbf{h}(\omega)\right] &= E\left\{\left|\mathcal{B}\left[\mathbf{h}(\omega),\theta\right]-\mathcal{B}_N\left(\theta\right)\right|^2\right\}\\ &= \mathbf{h}^H(\omega)\mathbf{\Phi_d}\mathbf{h}(\omega)-\mathbf{h}^H(\omega)\left[\mathbf{\Phi_{dt}}\mathbf{a}+\mathbf{\Phi_{ds}}\mathbf{b}\right]\\ &\quad -\left[\mathbf{a}^T\mathbf{\Phi}_{\mathbf{dt}}^H+\mathbf{b}^T\mathbf{\Phi}_{\mathbf{ds}}^H\right]\mathbf{h}(\omega)+\mathbf{a}^T\mathbf{\Phi_t}\mathbf{a}+\mathbf{b}^T\mathbf{\Phi_s}\mathbf{b}.\end{aligned} \tag{34}$$

where $E\left\{\cdot\right\}$ denotes mathematical expectation with respect to θ, $\mathbf{\Phi_d}=E\left[\mathbf{d}(\omega,\theta)\mathbf{d}^H(\omega,\theta)\right]$, $\mathbf{\Phi_{dt}}=E\left[\mathbf{d}(\omega,\theta)\mathbf{t}^T(\omega,\theta)\right]$, $\mathbf{\Phi_{ds}}=E\left[\mathbf{d}(\omega,\theta)\mathbf{s}^T(\omega,\theta)\right]$, $\mathbf{\Phi_t}=E\left[\mathbf{t}(\omega,\theta)\mathbf{t}^T(\omega,\theta)\right]$, and $\mathbf{\Phi_s}=E\left[\mathbf{s}(\omega,\theta)\mathbf{s}^T(\omega,\theta)\right]$.

To find the optimal filter in the MSE sense, it is important to minimize (34) subject to the distortionless constraint $\mathbf{d}^H\left(\omega,\theta_{\mathrm{s}}\right)\mathbf{h}(\omega)=1$, i.e.,

$$\min_{\mathbf{h}(\omega)} \;\mathrm{MSE}\left[\mathbf{h}(\omega)\right] \quad \text{subject to} \quad \mathbf{d}^H\left(\omega,\theta_{\mathrm{s}}\right)\mathbf{h}(\omega)=1. \tag{35}$$

The optimal solution is given by

$$\mathbf{h}_{\mathrm{opt}}(\omega)=\mathbf{h}_{\mathrm{u}}(\omega)+\frac{\left[1-\mathbf{d}(\omega,\theta_{\mathrm{s}})\mathbf{h}_{\mathrm{u}}\right]\mathbf{\Phi}_{\mathbf{ds}}^{-1}(\omega)\mathbf{d}(\omega,\theta_{\mathrm{s}})}{\mathbf{d}^H(\omega,\theta_{\mathrm{s}})\mathbf{\Phi}_{\mathbf{d}}^{-1}(\omega)\mathbf{d}(\omega,\theta_{\mathrm{s}})} \tag{36}$$

where $\mathbf{h}_{\mathrm{u}}(\omega)=\mathbf{\Phi}_{\mathbf{d}}^{-1}(\omega)\left[\mathbf{\Phi_{dt}}(\omega)\mathbf{b}+\mathbf{\Phi_{ds}}(\omega)\mathbf{a}\right]$ is the unconstrained filter obtained by minimizing $\mathrm{MSE}\left[\mathbf{h}(\omega)\right]$.

6. A DESIGN EXAMPLE

In this section, we present a design example of the third-order asymmetric supercardioid. Third-order designs require at least $M=7$ microphones. Let us assume that the steering angle is $\theta_{\mathrm{s}}=0^{\circ}$ and we would like to impose three nulls at $\theta_1=75^{\circ}$, $\theta_2=105^{\circ}$ and $\theta_3=220^{\circ}$. We choose $r=0.75$ cm which leads to $\delta=0.65$ cm.

First, we need to find the corresponding analytical asymmetric beampattern. Solving (26), the optimal coefficients vector, $\mathbf{c}$ (17) is calculated and substituted into (15). The three additional roots are $\theta_4=150^{\circ}$, $\theta_5=194^{\circ}$, and $\theta_6=260^{\circ}$. Figure 1 shows the analytical beampattern of the third-order asymmetric design (blue solid line), its symmetric version (black dashed line), i.e., the beampattern for the case that $\theta_4=140^{\circ}$, $\theta_5=255^{\circ}$, and $\theta_6=285^{\circ}$, and also the third-order unconstrained symmetric supercardioid (red circles line), which was derived in [4] and obtained for nulls at $\theta_1=98^{\circ}$, $\theta_2=125^{\circ}$ and $\theta_3=161^{\circ}$, and their symmetric directions. The

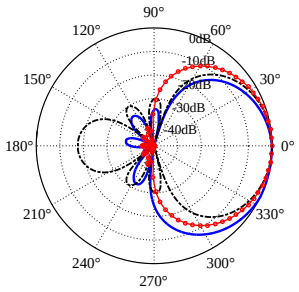

Fig. 1: Beampattern for the third-order asymmetric supercardioid (blue solid line) and its symmetric version (black dashed line). The red circles line is the unconstrained third-order symmetric supercardioid [4]. $\theta_1 = 75^\circ$, $\theta_2 = 105^\circ$, $\theta_3 = 220^\circ$.

latter is obtained by direct optimization of the FBR without any constraints on the null directions.

Using the calculated values of $\mathbf{c}$ (17) and of $\{\theta_i\}_{i=1}^{6}$, we can calculate (36) and design the third-order asymmetric CDMA. Figure 2 shows the beampattern of the third-order asymmetric supercardioid (a),(d), the third-order symmetric supercardioid (b),(e), and the third-order unconstrained symmetric supercardioid (c),(f), for different frequencies and steering angles. The black dashed line is the designed beampattern (27), while the blue circles line is the analytical beampattern (15).

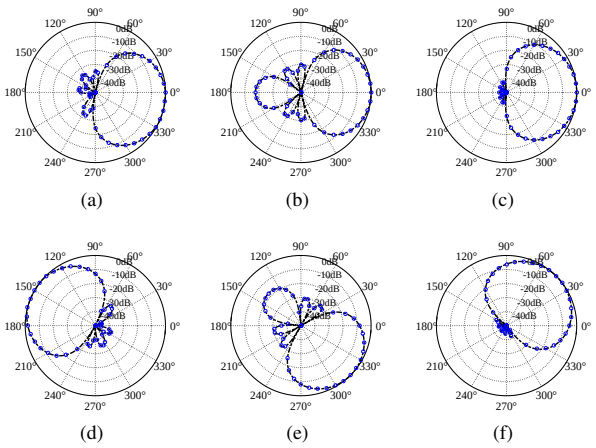

Fig. 2: Beampatterns for the third-order asymmetric supercardioid CDMAs with $M = 7$ sensors and three imposed nulls for different steering angles and frequencies: (a) $\theta_s = 0^\circ$, $f = 1000$ Hz, (d) $\theta_s = 165^\circ$, $f = 1800$ Hz. Beampatterns of the corresponding third-order symmetric design: (b) $\theta_s = 0^\circ$, $f = 200$ Hz, (e) $\theta_s = 315^\circ$, $f = 2200$ Hz . Beampatterns of the third-order unconstrained symmetric supercardioid: (c) $\theta_s = 0^\circ$, $f = 1500$ Hz, (f) $\theta_s = 43^\circ$, $f = 3000$ Hz. The black dashed line is the designed beampattern (27), while the blue circles line is the analytical beampattern (15).

Figure 3 shows the WNG, the DF, and the FBR as a function of frequency for the third-order asymmetric supercardioid (blue solid line), the third-order symmetric supercardioid (black dashed line), and the third-order unconstrained symmetric supercardioid (red circles line). The WNG, the DF, and the FBR are defined as [14, ch.2]

$$\mathcal{W}\left[\mathbf{h}(\omega)\right] = \frac{\left|\mathbf{h}^H(\omega)\mathbf{d}(\omega,\theta_s)\right|^2}{\mathbf{h}^H(\omega)\mathbf{h}(\omega)}, \tag{37}$$

$$\mathcal{D}\left[\mathbf{h}(\omega)\right] = \frac{\left|\mathbf{h}^H(\omega)\mathbf{d}(\omega,\theta_s)\right|^2}{\mathbf{h}^H(\omega)\mathbf{\Gamma}_{\rm dn}(\omega)\mathbf{h}(\omega)}, \tag{38}$$

$$\mathcal{F}\left[\mathbf{h}(\omega)\right] = \frac{\int_{-\pi/2}^{\pi/2}\mathcal{B}^2[\mathbf{h}(\omega),\theta]d\theta}{\int_{\pi/2}^{3\pi/2}\mathcal{B}^2[\mathbf{h}(\omega),\theta]d\theta}, \tag{39}$$

where $\left[\mathbf{\Gamma}_{\rm dn}(\omega)\right]_{ij} = \text{sinc}\left(2\varpi\left|\sin\left[\frac{\pi(i-j)}{M}\right]\right|\right)$.

The performance of the asymmetric design is very similar to that of the unconstrained supercardioid in terms of WNG, DF, and FBR while the symmetric design achieves much lower FBR but slightly higher DF, due to a narrower mainlobe. In [16], we derive also the asymmetric hypercardioid and show that the asymmetric design can achieve superior performance also in terms of DF. In addition, practical methods to improved the WNG, based either on regularization methods or increasing the number of sensors, can be found in [19].

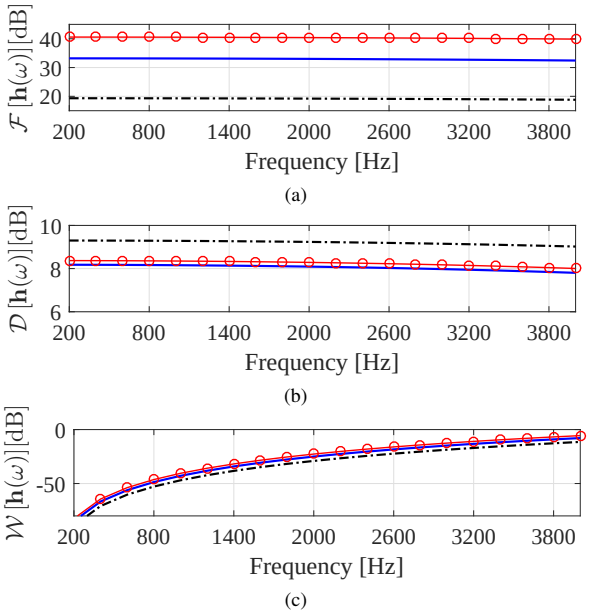

Fig. 3: FBR (a), DF (b), and WNG (c) vs. frequency for the third-order asymmetric supercardioid (blue solid line), the third-order symmetric design (black dashed line), and the third-order unconstrained symmetric supercardioid (red circles line) with $M = 7$ sensors.

7. CONCLUSIONS

We have presented an analytical model for asymmetric CDMAs, which includes the traditional symmetric model as a particular case. We have derived an analytical model for Nth-order asymmetric beampattern, and asymmetric version of the supercardioid. A practical design of an Nth-order asymmetric beamformer for a given number of microphones, based on the MSE criteria, is also proposed. Simulation results show that the asymmetric model allows more degrees of freedom, compared to a symmetric model, which can be exploited for better FBR.

8. REFERENCES

[1] J. Benesty, J. Chen, and Y. Huang, *Microphone Array Signal Processing*. Berlin, Germany: Springer-Verlag, 2008.

[2] H. Cox, R. M. Zeskind, and T. Kooij, "Practical supergain," *IEEE Trans. Acoust., Speech, Signal Processing*, vol. ASSP-34, no. 3, pp. 393–397, June 1986.

[3] M. Crocco and A. Trucco, "Design of robust superdirective arrays with a tunable tradeoff between directivity and frequency-invariance," *IEEE Trans. Signal Process.*, vol. 59, no. 5, pp. 2169–2181, May 2011.

[4] G. W. Elko, "Superdirectional microphone arrays," in *Acoustic Signal Processing for Telecommunication*, S. L. Gay and J. Benesty, Eds. Boston, MA: Kluwer Academic Publishers, 2000, ch. 10, pp. 181–237.

[5] T. D. Abhayapala and A. Gupta, "Higher order differential-integral microphone arrays," *J. Acoust. Soc. Amer.*, vol. 127, pp. 227–233, May 2010.

[6] J. Benesty and J. Chen, *Study and Design of Differential Microphone Arrays*. Berlin, Germany: Springer-Verlag, 2012.

[7] E. De Sena, H. Hacihabibğlu, and Z. Cavetković, "On the design and implementation of higher order differential microphones," *IEEE Trans. Audio, Speech, Language Process.*, vol. 20, no. 1, pp. 162–174, Jan. 2012.

[8] Y. Buchris, I. Cohen, and J. Benesty, "First-order differential microphone arrays from a time-domain broadband perspective," in *International Workshop on Acoustic Echo and Noise Control (IWAENC) 2016 conf.*

[9] H. Teutsch and W. Kellerman, "Acoustic source detection and localization based on wavefield decomposition using circular microphone arrays," *J. Acoust. Soc. Amer.*, vol. 120, no. 5, pp. 2724–2736, Nov. 2006.

[10] P. Ioannides and C. A. Balanis, "Uniform circular and rectangular arrays for adaptive beamforming applications," *IEEE Antennas Wireless Propagat. Lett.*, vol. 4, pp. 351–354, 2005.

[11] Y. L. Ma, Y. Yang, Z. He, K. Yang, C. Sun, and Y. Wang, "Theoretical and practical solutions for high-order superdirectivity of circular sensor arrays," *IEEE Trans. Ind. Electron.*, vol. 60, pp. 203–209, 2013.

[12] H. H. Chen, S. C. Chan, and K. L. Ho, "Adaptive beamforming using frequency invariant uniform concentric circular arrays," *IEEE Trans.Circuits Syst. I, Reg. Papers*, vol. 54, no. 9, pp. 1938–1949, Sept. 2007.

[13] X. Zhang, W. Ser, Z. Zhang, and A. K. Krishna, "Selective frequency invariant uniform circular broadband beamformer," *EURASIP Journal on Advances in Signal Processing*, pp. 1–11, 2010.

[14] J. Benesty, J. Chen, and I. Cohen, *Design of Circular Differential Microphone Arrays*. Berlin, Germany: Springer-Verlag, 2015.

[15] Y. Buchris, I. Cohen, and J. Benesty, "Analysis and design of time-domain first-order circular differential microphone arrays," in *the 22nd International Congress on Acoustics (ICA)*, 2016.

[16] ——, "Frequency-domain design of asymmetric circular differential microphone arrays," *submitted to IEEE/ACM Trans. Audio, Speech, Language Process.*

[17] S. Doclo and M. Moonen, "Design of far-field and near-field broadband beamformers using eigenfilters," *Signal Process.*, vol. 83, pp. 2641–2673, Dec. 2003.

[18] L. Zhao, J. Benesty, and J. Chen, "Optimal design of directivity patterns for endfire linear microphone arrays," in *in Proc. IEEE Int. Conf. Acoust., Speech, Signal Process.*, 2015, pp. 295–299.

[19] J. Benesty, J. Chen, and C. Pan, *Fundamentals of Differential Beamforming*. Springer, 2016.

Appendix IV:

This appendix contains the following manuscript:

Y. Buchris, I. Cohen, and J. Benesty, "Asymmetric Supercardioid Beamforming Using Circular Microphone Arrays," in Proc. 26th European Signal Processing Conference (EUSIPCO 2018) (pp. 627-631).

ASYMMETRIC SUPERCARDIOID BEAMFORMING USING CIRCULAR MICROPHONE ARRAYS

Yaakov Buchris and Israel Cohen

Technion, Israel Institute of Technology
Technion City, Haifa 32000, Israel
{bucris@campus, icohen@ee}.technion.ac.il

Jacob Benesty

INRS-EMT, University of Quebec
800 de la Gauchetiere Ouest, Suite 6900
Montreal, QC H5A 1K6, Canada
benesty@emt.inrs.ca

ABSTRACT

We present a joint-diagonalization based approach for a closed-form solution of the asymmetric supercardioid, implemented with circular differential microphone arrays. These arrays are characterized as compact frequency-invariant superdirective beamformers, allowing perfect steering for all azimuthal directions. Experimental results show that the asymmetric supercardioid yields superior performance in terms of white noise gain, directivity factor, and front-to-back ratio, when additional directional attenuation constraints are imposed in order to suppress interfering signals.

Index Terms— Circular differential microphone arrays (CDMAs), asymmetric beampatterns, supercardioid.

1. INTRODUCTION

In some applications involving broadband speech signals, circular differential microphone arrays (CDMAs) [1, 2] are advantageous due to several desired properties, such as frequency-invariant (FI) directivity pattern, small physical dimensions, superdirectivity [3,4], and perfect steering for all azimuthal directions. Circular geometry in general is beneficial for applications like 3D sound recording where signals may come from any direction [5–8].

Previous works on differential microphone arrays (DMAs), both for linear and circular geometries [9–13], have considered only the case of symmetric beampatterns, which is an inherent limitation of the linear geometry. Yet, in different array geometries like the circular one, asymmetric design may lead to a substantial performance improvement.

Recently we have proposed an analytical model for asymmetric CDMAs which generalizes the traditional symmetric model [14, 15]. It is shown that an asymmetric model, compared to a symmetric one, achieves higher performances in terms of white noise gain (WNG), directivity factor (DF), and front-to-back-ratio (FBR) due to a more flexible design under the constraints of the null directions. Herein, we propose an alternative approach to that in [14, 15], which yields a closed-form solution for the asymmetric FBR-optimal supercardioid directivity pattern, based on the joint-diagonalization approach. The proposed approach is computationally advantageous as it involves the inversion of a small-size matrix while the former solution requires calculation of a null-space matrix and maximization of a Rayleigh-quotient term. In the simulations section, we present a second-order asymmetric supercardioid design and demonstrate its benefits with respect to the symmetric design.

This research was supported by the Israel Science Foundation (grant no. 576/16), the ISF-NSFC joint research program (grant No. 2514/17), and MAFAAT-Israel Ministry of Defense.

2. SIGNAL MODEL

Consider an acoustic source signal, $X(\omega)$, with $\omega = 2\pi f$ denoting the angular frequency, that propagates in an anechoic acoustic environment at the speed of sound, i.e., $c \approx 340\,\mathrm{m/s}$, and impinges on a uniform circular array (UCA) of radius r, consisting of M omnidirectional microphones, where the distance between two successive sensors is equal to

$$\delta = 2r \sin\left(\frac{\pi}{M}\right) \approx \frac{2\pi r}{M}. \tag{1}$$

The direction of $X(\omega)$ to the array is denoted by the azimuth angle θ_{s}, measured anti-clockwise from the x axis, i.e., at $\theta = 0^\circ$.

Assuming the far-field propagation, the time delay between the mth microphone and the center of the array is $\tau_m(\theta_{\mathrm{s}}) = \frac{r}{c}\cos(\theta_{\mathrm{s}} - \psi_m)$, $m = 1, 2, ..., M$, where $\psi_m = \frac{2\pi(m-1)}{M}$ is the angular position of the mth array element. The mth microphone signal is

$$Y_m(\omega) = e^{j\varpi\cos(\theta_{\mathrm{s}}-\psi_m)}X(\omega) + V_m(\omega),\ m = 1, 2, ..., M, \tag{2}$$

where $\varpi = \frac{\omega r}{c}$, $j = \sqrt{-1}$, and $V_m(\omega)$ is the additive noise at the mth microphone. In a vector form, (2) becomes

$$\mathbf{y}(\omega) = [Y_1(\omega)\ \cdots\ Y_M(\omega)]^T = \mathbf{d}\left(\omega, \theta_{\mathrm{s}}\right) X(\omega) + \mathbf{v}(\omega), \tag{3}$$

where $\mathbf{d}(\omega,\theta_{\rm s})$ is the steering vector at $\theta=\theta_{\rm s}$, i.e.,

$$\mathbf{d}(\omega,\theta_{\rm s})=\left[e^{j\varpi\cos(\theta_{\rm s}-\psi_1)}\cdots e^{j\varpi\cos(\theta_{\rm s}-\psi_M)}\right]^T, \quad (4)$$

the superscript ^{T} is the transpose operator, the vector $\mathbf{v}(\omega)$ is defined similarly to $\mathbf{y}(\omega)$, and the acoustic wavelength is $\lambda=c/f$. It is assumed that $\delta\ll\lambda$, in order to approximate the differential of the pressure signal.

Assuming a 2D scenario, the FI beampattern of an Nth-order DMA is given, for any steering angle $\theta_{\rm s}$, as [9, 16]

$$\mathcal{B}_N(\theta-\theta_{\rm s})=\sum_{n=0}^{N}a_{N,n}\cos^n(\theta-\theta_{\rm s}), \quad (5)$$

where θ is the azimuth, and $\{a_{N,n}\}_{n=0}^N$ are real coefficients.

In order to design a practical beamformer, the vector $\mathbf{y}(\omega)$ should be multiplied by a complex vector, $\mathbf{h}(\omega)$, where $\mathbf{h}(\omega)=[H_1(\omega)\ H_2(\omega)\ \cdots\ H_M(\omega)]^T$. The corresponding designed beampattern is

$$\mathcal{B}[\mathbf{h}(\omega),\theta]=\mathbf{h}^H(\omega)\mathbf{d}(\omega,\theta). \quad (6)$$

The vector $\mathbf{h}(\omega)$ can be obtained using the approaches presented in [14, 15], which are aimed to design $\mathcal{B}[\mathbf{h}(\omega),\theta]$ as close as possible to $\mathcal{B}_N(\theta-\theta_{\rm s})$ (in the mean-square error sense).

3. ASYMMETRIC BEAMPATTERN FOR CDMAs

Traditional designs of DMAs focus mainly on linear geometry which inherently dictates a symmetric beampattern. Accordingly, (5) is sufficient for FI beampatterns associated with DMAs. Recently, we extended that design to include also asymmetric beampatterns. Specifically, an Nth-order asymmetric CDMA beampattern with the mainlobe steered to $\theta_{\rm s}$ is [14, 15]

$$\begin{aligned}\mathcal{B}_N(\theta-\theta_{\rm s})=&\sum_{n=0}^{N}\xi_n\cos^n(\theta-\theta_{\rm s})+\sum_{n=0}^{\lfloor\frac{N-1}{2}\rfloor}\mu_n\sin^{2n+1}(\theta-\theta_{\rm s})\\&+\sum_{n=1}^{\lfloor\frac{N}{2}\rfloor}\zeta_n\cos(\theta-\theta_{\rm s})\sin^{2n-1}(\theta-\theta_{\rm s}), \quad (7)\end{aligned}$$

which is a trigonometric polynomial of power N with $2N$ roots, and $\{\xi_0,...,\xi_N,\mu_0,...,\zeta_1,...\}$ are real coefficients. In fact, (7) can be equivalently expressed as

$$\mathcal{B}_N(\theta-\theta_{\rm s})=\sum_{n=0}^{N}a_n\cos\left[n(\theta-\theta_{\rm s})\right]+\sum_{n=1}^{N}b_n\sin\left[n(\theta-\theta_{\rm s})\right]. \quad (8)$$

In the following derivations, we use for convenience (8) instead of (7).

4. OPTIMAL ASYMMETRIC SUPERCARDIOID

The common directivity patterns in the context of microphone arrays are dipole, cardioid, hypercardioid, and supercardioid. These patterns, originally developed for linear geometry, are traditionally symmetric with respect to the steering angle, $\theta_{\rm s}$. In this section, we develop an asymmetric version of the supercardioid for CDMAs based on a joint-diagonalization approach. The supercardioid pattern maximizes the FBR [9], which is defined for a cylindrical noise field as

$$\mathcal{F}=\frac{\int_{-\pi/2}^{\pi/2}\mathcal{B}_N^2(\theta)\,d\theta}{\int_{\pi/2}^{3\pi/2}\mathcal{B}_N^2(\theta)\,d\theta}, \quad (9)$$

where we assume, without loss of generality, that the steering angle is $\theta_{\rm s}=0^\circ$. Let us define the following vector

$$\mathbf{q}(\theta)=[1,\cos(\theta),...,\cos(N\theta),\sin(\theta),...\sin(N\theta)]^T. \quad (10)$$

Then, we can write that $\int_{-\pi/2}^{\pi/2}\mathcal{B}_N^2(\theta)\,d\theta=\mathbf{c}^T\mathbf{\Gamma}_{\rm f}\mathbf{c}$ and $\int_{\pi/2}^{3\pi/2}\mathcal{B}_N^2(\theta)\,d\theta=\mathbf{c}^T\mathbf{\Gamma}_{\rm b}\mathbf{c}$, where

$$\mathbf{c}=[a_0,a_1,...,a_N,b_1,...,b_N]^T \quad (11)$$

is a vector of length $2N+1$ containing the coefficients of the asymmetric beampattern (8). The matrices $\mathbf{\Gamma}_{\rm f}$ and $\mathbf{\Gamma}_{\rm b}$ of size $(2N+1)\times(2N+1)$ are given by

$$\begin{aligned}[\mathbf{\Gamma}_{\rm f}]_{l,k}&=\int_{-\pi/2}^{\pi/2}q_l(\theta)q_k(\theta)d\theta\quad l,k=0,1,...,2N\\[\mathbf{\Gamma}_{\rm b}]_{l,k}&=\int_{\pi/2}^{3\pi/2}q_l(\theta)q_k(\theta)d\theta\quad l,k=0,1,...,2N,\end{aligned} \quad (12)$$

where $q_i(\theta)\triangleq[\mathbf{q}(\theta)]_i$ is the ith element of the vector $\mathbf{q}(\theta)$.

It can be shown that $[\mathbf{\Gamma}_{\rm f}]_{l,k}=0$ and $[\mathbf{\Gamma}_{\rm b}]_{l,k}=0$ for $0\le l\le N$ and $N+1\le k\le 2N$. Also, $[\mathbf{\Gamma}_{\rm f}]_{l,k}=0$ and $[\mathbf{\Gamma}_{\rm b}]_{l,k}=0$ for $N+1\le l\le 2N$ and $0\le k\le N$. Therefore, the coefficients $\{a_n\}_{n=0}^N$ and $\{b_n\}_{n=1}^N$ are independent. Hence, the circular geometry provides more degrees of freedom in the design of optimal patterns such as the supercardioid, and additional directional constraints should be imposed. The first one is the distortionless constraint:

$$\mathcal{B}_N(\theta_{\rm s}=0^\circ)=1, \quad (13)$$

leading to $\sum_{n=0}^N a_n=1$. We can add up to $L\le 2N$ attenuation constraints of the form:

$$\mathcal{B}_N(\theta=\theta_l)=g_l,\ \ l=1,2,...,L, \quad (14)$$

where $0\le g_l\le 1$. We formulate these constraints as

$$\mathbf{H}_{\rm c}\mathbf{c}=\mathbf{g}, \quad (15)$$

where $\mathbf{H}_{\rm c}$ is the constraint matrix of size $(L+1)\times(2N+1)$, typically non-diagonal. Vector $\mathbf{g}$ of length $L+1$ contains the coefficients $g_l,\ l=1,2,...,L$, and a single unity entry, satisfying (13).

Now we can formulate the optimization problem which provides the asymmetric supercardioid beampattern:

$$\max_{\mathbf{c}} \ \frac{\mathbf{c}^T\mathbf{\Gamma}_{\rm f}\mathbf{c}}{\mathbf{c}^T\mathbf{\Gamma}_{\rm b}\mathbf{c}} \quad \text{subject to } \mathbf{H}_{\rm c}\mathbf{c}=\mathbf{g}. \tag{16}$$

In order to solve (16), both $\mathbf{\Gamma}_{\rm f}$ and $\mathbf{\Gamma}_{\rm b}$ can be jointly diagonalized as follows [17]:

$$\mathbf{T}^T\mathbf{\Gamma}_{\rm f}\mathbf{T}=\mathbf{\Lambda}, \tag{17}$$

$$\mathbf{T}^T\mathbf{\Gamma}_{\rm b}\mathbf{T}=\mathbf{I}_{2N+1}, \tag{18}$$

where

$$\mathbf{T}=[\mathbf{t}_1\ \mathbf{t}_2\cdots\ \mathbf{t}_{2N+1}] \tag{19}$$

is a full-rank square matrix of size $(2N+1)\times(2N+1)$, $\mathbf{I}_{2N+1}$ is the identity matrix of size $(2N+1)\times(2N+1)$, and

$$\mathbf{\Lambda}=\text{diag}\left(\lambda_1,\lambda_2,...,\lambda_{2N+1}\right) \tag{20}$$

is a diagonal matrix of size $(2N+1)\times(2N+1)$ containing the eigenvalues of the matrix $\mathbf{\Gamma}_{\rm b}^{-1}\mathbf{\Gamma}_{\rm f}$ in a descending order, i.e., $\lambda_1\geq\lambda_2\geq\lambda_3\geq\cdots\geq\lambda_{2N+1}\geq 0$. The columns of the matrix $\mathbf{T}$ are

$$\mathbf{t}_l=\frac{\mathbf{t}'_l}{\sqrt{\mathbf{t}'^T_l\mathbf{\Gamma}_{\rm b}\mathbf{t}'_l}},\ \ l=1,2,...,2N+1, \tag{21}$$

where $\mathbf{t}'_l$ is the lth eigenvector of the matrix $\mathbf{\Gamma}_{\rm b}^{-1}\mathbf{\Gamma}_{\rm f}$, corresponding to the lth eigenvalue λ_l. We also define the vector:

$$\mathbf{c}'=\mathbf{T}^{-1}\mathbf{c}. \tag{22}$$

Substituting (17), (18) and (22) to (16), we get the equivalent optimization problem:

$$\max_{\mathbf{c}'} \ \frac{\mathbf{c}'^T\mathbf{\Lambda}\mathbf{c}'}{\mathbf{c}'^T\mathbf{c}'} \quad \text{subject to } \mathbf{H}_{\rm c}\mathbf{T}\mathbf{c}'=\mathbf{g}. \tag{23}$$

The solution to the unconstrained version of (23) is known to be $\lambda_{\max}=\lambda_1$, and for that case $\mathbf{c}'_{\rm opt}=[\gamma,0,0,...,0]$ where γ is a constant. Since we have $L+1$ constraints that should be satisfied, the optimal vector $\mathbf{c}'_{\rm opt}$ is of the form:

$$\mathbf{c}'_{\rm opt}=\left[\boldsymbol{\gamma}^T\ \mathbf{0}^T_{2N-L}\right]^T, \tag{24}$$

where $\boldsymbol{\gamma}$ is a vector of length $L+1$ and $\mathbf{0}_{2N-L}$ is a column vector containing $2N-L$ zeros. Taking a vector $\mathbf{c}'_{\rm opt}$ with more than $L+1$ non-zero elements may lead to inferior results as proven in [16] (See Property 2.3.1, pp.45). Therefore, (23) can be reduced to

$$\mathbf{H}_{\rm c}\tilde{\mathbf{T}}\boldsymbol{\gamma}=\mathbf{g}, \tag{25}$$

where

$$\tilde{\mathbf{T}}=[\mathbf{t}_1\ \mathbf{t}_2\cdots\ \mathbf{t}_{L+1}] \tag{26}$$

is a matrix of size $(2N+1)\times(L+1)$ that contains the $L+1$ eigenvectors corresponding to the $L+1$ largest eigenvalues of the matrix $\mathbf{\Gamma}_{\rm b}^{-1}\mathbf{\Gamma}_{\rm f}$. The solution to (25) is

$$\boldsymbol{\gamma}=\left(\mathbf{H}_{\rm c}\tilde{\mathbf{T}}\right)^{-1}\mathbf{g}. \tag{27}$$

Substituting (22) and (24) into (27), we have

$$\mathbf{c}_{\rm opt}=\tilde{\mathbf{T}}\left(\mathbf{H}_{\rm c}\tilde{\mathbf{T}}\right)^{-1}\mathbf{g}. \tag{28}$$

5. A DESIGN EXAMPLE

In this section, we present a design example of the second-order asymmetric supercardioid. Second-order designs require at least $M=5$ microphones. Let us assume that the steering angle is $\theta_{\rm s}=0^\circ$ and we would like to impose two nulls at $\theta_1=90^\circ$ and $\theta_2=245^\circ$. We choose $r=0.75$ cm which leads to $\delta=0.88$ cm.

First, we need to find the corresponding analytical asymmetric beampattern. Solving (28), the optimal coefficients vector, $\mathbf{c}$ (11), is calculated and substituted into (8). The two additional roots are $\theta_3=133^\circ$, and $\theta_4=190^\circ$. Figure 1(a) shows the analytical beampattern of the second-order asymmetric design (blue solid line), its symmetric version (black dashed line), i.e., the beampattern for the case that $\theta_3=115^\circ$, and $\theta_4=270^\circ$, and also the second-order unconstrained symmetric supercardioid (red circles line), which was derived in [9] and obtained for nulls at $\theta_1=106^\circ$, and $\theta_2=153^\circ$. The latter is obtained by a direct optimization of the FBR without any constraints on the null directions. Figure 1(b) shows a second example where two directional constraints $\theta_1=115^\circ$ and $\theta_2=230^\circ$ were imposed. Table 1 summarizes the FBR values obtained by the three compared approaches for both examples. One can see that compared to the symmetric approach, the asymmetric design is significantly less sensitive than the symmetric design to the values of θ_1 and θ_2. Furthermore, the asymmetric design achieves higher FBR values, which are closer to those values obtained by the unconstrained approach.

Table 1: Front-to-Back-Ratio, $\mathcal{F}$[dB], Achieved by Each of the Designs of a Second-Order Supercardioid for Two Different Choices of Constraints.

	$\theta_1=90^\circ$ $\theta_2=245^\circ$	$\theta_1=115^\circ$ $\theta_2=230^\circ$
Asymmetric	22.97	24.23
Symmetric	9.44	22.30
Unconstrained symmetric	26.31	26.31

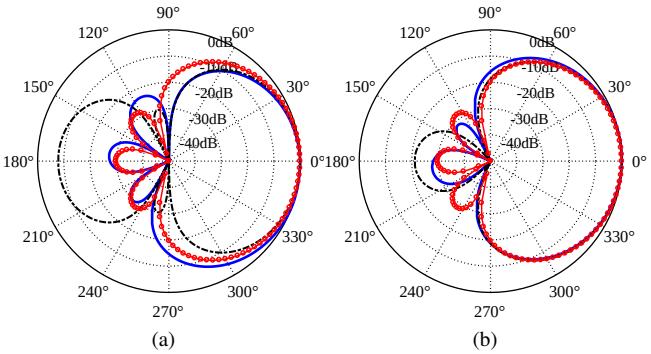

(a) (b)

Fig. 1: Beampatterns for the second-order asymmetric supercardioid (blue solid line) and its symmetric version (black dashed line). The red circles line is the unconstrained second-order symmetric supercardioid [9]. (a) $\theta_1 = 90°$, $\theta_2 = 245°$. (b) $\theta_1 = 115°$, $\theta_2 = 230°$.

Using the calculated values of $\mathbf{c}$ (11) and of $\{\theta_i\}_{i=1}^4$, we can calculate $\mathbf{h}(\omega)$ using one of the methods presented in our previous work [14,15] and design the second-order asymmetric supercardioid. In the following, we consider only the first example, i.e., the one with the parameters $\theta_1 = 90°$ and $\theta_2 = 245°$.

Figure 2 shows the WNG, the DF, and the FBR[1] as a function of frequency for the second-order asymmetric supercardioid (blue solid line), the second-order symmetric supercardioid (black dashed line), and the second-order unconstrained symmetric supercardioid (red circles line). These performance measures are defined as [16]

$$\mathcal{W}\left[\mathbf{h}(\omega)\right] = \frac{\left|\mathbf{h}^H\left(\omega\right)\mathbf{d}\left(\omega,\theta_{\mathrm{s}}\right)\right|^2}{\mathbf{h}^H\left(\omega\right)\mathbf{h}\left(\omega\right)}, \tag{29}$$

$$\mathcal{D}\left[\mathbf{h}(\omega)\right] = \frac{\left|\mathbf{h}^H\left(\omega\right)\mathbf{d}\left(\omega,\theta_{\mathrm{s}}\right)\right|^2}{\mathbf{h}^H\left(\omega\right)\mathbf{\Gamma}_{\mathrm{dn}}\left(\omega\right)\mathbf{h}\left(\omega\right)}, \tag{30}$$

$$\mathcal{F}\left[\mathbf{h}(\omega)\right] = \frac{\int_{-\pi/2}^{\pi/2}\mathcal{B}^2\left[\mathbf{h}(\omega),\theta\right]d\theta}{\int_{\pi/2}^{3\pi/2}\mathcal{B}^2\left[\mathbf{h}(\omega),\theta\right]d\theta}, \tag{31}$$

where

$$\left[\mathbf{\Gamma}_{\mathrm{dn}}\left(\omega\right)\right]_{ij} = \mathrm{sinc}\left(\frac{2\omega r}{c}\left|\sin\left[\frac{\pi\left(i-j\right)}{M}\right]\right|\right). \tag{32}$$

The performance of the asymmetric design is very similar to that of the unconstrained supercardioid in terms of WNG, DF, and FBR while the symmetric design achieves much lower FBR and similar DF. In [14], we derive also the asymmetric hypercardioid and show that the asymmetric

[1] for a cylindrical noise field

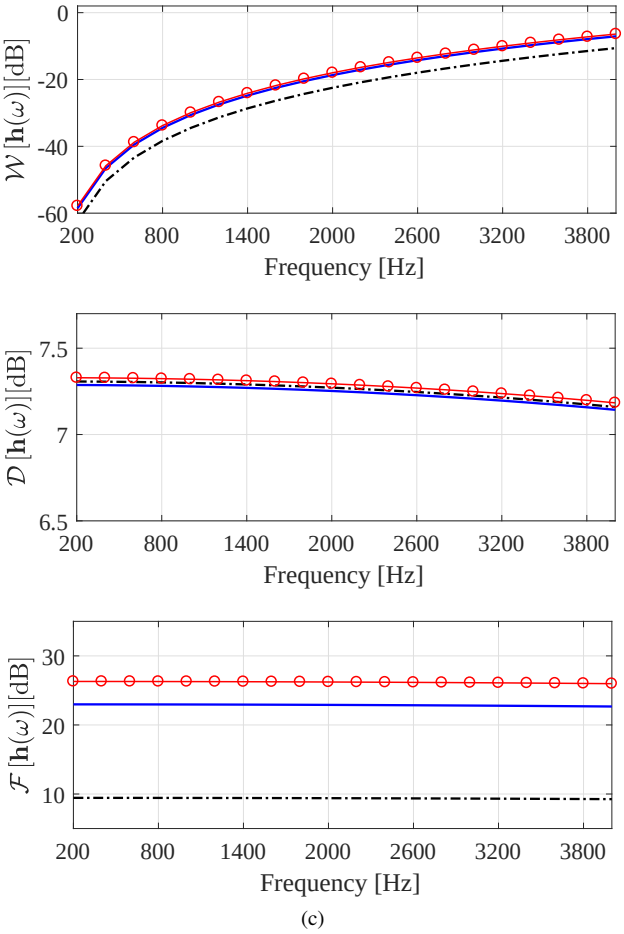

(c)

Fig. 2: WNG (a), DF (b), and FBR (c) vs. frequency for the second-order asymmetric supercardioid (blue solid line), the second-order symmetric design (black dashed line), and the second-order unconstrained symmetric supercardioid (red circles line) with $M = 5$ sensors. $\theta_1 = 90°$, $\theta_2 = 245°$.

design can achieve superior performance also in terms of DF. In addition, practical methods to improved the WNG, based either on regularization methods or increasing the number of sensors, can be found in [18] and are not included here as we would like to concentrate on the comparison between symmetric and asymmetric designs.

6. CONCLUSIONS

We have presented an alternative solution to an asymmetric supercardioid, which is based on the joint-diagonalization approach. The proposed solution is computationally more efficient than an existing alternative solution. Simulation results demonstrate that the asymmetric model yields a more flexible design and superior performance in several real-world applications involving beamforming for speech signals such as teleconferencing, hand-free communications, and more.

7. REFERENCES

[1] J. Benesty, J. Chen, and I. Cohen, *Design of Circular Differential Microphone Arrays*. Berlin, Germany: Springer-Verlag, 2015.

[2] Y. Buchris, I. Cohen, and J. Benesty, "Analysis and design of time-domain first-order circular differential microphone arrays," in *the 22nd International Congress on Acoustics (ICA)*, 2016.

[3] H. Cox, R. M. Zeskind, and T. Kooij, "Practical supergain," *IEEE Trans. Acoust., Speech, Signal Processing*, vol. ASSP-34, no. 3, pp. 393–397, June 1986.

[4] M. Crocco and A. Trucco, "Design of robust superdirective arrays with a tunable tradeoff between directivity and frequency-invariance," *IEEE Trans. Signal Process.*, vol. 59, no. 5, pp. 2169–2181, May 2011.

[5] H. Teutsch and W. Kellerman, "Acoustic source detection and localization based on wavefield decomposition using circular microphone arrays," *J. Acoust. Soc. Amer.*, vol. 120, no. 5, pp. 2724–2736, Nov. 2006.

[6] P. Ioannides and C. A. Balanis, "Uniform circular and rectangular arrays for adaptive beamforming applications," *IEEE Antennas Wireless Propagat. Lett.*, vol. 4, pp. 351–354, 2005.

[7] Y. L. Ma, Y. Yang, Z. He, K. Yang, C. Sun, and Y. Wang, "Theoretical and practical solutions for high-order superdirectivity of circular sensor arrays," *IEEE Trans. Ind. Electron.*, vol. 60, pp. 203–209, 2013.

[8] H. H. Chen, S. C. Chan, and K. L. Ho, "Adaptive beamforming using frequency invariant uniform concentric circular arrays," *IEEE Trans.Circuits Syst. I, Reg. Papers*, vol. 54, no. 9, pp. 1938–1949, Sept. 2007.

[9] G. W. Elko, "Superdirectional microphone arrays," in *Acoustic Signal Processing for Telecommunication*, S. L. Gay and J. Benesty, Eds. Boston, MA: Kluwer Academic Publishers, 2000, ch. 10, pp. 181–237.

[10] T. D. Abhayapala and A. Gupta, "Higher order differential-integral microphone arrays," *J. Acoust. Soc. Amer.*, vol. 127, pp. 227–233, May 2010.

[11] J. Benesty and J. Chen, *Study and Design of Differential Microphone Arrays*. Berlin, Germany: Springer-Verlag, 2012.

[12] E. De Sena, H. Hacihabibğlu, and Z. Cavetković, "On the design and implementation of higher order differential microphones," *IEEE Trans. Audio, Speech, Language Process.*, vol. 20, no. 1, pp. 162–174, Jan. 2012.

[13] Y. Buchris, I. Cohen, and J. Benesty, "First-order differential microphone arrays from a time-domain broadband perspective," in *International Workshop on Acoustic Echo and Noise Control (IWAENC) 2016 conf.*

[14] ——, "Frequency-domain design of asymmetric circular differential microphone arrays," *IEEE/ACM Transactions on Audio, Speech, and Language Processing*, 2018.

[15] ——, "Asymmetric beampatterns with circular differential microphone arrays," in *IEEE Workshop on Applications of Signal Processing to Audio and Acoustics (WASPAA)*, 2017.

[16] J. Benesty, I. Cohen, and J. Chen, *Fundamentals of Signal Enhancement and Array Signal Processing*. Wiley-IEEE Press, 2017.

[17] J. N. Franklin, *Matrix Theory*. Englewood Cliffs, NJ: Prentice-Hall, 1968.

[18] J. Benesty, J. Chen, and C. Pan, *Fundamentals of Differential Beamforming*. Springer, 2016.

שיטות תכן של מערכי מיקרופונים דיפרנציאליים רובוסטיים ודלילים

יעקב בוכריס

שיטות תכן של מערכי מיקרופונים דיפרנציאליים רובוסטיים ודלילים

חיבור על מחקר
לשם מילוי חלקי של הדרישות לקבלת התואר
דוקטור לפילוסופיה

יעקב בוכריס

הוגש לסנט הטכניון – מכון טכנולוגי לישראל

מר-חשוון תש"פ חיהפ נובמבר 2019

תודות

המחקר נעשה בהנחייתו של פרופסור ישראל כהן מהפקולטה להנדסת חשמל. פרופסור ג'ייקוב בניסטי ודוקטור אלון עמר היו אף הם מעורבים במחקר ותרמו רבות להצלחתו.

אני רוצה להודות למנחים שלי, פרופסור ישראל כהן, פרופסור ג'ייקוב בניסטי, ודוקטור אלון עמר, על שליוו אותי במהלך לימודיי לאורך התואר. תודה על ההדרכה ,ההכוונה ,על העצה טובה והעידוד .הייתם חלק משמעותי מאוד במסע שלי של לימודי הדוקטורט ואני מעריך מאוד שעזרתם לי לצלוח אותו .הענקתם לי כלים רבים וחשובים שעיצבו אותי וישמשו אותי רבות בהמשך דרכי.

אני רוצה להודות לצוות המעבדה לעיבוד אותות ותמונות בטכניון (SIPL), פרופסור דוד מלאך, מר נמרוד פלג, מר יאיר משה, ודוקטור אבי רוזן, על העזרה והתמיכה, העידוד והחברות לאורך כל הדרך.

לבסוף, תודה לך אורית ,אשתי המדהימה על היותך החצי השני שלי ועל תמיכתך הבלתי פוסקת במסע הארוך הזה. לך ולילדים המדהימים שלנו, תאיר, אליה-אבידן, אריאל, עמיחי, ואיתן, יש חלק לא מבוטל בהצלחה של העבודה הזו.
אתם האהובים שלי שהופכים אותי למי שאני.

אני מודה לטכניון ,לקרן הלאומית למדע(מענקים מס' 576/16) ולקרן הלאומית למדע (מענק מס' 2517/17) על התמיכה הכספית הנדיבה בהשתלמותי.

תקציר

מחקר זה עוסק בגישות תכן מתקדמות למערכי מיקרופונים דיפרנציאליים דלילים ורובוסטיים אשר יכולים להשתלב במגוון מערכות אקוסטיות בחזית הטכנולוגיה כגון: התקני שירות מבוסס דיבור (כדוגמת Amazon Alexa Device), התקני אודיו-וידאו לשיחות ועידה (video conference), כלים אוטונומיים תת מימיים (AUVs), רחפנים, ועוד. על מנת לקלוט את האות הרצוי באיכות טובה ולסנן אותות מפריעים ורעשים, מקובל להשתמש במערכי מיקרופונים ובשיטות של עיצוב אלומה רחב סרט. עם זאת, אחד האילוצים המשמעותיים במערכות אלו הינו הדרישה למערכים בעלי גודל פיסי קטן יחסית עקב מגבלות מקום ומשאבי חישוב וזיכרון. נדרש בנוסף שתגובת האלומה תהיה בקירוב קבועה בתדר, וזאת על מנת שלא ייכנסו עיוותים לאות כתוצאה מפעילות הסינון המרחבי. מתוך מגוון קונספטים למימוש עיצוב אלומה רחב סרט, מערכי מיקרופונים דיפרנציאליים (DMAs) הינם מערכים המאפשרים לקבל כיווניות גבוהה למרות הגודל הפיסי הקטן שלהם, ובנוסף, תגובת האלומה שלהם היא בקירוב קבועה בתדר. אחד המאפיינים של מערכים אלו הינו סדר המערך אשר מצביע על כמות החוסמים הכיווניים שניתן לממש בתגובת האלומה של המערך. למרות התכונות הרצויות שלהם, למערכי DMAs יש הגבר רעש משמעותי במוצא המערך, במיוחד בתדרים נמוכים. המשמעות המעשית של החיסרון הזה הינה רגישות גבוהה לשגיאות מודל ולאי וודאויות של הפרמטרים.

מחקר זה מתמקד בפיתוח גישות תכן מתקדמות למערכי DMAs המשיגים ביצועים טובים יותר בהשוואה לגישות קודמות, במונחים של הגבר מערך, כיווניות, סיבוכיות חישוב ותכונות נוספות רצויות. המחקר מורכב מארבעה חלקים עיקריים שיפורטו להלן.

הנושא הראשון שבו עוסק המחקר הוא תכן בתחום הזמן של מערכי DMAs, שהוא בעל חשיבות גבוהה עבור אפליקציות שבהן נדרשת השהייה קטנה ככל האפשר, כגון מערכות תקשורת אודיו בזמן אמת. יתר על כן, תכן בתחום הזמן עשוי להוריד את העומס החישובי לעומת תכן בתחום התדר, במיוחד כאשר מסננים בעלי מספר מקדמים קטן מספיקים לעמידה בביצועים הנדרשים. במסגרת עבודה זו, פיתחנו ביטוי אנליטי כללי לאות הנקלט במערך בתחום הזמן, עבור כל סדר DMA ומספר מיקרופונים. לביטוי שפותח יש מבנה ספרבילי, כלומר האות הינו מכפלה בין חלק שתלוי בגיאומטריה של הבעיה בלבד,

ובין חלק שתלוי במאפיינים של המקורות הנקלטים בלבד. התבנית שהתקבלה דומה לתבנית המתקבלת עבור מודל בתחום התדר, ולכן ניתן להשתמש באלגוריתמי עיצוב אלומה מגוונים שתוכננו לתחום התדר, ישירות גם בתחום הזמן עבור הייצוג המוצע. בנוסף פיתחנו פתרון אנליטי רובוסטי לווקטור המשקלים של מעצב האלומה בתחום הזמן, וגם הצגנו את מדדי הביצועים בתחום הזמן. תוצאות הסימולציה וההשוואה בין המודל בתחום התדר למודל המוצע בתחום הזמן מראים כי שני המודלים שקולים ומניבים ביצועים דומים. כמו כן, הראנו אנליטית כיצד המודל בתחום הזמן מתכנס תחת תנאים מתאימים למודל ה – DMAs הקלאסי.

בחלקו השני של המחקר הרחבנו את המודל הסימטרי הקלאסי של DMAs למודל אסימטרי עבור מערכי DMAs מעגליים. המודל המסורתי של DMAs התמקד בעיקר במערכים ליניאריים שעבורם תגובת האלומה הינה סימטרית ביחס לציר המערך. התכונה הזו גורמת למספר דרגות חופש מצומצם יחסית בקביעת כיווני החסימה של המערך. לעומת זאת, כאשר עוסקים בגיאומטריות אחרות כדוגמת הגיאומטריה המעגלית, ניתן להיפטר מהאילוץ הסימטרי ולאפשר תגובת אלומה כללית יותר וכתוצאה מכך יותר דרגות חופש בתכן התגובה. במסגרת העבודה הרחבנו את המודל הקלאסי של תגובת האלומה הסימטרית הקבועה בתדר של DMAs למודל רחב יותר המאפשר לתכנן מערכי DMAs מעגליים עם תגובת אלומה לא סימטרית, ואשר מכליל את המקרה הפרטי של תגובה סימטרית. על בסיס ההרחבה הזו, פיתחנו גרסה אסימטרית לשתי פתרונות נפוצים בספרות של תגובות אלומה. הראשון - הרחבה אסימטרית ל - hypercardioid אשר ידוע כממקסם את הכיווניות של המערך, והשני - הרחבה ל- supercardioid אשר ממקסם את היחס בין הספק המגיע אל חזית המערך להספק המגיע מהכיוון האחורי של המערך. תוצאות הסימולציה וההשוואה בין המודל האסימטרי למודל הקלאסי הראו שיפור ניכר בביצועים בהיבטים של הגבר מערך, שיפור בחסינות לשגיאות מודל ולרעש וגמישות גדולה יותר בקביעת מיקום כיווני החסימה של המערך.

החלק השלישי של המחקר עוסק בתכן מערכי DMAs דלילים, אשר במסגרתו מביאים לאופטימום גם את הגברי הסנסורים וגם את מיקומם ומספרם. במערכים דלילים, הסנסורים מרוחקים באופן לא אחיד זה מזה כך שחלקם נמצאים במרחק גדול ממחצית אורך הגל ולכן לא מקיימים את חוק הדגימה המרחבית, אולם חלקם קרובים מספיק בשביל למנוע אפקט של קיפולים מרחביים. כתוצאה מכך, מתקבלים מערכים רובוסטיים עם גודל פיסי

גדול יותר, ועם מספר כולל של סנסורים קטן יותר לעומת התכן הסטנדרטי האחיד. יתר על כן, כאשר מדובר על תכן רחב סרט, ובפרט על תכן רחב סרט עם תגובת אלומה קבועה בתדר, השימוש בכלים דלילים יאפשר גמישות גדולה יותר בהשגת תגובה קבועה בתדר. בספרות קיימות מגוון עבודות קודמות לתכן מערכים דלילים, אולם מרביתן טיפלו במקרה הצר סרט בעוד שכמעט ואין עבודות למקרה הרחב סרט. אחת העבודות הקודמות שעסקו בתכן דליל רחב סרט עשו שימוש בשיטות של אופטימיזציה קונווקסית מרובת אילוצים עקב העובדה שהתכן הוא עבור מערכת רחבת סרט. יחד עם זאת, השיטה הזו לא ישימה למקרים שבהם מדובר על מערכים עם כמות גדולה של סנסורים.

במסגרת המחקר פיתחנו גישת תכן למערכים דלילים רחבי סרט שבה בעיית האופטימיזציה מחושבת עבור כל תדר בנפרד. לאחר מכן מבוצע היתוך של התוצאות תוך שימוש בכלי ניתוח מידע מתקדמים כדוגמת כלים להורדת מימד ואלגוריתמי אשכול, כך שמתקבלת גיאומטריה דלילה אשר משותפת לכל התדרים. לתכונה האחרונה חשיבות רבה היות וניתן להשתמש בסט בודד של סנסורים עבור כל רוחב הסרט הרלוונטי. העובדה שהאופטימיזציה מבוצעת על כל תדר בנפרד מאפשרת להפעיל את השיטה גם עבור מקרים שבהם ניתן למקם סנסורים בהרבה מקומות הודות לסיבוכיות הנמוכה והאפשרות למקבל חישובים. ביצענו השוואה בין השיטה המוצעת לשיטה שבה האופטימיזציה מבוצעת על כל רוחב הסרט בבת אחת, וגם לתכן שבו הסנסורים נמצאים במרחקים אחידים זה מזה. הגישה המוצעת השיגה ביצועים אופטימאליים מבחינת רובוסטיות, תגובת אלומה קבועה בתדר, רמת אונות צד נמוכות וסיבוכיות חישוב ישימה. לעומת זאת שאר השיטות הראו יתרונות רק בחלק מהמדדים הנ"ל.

החלק האחרון של המחקר מרחיב את הגישה הדלילה שפותחה בחלק הקודם ואשר מוגבלת למקרים שבהם כיוון האלומה הראשית הוא קבוע ולא ניתן לשינוי. בחלק זה הכללנו את הקונספט הנ"ל על מנת שיתמוך במערכים בעלי גיאומטריה מסובכת יותר לעומת מערך ליניארי, אשר בהם נדרשת גמישות בקביעת כיוון האלומה הראשית. כמו כן נעשה שימוש בגישה חמדנית על מנת למצוא את מבנה המערך הדליל האופטימאלי. לגישה זו יש יתרון היות והיא מאפשרת בצורה יותר טבעית ופשוטה להעריך מה המספר המינימאלי הנדרש של סנסורים שבהם ניתן לעמוד בביצועים הנדרשים. התמקדנו במערכים בעלי גיאומטריה קונצנטרית (concentric) אשר להם תכונה של יכולת לייצר תגובת אלומה דומה בכיוונים אזימוטאליים שונים. על מנת לעמוד באילוץ הזה, התכן המוצע מורכב משלושה שלבים.

בשלב הראשון שימוש באלגוריתם חמדני למציאת מבנה המערך הנדרש עבור כיוון מסוים. השלב השני הינו שכפול המבנה לכיוונים נוספים, והשלב השלישי הינו צמצום יתירויות של סנסורים וקבלת פתרון דליל הן מבחינת מספר סנסורים והן מבחינת מספר טבעות של המערך. הראנו בסימולציות כי הגישה המוצעת אכן מאפשרת לקבל מערך דליל עם תגובת אלומה קבועה בתדר וקבועה בכיוונים אזימוטאליים שונים, ובנוסף התכן המוצע מספק ביצועים אופטימאליים באופן דומה למה שהושג בעבודה הקודמת בהשוואה למערכים אחידים ואף בהשוואה למערכים אקראיים.

לסיכום, בתיזה זו הצענו מספר גישות תכן חדשניות למערכי DMAs אשר מאפשרות לקבלת מערכים עם ביצועים משופרים. ההתקדמות המשמעותית שהושגה במחקר זה מאפשרת לשלב מערכים דיפרנציאליים בצורה יעילה יותר במערכות אקוסטיות עתידיות.